The Effect of Grain Refinement on the Castability of Magnesium-Aluminium Alloys

A thesis submitted

in partial fulfillment of the requirements for the degree of

Doctor of Philosophy

at

The University of Waikato

by

TIMOTHY KEVIN LOUGHNANE

February 2007

THE UNIVERSITY OF
WAIKATO
Te Whare Wānanga o Waikato

Abstract

Rapidly increasing fuel prices and global pressures to reduce the harmful effects of vehicle emissions are forcing vehicle manufacturers to look at alternative materials to reduce the mass of the vehicles they produce. This has led to an increase in the research and development of magnesium alloys for use in automotive applications, and the methods used to produce them. With a density two-thirds that of aluminium alloys, and one quarter that of steel, magnesium alloys are continually being investigated as possible replacements for the production of automotive castings such as wheels and engine blocks. However, there is presently a lack of understanding of the effects of common alloy additions that refine the as-cast microstructure on the castability of the casting alloys in question.

The most popular magnesium alloys for large automotive castings are based on the magnesium-aluminium alloy system. For the work presented in this thesis, two of the most common Mg-Al alloys, AZ91E and AM60B, were chosen to determine the effect of grain refinement on the castability of Mg-Al alloys. An experimental mould has been designed and developed to emulate the geometry, filling, and solidification of an alloy wheel casting. Two different grain refiners were investigated at varying addition levels to determine the effect of different levels of grain refinement on the castability of the two alloys. Castability, defined as the ability to produce sound castings from a particular alloy, has been assessed through visual examination of external casting defects, X-ray radiography of internal defects, as well as grain size and porosity level analysis of all samples produced.

It has been found that for both AZ91E and AM60B, an increase in the level of grain refinement achieved lead to an increase in the occurrence and severity of the surface slumping defect in the castings produced. Conversely, increased levels of grain refinement were found to reduce or totally eliminate the occurrence of the hot tearing defect in both alloys.

Contrary to popular belief, grain refinement was found to increase the level of internal shrinkage porosity in the Mg-Al castings. This was especially the case in

the poorly fed regions of the casting, such as the junction between the spoke and rim sections. This is due to the increased reliance on interdendritic feeding of liquid to compensate for shrinkage during the latter stages of solidification in such areas, where solidification does not proceed directionally towards the feeding reservoirs. An increase in the level of grain refinement means the interdendritic network becomes heavily constricted, resulting in a rapid increase in the feeding pressure required to feed metal to the areas where it is required.

This study has also resulted in the development of a novel method of successfully and consistently introducing carbon to a Mg-Al alloy melt. This has in the past been identified as a major issue to overcome when adding carbon based grain refiners to Mg-Al alloy melts.

Acknowledgements

I would like express my immense gratitude to Associate Professor Deliang Zhang for his learned direction, respected advice, and valued friendship during the last 10 years of my university career. Without his guidance this work would have never have reached completion. I would also like to acknowledge the support of my associate supervisors, Dr Darius Singh and Professor Thomas Neitzert.

Thank you to Technology New Zealand and the Bank of New Zealand who have supported me financially during this research through their respective scholarship schemes.

I would like to acknowledge Paul Ewart and Yuanji Zhang for their technical support during the experimental phase of this research, and especially for their assistance setting up the magnesium casting facility at Waikato University.

To my family, thank you for your support and encouragement over the past few years, especially to Daniel and Erin for their help in reviewing this thesis. I look forward to spending more time with all of you now that my weekends are my own.

I would like to gratefully acknowledge the staff at ION Automotive Ltd. for their help during the experimental stage of this research, and for teaching me the intricacies of magnesium alloy casting. Thank you also to Dr Paul Schaffer of Queensland University for his advice during the tough times and for looking after me whenever I was in Australia.

Finally I wish to express eternal gratitude to my fiancé, Jillian Kohler. Thank you for listening, understanding, and supporting me. Most of all, thank you for being you. *Ek is lief vir jou.*

Table of Contents

List of Figures

List of Tables

1.0 Introduction

Magnesium alloys are extremely attractive engineering materials due to their low density and high strength to weight ratio. After an initial surge in the use of magnesium alloys for aircraft and ballistic applications during World War II, magnesium has not continued on to realise its full potential in terms of annual production and use. The inherent difficulties associated with the production, processing, and corrosion protection of magnesium alloys have slowed its widespread uptake in many areas other than the high value aerospace and motor sport industries.

With increasing awareness of the need to control international fuel consumption and reduce harmful vehicle emissions, the automotive industry is now under extreme pressure to reduce the weight of the vehicles it produces. One of the simplest methods of reducing vehicle mass is to replace conventional materials such as steel with lightweight materials such as aluminium and magnesium. It is for this reason that in the last decade, research into the production and development of magnesium alloys specifically designed for use in the automotive industry has reached an all-time high. This has been reflected by a recent surge in the annual production of magnesium alloys, which is forecast to continue increasing by 12% per annum in coming years [1].

The most common method of using magnesium alloys to produce automotive components such as engine blocks, transmission cases, and alloy wheels is via the casting process. This method of production allows parts of complex shapes and sizes to be created more easily. To counter the lower strength of magnesium compared with other automotive materials; magnesium is often alloyed with up to 10% aluminium to increase strength and ductility. Of all the magnesium casting alloys used to date in the automotive industry, Mg-Al alloys are the most common.

As with other casting alloys, elemental additives are often made to a Mg-Al casting melt to refine the solidified microstructure of the finished component. A

finer microstructure gives further increases in strength and ductility, which is especially important when producing components that are required to withstand high impact forces such as an automobile wheel. This technique, known as grain refinement, has been studied in great detail to determine the most effective grain refinement treatments for magnesium alloys to further enhance their properties [1-4]. Where research is lacking however, is looking at how these treatments affect the *castability* of magnesium-aluminium alloys.

Castability is a measure of how easy it is to create a sound, dimensionally accurate, defect-free component using the casting process. It is very important to take into account castability when choosing a casting alloy and also to understand what effect any melt treatments such as grain refinement will have on castability. The aim of this thesis is to determine the effects of grain refinement on the castability of two of the most common Mg-Al casting alloys, which is reflected by the ease of defect formation. The experimental casting mould designed and studied in this project emulates the casting of an alloy wheel so that the results can be directly applied to a typical automotive casting. The outcomes of this work will further advance the understanding of the effects of grain refinement on Mg-Al castings.

1.1 Thesis Organisation

Following this brief introduction, Chapter 2 of this thesis will present a comprehensive review of the literature available on Mg-Al casting alloys, and in particular, research pertaining to the grain refinement and castability of these alloys.

Chapter 3 outlines the experimental methods and analytical techniques used throughout the course of the research, the results of which are presented and discussed in Chapters 4 and 5. Chapter 4 details the investigation into the effects of grain refinement on the castability of magnesium alloy AZ91E, with alloy AM60B being the subject of Chapter 5.

Chapter 6 of the thesis further discusses the results of both investigations and looks at any similarities or differences between the two alloys, with an aim to further understanding the effect of grain refinement on Mg-Al castability.

The thesis concludes with Chapter 7, which lists the significant findings of the study and identifies areas worthy of further investigation.

1.2 References

[1] Wallace, J. F., Schwam, D. and Zhu, Y., *The Influence of Potential Grain Refiners on Magnesium Foundry Alloys.* AFS 2003 1-15 (2003).

[2] Dahle, A. K., Lee, Y. C., Nave, M. D., Schaffer, P. L. and StJohn, D. H., *Development of the As-Cast Microstructure in Magnesium-Aluminium Alloys.* Journal of Light Metals **1** 61-72 (2001).

[3] Thomson, J., Fasoyinu, F. A., Sadayappan, M. and Sahoo, M., *Casting Characteristics of Permanent Mold Cast Mg-Alloy AZ91E.* AFS Transactions (2002).

[4] Thomson, J. P., Liu, P., Sadayappan, M. and Sahoo, M., *Effect of C_2Cl_6 on Mechanical Properties and Microstructure of Gravity Permanent Mold Cast AZ91E.* 108th American Foundryman's Society Metalcasting Congress Des Plaines, IL, USA AFS (2004).

2.0 Literature Review

This chapter presents a comprehensive review of the literature available on the casting of magnesium alloys and in particular, the grain refinement and castability of magnesium-aluminium alloys. The chapter begins with a brief introduction to magnesium alloys, before continuing with a review of the casting process including solidification mechanisms and grain refinement. The formation of casting defects is analysed with special focus on identifying the links between grain refinement and castability. The review of the literature will identify gaps in the current knowledge that require further attention to increase the understanding of the effect of grain refinement on the castability of magnesium-aluminium alloys.

2.1 Introduction to Magnesium Alloys

Magnesium is the lightest of all structural metals with a density two thirds that of aluminium and one quarter that of steel [1]. This low density accompanied by a high specific strength makes magnesium alloys an attractive option for component manufacturers where weight saving is of prime importance. An increase in the use of lightweight materials in the production of automotive components would lead to higher fuel economy and lower harmful exhaust emissions, and this is where the push for increased research and development of magnesium alloys stems from. Magnesium consumption in the automotive industry has increased at a rate of 15% per annum over the last decade and this is forecast to continue at a rate of at least 12% per year for the next ten years [2].

2.1.1 Magnesium Casting Alloys

The hexagonal close packed (HCP) crystal structure of magnesium gives limited opportunity for strengthening by thermo-mechanical processing and this is why cast magnesium components are more popular than wrought products. Magnesium is rarely used in engineering applications in an unalloyed state and the

favourable size factor of magnesium (atomic diameter 0.320nm) means solid solutions are formed easily with commercially significant elements such as Al, Zn, Mn, Cu, Ag, and Zr [3]. The decreasing solubility of such elements with temperature makes magnesium alloy castings responsive to precipitation hardening treatment, allowing higher strengths and ductility to be achieved through alloying and heat treatment.

Sand and permanent mould casting are the common casting processes that are employed in the manufacture of high integrity automotive components such as wheels and cylinder heads, and it is these casting alloys that will be the subject of this thesis. Table 2-1 gives the nominal compositions of magnesium casting alloys used for sand and permanent mould casting.

Table 2-1: Nominal compositions of magnesium casting alloys [4].

	Composition (weight %)					
Alloy	**Al**	**Zn**	**Mn**	**Rare Earths**	**Y**	**Zr**
AM50A	5.0	…	0.5	…	…	…
AM60A	6.0	…	0.13	…	…	…
AM60B	6.0	…	0.25	…	…	…
AM100A	10.0	…	0.10	…	…	…
AZ63A	6.0	3.0	0.15	…	…	…
AZ81A	8.0	0.7	0.13	…	…	…
AZ91C	9.0	0.7	0.13	…	…	…
AZ91E	9.0	1.0	0.10	…	…	…
EQ21A	…	…	…	2.0	…	0.60
EZ33A	…	2.7	…	3.3	…	0.60
QE22A	…	…	…	2.0	…	0.60
WE43A	…	…	…	3.4	4.0	0.70
WE54A	…	…	…	3.5	5.3	0.50
ZE41A	…	4.2	…	1.2	…	…
ZE63A	…	5.7	…	2.5	…	0.70
ZK51A	…	4.6	…	…	…	0.70
ZK61A	…	6.0	…	…	…	0.70

2.1.2 Magnesium-Aluminium Casting Alloys

The most widely used magnesium alloys for sand or permanent mould casting are magnesium-aluminium alloys. The addition of aluminium to magnesium alloys leads to increased strength, corrosion resistance and castability [5]. Aluminium also increases the fluidity of the alloys allowing it to fill thin casting sections more effectively. Increasing the aluminium content to 6.0 wt% or more allows the casting alloy to become heat treatable, although the aluminium content rarely exceeds 10 wt% as seen in Table 2-1.

Despite the popularity of magnesium-aluminium alloys there are two main barriers to the wider use of this material. The first limitation is the reduction in creep resistance of the alloy at temperatures exceeding 150°C, which restricts its use for automotive applications such as engines or powertrain components. The second major barrier is the reduction in ductility of the alloy as the aluminium content is increased [6]. This is due to the non-equilibrium cooling rates experienced in most casting processes leading to a completely divorced eutectic structure of α-Mg and β- $Mg_{17}Al_{12}$. The increased amount of the brittle $Mg_{17}Al_{12}$ compound reduces the alloy's ductility, as it forms at the grain boundaries of the microstructure.

The magnesium-aluminium equilibrium phase diagram is shown in Figure 2-1 to give a better understanding of the solidification patterns and microstructure constituents formed during the solidification of a magnesium-aluminium alloy casting. The processes involved during the solidification of a casting will be detailed in the following section.

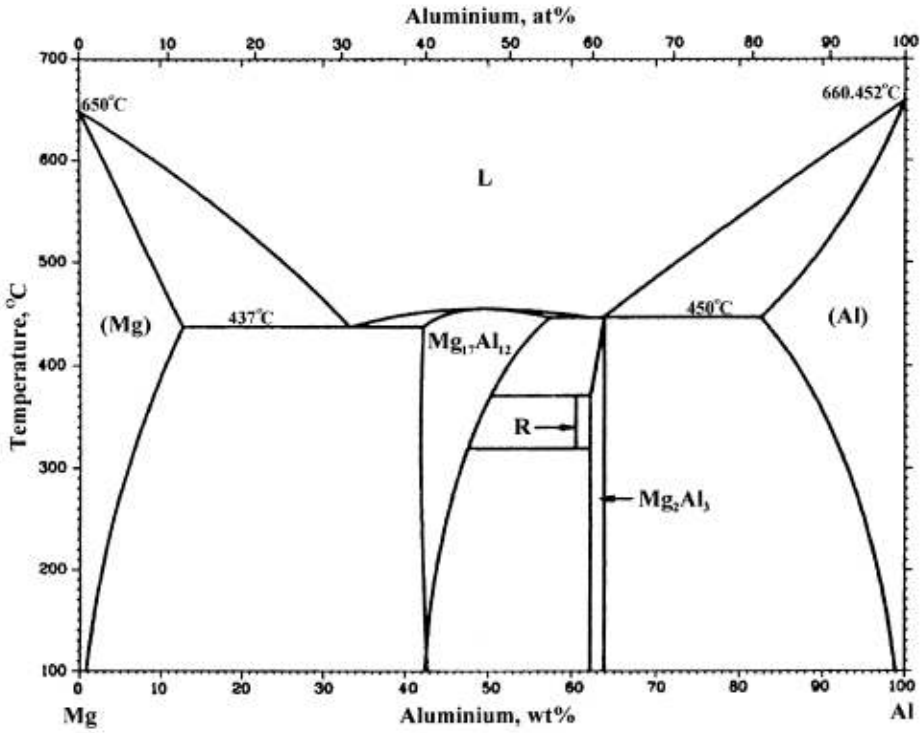

Figure 2-1: Equilibrium phase diagram of the binary magnesium-aluminium system [7].

2.2 Formation of the Cast Microstructure

Once a casting mould cavity has been filled with liquid metal, several complex occurrences must take place to convert the material into a fully solid object. These are dependant on several variables that will be discussed in this section.

2.2.1 Nucleation

By lowering an alloy to a temperature at or below its liquidus, the nucleation of small solid clusters or *embryos* is activated. For a solid crystal to grow, atoms must continue to diffuse from the surrounding liquid and attach to this embryo. The nucleation of the solid may be attributed to either *homogeneous* or *heterogeneous* nucleation. Homogeneous nucleation occurs when the solid phase forms within the body of the liquid without the aid of an external substrate, such as the mould wall or an impurity particle in the melt, to grow from. Homogeneous nucleation is seen rarely, if at all, when castings solidify due to the

large driving force required to overcome the energy of the new surface being created, requiring large undercooling of the melt.

The free energy change to form an embryo in the melt can be described by the summation of the energy of the new solid/liquid interface, and the change in chemical free energy between the solid and liquid phase, as is illustrated in Equation 2-1

$$\Delta G = 4\pi r^2\sigma + \frac{4}{3}\pi r^3 \Delta G_v$$

Equation 2-1

where σ is the interfacial energy between the solid and liquid per unit of area and ΔG_v is the free energy associate with the formation of a new volume. The system will lower its free energy by either dissolution or growth of the embryo.

The critical radius in order for a spherical embryo to become a nucleus is termed r^*. Below r^* an embryo will remelt and disappear into the liquid, while embryos larger than r^* will continue to grow, further lowering the total energy of the system. This is shown schematically in Figure 2-2:

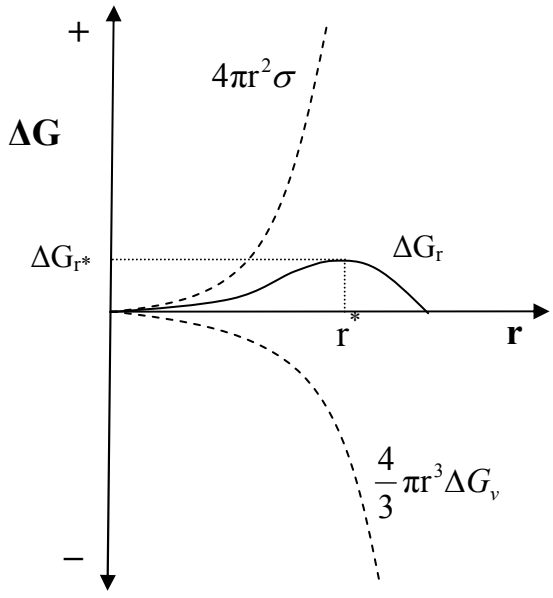

Figure 2-2: The free energy change for an embryo as a function of size. The two dashed lines represent the surface and volume free energies, with the summation of these energies represented by the solid line. The peak of this solid line (at r* and ΔG_{r^*}) is the point where an embryo becomes stable and forms a nuclei.

Where ΔG_r reaches a maximum value, as indicated in Figure 2-2, r* corresponds to the maximum free energy difference and the critical conditions for the formation of a stable nucleus have been met.

Large amounts of undercooling are required to overcome the energy barrier and form a stable nucleus in the melt that is larger than r*. It is doubtful whether this type of crystal nucleation is ever experienced during the solidification of castings, due to the abundant presence of solid substrates for the melt to nucleate against, such as the walls of the casting mould or solid impurities present in the liquid. The nucleation and growth of a solid phase against such a substrate is termed heterogeneous nucleation.

With heterogeneous nucleation, the presence of a substrate considerably lowers the thermodynamic barrier for nucleation. The contact between the substrate and the growing embryo requires a wetting term, $f(\theta)$, to be added to Equation 2-1.

$$\Delta G = \left[4\pi r^2 \sigma + \frac{4}{3} \pi r^3 \Delta G_v \right] f(\theta)$$

Equation 2-2

The term θ signifies the wetting angle between the solidifying nucleus and the substrate. Assuming the nuclei has the form of a spherical cap upon the substrate, the wetting angle can be visualised in Figure 2-3. Also shown are the various surfaces energies in the system.

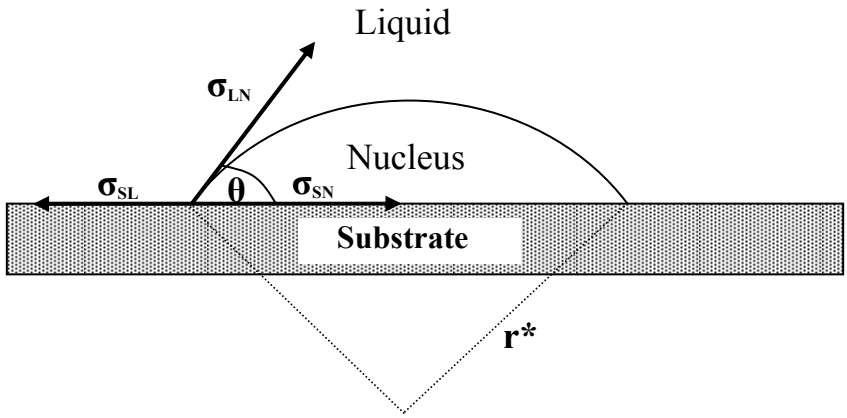

Figure 2-3: Schematic illustration of a heterogeneously nucleated solid growing against a substrate and surrounded by liquid. The wetting angle between the liquid and the substrate, θ, is also shown.

Figure 2-3 shows that the size of the wetting angle, θ, is strongly dependant on the surface energies, or surface tensions, of the various interfaces. The wetting angle will be greatly reduced if the surface energy between the nucleus and the substrate (σ_{SN}) is small. Equation 2-2 shows that a smaller wetting angle will reduce the barrier to nucleation of a viable embryo, so clearly the lower the interfacial energy between substrate and nucleus, the more potent that substrate will be at initiating solidification.

The addition of substances that produce potent nucleants in the melt is common practice in order to promote formation of new grains during solidification of a casting, and this will be discussed in more detail in Section 2.3.

2.2.2 Growth of the Solid

Once a stable nuclei has formed and begins to grow in the surrounding liquid there is a great reliance on the rate of solute distribution through both the solid and liquid phases. In perfect equilibrium conditions, solute homogenisation in both the solid and liquid phases is complete. The compositions of the solid and liquid phases are related by the lever rule as described in Equation 2-3:

$$\frac{C_l}{C_o} = \frac{1}{1 - pf_s}$$

Equation 2-3

where: C_l = the concentration of solute in the liquid

C_o = the initial concentration of solute in the system

p = 1-k

k = the partition coefficient

f_s = the fraction of solid in the system

The slow nature of diffusion of an element through a solid phase means a long period of time is required for appreciable solute redistribution. A more realistic relationship is given by the Scheil Equation, which is sometimes also called the

non-equilibrium lever rule. This equation predicts the solute concentration in the liquid during solidification assuming no solute diffusion through the solid phase, and complete solute homogenisation (or mixing) in the liquid. This is shown in Equation 2-4:

$$\frac{C_l}{C_o} = \frac{1}{(1 - f_s)^p}$$

Equation 2-4

In many situations, the homogenisation of solute in the liquid is also limited by solute diffusion in the liquid. In such cases, there is a solute concentration gradient ahead of the solidifying front. As the liquid ahead of the solid-liquid interface becomes less rich in solute with increasing distance, the liquidus temperature, T_{mp}, of the liquid increase with distance. However, the rate of heat transfer from the system is fixed due to the casting conditions, and the overall temperature distribution is controlled by the casting condition. Therefore a temperature difference between T_{mp} and T exists in the liquid ahead of the solid-liquid interface. This region is said to be "constitutionally undercooled".

The constitutional undercooling of the melt has a profound effect on the morphology of the solid-liquid interface during solidification. The transition from a planar to cellular morphology will allow a higher rate of solute rejection, with the transformation to a dendritic morphology allowing the highest rate of solute rejection. For this reason, constitutional undercooling plays a critical role in determining the final solidified microstructure. The transformation in morphology of the solid-liquid interface is shown schematically in Figure 2-4.

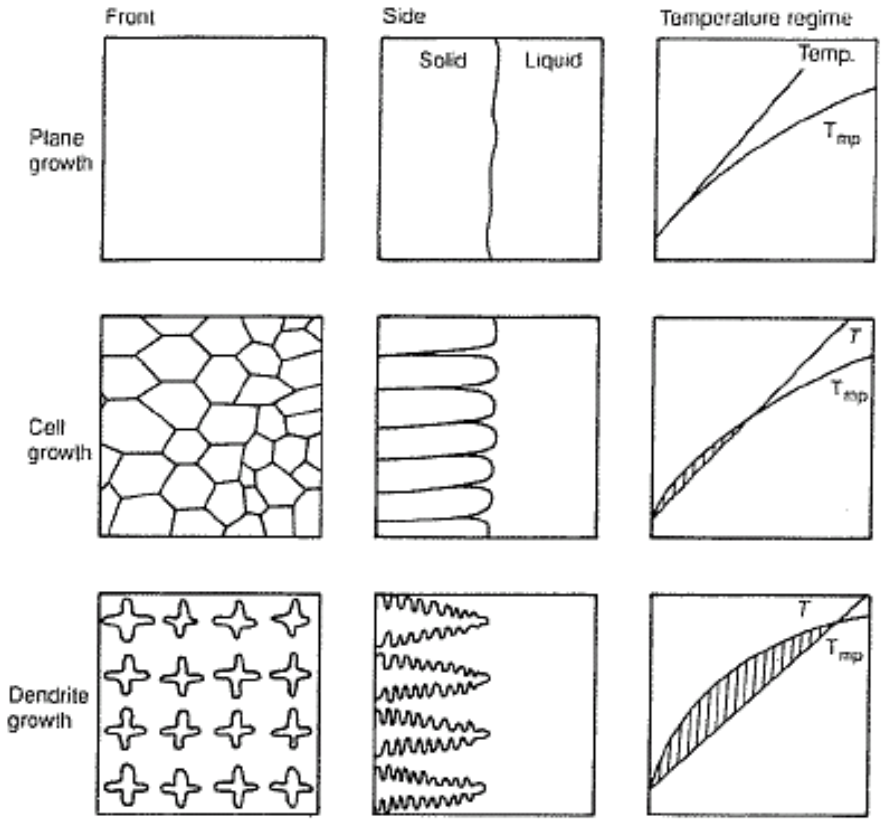

Figure 2-4: The transition of growth morphology from planar, to cellular, to dendritic as constitutional undercooling increases.

As magnesium possesses a hexagonal close packed (HCP) crystal structure, castings that are produced in non-equilibrium conditions contain a dendritic microstructure with six-fold symmetry. The preferred crystallographic direction for growth of magnesium dendrites is <210>.

The constitutional undercooling of the melt ahead of the solid-liquid interface does not only change the morphology of the growing solid. The likelihood of future nucleation events is also affected by this region of undercooling. As the constitutional undercooling reaches a point sufficient for nucleation (ΔT_n), new crystals nucleate and begin to grow in the undercooled region. The growth of these new crystals leads to further constitutional undercooling around them, which in turn facilitates the nucleation of other crystals. The rapid growth of closely grouped crystals leads to a restriction of crystal growth and a finer grain size results. Easton and StJohn [8] schematically illustrated this phenomenon in a diagram which is reproduced below in Figure 2-5.

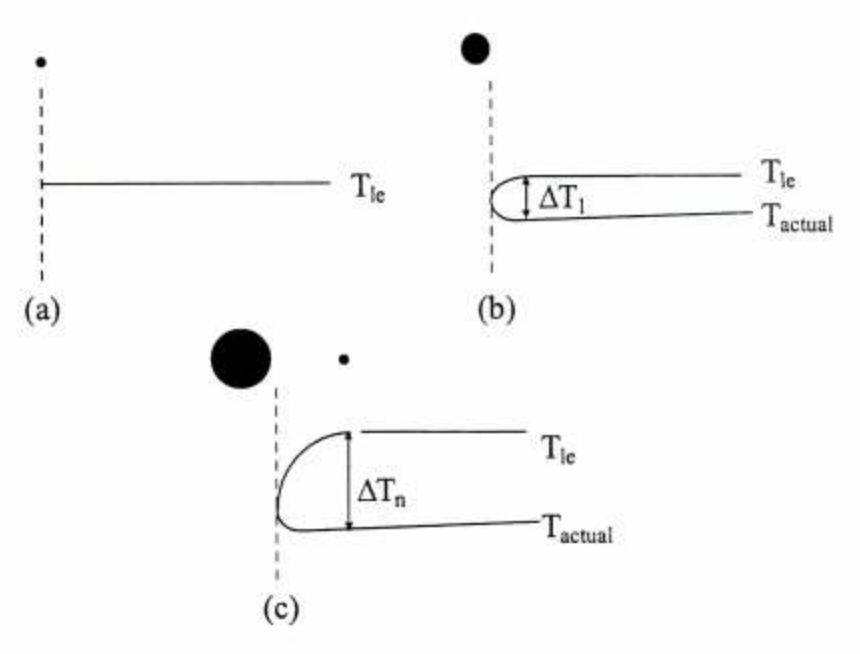

Figure 2-5: (a) through (c) shows the development of the constitutionally undercooled area in front of the growing interface so that further nucleation events can occur. In (b) a constitutionally undercooled area exists but is not sufficient to activate further nucleation. In (c) the undercooling reaches ΔT_n the sufficient level for nucleation to occur. T_{le} is the equilibrium liquidus temperature of the alloy. The dark circles represent growing solid crystals [8].

The growth restriction factor (GRF) is a measure of the growth restricting effects of solute elements on the growth of the solid-liquid interface of new grains as they grow into a melt [9]. The concept was first proposed by Maxwell and Hellawell as they developed the parameter $Q = m(k-1)C_o$, where m is the slope of the liquidus line, C_o is the concentration of solute in the alloy, and k is the partition coefficient between the liquid and solid. The value for Q can be determined from the equilibrium phase diagram under the assumption that the slopes of the liquidus line and the partition coefficient are constant.

The grain size of a casting is inversely proportional to the growth restriction factor. For this reason elements with high a GRF's are often added to the casting alloy to promote a fine casting microstructure.

The production of castings with small equiaxed grains has long been the desire of metal casters, with research in this area dating back to the 1940's [10]. Castings

with a fine grain structure have improved strength and ductility with increased resistance to corrosion due to a finer distribution of precipitates [9, 11, 12]. Also the avoidance of columnar grains in a casting means a component will have reduced anisotropy of mechanical properties.

The addition of grain refiners to the melt is designed to do one of two things; promote suitable sites for heterogeneous nucleation of grains, or restrict the growth of grains through the segregation of solute elements. As magnesium castings can possess a large and variable grain size, there has been much research undertaken to develop methods of grain refining magnesium casting alloys. The state of this research will be detailed and discussed in the following section.

2.3 The Grain Refinement of Mg-Al Alloys

The grain refinement of magnesium alloys is generally divided into two separate categories based on the presence or lack of aluminium in the alloy. Magnesium alloys that do not contain aluminium are extremely well grain refined by the addition of zirconium to the melt prior to casting. Many studies have found that adding as little as 0.5 wt% Zr to a magnesium alloy results in significant reduction in grain size [13-16]. It is also know that Zr is effective in reducing the iron level of a casting alloy by forming stable precipitates which settle from the melt after suitable holding time [17].

Zirconium can not be used to grain refine alloy containing aluminium, as stable intermetallic compounds are readily formed between Al and Zr. Consequently, much work has been conducted in the last 70 years to develop effective methods of grain refining magnesium-aluminium alloys (e.g. [10, 16, 18, 19]). The fundamental grain refinement methods developed in this time are detailed in the following sections.

2.3.1 The Superheating Method

Although raising a casting melt to temperatures well above the melting point is avoided in many casting alloys, it has been found to have beneficial effects for magnesium-aluminium alloys. Superheating of Mg-Al alloys differs from other grain refinement techniques, as no additions to the melt are required. The melt is simply heated to a temperature 150-260°C above the liquidus temperature and held for a short time. The temperature of the melt is then rapidly reduced back to the required casting temperature [10, 20]. It is to be noted that the significant effect of superheating on grain size is only apparent in aluminium containing magnesium alloys. In other magnesium alloys the effect is said to be marginal [20].

The exact reason for the grain refinement of Mg-Al alloys by superheating is not fully clarified in the literature; however there are many theories that propose the mechanisms of grain refinement. One theory explains the effect by the formation of various iron containing particles that promote the nucleation of α-Mg grains [21, 22]. This theory proposes that as iron becomes less soluble in molten magnesium, precipitates are formed as the melt is lowered from the superheating temperature, and the resulting precipitates act as suitable sites for heterogeneous nucleation.

A different theory proposed by Hall [23] is based on the formation of clouds of metallic oxides or other intermetallic compounds during superheating that also act as suitable nucleation sites during solidification. However this theory has been discredited to some degree by the research of Tiner [22] who obtained significant grain refinement by superheating the melt in a vacuum as well as in air, and Nelson [10] who also had successful refinement in a fully closed system.

A further theory to explain the grain refinement of Mg-Al alloys by superheating is proposed in the literature, called the temperature-solubility theory [10, 24]. It is thought that the change in particle size of compounds already present in the melt during superheating may transform them to more effective nucleants. Particles that are too coarse for heterogeneous nucleation may be dissolved during

superheating, and precipitated back out during subsequent cooling, with a finer morphology.

While the exact reason for the grain refinement effect obtained by the superheating method is not fully clarified in the literature, there are some underlying factors that are in general agreement [10, 21-26]. These are as follows:

- Aluminium appears to be an important alloying element for successful grain refinement using the superheating technique. Superheating effectiveness is increased with increasing aluminium content.

- Superheating relies heavily on treatment temperature and treatment time. A higher treatment temperature results in less holding time required for successful grain refinement. Grain size is independent of superheating temperature if holding time is sufficiently long. However, superheating at too high a temperature, or excessively long holding time results in grain coarsening.

- Presence of iron and manganese are essential for successful grain refinement. Too little iron results in a slow response to superheating, while too much manganese can also negate the grain refinement effect.

- The superheating effect is suppressed by the presence of zirconium, beryllium or titanium.

- Generally, the superheating effect will disappear when the alloy is remelted.

2.3.2 The Elfinal Process

The theory that iron played a part in the grain refinement achieved using the superheating process lead to the development of the Elfinal process for grain

refinement of magnesium alloys. Also called the $FeCl_3$ process, the Elfinal process involves the addition of anhydrous $FeCl_3$ to magnesium alloys at temperatures in the range of 740-780°C [26]. Although the process was first patented in 1942 [27], there is little coverage in the literature detailing experimental data and results. The lower operating temperature of the Elfinal process made it more attractive than the superheating process where energy and material costs were of great importance. Although the Elfinal process delivers similar grain refining efficiency as superheating, it is ineffective unless manganese is present in the melt. The presence of at least 3 wt% Al also aids the grain refinement process, and Emley suggests grain refinement is due to the formation of nucleant particles of Fe-Mn-Al [28].

Another theory as to the effectiveness of this process was suggested by Nelson [10], who said the addition of ferric chloride merely increased the melt temperature by local reaction into the range required for grain refinement by superheating.

Some elements such as zirconium and beryllium form stable compounds with iron when present in a melt treated with ferric chloride, and so lower the effectiveness of the process [16]. Other disadvantages of this process include the hazardous nature of $FeCl_3$ and the reduction in corrosion resistance of magnesium alloys that contain large amounts of iron.

2.3.3 Carbon Inoculation

The growing need for effective grain refinement, without the large energy requirements of superheating, lead to the development of the carbon addition method for grain refinement of Mg-Al based alloys. This method involves the addition of carbon to a Mg-Al based melt in such forms as graphite powder, CaC_2, C_2Cl_6, paraffin wax, or carbonaceous gases. The main benefit of the carbon addition method is the lower treatment temperature required for successful refinement compared with the superheating method [20, 25]. Successful

refinement is obtainable in the range of 760-815°C which gives the treatment practical advantages.

One method of introducing carbon is by bubbling carbonaceous gases such as carbon dioxide, acetylene and natural gas through the melt [10, 28, 29]. Davis and Eastwood [29] obtained successful grain refinement by bubbling natural gas through the melt at 760° for 5 minutes. The authors suggest that although this may be thought to introduce undesirable hydrogen to the melt, they found this was not the case. They mentioned that hydrogen present in the natural gas would most likely break down to molecular, not atomic hydrogen, which is not readily absorbed by molten magnesium.

Another method of carbon inoculation involves the addition of solid carbon or carbon containing materials to a magnesium melt. Such materials that have been investigated successfully include graphite powder, coal, lampblack, calcium carbide, silicon carbide, and paraffin wax [7, 29-31]. While all of these investigations have resulted in successful grain refinement, there were often reports of inconsistent results. This is said to be due to the difficulty in successfully introducing the carbon containing material into the melt. Fine powders may rise to the surface of the melt, and/or become entrapped in the oxide layer at the melt surface.

It is important to note that grain refinement of magnesium using carbon inoculation is only successful in alloys that contain aluminium [16, 25, 32, 33]. The presence of aluminium is necessary because the particles responsible for promoting nucleation of the α-Mg grains are thought to be either Al_4C_3 or a compound of Al-C-O [7, 18, 33].

This theory appears to be backed up by the experimental observations that higher treatment temperatures lead to more effective grain refinement, through improved dissolution of carbon. Holding the melt for long periods at lower temperatures (~700°C) also leads to a diminished effect, which suggests settling of nucleant particles.

More recently, there has been a dispute occurring in the literature as to the exact reason for the grain refinement of magnesium by carbon addition. Jin et al [34] report that although most researchers stand by the Al_4C_3 or Al-C-O nucleant theory, grain refinement through carbon addition may be due to constitutional undercooling. They mention that carbon has a strong segregation tendency in magnesium, so would restrict grain growth during solidification as explained in Section 2.2.2. However, Qian and Cao [35] published a negative response to this theory after conducting research of their own in this area. Their work states that carbon inoculation has no effect on magnesium alloys that do not contain aluminium. If grain refinement of magnesium is due to carbon segregation during solidification then surely the same effect would be seen in pure magnesium, or other magnesium alloys.

Although there is some conflict in the literature detailed above, underlying parameters for the successful grain refinement of magnesium alloys by carbon inoculation do exist. These are summarised as follows:

- Carbon inoculation is only successful for Mg alloys that contain aluminium.

- Grain refinement is suppressed by the presence of zirconium, beryllium, and titanium as these form more stable carbide compounds than aluminium.

- The optimal melt temperature range for carbon inoculation is 760-815°C.

- As with superheating, holding the carbon treated melt for extended periods results in a loss of grain refinement efficiency due to the settling of potential nucleant particles. The grain refinement is also not as effective upon remelting of a treated alloy.

2.3.4 Grain Refinement through Alloying Additions

Aside from the elements mentioned previously for the grain refinement of magnesium-aluminium alloys (Fe, Mn, Al, C), there has been much research into the effects of other alloying additions [7, 18, 24, 36-40]. Of all the elements investigated, the ones with the highest potential for grain refinement of Mg-Al alloys appear to be calcium and strontium.

To improve the high temperature creep resistance of Mg alloys, the use of calcium has been widely investigated [24, 37, 41, 42]. Researchers have found that calcium also has a beneficial effect in terms of grain refinement. Lee et al [24] produced significant grain refinement of pure magnesium with 0.4 wt% Ca. However there is only a small amount of detailed research into the effects of calcium as a grain refiner for Mg-Al alloys. In one investigation into the effects of calcium addition to Mg alloy AM60, Hu et al [37] found that adding 1.0 wt% Ca to the alloy resulted in a 57% reduction in grain size. They suggest that the mechanism responsible for the grain refinement is heterogeneous nucleation of the α-Mg grains by Mg_2Ca, and the restriction of grain growth by the presence of Al_2Ca.

Another investigation was carried out by Wang et al [43] on the effects of calcium addition to Mg alloy AZ91. It was found that the addition of calcium could refine the casting microstructure and reduce the amount of $Mg_{17}Al_{12}$ eutectic phase. Unfortunately this work did not detail the effect of calcium on the grain size of the casting samples.

Another element that is added to magnesium alloys to increase their creep resistance is strontium, due to the formation of grain boundary pinning Al_4Sr and Mg_2Sr particles. Strontium has also been found to refine the grain size of Mg-Al alloys [18, 24, 39, 40, 44].

Lee et al [18] found that strontium was an effective grain refiner for pure magnesium, but once the aluminium content was increased in the alloy, its effectiveness diminished. Gruzleski and Aliravci [44] however, reported

significant grain refinement of AZ91 with a small strontium addition to the melt. The authors mention that the grain refinement may be due to the presence of strontium altering the growth kinetics of the solid-liquid interface, and poisoning the fast growing direction of grains. This is said to be due to adsorption of Sr on the surface of the growing solid. One factor that brings the results of this study into question is that a C_2Cl_6 tablet was used prior to adding the strontium to degas the melt. As mentioned in Section 2.3.3, C_2Cl_6 may be an effective grain refiner in its own right, so this would have clouded the results somewhat. The true mechanism for grain refinement of Mg-Al alloys by strontium addition is yet to be clarified.

Nussbaum et al [45] also investigated the addition of strontium to AZ91 and found significant grain refinement. They also discovered the increased amounts of Al_4Sr and Mg_2Sr needles in the microstructure. It should be noted however, that precipitates of this nature are undesirable as they decrease the ductility of the alloy.

While the exact nature of grain refinement by strontium is yet to be fully understood, its effect on growth kinetics is well explained. The growth restriction effect detailed in Section 2.2.2 describes how the low solubility of Sr in magnesium leads to a build up of solute at the solid-liquid interface during solidification. This constitutional undercooling leads to an increase in the amount of nucleation events around this area which restricts further grain growth [24].

2.3.5 Grain Refinement through Direct Particle Additions

Particles that have a low wetting angle with molten magnesium and similar lattice parameters are said to be potentially effective nucleants for the grain refinement of magnesium alloys. Recent research by Luo has looked at the addition of silicon carbide particles to AZ91, and found significant grain refinement was achieved [46]. This was attributed to the low lattice disregistry of only 4% between SiC and Mg. It may also be attributed to the presence of foreign particles

interfering with the growth of the grains, forcing them to be pushed to the grain boundaries.

Lee et al [18] investigated the direct addition of TiC, SiC, AlN, and Al_4C_3 particles to magnesium alloys and experienced some grain refinement. The best results came from the addition of Al_4C_3 and SiC. Another investigation looked at the addition of AlB_2 in the form of a master alloy and found some grain refinement of the casting samples [11]. However there were difficulties associated with obtaining a homogenous distribution of particles in the melt.

As with the addition of carbon, there is still some difficulty in obtaining a homogeneous mix of particles in a magnesium casting melt. Particle settling and agglomeration are two problems that will need to be overcome to increase the use of these types of grain refiners. Perhaps the development of suitable master alloys, as is seen in the aluminium casting industry [47-51], would yield an increase in the effectiveness of direct particle additions for grain refinement.

2.3.6 Grain Refinement through Melt Stirring or Agitation

There are two methods of stirring or agitation of a casting melt which will lead to a refinement of the casting microstructure. The first method involves stirring the melt, either manually or automatically, immediately prior to pouring. Nelson [10] proclaimed that violent stirring of a small batch of magnesium results in successful grain refinement. He goes on to explain that the rapid stirring increases the dissolution of the nuclei forming phase in the alloy, thus increasing grain refinement. By this logic, stirring the melt at low temperatures should be avoided, as it would only lead to the coalescence of nucleant particles, and a reduction in grain refinement. Hultgren and Mitchell also reportedly obtained successful grain refinement of AZ92 by utilising the stirring method [52].

The other method to induce grain refinement through stirring or agitation is to upset the melt during solidification. This may be achieved through mechanical vibration, electromagnetic stirring, or by bubbling the melt. Many investigations have obtained successful grain refinement via this method [53-57]. The

mechanisms responsible for the grain refinement are improvement of heterogeneous nucleation through cavitation collapse and grain multiplication.

2.3.7 Measurement of Grain Size in Mg-Al Alloys

An unfortunate microstructural characteristic of Mg-Al alloys is the presence of large amounts of the brittle $Mg_{17}Al_{12}$ eutectic [6, 58-60]. This compound is often situated between dendrites and at the grain boundaries, and makes grain boundary identification difficult. As a result, Mg-Al castings are often solution heat treated prior to microstructural investigation. The solution heat treatment is designed to dissolve the eutectic compound, and helps reveal the grain boundaries for grain size measurement [61, 62]. A typical treatment regime is to heat the sample to 413°C and hold for 0.5 - 2.0 hours before cooling in air [18].

A major issue associated with solution treatment of metallic samples prior to microstructural characterisation is the potential for grain growth, or germination, during treatment. Germination can occur when the temperature of a metal is raised above half its melting temperature [63, 64]. The driving force for this growth is the reduction in the interfacial energy that exists between grains, by the growth of some or all of the grains in the sample. This phenomenon obviously negates whatever mechanical property advantages were gained through the grain refinement process. Germination also brings into question the validity of any data published for mean grain casting grain size of a casting, if the sample has been solution treated subsequent to casting. To truly determine the as-cast grain size of a casting sample, solution treatment should therefore be avoided.

Some researchers have investigated other methods of determining the true as-cast grain size of a Mg-Al casting [65-67]. George [65] developed etchants for Mg-Al alloys containing glacial acetic and picric acids. The etchant was designed to develop a colour contrast depending on crystallographic orientation and enabled clear distinction between differing grains. Unfortunately, some of the chemicals involved are highly undesirable due to safety concerns which have limited their use. More recently, Maltais et al have developed a reagent for determining the true as-cast grain size of magnesium alloy AZ91 [67]. Their process involves the

production of a cracked, dry film on the surface of the sample. The direction of cracks running parallel to each other on the surface of a grain is determined by the crystallographic orientation of the grain. This process allows grains to posses differing contrast when viewed under polarised light.

Figure 2-6 shows the contrast achieved in magnesium alloy AZ91 using the newly developed reagent of Maltais et al [67].

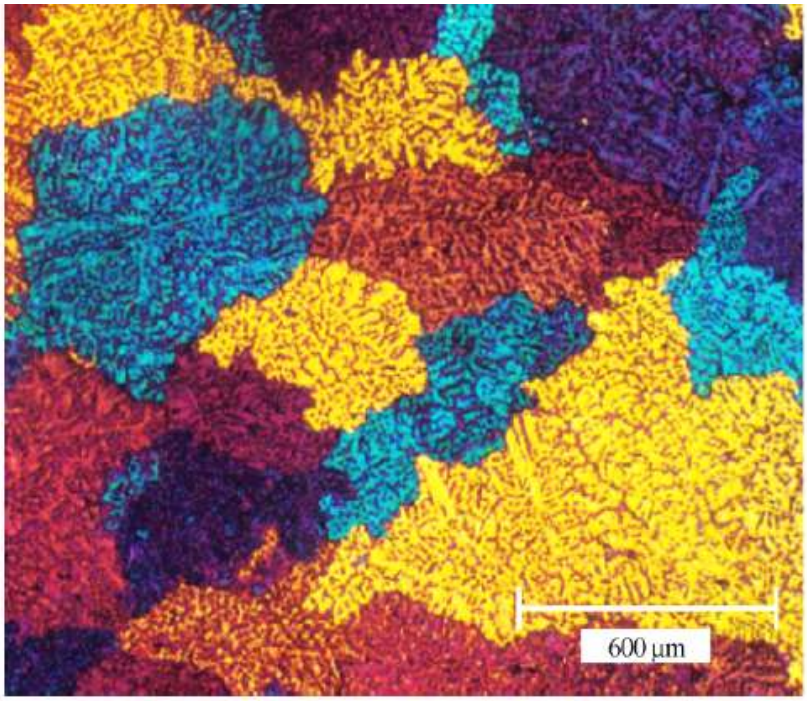

Figure 2-6: The microstructure of as-cast AZ91D. The image is viewed under light microscope using polarised light [67].

2.4 Casting Defect Formation

The formation of casting defects is a complex phenomenon which may be attributed to a single cause, or a combination of several factors. The shrinkage of solidifying metals, and the inefficient feeding of liquid metal to compensate for this shrinkage is a major cause of porosity in castings. The presence of dissolved gases and inclusions in the liquid metal may also lead to the formation of casting defects. The formation of common casting defects and the root causes of these defects are explained further in the following sections.

2.4.1 Feeding Mechanisms

The solidification of an alloy during casting results in significant contraction of the solid phase. To produce a fully dense component, effective feeding of liquid metal to compensate for this shrinkage is of prime importance. If the alloy has a long freezing range, the semi-solid network through which the compensatory liquid must travel may be tortuous and restrictive [68]. As the fraction of solid in the casting increases, it becomes more difficult for the liquid to flow between the dendrites. As a result the pressure gradient which drives the feeding of liquid varies greatly. The mechanisms of feeding liquid through a solidifying castings has been well defined by Campbell, who proposes five distinct feeding mechanisms [69]. These mechanisms are listed below and are illustrated in Figure 2-7.

- Liquid Feeding
- Mass Feeding
- Interdendritic Feeding
- Burst Feeding
- Solid Feeding

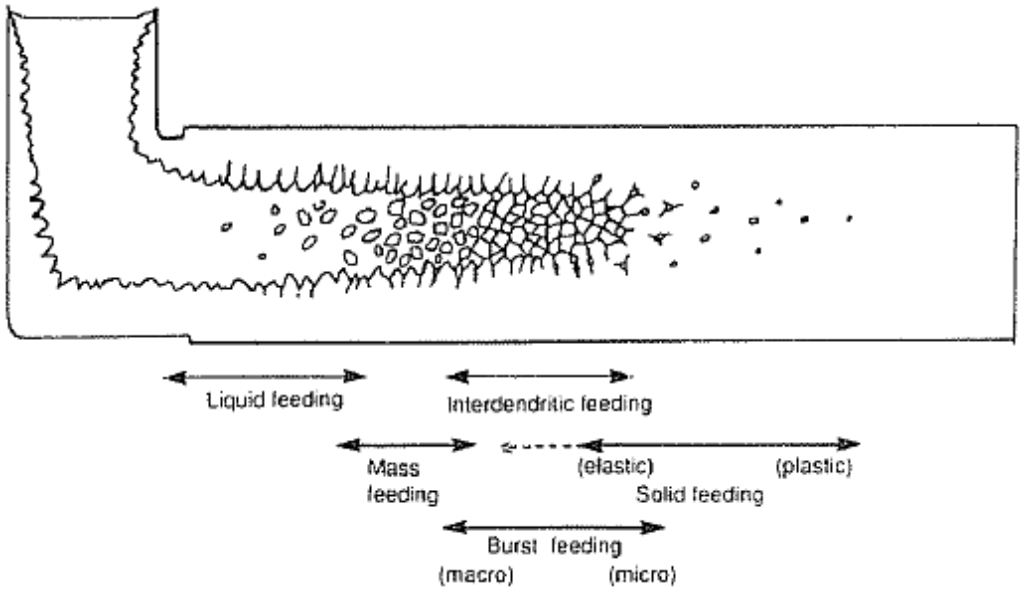

Figure 2-7: A schematic of a solidifying casting showing the different feeding mechanisms that operate during solidification [69].

Liquid feeding usually precedes all other forms of feeding and is the least restrained form of feeding. It occurs at temperatures above the liquidus of an alloy. Due to the insignificant stresses invoked by the small pressure gradient, the fluid can flow freely to areas of the casting where it is required.

Mass feeding occurs when the temperature of the alloy drops to below the liquidus temperature, and the fluid is a mixture of solid and liquid. The semi solid nature of the material increases its viscosity and the fluid behaves more like a slurry. Like liquid feeding there are insignificant stresses induced by the small pressure gradient, and mass feeding continues until the solid crystals begin to impinge on each other. At the stage where a solid network of dendrites has developed, mass feeding ceases. The point at which the dendrites are locked together is termed the coherency point.

Dendrite coherency usually occurs in an alloy between 10-50% solid fraction. The exact point of coherency is influenced by the grain size and morphology of the alloy. Large grain size leads to coherency being reached earlier in solidification, while more spherical grains impinge later in solidification. After dendrite coherency is reached, a transition from mass to interdendritic feeding occurs.

Interdendritic feeding is the most difficult feeding mechanism and is extremely important in relation to the formation of defects. Once the dendritic network is strong enough to withstand the forces imposed by the pressure gradient, feeding must proceed via liquid flowing through the channels that exist between the dendrites. The pressure gradient (dp/dx) required to drive the fluid to flow through this interdendritic network can be estimated using Darcy's Law:

$$\frac{dp}{dx} = -\frac{v\mu}{K_S}$$

Equation 2-5

where ν is the volumetric velocity of the liquid through the network, K_s is the permeability of the semi-solid medium and μ is the viscosity of the liquid. By

using the permeability component of the Darcy's Law, the resistance to feeding of liquid metal through the interdendritic network can also be estimated. The Kozeny-Carman equation gives the liquid permeability, K_s as follows:

$$K_S = \frac{g_L^3}{k_C S_V^2}$$

Equation 2-6

where g_L is the liquid volume fraction, S_V is the specific surface area, and k_C is the Kozeny-Carman constant which is determined by the characteristic of the porous network. Equation 2-6 suggests that permeability is decreased as solid fraction increases, or in other words, as g_L is decreased.

As seen in Figure 2-7, burst feeding may occur around the same time as interdendritic feeding. This is due to the stresses developed by solidification shrinkage, overcoming the strength of the dendritic network. When this occurs, it is possible for the network to collapse inwards, allowing mass and interdendritic feeding to overcome the pressure gradient. Alloys with long freezing ranges are more prone to burst feeding, as the long interdendritic feeding paths created in these alloys allows for the build up of a high pressure differential.

The final feeding mechanism occurs in the latter stages of solidification and is termed solid feeding. This feeding stage is caused by high temperature deformation of an already solidified region in the casting. If a region is prematurely isolated from adequate feed metal to compensate for the solidification shrinkage, the hydrostatic stress that is created may be sufficient to overcome the yield stress of the solidified casting. When this occurs, the solidified casting may be drawn inwards to overcome the shrinkage pressure, hence the term "solid feeding". This type of feeding mechanism is the main cause of a casting defect relating to slumping of the casting surface. This will be discussed in greater detail in Section 2.4.3.

2.4.2 Porosity Formation

The formation of pores in a solidifying casting is defined as being possible by the following equation [69, 70]:

$$P_G + P_S > P_{ATM} + P_H + P_{ST}$$

Equation 2-7

where:

P_G	=	Pressure of dissolved gas in the liquid
P_S	=	Pressure resulting from solidification shrinkage
P_{ATM}	=	Atmospheric pressure
P_H	=	Pressure from metallostatic head
P_{ST}	=	Pressure due to the surface tension between the liquid/pore

The left side of Equation 2-7 defines the pressures promoting the formation of pores; with the terms on the right defining the resistance to pore formation. Once the left side of the equation is greater than the right side, the formation of pores becomes feasible.

The most common dissolved gas that affects aluminium and magnesium casting alloys is hydrogen. The two methods of introducing hydrogen to molten magnesium alloys are via absorption from hydrogen in the atmosphere, and by reaction between molten magnesium and moisture. The reaction between molten magnesium and moisture is defined by the following equation:

$$Mg + H_2O \Rightarrow MgO + 2H$$

Equation 2-8

Dissolved hydrogen has a potential for porosity formation due to the difference in its solubility in solid and liquid magnesium as shown in Figure 2-8. As solidification progresses the alloy is unable to keep as much hydrogen in solution, and so gas pores may be nucleated. The role of hydrogen in porosity formation in

magnesium alloys is not as important as it is with aluminium alloys, due to higher hydrogen solubility in solid magnesium. The solid solubility of hydrogen in aluminium alloys is around 0.04ppm [71], while for AZ91 it is as high as 24ppm [72].

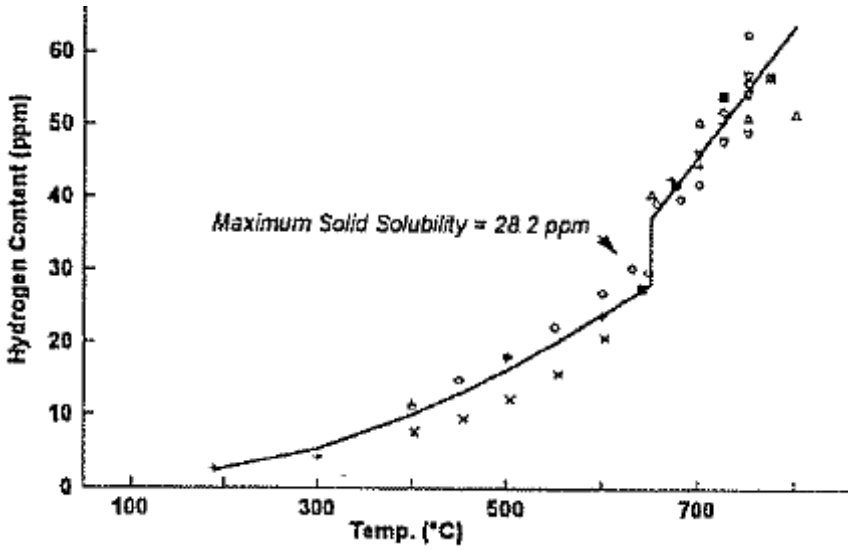

Figure 2-8: The solubility of hydrogen in pure magnesium [72].

For porosity to form during solidification, the critical pressure for pore nucleation must be overcome. Homogeneous nucleation of pores requires that extremely high pressures be overcome, and this is extremely unlikely. Therefore, similar to crystal nucleation during solidification, heterogeneous nucleation of pores is much more likely. Nucleation substrates such as oxide films and other inclusions introduce an interfacial energy factor which substantially reduces the pressure barrier for pore formation.

The other term on the left side of Equation 2-7, P_S, refers to the pressure created by the solidification shrinkage. If the feeding mechanisms discussed in Section 2.4.1 are not able to compensate for this shrinkage, pores may form to relieve the associated pressure. This is known as shrinkage porosity. Shrinkage porosity may form on a large scale, as a sizeable defect in a hot spot, or on a smaller scale such as between dendrites in the dendritic networks. Small-scale shrinkage porosity is termed shrinkage microporosity.

The terms on the right hand side of Equation 2-7 work against the formation of porosity during solidification. Of all these terms, it is the pressure associated with surface tension between the liquid and the pore, P_{ST}, which creates the most resistance. Once again, if a nucleating substrate is present in the melt, this pressure term is reduced by a degree dependant on the wetting angle between the molten liquid and the substrate. This wetting angle depends on the geometry of the substrate and the degree of wetting between the liquid and the substrate. It is for this reason that casting melts should be as clean and free from inclusions as possible, to make the formation of porosity more difficult.

It is unlikely that the formation of porosity is solely due to the presence of dissolved gas or shrinkage pressure. Porosity formation is more likely to be due to contributions from both factors. When a pore is nucleated, the presence of dissolved gas aids the growth of the pore by being diffused into the newly created space. The pressure invoked by this diffusion will push against the melt with a pressure $P_{g,}$ while the solidification shrinkage will impart a negative pressure on the pore, P_s, which is effectively pulling at the pore. The combination of these pressures is shown by Equation 2-9 [69]:

$$P_T = P_g + P_s$$

Equation 2-9

The total pressure, P_T, promotes the formation and growth of porosity by helping overcome the critical pressure required to separate the body of liquid.

2.4.3 Surface Slumping

Inward slumping of the casting surface is a common casting defect that affects metal castings. Slumping occurs as a direct result of the solid feeding process discussed in Section 2.4.1. When a hot spot in a casting is isolated from the feed metal which compensates for volumetric shrinkage upon solidification, a great deal of internal pressure is imparted on the surrounding solid. If these stresses are sufficient to overcome the yield strength of the alloy, which is not very high at

elevated temperatures, the surrounding solid phase will be drawn inwards to compensate for the shrinkage. This is schematically illustrated in Figure 2-9.

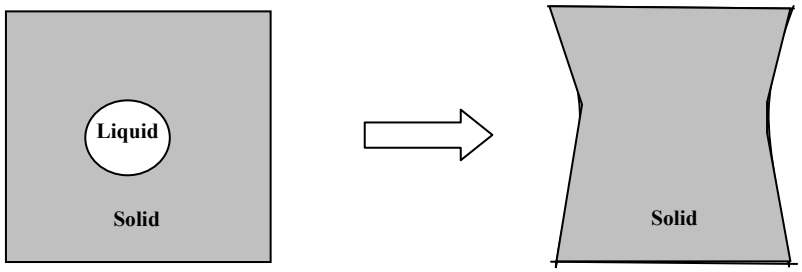

Figure 2-9: Schematic illustration of how a hot spot in a casting can result in the slumping inward of the casting surface. The isolated pool of solidifying liquid imparts pressure on the surrounding solid through solidification shrinkage. If this pressure is higher than the yield strength of the casting, surface slumping will result.

2.4.4 Hot Tearing

Hot tearing is one of the most serious defects from which a casting may suffer [73]. The defect takes the form of a ragged tear through the casting, often following a path through the interdendritic network or along grain boundaries. The defect results from the uniaxial tensile failure of the casting due to stresses imparted on the casting during solidification. Above the solidus temperature, the presence of intergranular liquid films facilitates the formation of hot tears by weakening the material [74].

As a casting is often fully restrained inside a sand or permanent mould, the shrinkage forces may build to a point where the casting is literally torn apart. Hot tears are usually situated around a hot spot created by a junction between two thin casting sections. The shrinkage of the hot spot may create tension around this junction causing a crack to form in the later stages of solidification. Hot tearing of castings tends to be more prominent in alloys with longer freezing ranges [75]. Magnesium alloy AZ91 is highly susceptible to tearing, with a freezing range of 125°C [76].

A common method of determining the hot tearing susceptibility of an alloy is to use a restrained rod test mould. As shown in Figure 2-10, this mould contains a

series of rods of increasing lengths, to create a range of stresses in the casting to determine the ease of hot tear formation. Cracking in the shorter rods indicates a highly susceptible alloy, while little or no cracking in any of the longer rods means the alloy is relatively immune to hot tearing. Of course mould design plays a large part in the occurrence of hot tearing, with sharp corners and abrupt changes in section thickness increasing the likelihood of hot tearing.

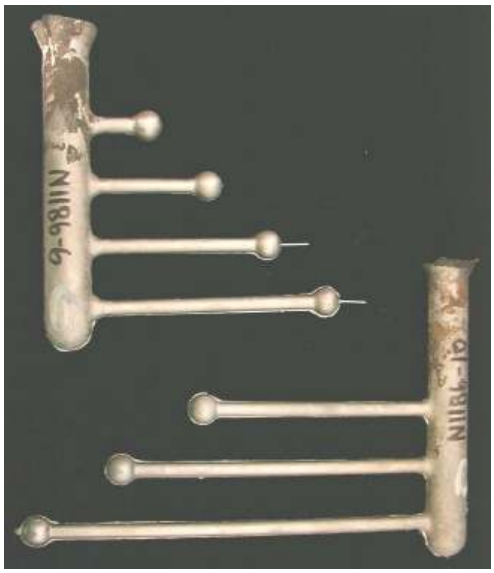

Figure 2-10: An example of two restrained rod hot tearing test castings. The bulb at the ends of the casting creates tension through the rod during solidification [77].

2.4.5 The Link between Hot Tearing and Shrinkage Related Defects

While the above sections on porosity, surface slumping, and hot tearing formation during solidification of a casting have been addressed separately, it is highly likely that the formation of one defect will affect the formation of another for a given set of casting conditions. Shrinkage related defects such as shrinkage porosity and surface slumping arise from hydrostatic (and therefore triaxial) stress imparted on the residual liquid during solidification [73]. Hot tearing on the other hand is the result of a uniaxial tensile failure of the casting structure. Both types of defects however, require high levels of stress to initiate and grow. It is therefore reasonable to suggest that the formation of one type of defect would alter the stresses acting on the casting and potentially reduce the chances of formation of another.

An investigation into the castability of aluminium alloys by Easton and StJohn [78] produced results that support this theory. They discovered that the susceptibility of an alloy to form hot tearing defects was increased as shrinkage related defects were reduced (and vice versa) for a given grain size. This is schematically illustrated in Figure 2-11.

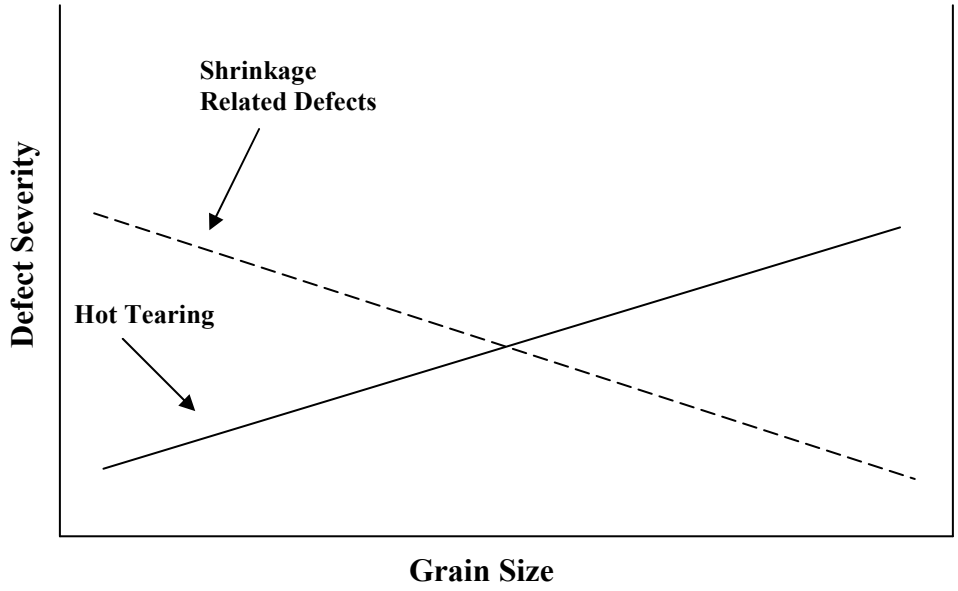

Figure 2-11: Schematic illustration of the relationship between the severity of shrinkage related defects and hot tearing with respect to grain size as shown by Easton and StJohn [78].

The formation of one type of defect over another will depend on such factors as grain size, mould geometry and the availability of feed liquid during solidification, which is in turn affected by the alloy composition and the thermal field of the casting. In a casting that is prone to hot tearing due to a hot spot giving rise to a large concentration of strain in that area, the formation of an internal pore would relieve some of the stress in that region. Conversely, there may be an isolated pool of liquid metal that results in large hydrostatic tension inside the casting. If a hot tear was to form at this region some of the stress would be alleviated and alternate feed paths may open up to allow feeding of liquid metal and a subsidence of the hydrostatic stress. This relationship is illustrated schematically in Figure 2-12 where the total stress in the casting (whether uniaxial or triaxial) is increased as solidification progresses. Once the total stress reaches a

level sufficient to initiate the formation of a defect, the stress is relieved making the formation of another type of defect less likely. Although in this simplistic case only one type of defect (defect 1) may form at the expense of another, it shows that if the casting was one in which the formation of shrinkage porosity required less stress than that required to form hot tearing (defect 2), then the formation of a shrinkage pore would relieve some of the stress acting on the casting and reduce the likelihood of a hot tear forming. Likewise for a casting that was more prone to hot tearing formation (now hot tearing becomes defect 1) then the initiation and growth of a tear would reduce the total stress acting on the casting and would reduce the likelihood of pore formation.

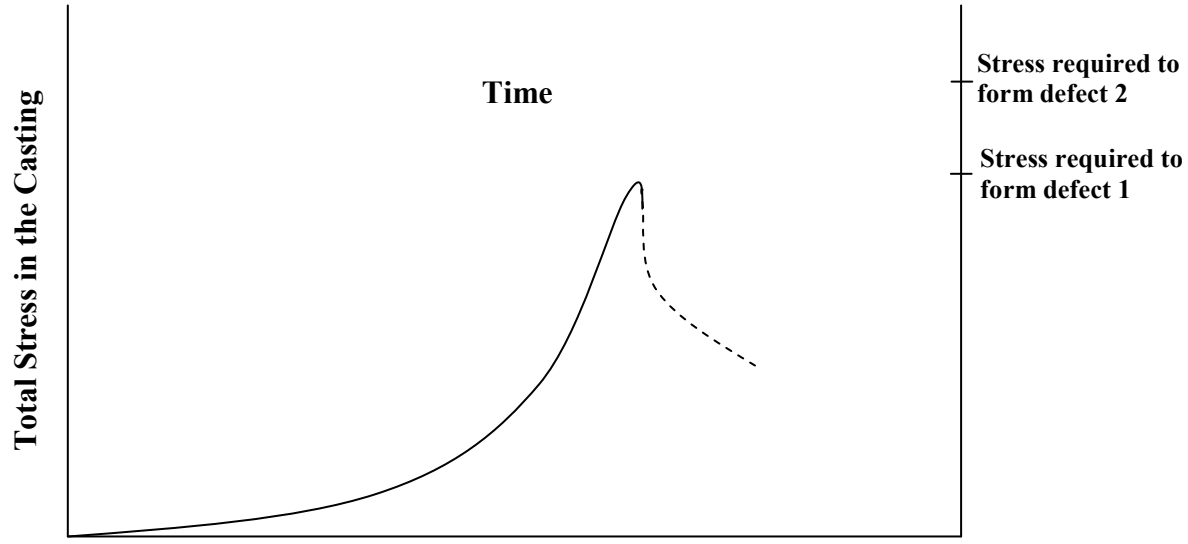

Figure 2-12: Schematic illustration of the critical stress required to form a casting defect for a given set of casting conditions.

2.5 The Castability of an Alloy

2.5.1 What is Castability?

While there is nothing to stop a manufacturer from producing cast components of any metal or alloy available, some alloys are more suited to the casting process than others. These alloys are said to have good *castability.* Castability has been defined as "the ability of an alloy to form a dimensionally accurate casting of acceptable soundness and integrity" [79]. There are many methods for assessing

the castability of an alloy, but the most common assessments include some or all of the following [75, 80-83]:

- Metal Fluidity
- Feedability
- Casting Grain Size
- Casting Porosity Level
- Hot Tearing Resistance
- Surface Abnormalities

Metal fluidity is a definition of how well an alloy will flow inside a casting mould, while it continues to lose heat and begins to solidify. The term should not to be confused with its use in physics, where fluidity is the inverse of viscosity [84]. Metals that have a high fluidity will be able to fill intricate moulds and thin casting sections without freezing off or becoming too thick to flow efficiently and fill the casting cavity. Magnesium alloys have extremely good fluidity rating and are considered one of the best casting alloys in this regard.

Feedability relates to how well an alloy can compensate for the solidification shrinkage by supplying liquid through different kinds of channels. Liquid metal is required to feed these areas during solidification or a defective casting may result. Castings that are not fed efficiently may have high porosity and hot tearing levels as well as surface abnormalities such as surface slumping.

2.5.2 Recent Studies on Magnesium Alloy Castability

There has been much research undertaken to understand the behaviour of certain alloys employed to produce components using the casting process. A wide range of literature is available on the castability of aluminium foundry alloys, and this remains the focus for many researchers [85-89]. With increased demand for the use of magnesium alloys, especially in the automotive industry, the investigation into the casting behaviour of magnesium alloys is receiving growing attention.

A few researchers in the early 1990's focussed on determining the origin and behaviour of microporosity formation in the magnesium casting alloy AZ91 [40, 72]. Shearhouse and Mikucki [72] focussed on the effect of dissolved hydrogen on the formation of microporosity in AZ91. They argued that although hydrogen has negligible effect on porosity in elemental magnesium castings due to its high solid solubility, the dissolved gas does play a role in the formation of porosity in AZ91 alloy castings. This is said to be due to the intermetallic eutectic compound $Mg_{17}Al_{12}$ having negligible hydrogen solubility in the solid state, so when eutectic solidification commences late in the overall solidification process, the excess hydrogen is evolved in the form of gas bubble pores.

While this research highlights the potential for hydrogen porosity formation, it is interesting to note that the metal used to produce the experimental castings was not filtered at any stage. As discussed in Section 2.4.2, the presence of nucleating substrates, such as oxide films, makes the formation of porosity much more favourable. Therefore the cleaner the casting melt, the more difficult it is for porosity to form. While this does not overshadow the results of this research, it would be interesting to note whether the porosity levels would be as high in castings that had been filtered.

In their study on microporosity formation in AZ91 sand castings, Aliravci et al [40] found that the addition of strontium concentrated the shrinkage microporosity to the thickest parts of the casting. They mention that the grain refining effect of strontium improved the mass feeding during solidification and hence, aided in the production of denser castings. While definite grain size reduction was achieved in this study, it is important to note that the authors had degassed the melt using C_2Cl_6 tablets which are known to be effective grain refiners in their own right. While the Sr addition may have had an additional effect, some clouding of the results is inevitable.

The exact effect of C_2Cl_6 tablets on the casting microstructure of AZ91E permanent mould castings was researched by Thompson et al [90]. They wanted to determine whether the increase in mechanical properties was due more to the grain refinement achieved, or by a reduction in porosity due to the degassing

effect of the tablets. They found that the optimal addition rate of 0.3 wt% produced the smallest grain size and further addition had little effect. The hydrogen level was found to be lowest at an addition rate of 0.06% and increasing the amount of C_2Cl_6 did not lower the dissolved gas level any further. From the results they concluded that the increase in mechanical properties comes from the grain size reduction, and hydrogen level does not have much effect on properties.

In their comprehensive study of the development of the as-cast microstructure in magnesium-aluminium alloys [7], Dahle et al discussed the formation of porosity in their permanent mould castings. They described the porosity formation as arising not from either dissolved hydrogen or inefficient shrinkage feeding, but a combination of both. They do concur that the role of the eutectic component of the solidified alloy is an area that requires more research to determine its effect on porosity formation.

Schaffer [91] discovered that porosity levels in magnesium-aluminium alloy castings increased with increasing aluminium content. This pattern continues up to a peak level at 11 wt% Al, whereupon porosity level decreases until the eutectic composition is reached. This peak in porosity arises from the worst feeding conditions of the wide mushy zone and low permeability of the interdendritic network. The author also concluded that pore size increases as aluminium content is increased.

Another factor that affects an alloy's castability is hot tearing susceptibility. Many studies have been conducted using magnesium alloys to investigate the characteristics of this defect [41, 92-94]. Argo et al [93] found that Mg-Al-Sr alloys were prone to hot tearing when they investigated the use of this alloy for the casting of an engine valve cover. They found the tears were mostly located around flanges and other raised areas. This is most likely due to the increase in section thickness creating hot spots in these regions. The contraction created during solidification in these areas would have created tensile forces to build to a point where the weaker, semisolid areas surrounding the hotspots were torn apart. Further indication of the sensitivity of this defect is given by Koike et al [94], who found that hot tearing was influenced by alloy content. They found major hot

tearing with 2-3% Al, but a reduction of tearing with increased aluminium content.

The methods and mechanisms of grain refinement of magnesium alloys have been discussed previously in this chapter, but one area where the literature seems to be lacking is what effect the addition of grain refiners has on the castability of an alloy. One comprehensive study was carried out by Easton and StJohn [78] where the effect of grain refinement on the formation of casting defects in aluminium alloys A356 was investigated. This type of study is of prime importance to casting manufacturers, as promotional material from grain refinement suppliers often states the importance of grain refinement in increasing mechanical properties, but rarely focuses on the effect of these additions to defect levels. The study was separated into two parts, a casting trial conducted in an industrial setting and a laboratory controlled investigation.

The industrial trial found that the level of porosity found in the spoke-rim junction of an alloy wheel casting was increased by the addition of grain refiners. It appeared that a larger grain size was required for the reduction of defective castings. A segregated channel of eutectic was observed in the centre of the spoke when low levels of grain refiner were used, which would have assisted the feeding of the hot spot in the spoke rim junction. The main reason for the rejection of the grain refined castings was the presence of large amounts of interconnected porosity. This was said to be formed by the "sucking" of eutectic liquid into the hot spot during solidification, leaving behind a network of connected porosity.

To fully understand this phenomenon a relatively crude experimental mould was produced to simulate the filling and solidification in this area of the casting. Laboratory experiments using the mould found that again, porosity level increased with decreasing grain size. The grain refinement did however reduce the severity of hot tearing in the experimental castings.

The experimental mould did have some limitations however. The castings produced consisted of a cylindrical elbow running into a rectangular plate to create the junction that they wished to emulate. There was no attempt made to

control the flow of the metal stream as it entered the mould, and the casting melt was not filtered in any way. The authors even admit that the experimental methods were crude and uncontrolled, but say this was deliberate to simulate industrial conditions. As the quality of metal used and presence of oxide films is a contributing factor to the initiation of porosity [69], it is again difficult to completely rely on the porosity data obtained. A mould that possessed an adequate running system and allowance for the placement of a filtration system would have greatly aided this otherwise excellent study.

Details available in the literature on the effect of grain refinement on the castability of Mg-Al alloys are scarce. In recent years, a few studies have tried to establish the effect of melt additions on Mg-Al castability to varying degrees of success [39, 77]. These studies utilise a range of test moulds to analyse melt fluidity, hot tearing susceptibility, porosity levels and as-cast grain size. There is however, some disagreement in the results published.

Thomson et al [77] say that the addition of C_2Cl_6 grain refiner had no significant effect on the grain size of permanent mould cast AZ91E, whereas Wallace et al [39] stated they obtained significant grain refinement from a range of melt additions, including C_2Cl_6. The latter appears to be the more reliable source, as Thompson states that there was difficulty in revealing the grain boundaries for microscopic examination, which would have made accurate grain size measurements impossible.

Both of these studies investigated the presence of porosity, however no attempt was made to accurately measure porosity level in the casting samples. Instead microscopic images were given to show the presence or lack of porosity in the castings.

Again both studies investigated the hot tearing susceptibility of the alloys, this time using the restrained rod test mould (see Figure 2-10). Unfortunately there was also disagreement in the results. Thomson was unable to detect a trend in the hot tearing results and concluded that it is difficult to determine the hot tearing tendency of alloy AZ91E using this type of mould. Wallace did conclude that the

addition of grain refiners provided resistance to hot tearing. Looking at the results presented however, it is difficult to gain any real insight into the effects of grain refinement on hot tearing susceptibility. In the unrefined samples, two of the four rods in the mould exhibited cracking, whereas the rest of the grain refined samples still had one of the four test bars showing signs of hot tearing. Only one out of the total of nine samples was completely free from cracking, this sample was refined with C_2Cl_6.

While the previous studies on the effect of grain refinement on the castability of magnesium-aluminium alloys do present useful results, a comprehensive investigation to determine the sensitivity of casting defects to grain refinement is still lacking from the literature.

2.6 Questions Arising from the Literature Review

It is clear from the literature review that many areas of knowledge concerned with the grain refinement of magnesium alloys and its effect on castability have yet to be clarified. With increased demand for the use of magnesium alloys in the automotive industry, there is a definite need for more focussed research in the area of defect formation during magnesium alloy casting.

Effective methods for the grain refinement of magnesium-aluminium alloys have been discovered, although the mechanisms of many of these methods have yet to be fully clarified. This however, is not as pertinent as the effect that successful grain refinement has on the formation of defects during the production of magnesium castings. The automotive industry is already increasing the use of magnesium alloys, with magnesium-aluminium alloys AZ91 and AM60 being two of the most commonly utilised. At the present time there is little understanding of whether the beneficial effects of grain refinement are to some extent negated by reduced castability of the alloy being treated. A systematic study is required to clarify this issue, and the work presented in the following chapters attempts to answer the following questions arising from the literature:

- Can an experimental mould be developed that effectively emulates the filling and solidification of a notoriously difficult automotive casting?

- How does grain refinement effectiveness vary with addition rate in Mg-Al alloys?

- Is there a better method of consistently and effectively introducing carbon to a Mg-Al casting melt?

- What effect does grain refinement have on the internal porosity levels of the castings produced?

- What is the sensitivity of the hot tearing defect to grain refinement?

- How do surface abnormalities such as slumping vary with the degree of grain refinement achieved?

- What effect does the refinement of the casting macrostructure have on porosity morphology and distribution?

The overall aim of the research presented in this thesis is to increase the understanding of the effect of grain refinement on the castability of magnesium-aluminium alloy castings.

2.7 References

[1] Askeland, D. R., *The Science and Engineering of Materials.* London Chapman and Hall 830-831 (1996).

[2] Luo, A., *Magnesium: Current and Potential Applications.* JOM 42-48 (2001).

[3] Froes, F. H. and Aighion, E., *The Science, Technology, and Applications of Magnesium.* JOM 30-34 (1998).

[4] ASM, *Gravity and Low Pressure Casting.* Magnesium and Magnesium Alloys M. M. Avedesian and H. Baker ASM International 55-65 (1999).

[5] Giley, E., *Magnesium Alloys: Property, Corrosion, and Automotive Uses.* Ford Research Laboratory Report (2000).

[6] Nave, M. D., Dahle, A. K. and StJohn, D. H., *Eutectic Growth Morphologies in Magnesium-Aluminium Alloys.* Magnesium Technology 2000 H. I. Kaplan, et al. TMS 233-242 (2000).

[7] Dahle, A. K., Lee, Y. C., Nave, M. D., Schaffer, P. L. and StJohn, D. H., *Development of the As-Cast Microstructure in Magnesium-Aluminium Alloys.* Journal of Light Metals **1** 61-72 (2001).

[8] Easton, M. and StJohn, D. H., *Grain Refinement of Aluminium Alloys: Part II. Confirmation of, and a Mechanism for, the Solute Paradigm.* Metallurgical and Materials Transactions A **30A** 1625-1633 (1999).

[9] Easton, M. and StJohn, D. H., *Grain Refinement of Aluminium Alloys: Part I. The Nucleant and Solute Paradigms-A Review of the Literature.* Metallurgical and Materials Transactions A **30A** 1613-1623 (1999).

[10] Nelson, C. E., *Grain Size Behaviour in Magnesium Casting Alloys.* AFS 52nd Annual Meeting Chicago, IL. American Foundryman's Society 1-23 (1948).

[11] Nishino, N., Kawahara, H., Shimizu, Y. and Iwahori, H., *Grain Refinement of Magnesium Casting Alloys by Boron Addition.* Magnesium Alloys and their Applications K. U. Kainer Wiley-VCH 59-64 (2000).

[12] Renger, K. and Simon, R., *Grain Refinement of AZ91 by Nucleant 5000.* 1st Int. Light Metals Technology Conf. 2003 A. K. Dahle Brisbane (2003).

[13] Qian, M., StJohn, D. H. and Frost, M. T., *Zirconium Alloying and Grain Refinement of Mg Alloys.* Magnesium Technology 2003 H. I. Kaplan TMS (2003).

[14] Qian, M., Zheng, L., Graham, D. A., Frost, M. T. and StJohn, D. H., *Settling of Undissolved Zirconium Particles in Pure Magnesium Melts.* Journal of Light Metals **1** 157-165 (2001).

[15] Hildebrand, Z. C. G., Qian, M., StJohn, D. H. and Frost, M. T., *Dissolution of Zirconium as AM-cast in Magnesium.* Light Metals Technology 2003 A. K. Dahle (2003).

[16] Glasson, F. L. and Emley, E. F., *Heterogeneous Nucleation in the Solidification of Aluminium and Magnesium Alloys.* The Solidification of Metals London 1-9 (1967).

[17] Cao, P., Qian, M., StJohn, D. H. and Frost, M. T., *Influence of the Uptake of Iron on the Grain Refinement of Pure Magnesium by Zirconium.* Light Metals Technology 2003 A. K. Dahle (2003).

[18] Lee, Y. C., Dahle, A. K. and StJohn, D. H., *Grain Refinement of Magnesium.* Magnesium Technology 2000 H. I. Kaplan, et al. TMS 211-218 (2000).

[19] Schaffer, P. L., Lee, Y. C. and Dahle, A. K., *The Effects of Aluminium Content and Grain Refinement on Porosity Formation in Mg-Al Alloys.* Magnesium Technology 2001 J. Hyrn TMS 87-94 (2001).

[20] Bamberger, M., *Structural Refinement of Cast Magnesium Alloys.* Materials Science and Technology **17** (2001).

[21] Wood, R. T., *The Foundryman.* 98 (1953).

[22] Tiner, N., Trans AIME **161** 351 (1945).

[23] Hall, H. T., *Magnesium Review and Abstracts.* **3** 68-72 (1945).

[24] Lee, Y. C., Dahle, A. K. and StJohn, D. H., *The Role of the Solute in Grain Refinement of Magnesium.* Metallurgical and Materials Transactions A **31A** 2895-2906 (2000).

[25] Motegi, T., Yano, E., Tamura, Y. and Sato, E., *Clarification of Grain Refining Mechanisms of Superheat Treated Mg-Al-Zn Alloy Castings.* Materials Science Forum **350** 191-198 (2000).

[26] Cao, P., Qian, M. and StJohn, D. H., *Effect of Iron on Grain Refinement of High-Purity Mg-Al Alloys.* Scripta Materialia **51** 125-129 (2004).

[27] Farbenindustrie, I., *Procedure for Grain Refining Magnesium and its Alloys.* Belgian Patents (1942).

[28] Emley, E. F., *Principles of Magnesium Technology.* NY Pergamon (1966).

[29] Davis, J. A., Eastwood, L. W. and DeHaven, J. C., *Grain Refinement in Magnesium Casting Alloys.* AFS Transactions **53** 352-362 (1945).

[30] Holm, V. C. F. and Krynitsky, A. I., *Control of Grain Size in Magnesium Casting Alloys.* The Foundry **75** 228-240 (1947).

[31] Kurfman, V. B., *Hydrogen Escape from Magnesium Alloys.* Modern Castings **45** 9-12 (1964).

[32] Liu, Y., Liu, X. and Xiufang, B., *Grain Refinement of Mg-Al Alloys with Al4C3-SiC/Al Master Alloy.* Materials Letters **58** 1282-1287 (2004).

[33] Zhang, M. X., Kelly, P. M., Qian, M. and Taylor, J., *Crystallography of Grain Refinement in Mg-Al Based Alloys.* Acta Mater **53** 3261-3270 (2005).

[34] Jin, Q., Eom, J. P., Lim, S. G., Park, W. W. and You, B. S., *Grain Refining Mechanism of a Carbon Addition Method in a Mg-Al Magnesium Alloy.* Scripta Materialia **49** 1129-1132 (2003).

[35] Qian, M. and Cao, P., *Discussions on Grain Refinement of Magnesium Alloys by Carbon Inoculation.* Scripta Materialia **52** 415 - 419 (2005).

[36] Yuan, G. Y., Liu, Z. L., Wang, Q. and Ding, W., *Microstructure Refinement of Mg-Al-Zn-Si Alloys.* Materials Letters **56** 53-58 (2002).

[37] Hu, H., Shang, R. and Li, N., *Effect of Ca Addition on Grain Microstructure Development of Mg Alloy AM60.* AFS 2003 (2003).

[38] Lee, S. L., Lee, H. L. and Kim, D. H., *Effect of Y, Sr, and Nd Additions on the Microstructure and Microfracture Mechanism of Squeeze Cast AZ91-X Magnesium Alloys.* Metallurgical and Materials Transactions A **29A** (1998).

[39] Wallace, J. F., Schwam, D. and Zhu, Y., *The Influence of Potential Grain Refiners on Magnesium Foundry Alloys.* AFS 2003 1-15 (2003).

[40] Aliravci, C. A., Gruzleski, J. E. and Dimayuga, F. C., *Effect of Strontium on the Shrinkage Microporosity in Magnesium Sand Castings.* AFS Transactions 1992 AFS **100** 353-362 (1992).

[41] Powell, B. R., Luo, A., Tiwari, B. L. and Rezhets, V., *The Diecastability of Calcium Containing Magnesium Alloys: Thin Wall Computer Case.* Magnesium Technology 2002 H. I. Kaplan (2002).

[42] King, J. F., *Development of Magnesium Die Casting Alloys.* Magnesium Alloys and their Applications B. L. Mordike and K. U. Kainer Frankfurt Werkstoff-Informationgesellschaft mbH 37-47 (1998).

[43] Wang, Q. D., Chen, W. Z., Ding, W., Zhu, Y. P. and Xu, X. P., *Effects of Ca Addition on the Microstructure and Mechanical Properties of AZ91 Magnesium Alloy.* Journal of Materials Science **36** 3035-3040 (2001).

[44] Gruzleski, J. E. and Aliravci, C. A., *Low Porosity Fine Grained Strontium Treated Magnesium Alloy Castings.* United States Patent Office (1992).

[45] Nussbaum, G., Bridot, P., Warner, T. J., Charbonnier, J. and Regazzoni, G., *New Mg-Al Based Alloys with Improved Casting and Corrosion Properties.* Magnesium Alloys and their Applications B. L. Mordike and F. Hehmann DGM Informationsgesellschaft mbH 351-358 (1992).

[46] Luo, A., *Heterogeneous Nucleation and Grain Refinement in Cast Mg(AX91)/SiC Metal Matrix Composites.* Canadian Metallurgical Quarterly **35** 375-383 (1996).

[47] Venkateswarlu, K., Murty, B. S. and Chakraborty, M., *Effect of Hot Rolling and Heat Treatment of Al-5Ti-1B Master Alloy on the Grain Refining Efficiency of Aluminium.* Materials Science and Engineering **A301** 180-186 (2001).

[48] Schneider, W. A., Quested, T. E., Greer, A. L. and Cooper, P. S., *A Comparison of the Family of AlTiB Refiners and Their Ability to Achieve a Fully Equiaxed Grain Structure in DC Casting.* Light Metals 2003 P. Crepeau (2003).

[49] Schaffer, P. L., Dahle, A. K. and Zindel, J. W., *Grain Refiner Fade in Aluminium Alloys.* Light Metals 2004 A. T. Tabereaux TMS 821-826 (2004).

[50] Sato, K. and Flemings, M. C., *Grain Refining of Al-4.5Cu Alloy by Adding an Al-30TiC Master Alloy.* Metallurgical and Materials Transactions A **29A** 1707-1710 (1998).

[51] Kori, S. A., Murty, B. S. and Chakraborty, M., *Development of an Efficient Grain Refiner for Al-7Si Alloy and its Modification with Strontium.* Materials Science and Engineering **A283** 94-104 (2000).

[52] Hultgren, R. and Mitchell, D. W., *Grain Refinement of Magnesium Alloys without Superheating.* Trans AIME **161** 323-327 (1945).

[53] Campbell, J., *Effects of Vibration During Solidification.* International Metals Review **26** 71-108 (1981).

[54] Maltais, A., Fiset, M. and Dube, D., *Grain Refinement of Magnesium Alloys AZ91D Cast in Permanent Mould Using Mechanical Vibration.* Materials Science Forum 527-532 (2003).

[55] Flemings, M. C., *Solidification Processing.* NY McGraw-Hill (1974).

[56] Wallace, J. F., *Grain Refinement of Steels.* Journal of Metals **15** 372-376 (1963).

[57] Campbell, J., *Grain Refinement of Solidifying Metals by Vibration: A Review.* Solidification Technology in the Foundry and Cast House London Metals Society (1983).

[58] Han, Q., Kenik, E. A., Agnew, S. R. and Viswanathan, S., *Solidification Behaviour of Commercial Magnesium Alloys.* Magnesium Technology 2001 J. R. Hyrn TMS (2001).

[59] Shepeleva, L., Manov, E. and Bamberger, M., *TEM Study of the As-Cast and Aged Microstructures of Mg-Al-Zn Alloys and the Influence of Zn Content on Precipitation.* Magnesium Technology J. Hyrn TMS 189-194 (2001).

[60] Bakke, P., Fuerst, C. D. and Westegen, H., *Solidification Induced Inhomogeneities in Magnesium-Aluminium Alloy AZ91 Ingots.* Magnesium Technology 2000 H. I. Kaplan, et al. TMS 201-210 (2000).

[61] ASM, *Microstructure of Magnesium Alloys.* Metals Handbook, Atlas of Microstructures for Industrial Alloys ASM **7** (1972).

[62] Cabibbo, M., Cerri, E. and Evangelista, E., *Microstructural Study After Solution Treatments of a Thixocast AZ91.* Magnesium Technology J. Hyrn TMS 211-216 (2001).

[63] Matsumoto, K., Shibayanagi, T. and Umakoshi, Y., *On the Role of Grain Boundary Character Distribution in Grain Growth of Al-Mg Alloys.* Acta Mater **45** 439-451 (1997).

[64] Henry, S., Rappaz, M. and Jarry, P., *<110> Dendrite Growth in Aluminium Feathery Grains.* Metallurgical and Materials Transactions A **29A** 2807-2817 (1998).

[65] George, P. F., *Some Special Metallographic Techniques for Magnesium Alloys.* Trans ASM **38** 686-708 (1947).

[66] ASM, *Metallography and Microstructures.* Metals Handbook M. Park **9** 425-434 (1989).

[67] Maltais, A., Dube, D., Fiset, M., Laroche, G. and Turgeon, S., *Improvements in the Metallography of as-cast AZ91 Alloy.* Materials Characterization **52** 103-119 (2004).

[68] Dash, M. and Makhlouf, M. M., *Effect of Key Alloying Elements on the Feeding Characteristics of Aluminium-Silicon Casting Alloys.* Journal of Light Metals **1** 251-265 (2001).

[69] Campbell, J., *Solidification Shrinkage.* Castings Oxford Butterworth-Heinemann Ltd 175-208 (1991).

[70] Gruzleski, J. E. and Closset, B. M., *The Treatment of Liquid Aluminium Silicon Alloys.* Des Plaines, Illinois AFS (1990).

[71] ASM, *The Influence and Control of Porosity and Inclusions in Aluminium Alloy Castings.* Aluminium Alloy Castings: Properties, Processes, and Applications ASM International 47-53 (1988).

[72] Shearouse III, J. D. and Mikucki, B. A., *The Origin of Microporosity in Magnesium Alloy AZ91.* SAE Technical Paper Series (1994).

[73] Campbell, J., *Linear Contraction of the Casting.* Castings Butterworth-Heinemann Ltd 209-240 (1991).

[74] Barnett, R. S., Taylor, J. A. and StJohn, D. H., *A Method for Reducing Hot tearing in 356 Alloy Air-Intake Manifolds.* Light Metals Technology 2003 A. K. Dahle (2003).

[75] Viano, D., StJohn, D. H., Caceres, C. H. and Grandfield, J., *Hot tearing of Aluminium-Copper Alloys.* 1st Int. Light Metals Technology Conf. 2003 A. K. Dahle Brisbane 247-250 (2003).

[76] www.matweb.com *Online Materials Database.*

[77] Thomson, J., Fasoyinu, F. A., Sadayappan, M. and Sahoo, M., *Casting Characteristics of Permanent Mold Cast Mg-Alloy AZ91E.* AFS Transactions (2002).

[78] Easton, M. and StJohn, D. H., *The Effect of Grain Refinement on the Formation of Casting Defects in Alloy 356 Castings.* Int. J. Cast Metals Res. **12** 393-408 (2000).

[79] Taylor, J., *Metal-Related Castability Effects in Aluminium Foundry Alloys.* Cast Metals **8** 225-252 (1996).

[80] Dinnis, C., Otte, M. O., Taylor, J. A. and Dahle, A. K., *Sr-Modification and Casting Design Effects on Porosity in Al-Si Alloys.* Light Metals Technology 2003 A. K. Dahle (2003).

[81] Taylor, J., Otte, M. O. and McDonald, S. D., *Aluminium Alloy Castability.* Materials Australia 16-18 (1999).

[82] Watanabe, I., Woldu, M., Watanabe, K. and Okabe, T., *Effect of Casting Method on Castability of Titanium and Dental Alloys.* Journal of Materials Science **11** 547-553 (2000).

[83] Zhang, J. and Singer, R. F., *Effect of Grain Boundary Characteristics on Castability of Nickel Based Super Alloys.* Metallurgical and Materials Transactions A **35A** 939 (2004).

[84] Campbell, J., *Fluid Dynamics.* Castings Butterworth-Heinemann Ltd Butterworth-Heinemann Ltd 74-84 (1991).

[85] Conley, J. G., Huang, J., Asada, J. and Akiba, K., *Modelling the Effects of Cooling Rate, Hydrogen Content, Grain Refiner and Modifier on Microporosity Formation in Al A356 Alloys.* Materials Science and Engineering **A285** 49-55 (2000).

[86] Taylor, J., StJohn, D. H. and Schaffer, G., *Aluminium Alloys and Processing Problems: Castability of Alloys used for High Integrity Castings.* 4th Australian Asian Pacific Course and Conference: Aluminium Cast House Technology: Theory and Practice M. Nilmani 237-247 (1995).

[87] Taylor, J., Schaffer, G. and StJohn, D. H., *Shrinkage Porosity Formation in Iron Containing Al-Si-Cu-Mg Casting Alloys.* (1997).

[88] Sigworth, G. K. and De Hart, F., *Recent Developments in the High Strength Aluminium-Copper Alloy Casting Alloy 206.* AFS Transactions (2002).

[89] de Looze, G., Carrig, J., Alguine, V. and Nguyen, T., *The Effect of Process Parameters on Porosity in Low Pressure Die Casting.* Proc. of the 12th Int. Die Casting Conference of the Australian Die Casting Association Melbourne, Australia (2004).

[90] Thomson, J. P., Liu, P., Sadayappan, M. and Sahoo, M., *Effect of C_2Cl_6 on Mechanical Properties and Microstructure of Gravity Permanent Mold Cast AZ91E.* 108th American Foundryman's Society Metalcasting Congress Des Plaines, IL, USA AFS (2004).

[91] Schaffer, P. L., *The Effect of Aluminium Content and Grain Refinement on Porosity Formation in Mg-Al Alloys.* Mining Minerals and Materials Engineering Brisbane University of Queensland 70 (2000).

[92] Grandfield, J., Davidson, C. and Taylor, J., *Application of a new Hot Tearing Analysis to Horizontal Direct Chill Cast Magnesium Alloy AZ91.* Light Metals 2001 (2001).

[93] Argo, D., Pekguleryuz, M. O., Labelle, P., Dierks, M., Sparks, T. and Waltemate, T., *Diecastability and Properties of Mg-Al-Sr Based Alloys.* Magnesium Technology J. Hyrn TMS 131-136 (2001).

[94] Koike, S., Washzu, K., Tanaka, S., Baba, T. and Kikawa, K., *Development of Lightweight Oil Pans Made of a Heat-Resistant Magnesium Alloy for Hybrid Engines.* SAE Technical Paper Series **2000-01-1117** (2000).

3.0 Experimental Methodology

3.1 Source Materials

As the aim of this study is to investigate the castability of magnesium alloys for use in the production of automotive components, two of the most common casting alloys were chosen as a baseline for the study. Dead Sea Magnesium of Israel supplied commercial purity magnesium alloys AZ91E and AM60B for use in the experimental phase of this research. Inductively Coupled Plasma Atomic Emission Spectroscopy (ICP-AES) was performed to determine the chemical composition of the alloys, which are listed in Table 3-1.

Table 3-1: Chemical composition of the magnesium alloys used in the experimental phase of this research. All figures are expressed in weight percent.

	Mg	Al	Zn	Mn	Sr	Pb	Be	Fe	Cu	Zr
AM60B	Bal	5.82	<0.005	0.29	<0.001	<0.002	0.001	<0.002	<0.002	<0.002
AZ91E	Bal	8.69	0.63	0.22	<0.001	<0.002	0.001	<0.002	<0.002	<0.002

3.2 Alloy Preparation and Melting

3.2.1 Preparation of Melting Equipment

The melting of magnesium can be extremely dangerous due to the highly exothermic and potentially explosive reactions that can occur when molten magnesium is exposed to moisture and impurities such as oil or rust. To eliminate the potential for these reactions, the alloy was ground using coarse silicon carbide paper to remove the surface layer of oxidation and preheated to 200°C in an electrical resistance furnace to ensure the alloy was completely free from moisture prior to melting.

The mild steel crucible used for melting the alloy was bead blasted thoroughly prior to each melt procedure to remove any surface oxidation and debris left from previous experiments. This ensured that melting process was performed in consistent conditions for each casting experiment. The melt crucible and all related equipment were preheated to 200°C to remove residual moisture and subsequently coated with boron nitride, a non-wetting agent, to prevent the molten magnesium from coming into contact with the melting equipment.

3.2.2 Melt Procedure

The preheated alloy and crucible were placed inside the water-cooled coils of an Inductotherm induction furnace and heated to 700°C at which point the melt was drossed to remove the surface layer of oxide that was present. The melt was then raised to the required temperature for the addition of grain refiners as explained in Section 3.3. Once the grain refiner additions had been made, the melt was again drossed and lowered to the desired pouring temperature of 100°C above the liquidus temperature of the alloy (i.e. 715°C for AM60B and 695°C for AZ91E).

3.2.3 Oxidation Prevention

To prevent the oxidation and subsequent burning of magnesium at elevated temperatures some form of oxidation prevention is always required. During the course of these experiments a cover gas containing 50% carbon dioxide (CO_2), 49% dry air, and 1% sulphur hexafluoride (SF_6) was used to prevent reaction between the magnesium alloy and the surrounding air. The cover gas was introduced to the crucible through a specially designed lid that contained holes for gas intake, exhaust, and for the positioning of a K-type thermocouple for temperature measurement.

Figure 3-1 shows the melting station used throughout the magnesium casting experiments.

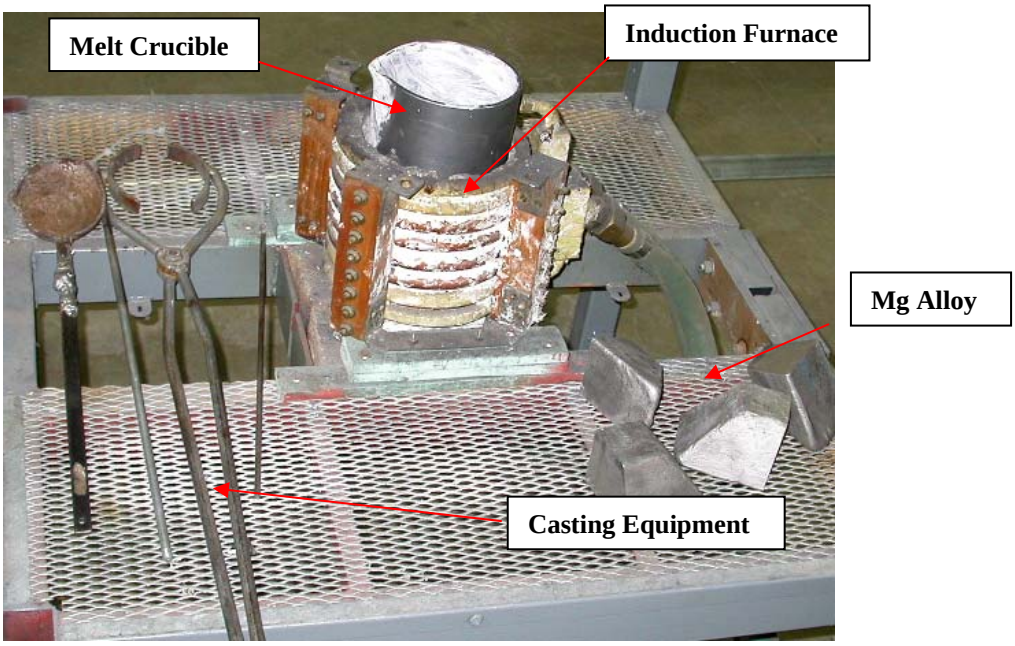

Figure 3-1: The melting station used for the magnesium casting experiments.

3.3 Melt Additions

3.3.1 Strontium Additions

A strontium-containing aluminium master alloy was used to investigate the effect of strontium as a grain refiner on the castability of the two magnesium-aluminium alloys AZ91E and AM60B. The master alloy used was an Al-10Sr alloy containing 90 wt% of aluminium and 10 wt% of strontium supplied by Cometals Pty of Sydney, Australia. Two separate levels of strontium addition, 0.05 wt% Sr and 0.10 wt% Sr were added to the alloy prior to casting. The master alloy was cut to the appropriate size and preheated to 200°C to remove any residual moisture before it was added to the melt at 725°C. The master alloy was held under the melt surface for a short period to facilitate melting and then manually stirred for a period of 60 seconds to ensure dissolution of the strontium.

3.3.2 Carbon Additions

Two different methods were employed to investigate the effects of carbon on the grain refinement of AZ91E and AM60B. The first method involved the addition of carbon black powder wrapped in aluminium foil preheated to 200°C and held under the melt surface for a short period. The melt was then manually stirred for a period of 60 seconds to disperse the carbon powder and promote dissolution in the magnesium alloy. As literature suggested the minimum temperature for effective grain refinement of aluminium containing magnesium alloys is 760°C [1], the carbon was introduced to the melt at this temperature. Higher melt temperatures were avoided to discount the grain refinement effect that can be achieved by superheating a magnesium melt to around 800°C and cooling to the pouring temperature, as detailed in Chapter 2. Using this method, carbon was added to the melts at two nominal addition levels of 0.05 wt% C and 0.10 wt% C respectively.

The second technique employed involved the mechanical milling of carbon black powder added to a 50:50 mix of magnesium and aluminium powder. For each milling run, 8g of the powder mixture was placed in a steel vial with eight hardened steel ball bearings under an argon atmosphere to prevent oxidation and burning of the powders during milling. The vial was inserted into a vibratory ball mill and milled continuously for periods of 8 and 24 hours. X-ray Diffraction (XRD) analysis was performed on the powder mixes subsequent to milling using a Phillips X'Pert powder diffractometer, using CuKα radiation and a 2θ range of 0 to 120˚.

The mechanically milled powder was then pressed in a 10mm x 5mm steel die at 50 MPa to form small tablets, with half of the tablets produced being sintered under argon at 430°C for 4 hours. For grain refinement addition, the tablets were preheated to 200°C before being submersed in the magnesium melt and held for a short time to facilitate melting of the Mg/Al matrix. The melt was subsequently stirred for 60 seconds to ensure dissolution. In this case, the nominal carbon addition level was controlled at 0.05 wt% C.

3.4 Casting

3.4.1 Design of the Casting Mould

An experimental mould was developed with a casting geometry closely related to that found in an alloy wheel casting. A great amount of effort was expended to ensure the mould reflected the filling and solidification patterns that would be experienced in an actual alloy wheel casting. Figure 3-2 shows the typical geometry of an alloy wheel casting and highlights the four main regions; the hub, the spoke, the spoke/rim junction and the rim. Due to the thick to thin transition between these areas, a casting of this nature is prone to porosity and hot tearing defects and it is these defects that were to be promoted for investigation during the study.

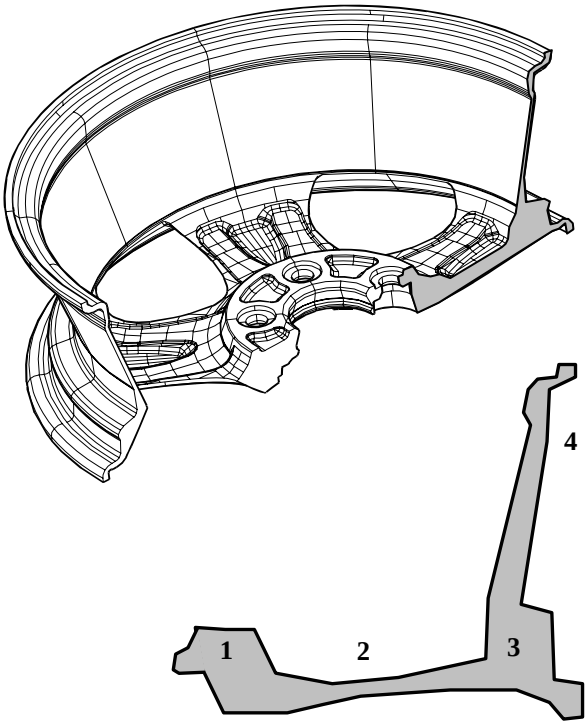

Figure 3-2: Schematic illustration of the cross-section geometry of a typical wheel casting. The four areas labelled are (1) the hub, (2) the spoke, (3) the spoke/rim junction, and (4) the rim.

As mentioned in Chapter 2, previous attempts to emulate the filling and solidification of an alloy wheel have all had limited control of filling speed, leading to turbulence and oxidation of the melt stream. Uncontrolled filling of a casting makes it difficult

to identify the root causes of hot tearing and porosity, as the presence of oxide inclusions is unable to be predicted accurately. In the design of the experimental mould used in this study, every effort was made to control the filling and eliminate inclusions so the mould filled in a smooth and controlled manner. The first means of achieving this was to have an appropriately designed tapered sprue and well to collect the metal stream and slow its progress before entering the casting cavity. It is suggested that one of the most important effects of a properly sized well is that of preventing the splash of the melt along the runner when the metal first impacts at the base of the sprue. Without a sprue well, this first splash would shoot unconstrained along the length of the runner. The recommended dimensions of a sprue well are illustrated in Figure 3-3 [2].

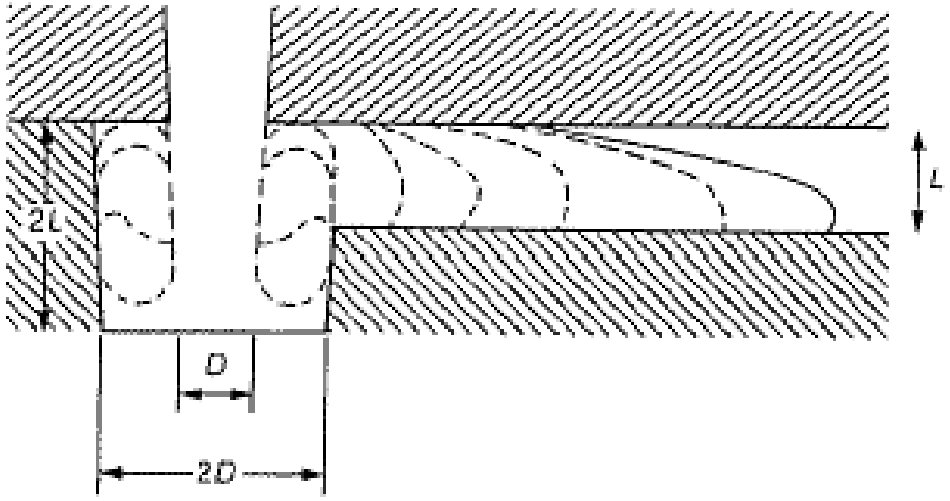

Figure 3-3: The dimensions of an effective sprue well [2].

Once the metal has travelled in an uncontrolled fashion down the sprue of the experimental mould, the sprue well collects the broken metal stream and allows it to flow smoothly into the runner. The experimental mould was also designed with a section to allow for the placement of a ceramic foam filter at the entrance to the casting cavity that would further control the flow of metal and remove any oxides and inclusions present in the melt stream.

The 3D solid modelling software Solidworks™ was used to design and model a casting part that would emulate the filling and solidification of an alloy wheel. The part was modelled with features purposely added to promote the formation of defects, such as sharp corners to promote hot tearing, and sudden transitions between thick and thin sections to promote porosity. By designing the mould in this fashion, it has allowed the sensitivity of these defects to melt chemistry and grain refinement to be investigated.

To enable the casting to be removed easily from the mould, draft angles needed to be introduced to taper the surfaces of the casting. The Mg Diecasting Handbook states that draft angles in the range of 2-5 degrees are generally recommended, however it is not uncommon to find draft angles in the range of 1-3 degrees, and even zero draft [3]. A draft angle of 3 degrees was chosen to facilitate the removal of the casting without changing the dimensions of the casting greatly through its cross section. Figure 3-4 shows the finished model of the experimental casting.

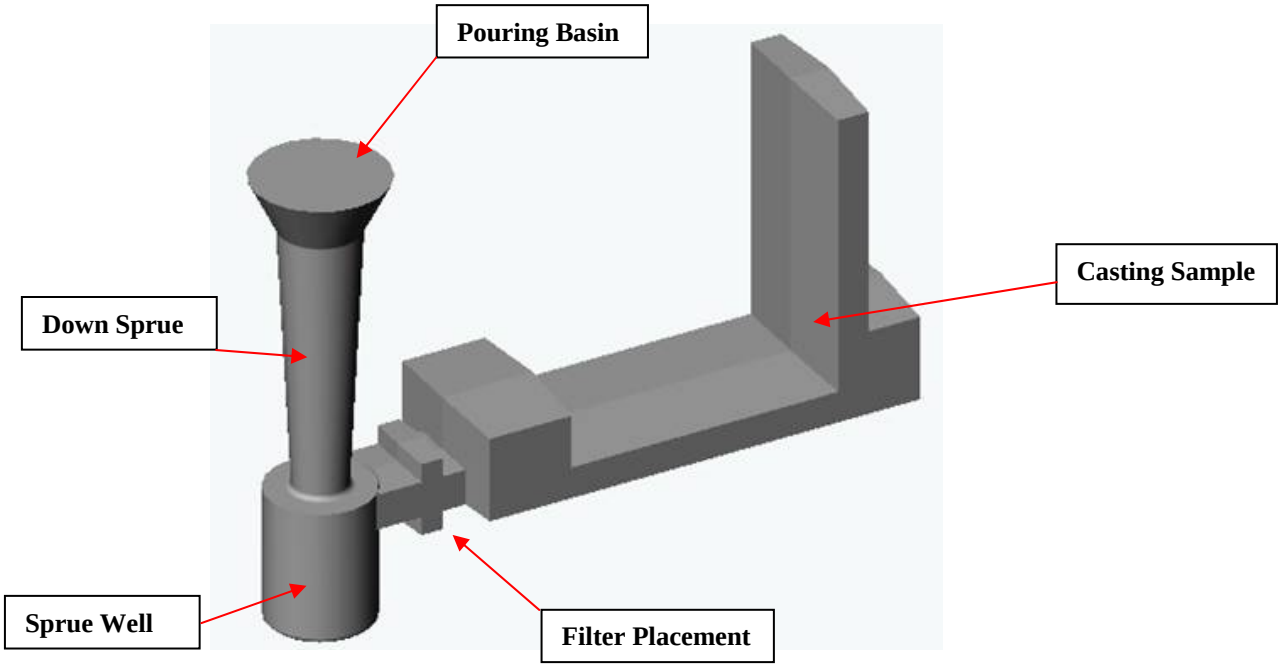

Figure 3-4: Solidworks™ model of the experimental casting designed to emulate the filling and solidification of an alloy wheel casting.

The Solidworks™ model was imported into 3D modelling software IDEAS™ to transform the casting model into the solid model of a casting mould. A two-piece mould was chosen with a symmetrically identical geometry with one half of the casting situated in each mould section. Recesses were placed in the mould to allow it to be easily pried open after the casting had solidified. Once the model was completed, it was sent to Barracuda Engineering of Auckland for CNC machining of a mild steel block to produce the mould. Samples of the IDEAS™ model are shown in Figure 3-5.

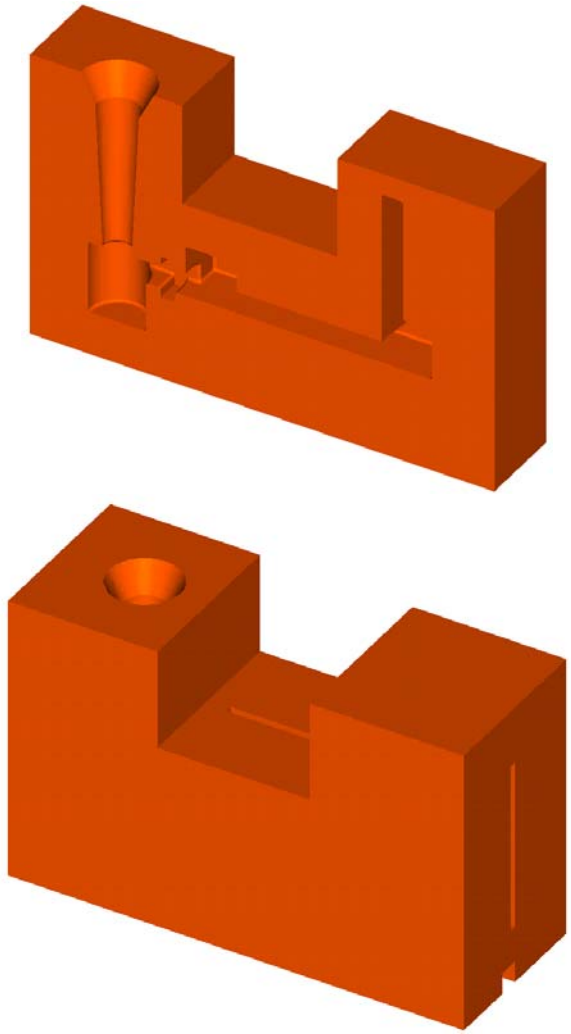

Figure 3-5: IDEAS™ model of the two-piece experimental casting mould.

Figure 3-6 shows an image of the finished experimental casting mould with the section of alloy wheel that its design was based upon. The image shows the close relationship between the experimental casting mould geometry and the geometry of an alloy wheel casting. Notice the sectional thickness transitions from thick to thin from the hub to the rim in both cases.

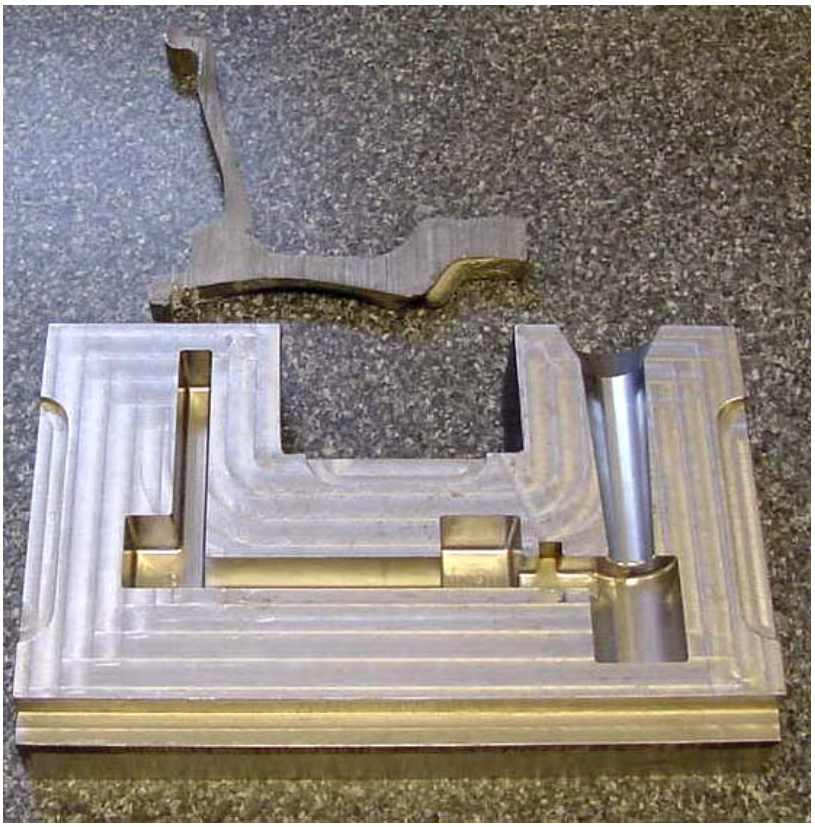

Figure 3-6: One half of the casting mould with the section of alloy wheel its design was based upon.

3.4.2 Thermocouple placement

To monitor temperature of the casting mould during heating, filling and solidification, four 1.5mm diameter K-type thermocouples were inserted in the mould walls. The thermocouples were placed slightly behind the casting surface to gauge mould temperatures for accurate and consistent casting conditions between each experiment. Figure 3-7 shows the poisoning of the four K-type thermocouples.

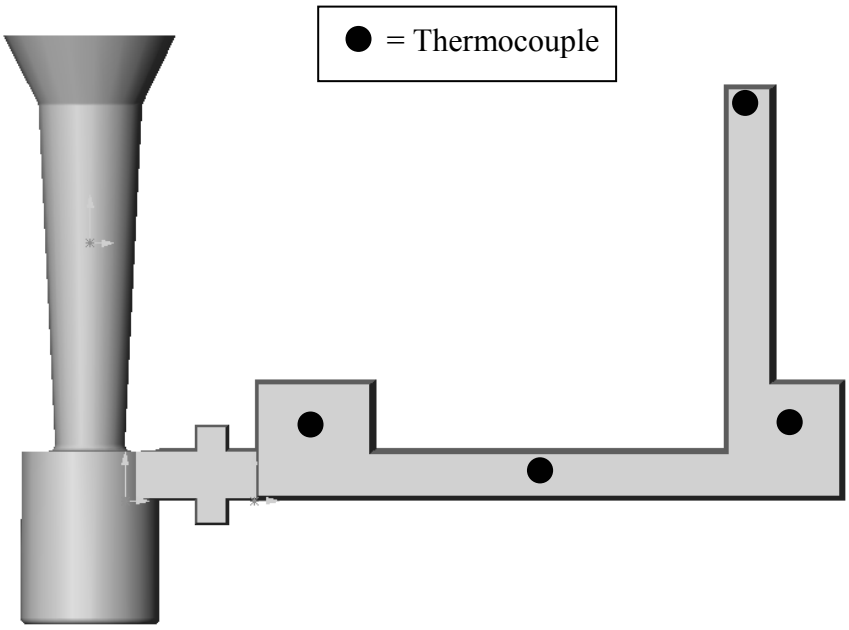

Figure 3-7: The positioning of the K-type thermocouples in the casting mould.

3.4.3 Development of the Casting Procedure

Due to the complex geometry of the specially designed experimental casting, a casting procedure had to first be developed so that complete castings could be produced consistently from both alloys. This would ensure every casting trial would be completed with consistent experimental parameters meaning confident conclusions could be drawn from the results.

Initial trials investigated the feasibility of producing a set of experimental castings consecutively from the same heat of melt, as is done in high-production casting foundries. It was hoped that the heat transfer from the casting to the mould would be enough to keep the mould at a sufficient temperature to allow complete filling of the mould meaning solidification would commence once the cavity was completely filled with molten metal.

In the initial casting trial, 3.5kg of AZ91E was melted and the mould heated to 500°C using a gas burner positioned under the mould. The mould was heated until the thermocouples in the lower part of the mould reached 600°C at which time the heat source was removed. This allowed the cooler top half of the mould to continue heating through internal conduction within the mould until equilibrium. When the equilibrium temperature of the mould had reached 500°C the melt was poured into the mould cavity, which had been filled with SF_6 cover gas to prevent oxidation during the filling process. It was found that although the first few castings progressed well, the heat from the magnesium castings was not sufficient to keep the mould at a high enough temperature so that subsequent castings could be poured at the same initial mould temperature of 500°C. As the mould continued to cool, the third casting did not completely fill the cavity due to premature solidification during filling with the rim of the casting only 80% filled. The fourth and final casting was another misrun with a partially filled rim, and by this time, the mould had cooled to such a level that the casting had contracted forcefully onto the mould and was unable to be removed.

After determining that multiple castings could not be consistently produced from one large heat of melt the experimental procedure was refined so that enough magnesium for one casting was melted each time (1kg). After the casting was removed from the mould, the gas burner was repositioned to regain optimum mould temperature prior to casting. The time taken to reheat the mould was also sufficient time to melt another kilogram of metal for the following casting. This stop-start approach to casting, although not entirely efficient, allowed every casting to be produced with a consistent melt and mould temperature, which is extremely important for the collection of meaningful data.

The only other modification to this process was made when castings were produced using AM60B. With the initial mould temperature of 500°C, these castings took a long time to solidify and were often damaged during removal. This was remedied by lowering the mould temperature by 50°C to allow a slightly higher cooling rate of the

casting, and thus producing sound solid castings in the same time frame as the AZ91E. To ensure the repeatability of the results gathered during experimentation, two separate castings were produced for each experimental parameter being investigated.

After refining the casting procedure to a point where complete castings could be made consistently from both alloys, the experimental set up now closely emulated the procedures found in a high production automotive casting foundry. This coupled with a casting design that emulates the filling and solidification of an alloy wheel meant that the results gained from the magnesium castability study would be directly relevant to the magnesium casting industry.

3.5 Casting Analysis

3.5.1 Chemical Analysis

Subsequent to each casting being poured, a small sample from the melt was also poured into a small cylindrical steel mould for chemical analysis of the melt. The samples were sent to Spectrometer Services Pty. Ltd. in Australia for compositional analysis using the Inductively Coupled Plasma Atomic Emission Spectroscopy (ICP-AES) analysis method. The claimed accuracy of this analysis method was ±2% relative to the total given on major elements (> 0.5 wt %) and ±5% relative to the total given for minor elements (< 0.5 wt %).

In Chapter 2 it was suggested that carbon levels in aluminium containing magnesium alloys is of great interest to grain refinement research. As the ICP-AES method of chemical analysis is unable to detect the presence of carbon, the Leco-Combustion method was also employed for the samples where carbon content was required to be analysed. Throughout the remainder of the thesis, when referring to an individual

casting the analysed chemical content will be stated unless otherwise specified. When referring to a group of castings the nominal composition will be used.

3.5.2 Visual Inspection

After each experiment was complete, the running system and filter sections of the castings were removed using a band saw. The castings were then visually inspected for the externally visible casting defects of surface slumping, external shrinkage porosity and hot tearing. The defects were exclusively found in four main areas labelled A-D, which are highlighted in Figure 3-8.

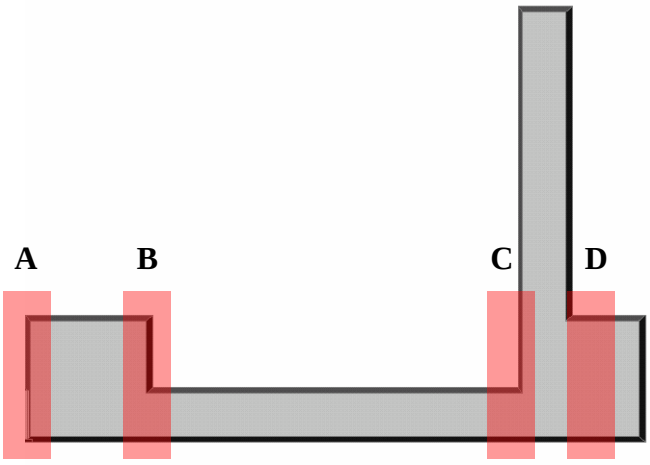

Figure 3-8: The four main areas of casting defects found in the magnesium castings.

Figure 3-9 shows examples of the three types of externally visible defects that were encountered during the course of the research. These are the types of defects which, in common casting situations, would cause castings to be rejected shortly after they were removed from the casting mould. For this reason, the recording and analysis of the these defects during the experiential phase was completed.

Surface Slumping **External Shrinkage Porosity** **Hot Tearing**

Figure 3-9: Examples of the three types of externally visible casting defects experienced during the experimental casting trials.

During the qualitative analysis, the severity of each defect was given a rating from 0 to 3 to give data that could be quantitatively assessed. By doing this, comparisons between different experimental castings could be made easily. Explanations of each of the ratings are given in Table 3-2.

Table 3-2: Severity ratings of the casting defects found in the magnesium alloy castings.

	Surface Slumping	**Shrinkage Porosity**	**Hot Tearing**
Grade 0	No surface slumping	No visible porosity	No tears present
Grade 1	Small amount of surface slumping	Slight traces of porosity	Small tears present
Grade 2	Moderate amount of surface slumping	Moderate amounts of porosity visible	Moderate amount of tearing
Grade 3	Large amount of surface slumping	Large amount of porosity present	Large tears apparent

3.5.3 X-Ray Radiography

To inspect the internal soundness of the samples, each casting was sent to X-Ray Laboratories in Auckland for radiographic inspection using a Philips Industrial X-Ray Set machine. The rim of the castings was removed and laid flat in the same plane as

the rest of the casting so a thorough insight into casting soundness could be obtained. The samples were exposed for 120 seconds at 90kV and 5mA. This exposure time was chosen due to the varying thickness of the samples from the hub to the spoke, the spoke rim junction and the rim.

3.5.4 Porosity Measurement

To determine the porosity levels in the castings two separate porosity measurements were made. Firstly, the density of the entire casting sample was measured to determine the overall porosity in the casting. The ASTM Test Method for Density Determination for Powder Metallurgy Materials Containing Less Than Two Percent Porosity was used (ASTM B311-93 Reapproved 1997). This involved using the Archimedes principle of weighing the samples in air and then in water with the temperature of the water measured. These masses, along with the density of the water at a given temperature, were used to obtain the Apparent Density of the sample using Equation 3-1.

$$(\rho_{apparent(T)}) = \rho_{water(T)} \times \left(\frac{mass_{dry}}{mass_{dry} - mass_{wet}} \right)$$

Equation 3-1: Equation for measuring the apparent density of the entire casting.

The apparent density of the casting was then related to the theoretical density to determine the porosity of the casting. The theoretical density was obtained by cutting a small section from the rim of the casting and placing it in a Hot Isostatic Press (HIP) for one hour at 390°C and 100 MPa. The rim section was chosen for this, as it is a fast freezing thin section and so would inherently have very low levels of porosity. The samples were HIPed to densify the sample further and remove any internal porosity that was present. The densities of the samples were measured using

Equation 3-1 and this value was used as the theoretical density in the porosity calculations given in Equation 3-2.

$$(P) = \left(\frac{\rho_{theoretica(T)} - \rho_{apparent(T)}}{\rho_{theoretical(T)}} \right) \times 100$$

Equation 3-2: The equation used to determine porosity level in the castings.

The second method for porosity measurement involved cutting the casting symmetrically in half to expose its centre and then separating each of the sections, i.e. the hub, the spoke, the spoke/rim junction, and the rim. This was done to negate the effect of large pores in the hub and spoke/rim junction clouding the porosity measurements. Without doing this, in cases where a large pore was completely encased in the casting a large porosity value would be obtained, however if an equally large pore had breached the surface of the casting and allowed water to enter it during density measurement, a lesser porosity value could be obtained. By sectioning the casting down the centre, any large pores would be exposed and accurate measurements for the internal porosity of each separate casting section could be made. Porosity calculations were made using techniques described above and employing Equation 3-1 and Equation 3-2.

3.6 Metallography

The samples used for metallographic examination of the macrostructure and microstructure of the castings were the same as those used for the internal porosity measurements of the separate casting sections as described in Section 3.5.4. Samples were ground using 220, 400, 800, 1200, and 4000 grade silicon carbide grinding papers to achieve a smooth flat surface. Each sample was then polished for 2 minutes using 3μm and 1μm diamond solutions respectively, with the samples being washed in water and ethanol between each stage.

To obtain grain contrast and prepare the samples for grain size measurement, two separate chemical etchants were used. For the lower aluminium content AM60B, acetic-picral etchant was used (10ml acetic acid, 4.2g picric acid, 10ml H_2O, and 70ml ethanol). This etchant enabled the different grains in the sample to become visible by producing a distinct colour contrast depending on the crystallographic orientation of each grain. Samples were immersed in the etchant for a period of 15 seconds until a brown film covered the polished surface. The specimens were then washed in ethanol and dried with a blast of warm air from a hair drier.

A second etchant was used for the higher aluminium content of AZ91E. 1ml acetic acid, 50ml H_2O, and 150ml ethanol was used to develop a contrast between neighbouring grains. This contrast was achieved through a fine and continuously oriented series of microscopic cracks formed on the surface of the sample with the orientation of the cracking related to the crystallographic orientation of the grains achieving a definite contrast between grains. The polished samples were immersed in the etchant for 120 seconds before being rinsed in ethanol and dried in a blast of warm air. The contrast in the grains did not become evident until the drying stage. Once the etching had been performed, macrographs of the casting samples were taken by using a high resolution Hewlett Packard digital scanner at 1200 dpi.

3.6.1 Grain Size Measurements

Image analysis software ImagePRO™ was used to achieve an improved contrast in the scanned images to assist in the distinction between neighbouring grains during grain size measurement. The grain size measurement technique employed was based on the Lineal Intercept Method outlined in the ASTM standard E112-96, 2003. Wherever possible at least 50 counts were made for each field and at least 5 fields were measured for each sample. This large number of sample points allowed quantitative statistics such as mean, median and standard deviation to be gathered with confidence. It should be noted that in some of the samples with much smaller grain sizes a higher magnification was used to measure the grain size. This may have

allowed grains to be distinguished that would not have been visible under a lower magnification.

3.6.2 Optical Microscopy

Optical microscopic examination of the etched samples was performed using an Olympus BX60 optical microscope with an attached Polaroid DMC 1 digital camera for image capture. Samples were viewed under polarised light to obtain micrographs of the casting microstructure. By alternating between non-polarised and polarised light the location of porosity in relation to grain structure could also be determined for a given area.

3.6.3 Scanning Electron Microscopy (SEM)

Porosity distribution analysis of the polished and etched casting samples was achieved using a Hitachi S4000 Scanning Electron Microscope (SEM). The SEM was used to obtain secondary electron and back scattered electron micrographs. The Hitachi S4000 also had an attached Energy Dispersive X-Ray (EDX) spectrometer for determining elemental composition of selected areas in the samples.

3.7 Casting Simulation

Filling and solidification modelling of the permanent mould casting was performed using the finite difference software package, MAGMAsoft ®. The purpose of the modelling was to simulate the filling and solidification of the magnesium castings and estimate temperature distribution and solidification times throughout the casting. The model would also confirm that marginal (non-directional) solidification conditions existed in the casting. An example of the temperature distribution simulated by the model during the casting of AZ91E can be seen in Figure 3-10.

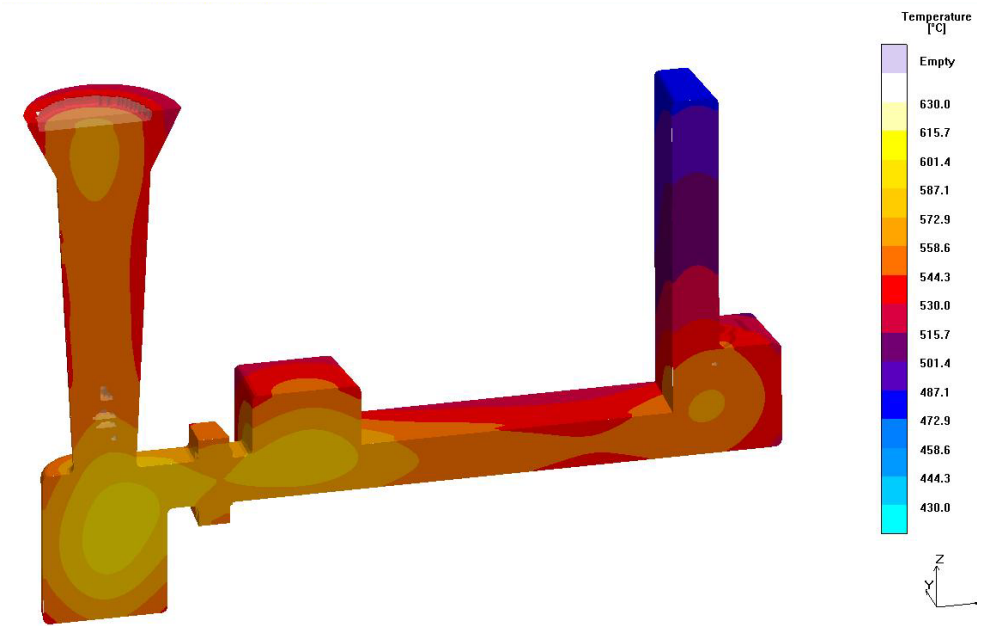

Figure 3-10 A three dimensional representation of the temperature distribution during solidification of AZ91E as predicted by the MAGMAsoft® model.

3.8 References

[1] Nelson, C. E., *Grain Size Behaviour in Magnesium Casting Alloys.* AFS 52nd Annual Meeting Chicago, IL. American Foundryman's Society 1-23 (1948).

[2] Campbell, J., *Fluid Dynamics.* Castings Butterworth-Heinemann Ltd Butterworth-Heinemann Ltd 74-84 (1991).

[3] NADCA, *Magnesium Die-Casting Handbook.* North American Die Casting Association 85-100 (1998).

4.0 The Effect of Grain Refinement on the Castability of Magnesium Alloy AZ91E

This chapter presents the results of the investigation conducted to assess the effect of grain refinement, achieved by additions of strontium and carbon, on the castability of commercial purity Mg-Al alloy AZ91E. The chapter begins with an introduction to the alloy being investigated and a brief summary of the experimental techniques used. Presentation and discussion of the results gathered in relation to the literature is followed by a section summarising the conclusions drawn from the investigation.

4.1 Introduction

Of all the magnesium alloys available for use in the production of cast components, the most widely utilised is AZ91. This alloy is one of the group of aluminium containing magnesium alloys which offer improved castability, mechanical properties and corrosion resistance over other alloys. Based on the ASTM standard designation, the composition limits of AZ91E are listed in Table 4-1. The solidification behaviour of AZ91 has been extensively studied in recent years [1-5] aiming at improving the solidified microstructure and mechanical properties of the alloy. It has been found that an improvement in the microstructure and properties of the alloy can be achieved through the addition of minor elements [3]. While much of this work is of great benefit to metal casters dealing with magnesium alloys, little work has been done to investigate the effect of so called "beneficial elements" on the behaviour of the material during processing. The aim of this investigation is to determine the effect of grain refinement additions on the castability of AZ91E. Samples have been cast in a realistic gravity permanent mould under strict laboratory conditions so that the impact and effectiveness of grain refiner type and addition level on the castings can be assessed. The results of this investigation will be an important guide to the parameters used in the full scale casting of AZ91E components.

Table 4-1: Alloy compositional limits for ASTM alloy designation AZ91E [6] .

Element	Composition (wt%)
Mg	Balance
Al	8.3 - 9.7
Mn	0.17 - 0.35
Zn	0.35 – 1.0
Si	0.1 max
Fe	0.005 max
Cu	0.03 max
Ni	0.002 max
Other (each)	0.01 max
Other (total)	0.30 max

4.2 Casting Procedure

Commercial purity Mg-Al alloy AZ91E was melted in 1kg batches using an Inductotherm induction furnace under a protective atmosphere of 50% CO_2, 49% dry air, and 1% SF_6. The alloy ingots were first ground using silicon carbide papers to remove the thick oxide layer formed on the surface. This prevents the oxide from becoming entrained in the melt during melting and casting. Prior to placement in a boron nitride coated mild steel crucible, the alloy was preheated to 200°C to ensure it was free from moisture.

Two different grain refiners were chosen for this study based on their proposed mechanisms for grain refinement. Strontium was chosen for the addition of a solute element to promote constitutional undercooling during solidification. Carbon was chosen as the other grain refiner to promote the distribution of suitable sites for heterogeneous nucleation. The three nominal addition levels investigated were no grain refiner addition, 0.05 wt% and 0.10 wt%. Once the melt had reached 700°C it

was drossed to remove the layer of oxide on the surface. The melt was then raised to the required temperature for grain refiner addition, i.e. 725°C for strontium and 760°C for carbon. Subsequent to adding the grain refiner, the melt was stirred continuously for 60 seconds to ensure dissolution prior to casting. After adding the grain refiner the melt was lowered to the pouring temperature of 695°C, which is 100°C above the liquidus temperature of the alloy.

The experimental casting mould was coated with boron nitride and preheated to the required casting temperature as discussed in Chapter 3. The mould cavity was purged with the protective gas to prevent oxidation and burning during casting. A small 10ppi ceramic foam filter was placed at the entrance to the mould cavity to remove non-metallic inclusions from the melt. Once the casting was poured, the remaining 10% of the melt was poured into a small cylindrical mild steel chill mould to form a sample for ICP-AES analysis to determine the actual alloy composition of each batch.

The resulting castings were analysed in accordance with the techniques outlined in Section 3.5 of Chapter 3, with raw data and summary statistics presented in Appendices I-IV.

4.3 Results

4.3.1 The Effect of Strontium on Grain Size

The first stage of the investigation into the effect of grain refinement on the castability of AZ91E involved the addition of an Al 10 wt% Sr master alloy to the melt. The initial set of castings produced had no strontium added, with following sets containing 0.05 wt% and 0.10 wt% Sr respectively. A sample from each of the melts used to produce the castings was analysed using ICP-AES spectrographic analysis to determine the chemical composition of the alloy and to ensure the desired strontium level was being achieved in each case. The results of the analysis, as shown in Table 4-2, confirmed that the addition of the Al 10wt% Sr master alloy to the melt

prior to casting increased the strontium level to the required composition for the investigation.

Table 4-2: Composition of the melts used for the casting experiments. All figures are in wt%.

Nominal Addition	Mg	Al	Zn	Mn	Be	Fe	Sr
AZ91E	Bal	8.69	0.63	0.22	0.001	<0.002	**<0.001**
AZ91E + 0.05 wt% Sr	Bal	8.97	0.61	0.22	0.001	<0.002	**0.05**
AZ91E + 0.10 wt% Sr	Bal	9.64	0.62	0.23	0.001	<0.002	**0.10**

The grain size of each section of the castings was measured in accordance with ASTM standard E 112-96 using the linear intercept method. A total of at least 50 grains were counted for each field of investigation, with five fields selected in each case. This high sample number allowed accurate statistics to be gathered for the mean and standard deviation of the grain size. The effect of strontium on the grain size of the different sections of AZ91E castings can be seen in Figure 4-1.

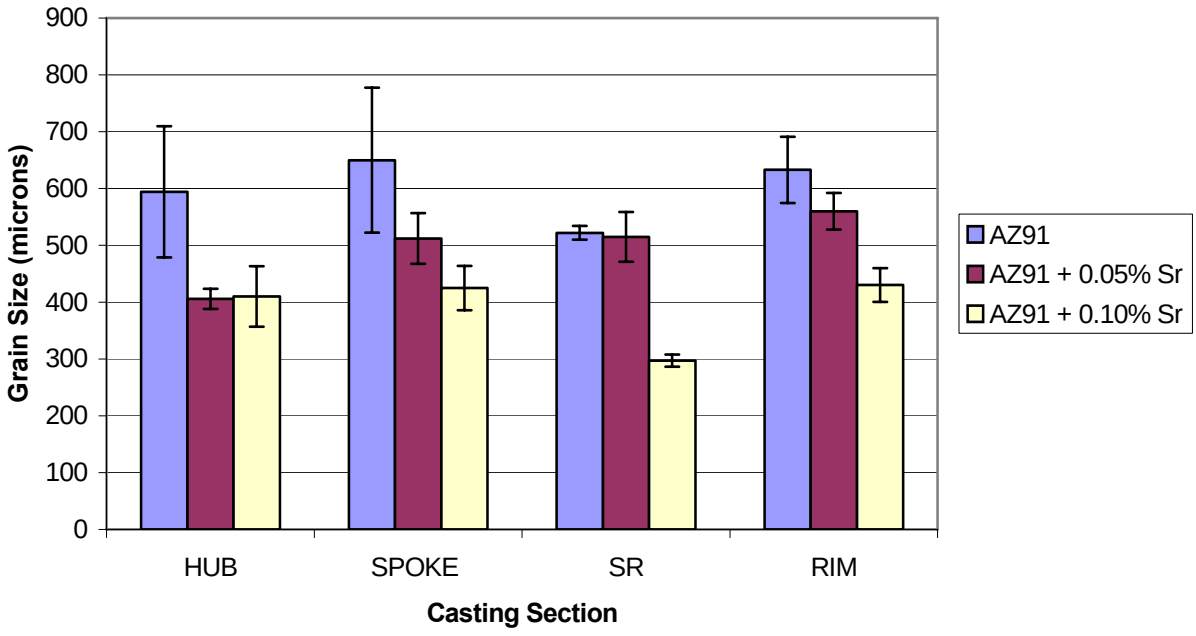

Figure 4-1: The grain size of different sections of AZ91E castings with different levels of Sr addition. The error bars represent plus or minus one standard deviation from the mean.

The addition of strontium to the AZ91E had a noticeable effect on the grain size of the castings. Three of the four casting sections exhibited a decrease in grain size with 0.05 wt% Sr added, with all four casting sections exhibiting significant grain refinement with 0.10 wt% Sr. As an example, the reduction in grain size with strontium addition to the AZ91E alloy can be seen in Figure 4-2, which shows macrographs of the rim section of the castings with increasing strontium level.

Figure 4-2:Macrographs of the rim section of the AZ91E castings with AZ91E untreated (left) AZ91E + 0.05 wt% Sr (centre), and AZ91E + 0.10 wt% Sr (right).

4.3.2 The Effect of Carbon Addition on Grain Size

Literature suggests that the addition of carbon, or carbon containing materials, to magnesium alloys that contain aluminium (such as AZ91E and AM60B) can yield significant grain refinement [4, 7-13]. However, this often produces inconsistent results in terms of its effectiveness. It is widely accepted that this inconsistency is due to the difficulties associated with getting the carbon homogenously distributed throughout the melt prior to casting. One method of adding carbon to the melt is by plunging a sample of ultra fine carbon black powder wrapped in aluminium foil under the melt surface, and then stirring to promote dispersion of the carbon powder. Due to the comparatively low bulk density of carbon black powder (0.27 g/cm^3 *cf.* 1.81 g/cm^{3}for AZ91E [6]) the powder may simply rise to the melt surface and become trapped in the oxide layer which is skimmed off during the drossing procedure conducted prior to pouring. To address the issues relating to getting carbon adequately dispersed through the melt prior to casting, work has

been undertaken during this investigation to develop a new method of adding carbon to a magnesium alloy melt.

An initial investigation hypothesised that if a tablet of similar density and melting temperature to the magnesium alloy could be produced which contained a fine dispersion of carbon, the tablet would slowly release carbon particles as it was dissolved allowing adequate contact time between the carbon and the molten magnesium alloy. The investigation involved the mixing of AZ91E powder with pure aluminium powder to produce a 50:50 ratio of aluminium to magnesium, with carbon black powder added to this powder mixture at levels of 10 and 20 wt% respectively. The powder mixtures were subsequently milled for 8 and 24 hours respectively under argon atmosphere using a SPEX 8000 Mixer/Mill. Mechanical milling was used to produce a composite powder, and also to promote the mechanical alloying of the phases to produce compounds that can be highly effective nucleation sites during the solidification of magnesium-aluminium alloys.

To determine the effect of milling time and initial carbon concentration on the final composition of the milled powders, X-ray diffraction (XRD) analysis was carried out on the powders subsequent to milling using the techniques outlined in Section 3.3.2 of Chapter 3. Figure 4-3 shows the results of the XRD analysis and how the relative composition of the carbon, magnesium, magnesium aluminide, and aluminium phases changed with respect to milling time and initial composition. In the case of the Al/Mg + 10 wt% C powders, increasing the milling time from 8 to 24 hours resulted in little change in the XRD pattern, other than a reduction in intensity of the magnesium phase and an overall broadening of the peaks. As the milling was conducted under an argon atmosphere, this is unlikely to be due to oxidation of the magnesium during milling. Instead there appears to be a slight increase in the relative intensity of the $Mg_{17}Al_{12}$ phase around a 2θ of 35º, indicating the milling resulted in the mechanical alloying of the magnesium and aluminium phases to increase the relative amount of this compound.

For the powder mixture containing 20 wt% C, a much larger change in the phase structure is evident, as a result of milling. Here, two distinct peaks can be seen to appear at a 2θ of around 42º and 62º after 8 hours of milling. These peaks were identified as $Mg_{17}Al_{12}$. The relative intensity of the aluminium phase is also reduced as milling time was increased. More interestingly, two other distinct peaks (at a 2θ of 32º and 55º) appeared in the XRD pattern of the Al/Mg + 20 wt% C sample milled for 24 hours. These peaks were identified as aluminium carbide (Al_4C_3), which is thought to be a powerful nucleant for magnesium during solidification [14].

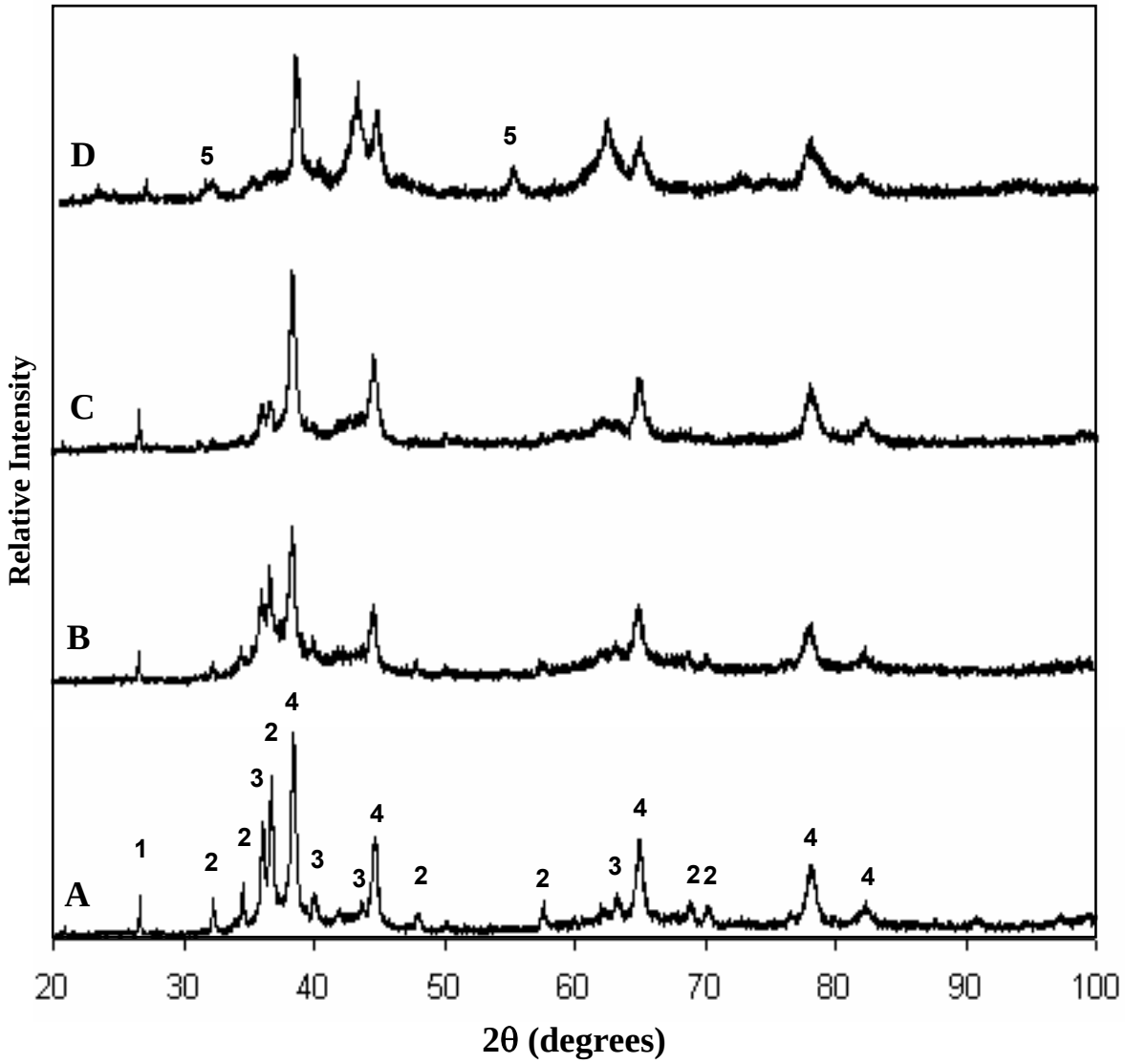

Key:

- 1 = C
- 2 = Mg
- 3 = $Mg_{17}Al_{12}$
- 4 = Al
- 5 = Al_4C_3

Figure 4-3: X-ray diffraction spectra of the four Al/Mg/C powder mixes milled for different lengths of time: (A) Al/Mg + 10 wt% C milled for 8 hours (B) Al/Mg + 10 wt% C milled for 24 hours (C) Al/Mg + 20 wt% C milled for 8 hours (D) Al/Mg + 20 wt% C milled for 24 hours.

The powders were then compacted in a cylindrical mould with a diameter of 10mm and a height of 5mm under a pressure of 50MPa using a hydraulic press. This produced solid cylindrical tablets that were subsequently labelled to reflect their composition. Half of the tablets produced were sintered under an argon atmosphere at 430°C for 4 hours to further promote the production of carbide compounds that are thought to be primarily responsible for grain refinement of magnesium castings. The experimental parameters used to produce the eight carbon containing tablets are summarised in Table 4-3.

Table 4-3: The experimental parameters used to produce the carbon containing tablets.

Tablet No.	Carbon Content	Milling Time	Sintered
1	10 wt%	8 hours	No
2	10 wt%	24 hours	No
3	20 wt%	8 hours	No
4	20 wt%	24 hours	No
5	10 wt%	8 hours	Yes
6	10 wt%	24 hours	Yes
7	20 wt%	8 hours	Yes
8	20 wt%	24 hours	Yes

To assess the effectiveness of the tablets in introducing carbon to the casting melt, batches of 500g of AZ91E melt were prepared, with the tablets being plunged and stirred into the melt for 60 seconds at 760°C. The tablets contained enough carbon to give a nominal addition rate of 0.05 wt% C. A cylindrical steel mould with a diameter of 60mm and a height of 80mm that had been preheated to 200°C was used to make the castings. One casting was also poured without the addition of a carbon tablet for comparison purposes. Once the castings had cooled they were sectioned in half, with one half used for leco-combustion analysis to determine carbon content, and the other polished and etched for grain size measurement.

The results of the leco-combustion analysis for carbon content of the treated castings are shown in Table 4-4. This shows that the carbon content of the castings was much lower than the nominal addition of 0.05 wt%. Much of the carbon released by the dissolution of the tablets may have been removed during drossing immediately before the castings were poured. From the leco-combustion analysis results it appears there is no significant effect of sintering, increasing the milling time from 8 to 24 hours, or changing the carbon content of the composite powder from 10 to 20 wt% on the resulting carbon level of the castings.

Table 4-4: The leco-combustion analysis of the castings produced using the carbon tablets.

Sample	Wt% C
AZ91E + Tablet 1	0.006
AZ91E + Tablet 2	0.011
AZ91E + Tablet 3	0.006
AZ91E + Tablet 4	0.010
AZ91E + Tablet 5	0.010
AZ91E + Tablet 6	0.009
AZ91E + Tablet 7	0.005
AZ91E + Tablet 8	0.005

The castings were analysed to determine whether the tablets were effective in altering the grain size of the castings, and to determine whether any of the tablets performed more effectively than the others. As shown in Figure 4-4, significant grain size reduction was achieved when the carbon tablets were added to the melt. Examples of the grain size reduction achieved in the casting samples are also shown in Figure 4-5.

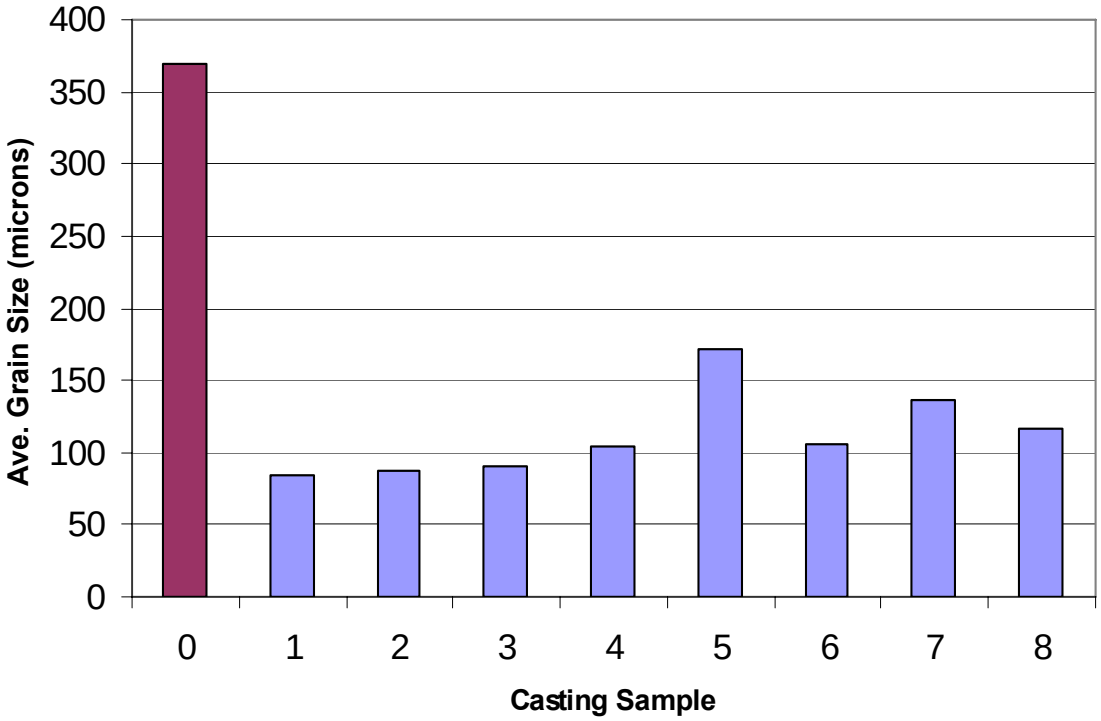

Figure 4-4: Resulting grain sizes of casting samples produced with additions of the different carbon containing tablets.

When no tablet was added to the melt (Sample 0) the mean grain size of the cylindrical casting was 369µm. After the addition of the carbon-containing tablets, the mean grain sizes achieved ranged from 75-175µm. The minimum average grain size of 75µm was achieved in the casting produced with a tablet consisting of Al/Mg + 10 wt% C powder milled for 8 hours without sintering (Sample 1), though this was not significantly lower than the other casting samples. The highest average grain size of the treated castings which was 175µm was achieved using the tablet containing Al/Mg + 10 wt% C powder milled for 8 hours with subsequent sintering (Sample 5). A slight trend in the results was apparent with the grain sizes of castings refined using the unsintered tablets (Samples 1-4) being more consistent and, on average, slightly lower than average grain size of the castings refined using the sintered tablets (Samples 5-8). Overall, although the actual carbon content of the castings is still significantly lower than the nominal content to be achieved by adding the carbon containing tablets, the grain refinement effect is significant. This shows that only a relatively small amount of carbon is required to be added to AZ91E before significant grain refinement is achieved.

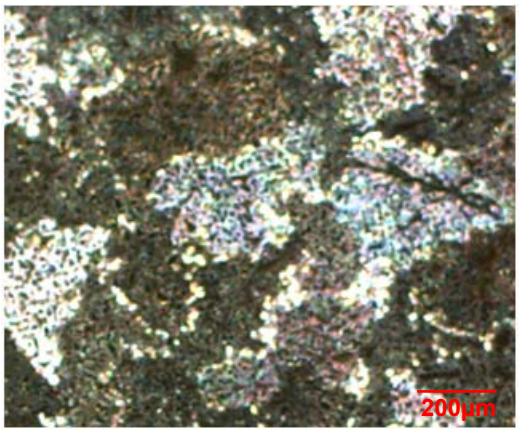

Sample 0

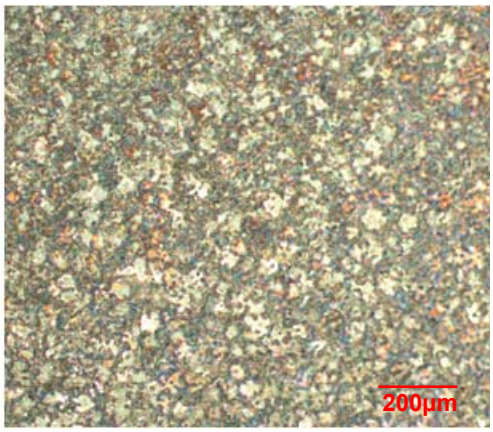

Sample 1

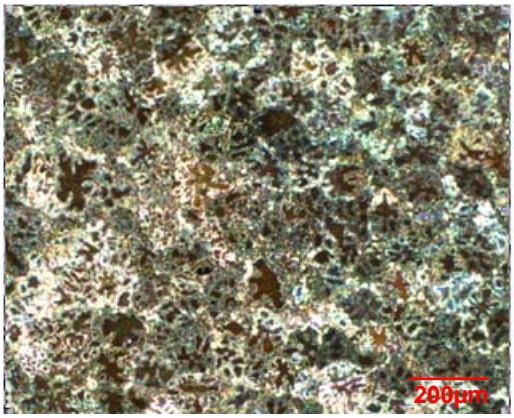

Sample 2

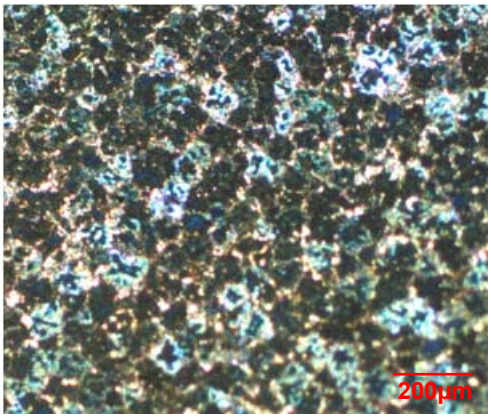

Sample 3

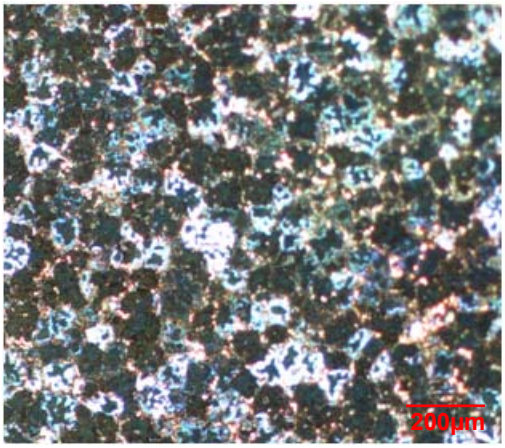

Sample 4

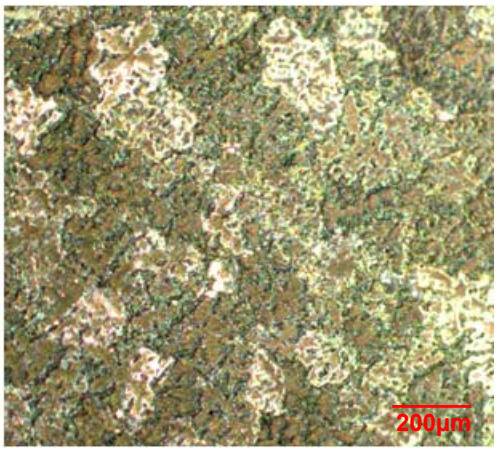

Sample 5

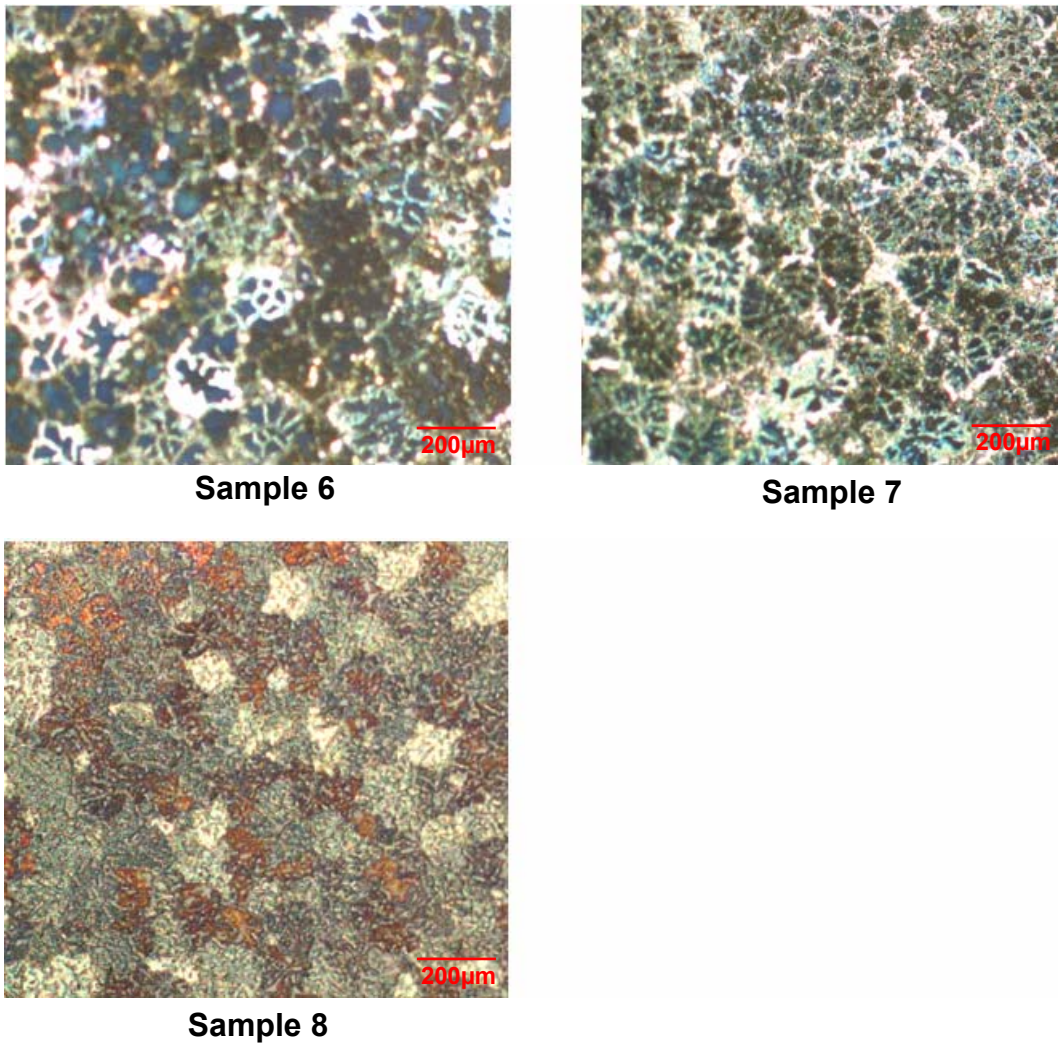

Figure 4-5: Optical microscopy images of the grain structure of the samples produced in the carbon tablet trial. Sample 0 is the untreated casting and the details of samples 1-8 are listed in Table 4-3.

Once the hypotheses that a "slow release" carbon containing tablet would be an effective means of introducing carbon to a magnesium-aluminium alloy melt had been proven, the experiments moved towards the use of the specially designed experimental casting mould. Four separate melt treatments were used to produce two castings from each to determine the effect of grain refinement achieved using carbon on the castability of AZ91E. The melt treatments investigated were AZ91E untreated, 0.05 and 0.10 wt% C (nominal) added in the form of carbon powder wrapped in aluminium foil, and addition of a carbon tablet at a nominal addition rate of 0.05 wt% C. This would give a comparison between the effects of differing amounts of carbon added on grain

refinement, and also the effectiveness of adding carbon to the melt by the use of aluminium foil and a pressed tablet. The carbon tablet chosen from the initial experiments was based on Sample 4, that being Al/Mg + 20 wt% C powder milled for 24 hours without sintering of the pressed tablet. This tablet was chosen because it resulted in one of the highest carbon contents of the finished castings, and it contained a greater amount of carbon black than the other leading unsintered tablet (Tablet 2).

As with the casting trial using strontium as a grain refiner, a small cylindrical casting was poured from each melt for ICP-AES analysis to determine alloy chemistry. Leco-combustion analysis was also employed to determine the resulting carbon level in the castings. The results of the analyses are presented in Table 4-5.

Table 4-5: Alloy chemistry of castings produced in carbon treatment investigation.

Nominal Composition	Addition Method	Al	Zn	Mn	Be	Fe	C
AZ91E	Nil	8.69	0.63	0.22	<0.001	<0.005	**<0.005**
AZ91E + 0.05 wt% C	Carbon black wrapped in foil	9.12	0.55	0.27	<0.001	<0.005	**0.005**
AZ91E + 0.10 wt% C	Carbon black wrapped in foil	9.09	0.56	0.27	<0.001	<0.005	**0.007**
AZ91E + 0.05 wt%	Al/Mg + C tablet	9.21	0.56	0.29	<0.001	<0.005	**0.020**

Table 4-5 shows that the alloy chemistry of all four castings fits in with that designated for AZ91E alloy specification. Leco-combustion analysis of the samples revealed that the nominal compositions of 0.05 wt% C and 0.10 wt% C were not achieved when carbon powder wrapped in an aluminium foil was plunged into the melt. In fact, less than 10% of the desired carbon compositions were achieved in this case. This reiterates the difficulty of introducing carbon into magnesium-aluminium melts effectively. A much higher carbon level was achieved when the newly developed carbon containing tablet was employed with the resulting 0.02 wt% C being only slightly lower than the desired

carbon level of 0.05 wt% C. The castings produced using the tablet had a carbon level three to four times higher than when the carbon black was added in foil. This proves the benefits of using the specially designed tablets for the grain refinement of magnesium-aluminium alloys.

To determine the effect of carbon content on the grain refinement of AZ91E, the castings were sectioned and prepared using the techniques outlined in Section 3.6 for grain size measurement. The results of the grain size measurements are presented in Figure 4-6 with detailed summary statistics presented in Appendix I.

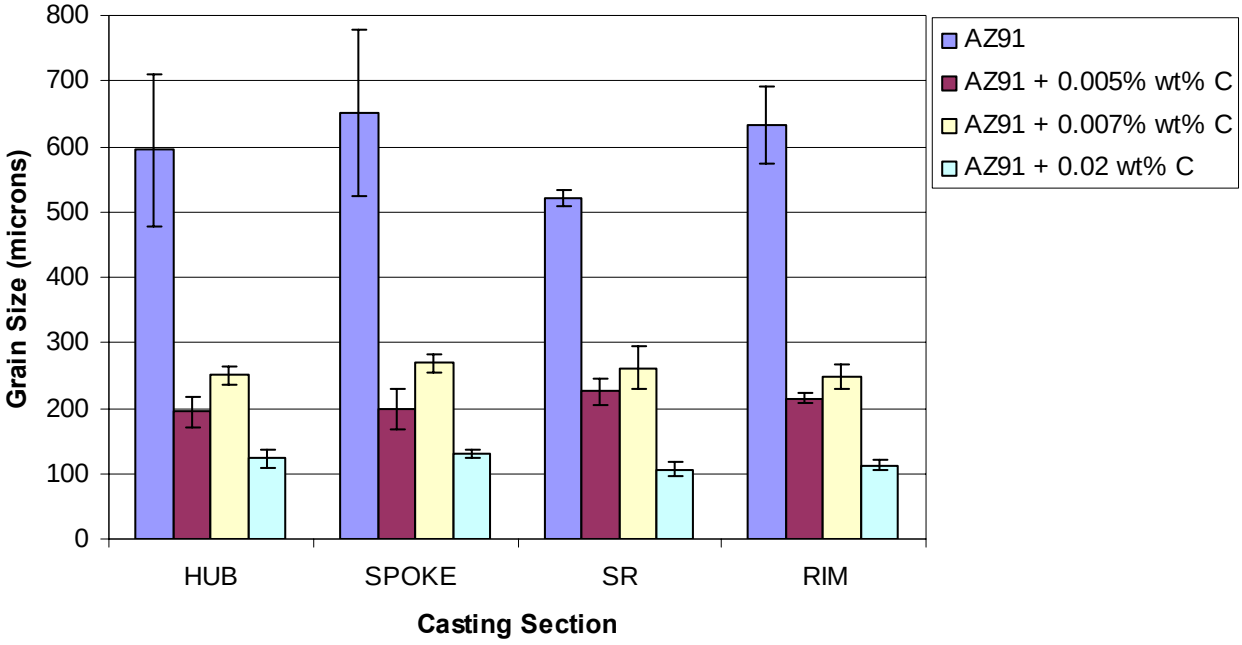

Figure 4-6: Grain sizes of the different sections of the castings with differing carbon contents. The error bars represent plus and minus one standard deviation from the mean value.

As an example, Figure 4-7 shows macrographs of the rim section of the castings, which clearly illustrate the effect of carbon on the grain size of AZ91E alloy castings.

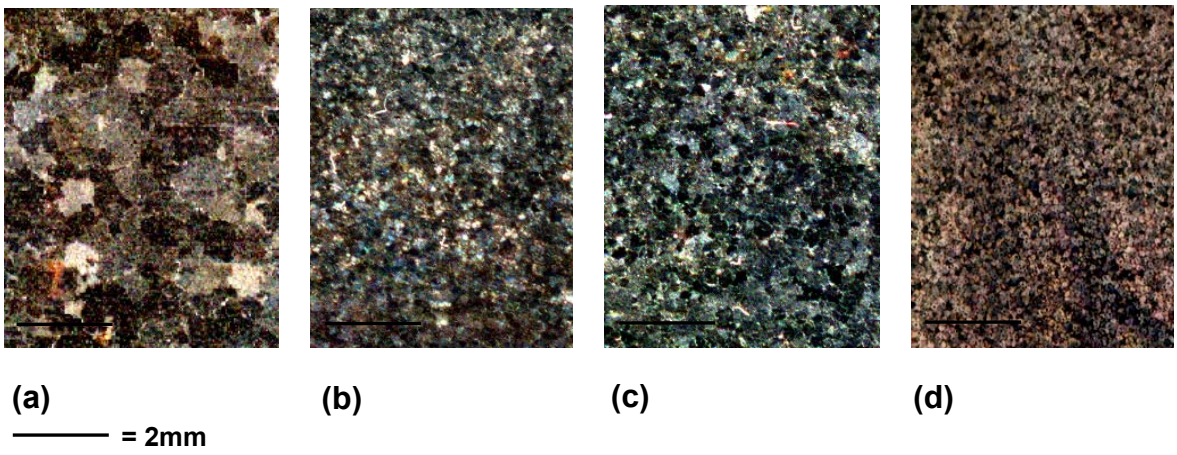

Figure 4-7: Casting macrographs of the rim section of the castings produced during the carbon investigation: (a) AZ91E untreated (b) AZ91E + 0.005wt% C (c) AZ91E + 0.007 wt% C (d) AZ91E + 0.02 wt% C.

The addition of carbon to AZ91E had a significant effect on the grain size of every section of the castings produced. Adding 0.005 wt% C, reduced the grain size of the castings by approximately 70%, though adding 0.007 wt% C resulted in a slightly less effective grain refinement. Increasing the addition to 0.02 wt% C gave a consistently smaller grain size than those of AZ91E + 0.005 wt% C, AZ91E + 0.007 wt% C castings and of course the untreated AZ91E castings. As an example, the spoke section of the untreated AZ91E castings had a mean grain size of 650µm, while the grain size of the same section of the casting with 0.02 wt% C added was only 130µm.

4.3.3 Summary on the Study of Grain Refiner Effectiveness

Both of the grain refiners chosen for this investigation modified the as-cast grain size of the experimental castings as desired. This has allowed the effect of grain refinement on the castability of AZ91E to be determined. The addition of 0.05 wt% Sr reduced the grain size of all but one of the casting sections, with 0.10 wt% Sr yielding further refinement of all casting sections. The addition of carbon in powder form wrapped in foil to the alloy melt at the nominal addition rate of 0.05 and 0.10 wt% C leads to actual carbon level in the castings being 0.005 and 0.007 wt% C respectively. These levels of carbon resulted in considerable grain refinement in the casting. With a nominal addition

rate of 0.05 wt% C, the development and employment of the mechanically milled magnesium-aluminium-carbon powders pressed into tablet form brought the highest carbon content of 0.02 wt% C and hence, the greatest degree of grain refinement. A prime example is seen in the rim section, where the as-cast grain size was lowered from 633µm to 113µm. Another trend apparent from the addition of the two different grain refining elements to AZ91E was that the variability of grain size throughout the casting section was lowered considerably. This meant that the grain sizes were not only smaller but also more consistent after grain refinement addition.

4.3.4 External Defect Inspection

As outlined in Section 3.5.2 of Chapter 3, each of the AZ91E castings produced from the experimental mould was visually inspected for external defects. Two castings were produced for each experimental parameter to ensure the results were consistent and reproducible, and this was found to be the case. The severity of the defects was graded on a scale from 0-3. Grade 0 means no visible defect was present and grade 3 means the visible defect was severe. The defects were classified by which area in the casting they occurred, and the grades from both castings were averaged to give a score for each experimental parameter. Details of the analysis are presented in Appendix III.

The three types of visible defects found were external slumping of the casting surface, shrinkage porosity that had broken through and was visible on the casting surface, and hot tearing of the casting. The areas inspected for external defects in the casting samples are shown in Figure 4-8.

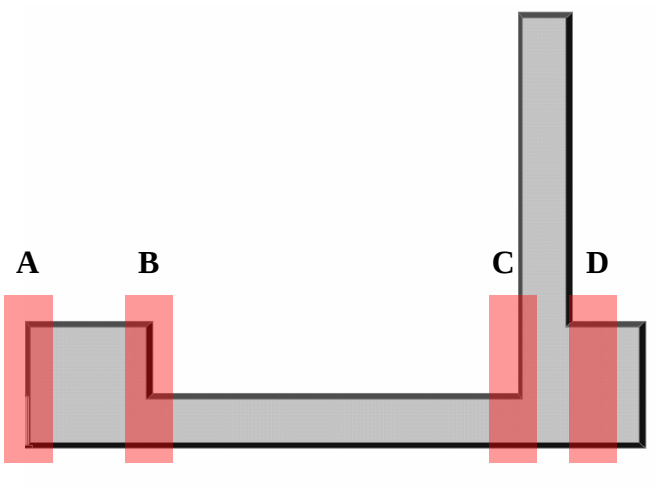

Figure 4-8: The four areas of the casting that were assessed for external casting defect levels.

The results of the analysis of the AZ91E castings treated with 0.05 wt% Sr and 0.10 wt% Sr are shown in Table 4-6, which shows that the presence of external shrinkage porosity was completely eliminated when Sr was added to the melt, although its occurrence in the casting without any strontium was minor, with an average score of 1. Addition of Sr had an inconclusive effect on surface slumping. A slight decrease was observed after the addition of 0.05 wt% Sr, but a sharp increase in slumping occurred when 0.10 wt% Sr was added. The greatest effect of adding strontium was observed to be the reduction of hot tearing. Without adding strontium, hot tearing in the castings was severe, especially in regions C and D around the spoke to rim junction of the experimental casting. The addition of Sr decreased the level of hot tearing greatly with only one of the castings produced displaying a minor tear in region C.

Table 4-6: External defect levels of the AZ91E castings treated with strontium.

AZ91E + 0 wt% Sr					
	A	**B**	**C**	**D**	**TOTAL**
Slumping	0	0.5	0.5	1	**2**
Shrinkage	0	0.5	0.5	0	**1**
Hot Tearing	0	0	2.5	1.5	**4**
AZ91E + 0.05 wt% Sr					
	A	**B**	**C**	**D**	**TOTAL**
Slumping	0	0	0.5	0.5	**1**
Shrinkage	0	0	0	0	**0**
Hot Tearing	0	0	1.5	0	**1.5**
AZ91E + 0.10 wt% Sr					
	A	**B**	**C**	**D**	**TOTAL**
Slumping	0	1.5	0.5	1.5	**3.5**
Shrinkage	0	0	0	0	**0**
Hot Tearing	0	0	0.5	0	**0.5**

The effect of carbon addition on defect levels of the castings is shown in Table 4-7, which shows that the results for the castings produced with a carbon grain refiner were similar to those produced when strontium was added. The addition of carbon grain refiner increased the level of surface slumping in the castings, but eventually eliminated external shrinkage porosity. The occurrence of hot tearing was completely eliminated in all of the carbon grain refined castings.

Table 4-7: External defect levels of the AZ91E castings treated with carbon.

AZ91E					
	A	**B**	**C**	**D**	**TOTAL**
Slumping	0	0.5	0.5	1	**2**
Shrinkage	0	0.5	0.5	0	**1**
Hot Tearing	0	0	2.5	1.5	**4**
AZ91E + 0.005 wt% C					
	A	**B**	**C**	**D**	**TOTAL**
Slumping	1.5	0	0	2	**3.5**
Shrinkage	0	0	0	0	**0**
Hot Tearing	0	0	0	0	**0**
AZ91E + 0.007 wt% C					
	A	**B**	**C**	**D**	**TOTAL**
Slumping	0	0.5	1.5	1	**3**
Shrinkage	0	0	0	1	**1**
Hot Tearing	0	0	0	0	**0**
AZ91E + 0.02 wt% C					
	A	**B**	**C**	**D**	**TOTAL**
Slumping	0.5	1	0.5	2.5	**4.5**
Shrinkage	0	0	0	0	**0**
Hot Tearing	0	0	0	0	**0**

Subsequent to the visual inspection of the external quality of the experimental castings, all of the samples produced were x-rayed to inspect their internal soundness. This would determine whether internal macro-porosity was visibly affected by grain refinement of the castings. Figure 4-9 and Figure 4-10 show x-ray radiographs of the AZ91E castings before and after grain refinement with strontium and carbon respectively.

	AZ91E	**AZ91E + 0.05 wt% Sr**	**AZ91E + 0.10 wt% Sr**
Hub	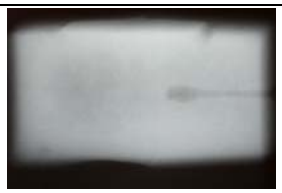		
Spoke			
Spoke/Rim Junction			
Rim			

Figure 4-9: X-Ray radiographs of the casting sections of the AZ91E castings, with and without being treated with strontium.

Figure 4-9 shows that for AZ91E castings without any strontium added there are large internal pores in the hub and the spoke to rim junction, which are the thicker sections of the casting. This is illustrated by the darkened areas inside the lighter coloured magnesium casting. These large cavities are not as severe when the melt is treated with strontium.

There is a slightly darker area in the spoke to rim junction of the AZ91E casting with 0.10 wt% Sr added. This was due to surface slumping of the casting surface resulting in

a reduction in section thickness of the casting in that area, yielding a change in contrast. This area is not to be confused with the presence of a large internal pore, which would display a much more distinct darkened area in the radiograph.

The x-ray radiographs of the castings produced with carbon as the grain refiner are shown below in Figure 4-10.

	AZ91E	**AZ91E + 0.005 wt% C**	**AZ91E + 0.007 wt% C**	**AZ91E + 0.02 wt% C**
Hub				
Spoke				
Spoke/Rim Junction				
Rim				

Figure 4-10: X-Ray radiographs of the casting sections of the AZ91E castings with and without being treated with carbon.

Little change to the thinner casting sections of the spoke and rim is observed in the radiographs when carbon is added to the melt. In the thicker, slower cooling sections of the hub and the spoke/rim junction it appears that the level of internal porosity increases slightly when carbon is added. The images contain areas of dark cloudiness which indicates an area of lower density. As the internal inspection of the AZ91E castings shows up many instances of internal defects in the castings, the next step in the castability investigation was to measure the overall porosity levels of the castings. The porosity level of each separate casting section was also measured to quantify the effect of grain refinement on internal porosity of AZ91E castings.

4.3.5 Overall Casting Porosity Levels

The overall casting porosity levels were determined by measuring the apparent density of the entire castings using the Archimedes principle. This was then compared to the density of a densified sample. The densified sample was produced by hot isostatic pressing of a section of AZ91E casting at 390°C and a pressure of 100 MPa for one hour. In each case, castings produced for both alloy conditions were measured for porosity with the results averaged to yield the porosity percentage for the casting condition. The results of the porosity measurements for the castings treated with strontium and carbon can be seen in Figure 4-11 and Figure 4-12 respectively.

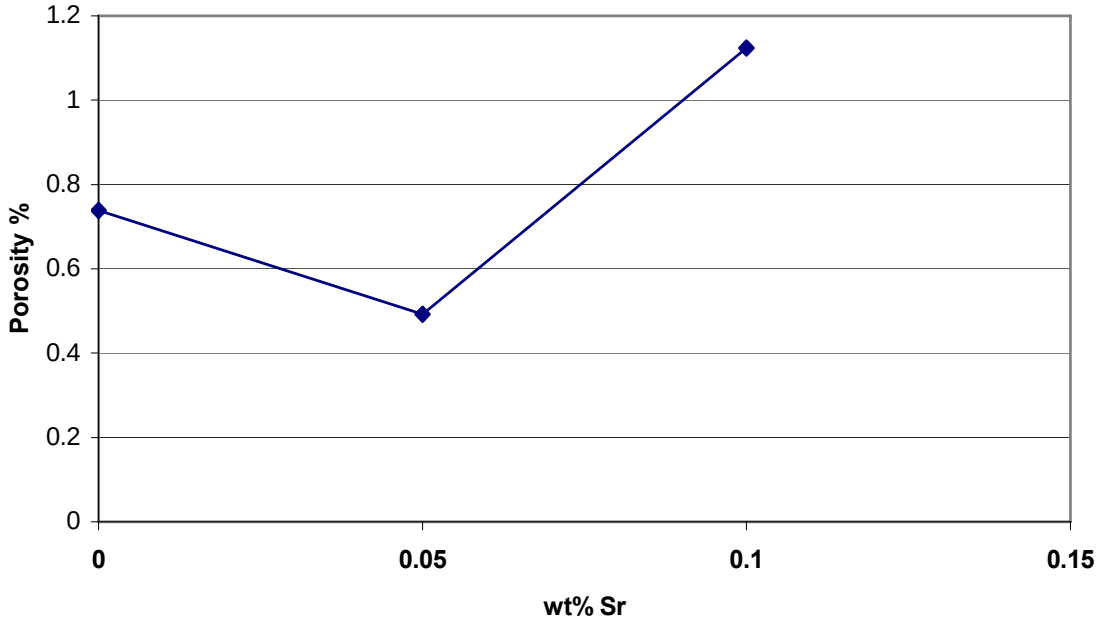

Figure 4-11: Casting porosity levels for AZ91E with increasing Sr levels.

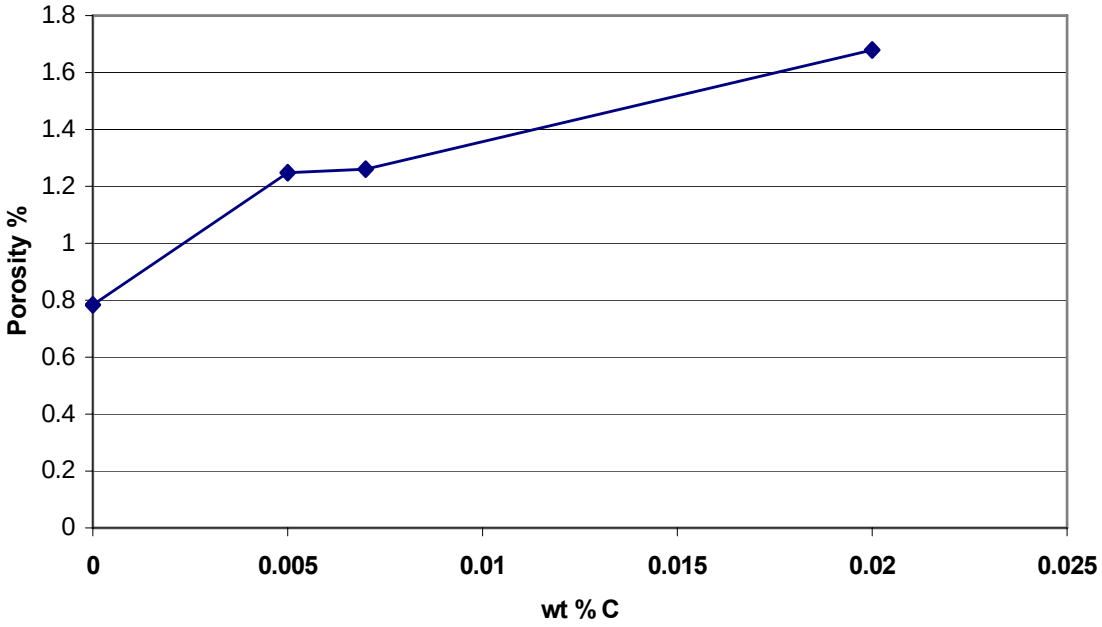

Figure 4-12: Casting porosity levels for AZ91E with increasing C addition levels.

The effect of strontium on the overall porosity of the castings did not show a clear trend with the amount of Sr added. The addition of 0.05 wt% Sr to the melt resulted in slight decrease in the overall porosity level from 0.73% to 0.49%, but the addition of 0.10 wt% Sr resulted in a clear increase of the overall porosity level to 1.12%.

The inconsistency in the results of the castings treated with strontium may be due to the fact that a large shrinkage porosity pore in the hub or spoke/rim junction of a casting may or may not be connected to the surface of the casting. Hence, the pore could interfere with the Archimedes density measurements. More reliable assessment of the effect of grain refinement on casting porosity levels will be shown in Section 4.3.6 where the samples have been sectioned to expose all large pores to the surface, so that the results are a true measure of internal microporosity levels.

In the case of the melts treated with carbon, a far clearer trend was apparent. When the casting contained 0.005 wt% C, there was a significant increase in overall porosity level from 0.74% to 1.27%. Slightly increasing the amount of carbon added to 0.007 wt% C had no further effect on porosity level. However, when the amount of carbon in the sample was increased to 0.02 wt% C the porosity level of the sample was increased further to 1.68%.

4.3.6 Porosity Levels of the Individual Casting Sections

Each casting was sectioned using a band saw to separate the four distinct regions of the hub, spoke, spoke/rim junction and the rim. These sections were then measured for internal porosity levels using the techniques outlined in Section 3.5.4 of Chapter 3.

The effect of strontium addition on the internal porosity levels of the different sections of the AZ91E casting is illustrated in Figure 4-13. With the addition of strontium to the AZ91E castings, a reduction in the porosity levels of the thinner sections of the spoke and rim is apparent. The porosity level dropped sharply after the addition of only 0.05 wt%

Sr to the melt, however increasing the addition to 0.10 wt% had no further effect. The effect of strontium on the internal porosity levels of the thicker sections was inconclusive. Only when comparing the thicker casting sections of the untreated AZ91E with the 0.10 wt% Sr addition castings, can it be said that the addition of Sr resulted in an increase in internal porosity level.

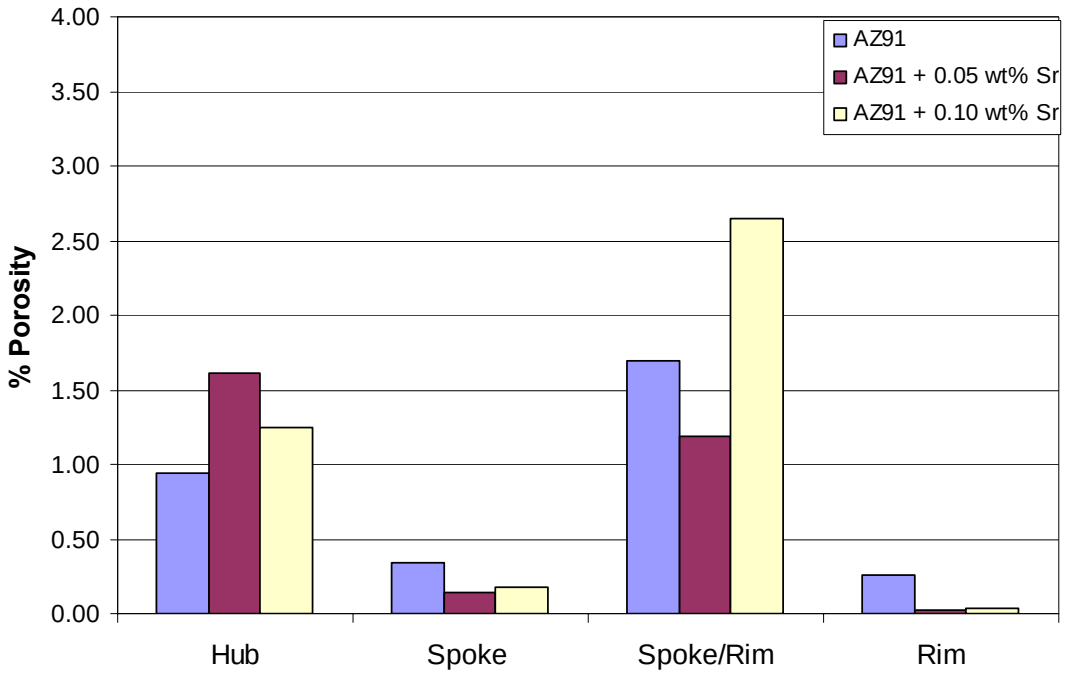

Figure 4-13: Internal porosity levels of the separate sections of the AZ91E castings with increasing strontium levels.

The addition of carbon to the AZ91E melt prior to casting had a more marked effect on porosity levels of the different casting sections. Figure 4-14 shows the porosity levels of the different sections as a function of carbon content in the melt.

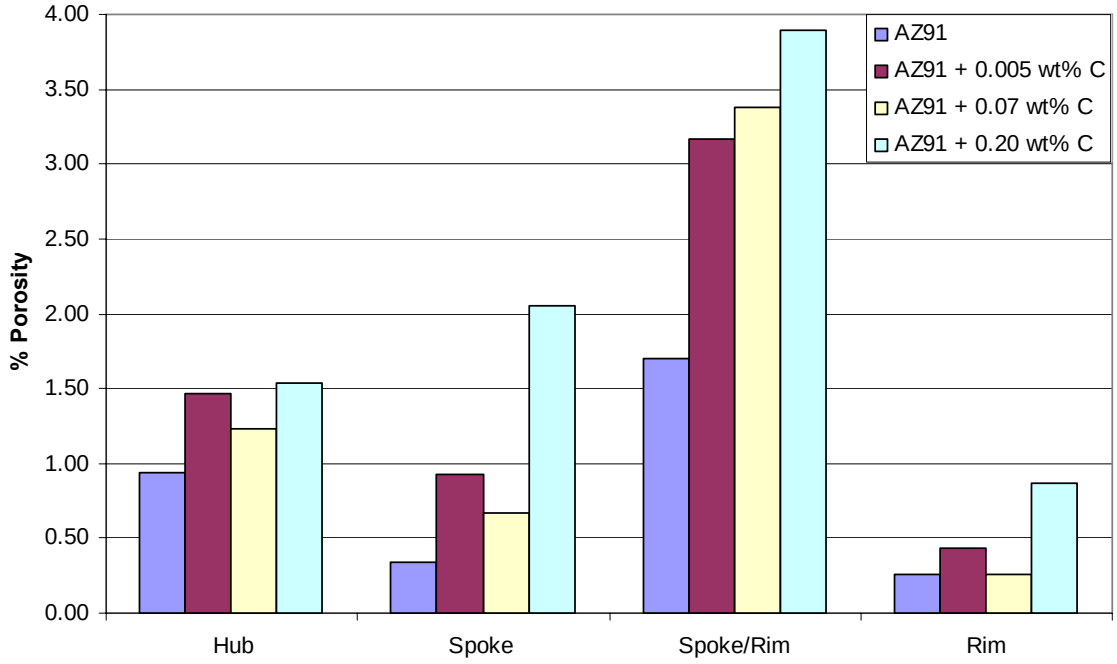

Figure 4-14: Internal porosity levels of the separate sections of the AZ91E castings with increasing carbon addition levels.

Compared to the untreated AZ91E castings, each section of the castings treated with carbon as a grain refiner exhibited an increase in internal porosity levels. This correlates well with the results of the overall porosity measurements which yielded an increase in porosity with carbon treatment. The highest internal porosity levels attained in the castings were in the 0.02 wt% C castings produced using the carbon containing tablet.

4.3.7 MAGMAsoft™ Casting Simulation

To highlight the intricacies of solidification of the experimental casting and the reliance on effective feeding mechanisms, a MAGMAsoft simulation was produced. The images in Figure 4-15 and Figure 4-16 show the temperature profiles through the casting at the commencement of, and mid way through solidification respectively. Note the confirmation of the presence of hotspots in the hub and spoke/rim junction.

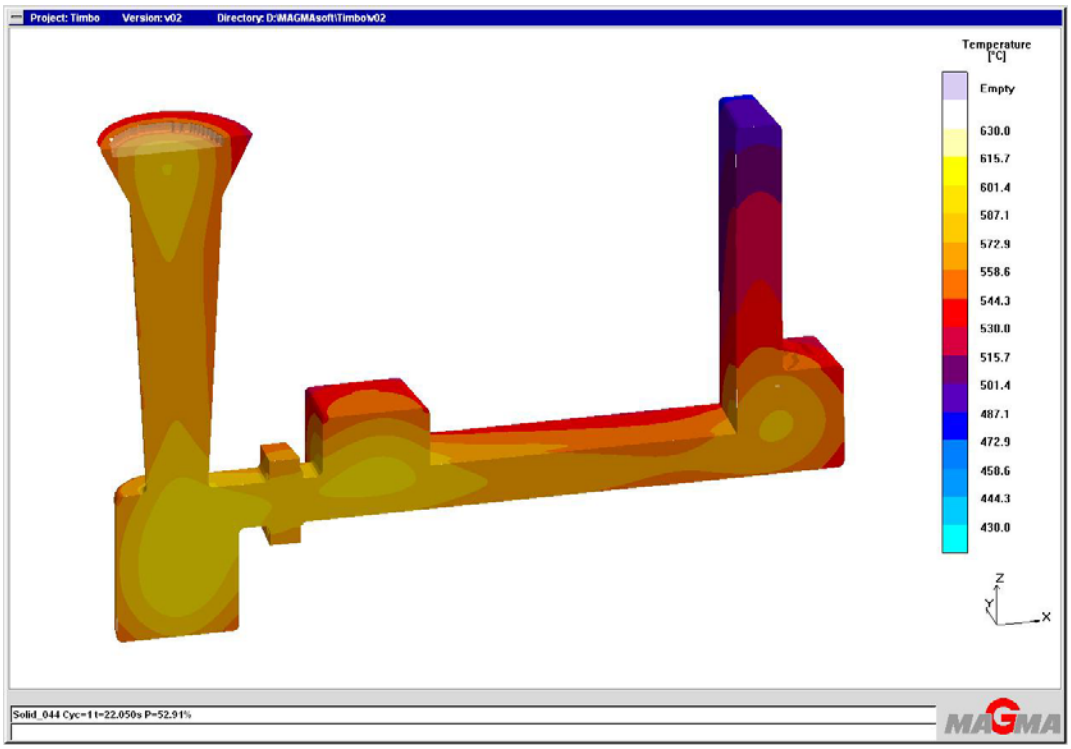

Figure 4-15: Screen capture of the MAGMAsoft simulation at the commencement of solidification in the AZ91E experimental casting.

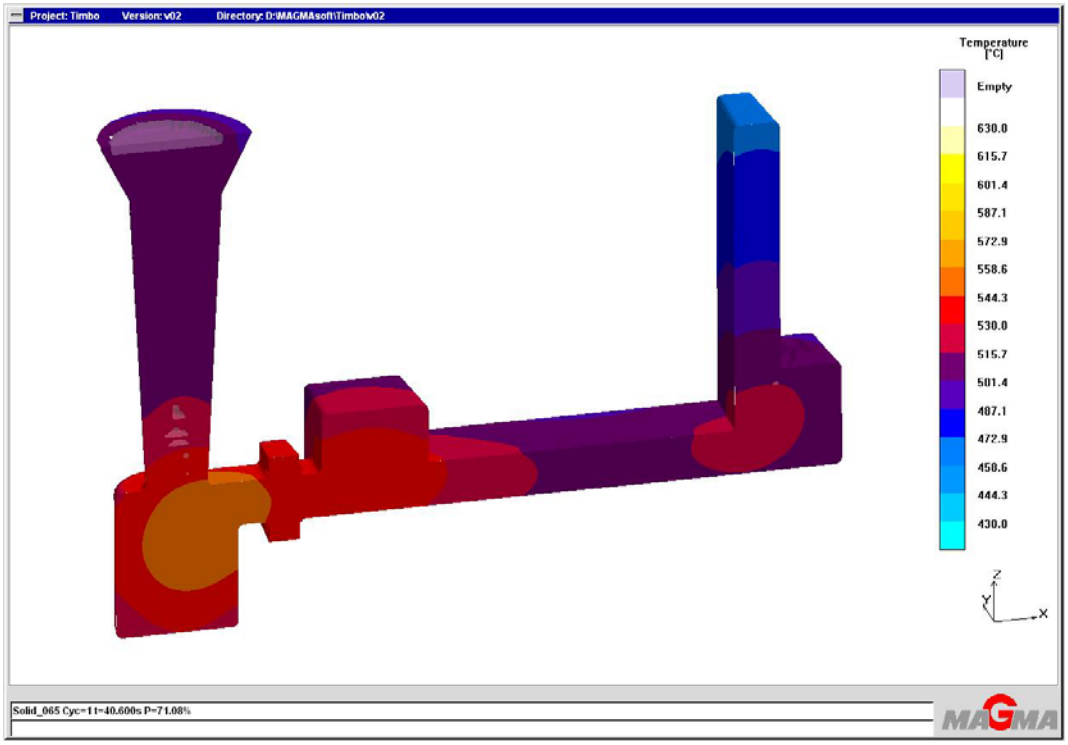

Figure 4-16: Screen capture of the MAGMAsoft simulation midway through solidification in the AZ91E experimental casting.

Figure 4-15 shows that in the experimental casting, solidification begins at the top of the rim section furthest from the pouring basin. This is the ideal situation when producing a casting of this type such as an alloy wheel, as the rim is always furthest from the feed metal in a riser for gravity castings, or the sprue in a low pressure casting. In ideal conditions solidification would proceed from the furthest point directionally towards the feed metal so that a path for metal to compensate solidification shrinkage remains open. This is often difficult to achieve, especially with several changes in section thickness as is common in alloy wheel castings of which this mould is based upon.

Figure 4-16 shows that as the casting continues to cool and solidification progresses, it is obvious that the casting is not solidifying directionally. The figure shows that the spoke section will begin to freeze off before the hot spot in the spoke rim junction. This means there will be limited feed metal available to compensate for shrinkage in this hot spot, and porosity will result. This helps to explain why grain refinement had such an adverse effect on porosity levels in the castings.

4.3.8 Microscopic Examination of Porosity

During the investigation the etchants used to reveal the microstructure of the casting samples distinguished the individual grains effectively. Optical microscopy was employed to determine whether the location, size, and morphology of the porosity in the samples changed with respect to the casting macrostructure as the grain size was reduced. For the AZ91E castings the spoke-rim junction and the rim section were analysed giving a contrast in section thickness. Samples were selected from all of the castings produced to give a range of grain sizes from completely unrefined to fully refined.

The samples chosen are listed below, with the contrast in average as-cast grain size being shown in Figure 4-17.

- AZ91E untreated
- AZ91E + 0.10 wt% Sr
- AZ91E + 0.005 wt% C
- AZ91E + 0.02 wt% C

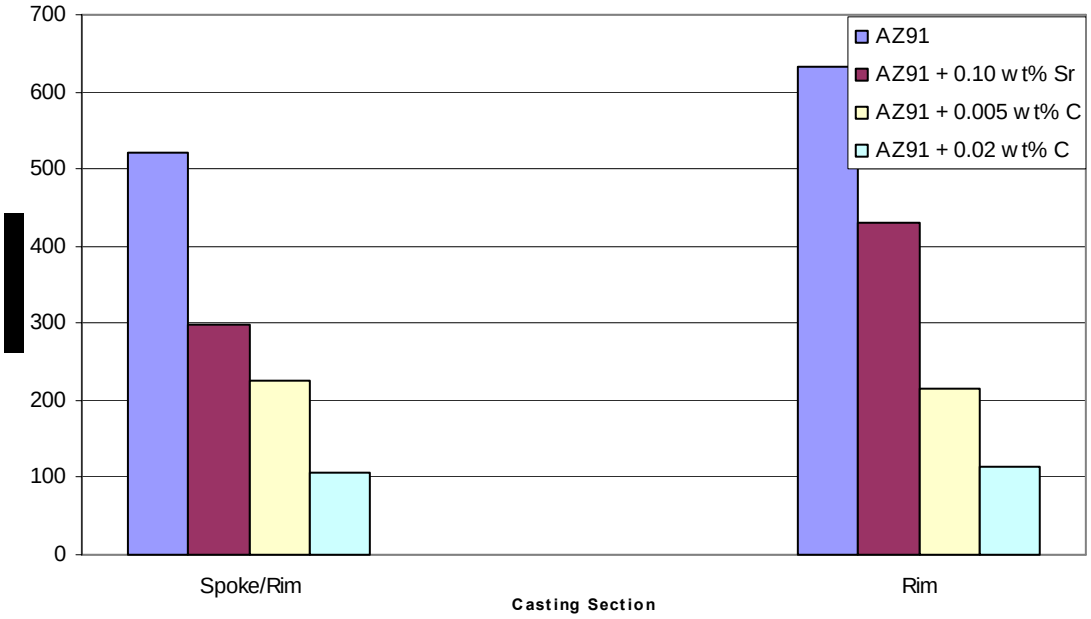

Figure 4-17: The mean grain sizes of the casting samples chosen for the microscopic porosity investigation

Unfortunately the polarised light used to reveal the grain structure tended to obscure the position of the pores in the samples. Conversely, removing the polarised light would identify the porosity in the sample but the contrast of grain boundaries would become lost. To counter this, a separate micrograph for each lighting condition was taken from the identical position in the sample. This allowed for further processing of the grain-highlighting images under high magnification to trace the outline of the grain boundaries. The traced outline of the grain boundaries was then overlaid onto the image which highlighted the location of pores, thereby giving a combined image where both of the microstructural characteristics could be observed simultaneously.

Processing the images in this way allowed for the analysis of the effect of grain refinement on porosity characteristics in the casting samples. The resulting micrographs showed how the pore size, shape and distribution altered as the grain size was reduced through the samples. As mentioned previously, the samples were chosen to yield a steady reduction in grain size to help identify any trends with increasing levels of grain refinement.

Figure 4-18 through Figure 4-21 show the micrographs of the spoke-rim junction and rim sections of the castings with decreasing grain size. The image at the top illustrates the grain structure of the sample, with the lower image showing the pores in the casting. The grain structure network has been overlaid in yellow so as not to obscure the darker areas where pores are present. The two images displayed in Figure 4-18 show the presence of both intergranular and interdendritic pores. Here, branches of connected pores can be seen following sections of grain boundaries, but also entering inside the grains and spreading between dendrite arms. The pores are a result of insufficient liquid feed metal to these areas, which are the last to solidify during the casting process.

When the mean grain size of the sample is reduced from 522μm to 297μm, a major change is evident. Figure 4-19 shows that the pores are no longer widespread inside the grains and between dendrite arms. Nearly all of the pores that are present in the sample are distributed along the grain boundaries. This is again illustrated in Figure 4-20 with a further reduction in grain size to 225μm showing almost a complete elimination of interdendritic pores. An overall increase in the amount of porosity is also clearly evident. With a further reduction in grain size to 106μm, the pores are located more in isolated pools at the corner junctions between 3 or more grains, instead of being spread right along the grain boundaries.

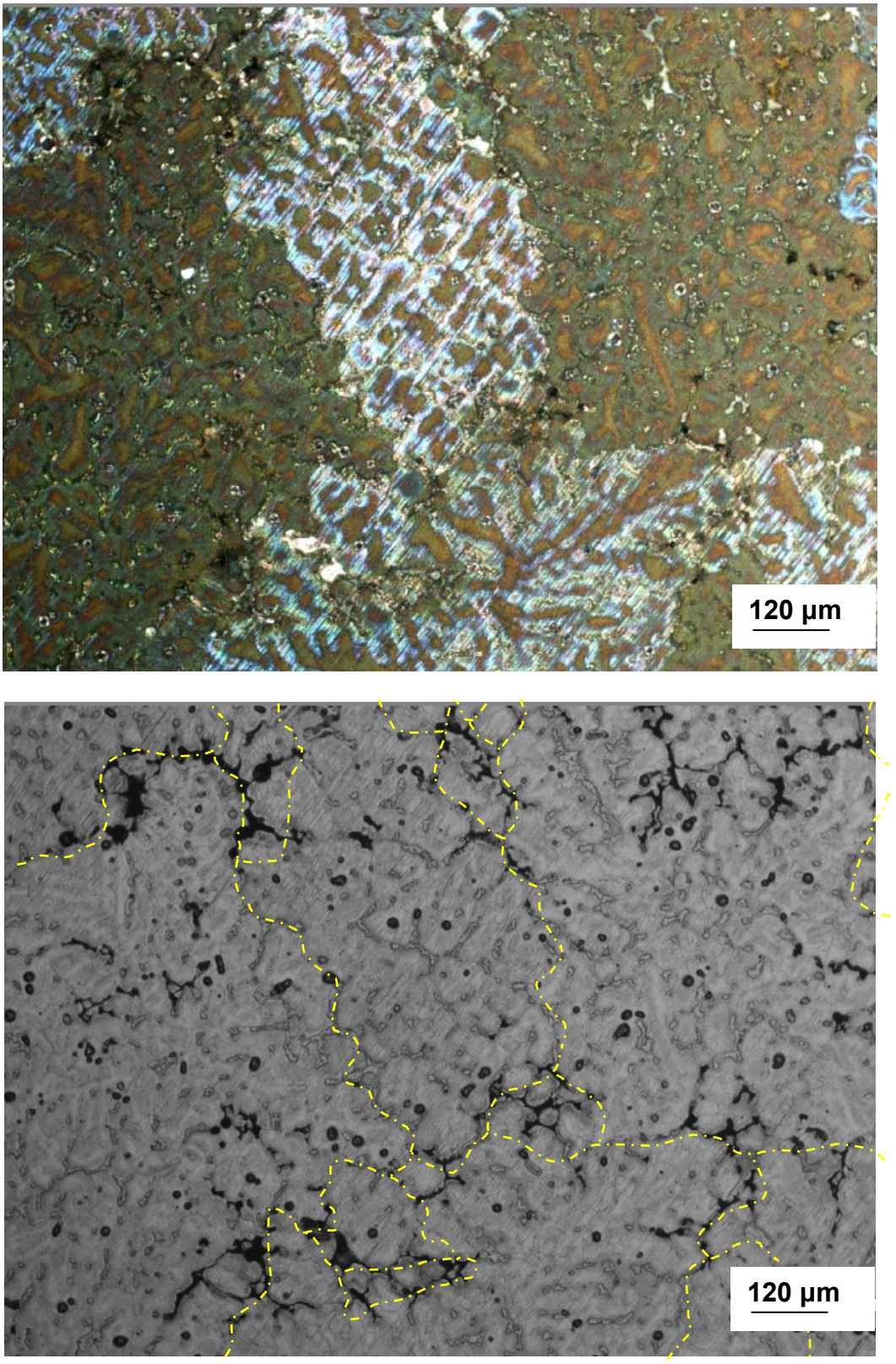

Figure 4-18: Micrographs showing the relationship between grain structure and the distribution of pores in the spoke-rim junction of the untreated AZ91E casting. The mean grain size of this sample is 522µm.

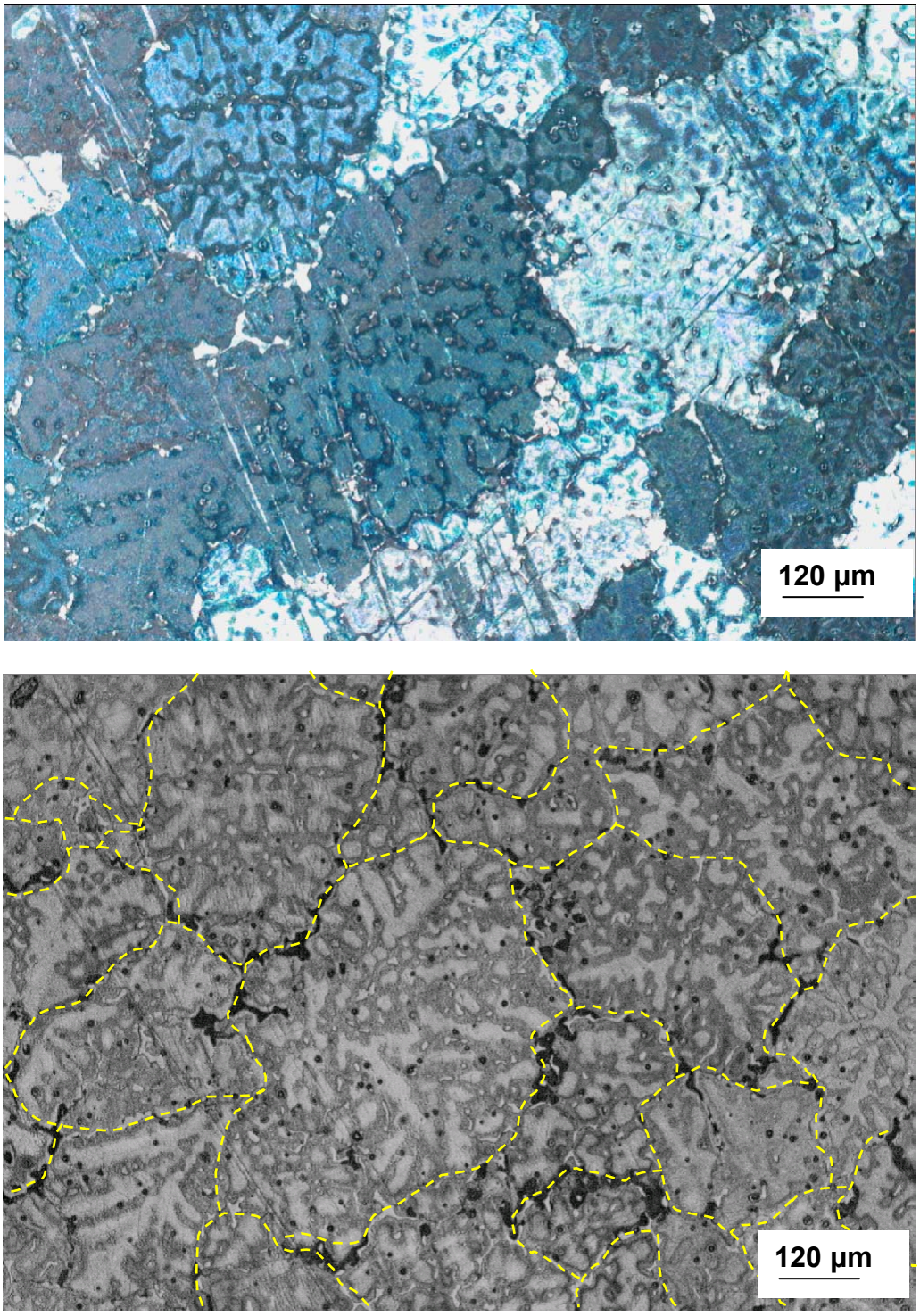

Figure 4-19: Micrographs showing the relationship between the grain structure and distribution of pores in the spoke-rim junction of the AZ91E casting treated with 0.10 wt% Sr. The mean grain size of this sample is 297µm.

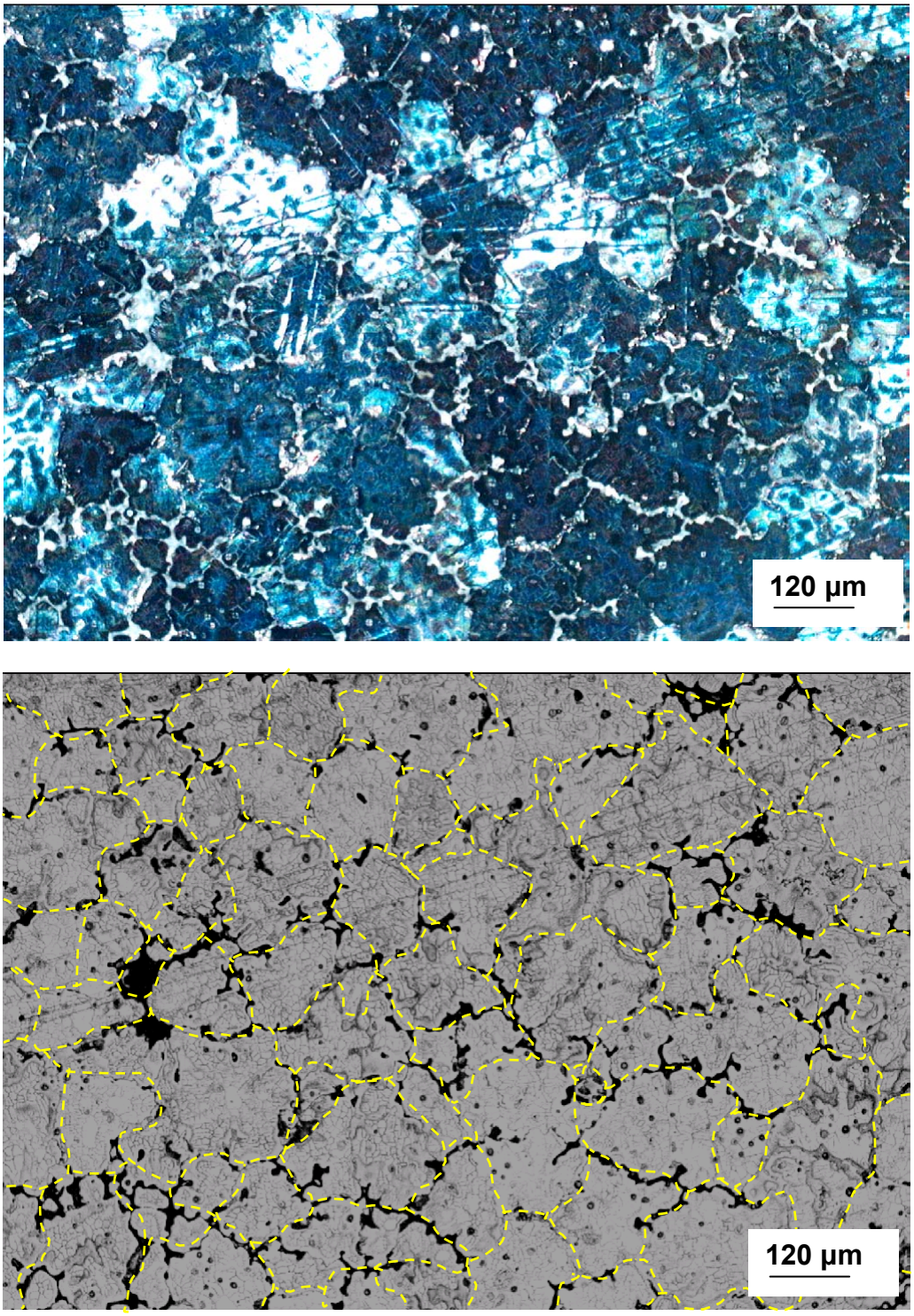

Figure 4-20: Micrographs showing the relationship between the grain structure and the distribution of pores in the spoke-rim junction of the casting treated with 0.005 w% C. The mean grain size of this sample is 225µm.

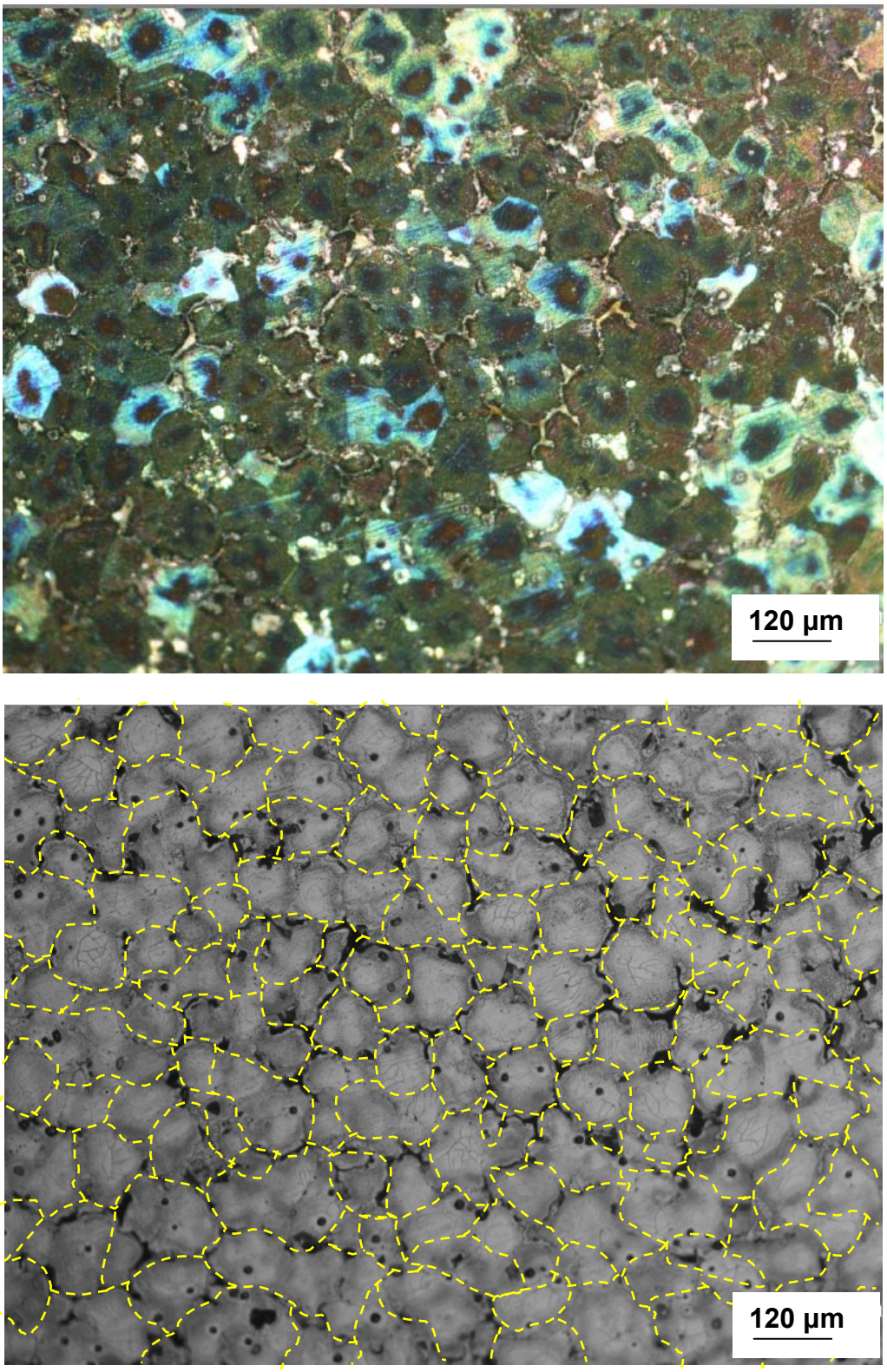

Figure 4-21: Micrographs showing the relationship between the grain structure and the distribution of pores in the spoke-rim junction of the AZ91 E casting treated with 0.02 wt% C. The mean grain size of this sample is 106µm.

To determine whether section thickness plays a role in the effect of grain refinement on casting porosity characteristics, the thinner rim section of the casting samples was also investigated. Figure 4-22 through Figure 4-25 show the results of this optical microscopy investigation. Here the trend of changing the distribution of pores with increased degree of grain refinement remains the same. Figure 4-22 shows the unrefined rim section with a large mean grain size of 633μm. A small number of shrinkage pores can be seen being distributed along the grain boundaries and also between the dendrites inside some of the grains. A significant reduction in grain size down to 430μm, as illustrated in Figure 4-23, results in a significant increase in the number of pores, though the distribution of the pores is still divided between intergranular and interdendritic. Figure 4-24 displays a further reduction in mean grain size, down to 215μm, and it is here where there is a noticeable change in the distribution of pores. Almost all pores in the sample are distributed along the grain boundaries. This phenomenon is illustrated again with a further reduction in mean grain size to 113μm, as shown in Figure 4-25. Again, almost all pores are distributed and grouped along the grain boundaries and the pores in each group are connected.

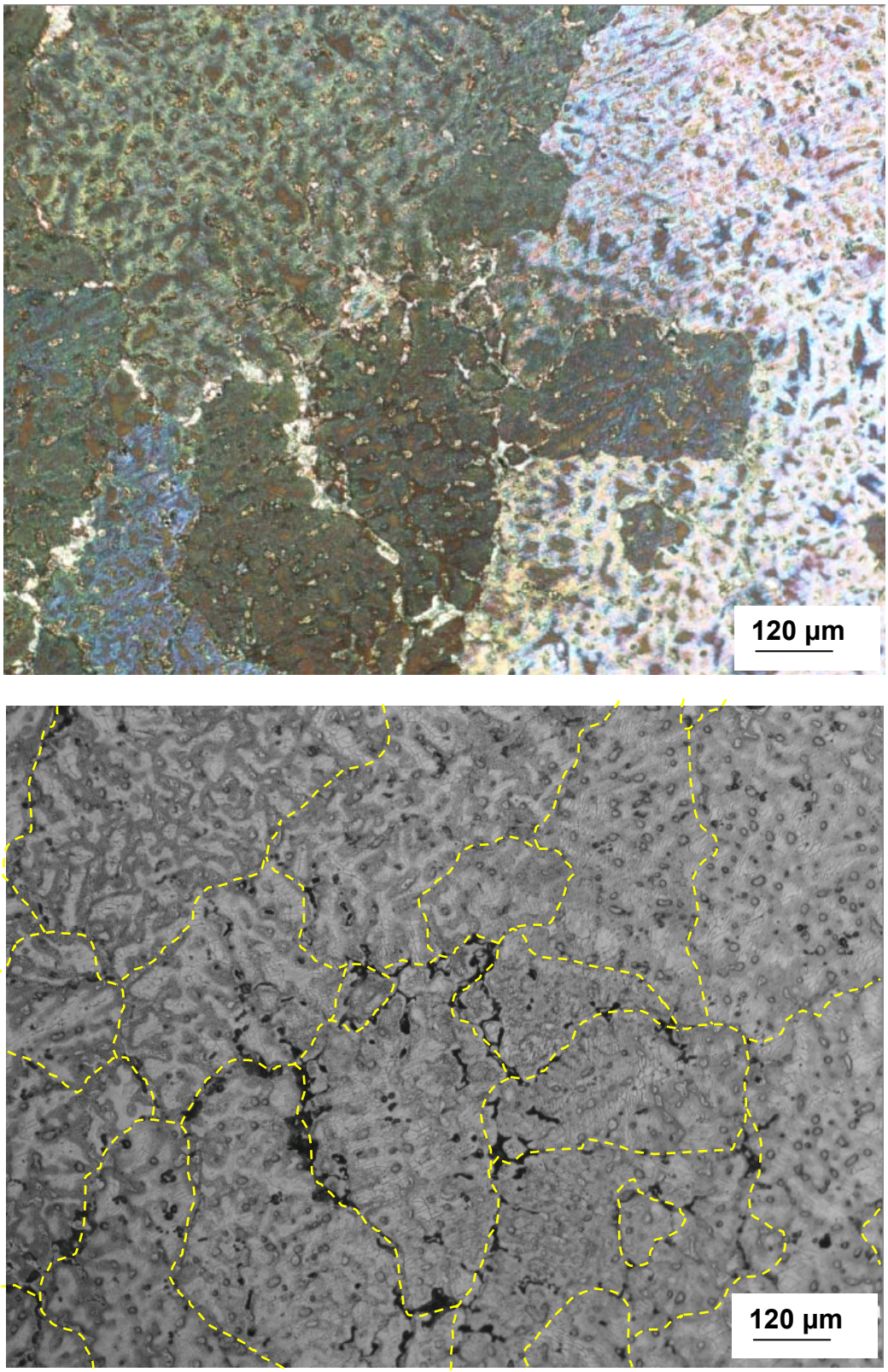

Figure 4-22: Micrographs showing the relationship between the grain structure and the distribution of pores in the-rim section of the untreated AZ91E casting.. The mean grain size of this sample is 633µm.

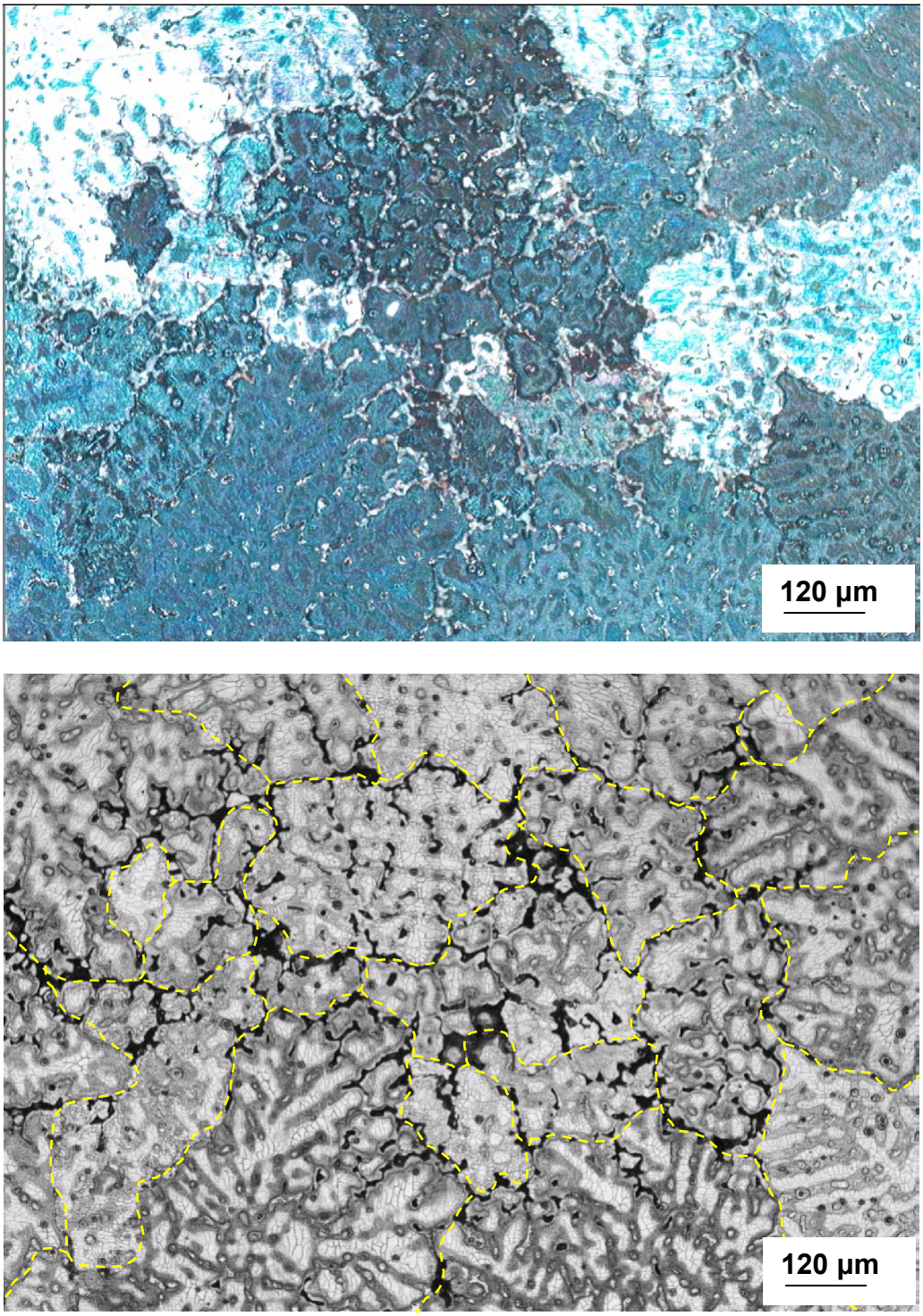

Figure 4-23: Micrographs showing the relationship between the grain structure and the distribution of pores in the rim section of the AZ91E casting treated with 0.10 wt% Sr. The mean grain size of this sample is 430µm.

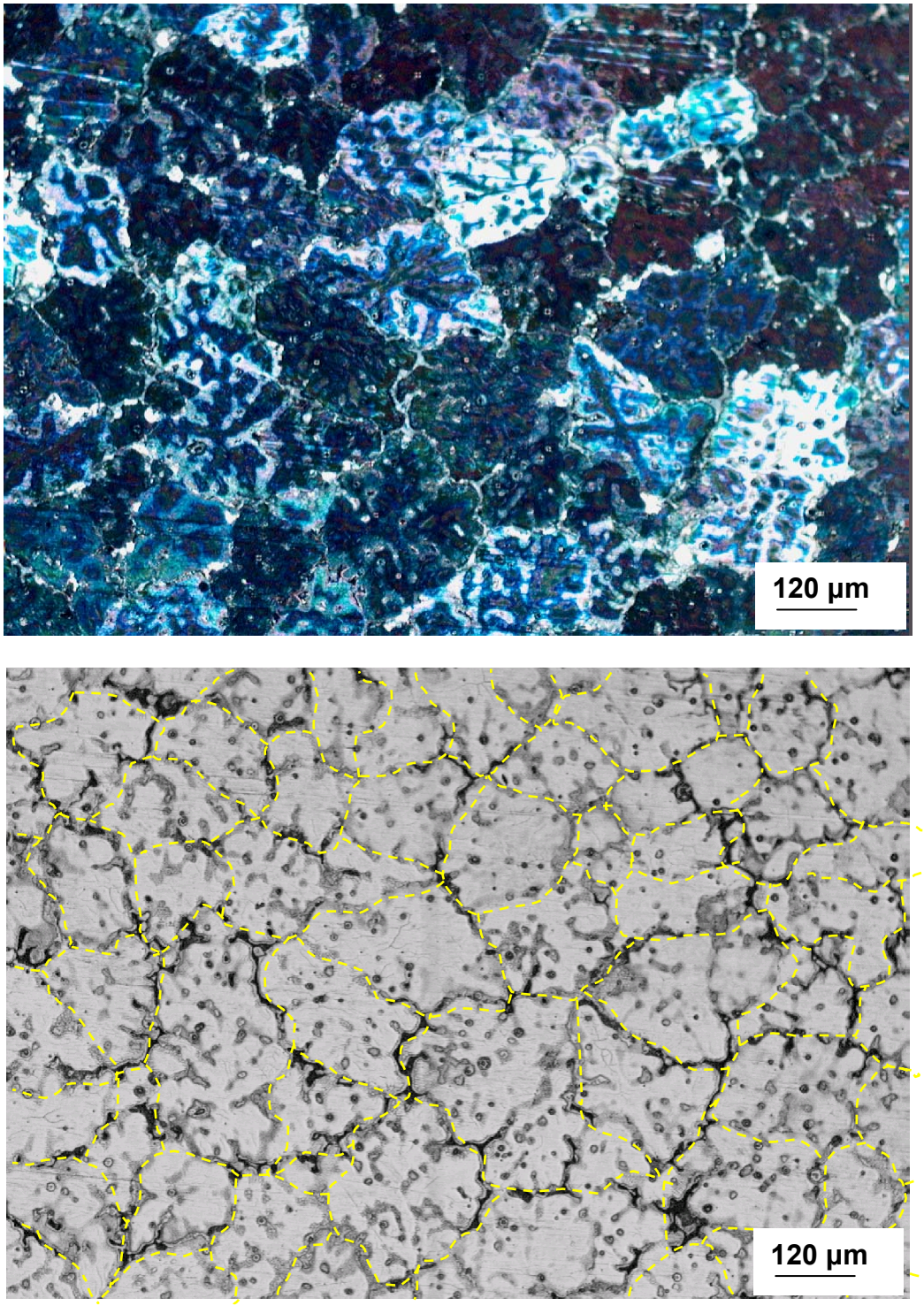

Figure 4-24: Micrographs showing the relationship between the grain structure and the distribution of pores in the rim section of the AZ91E casting treated with 0.005 w% C. The mean grain size of this sample is 215µm.

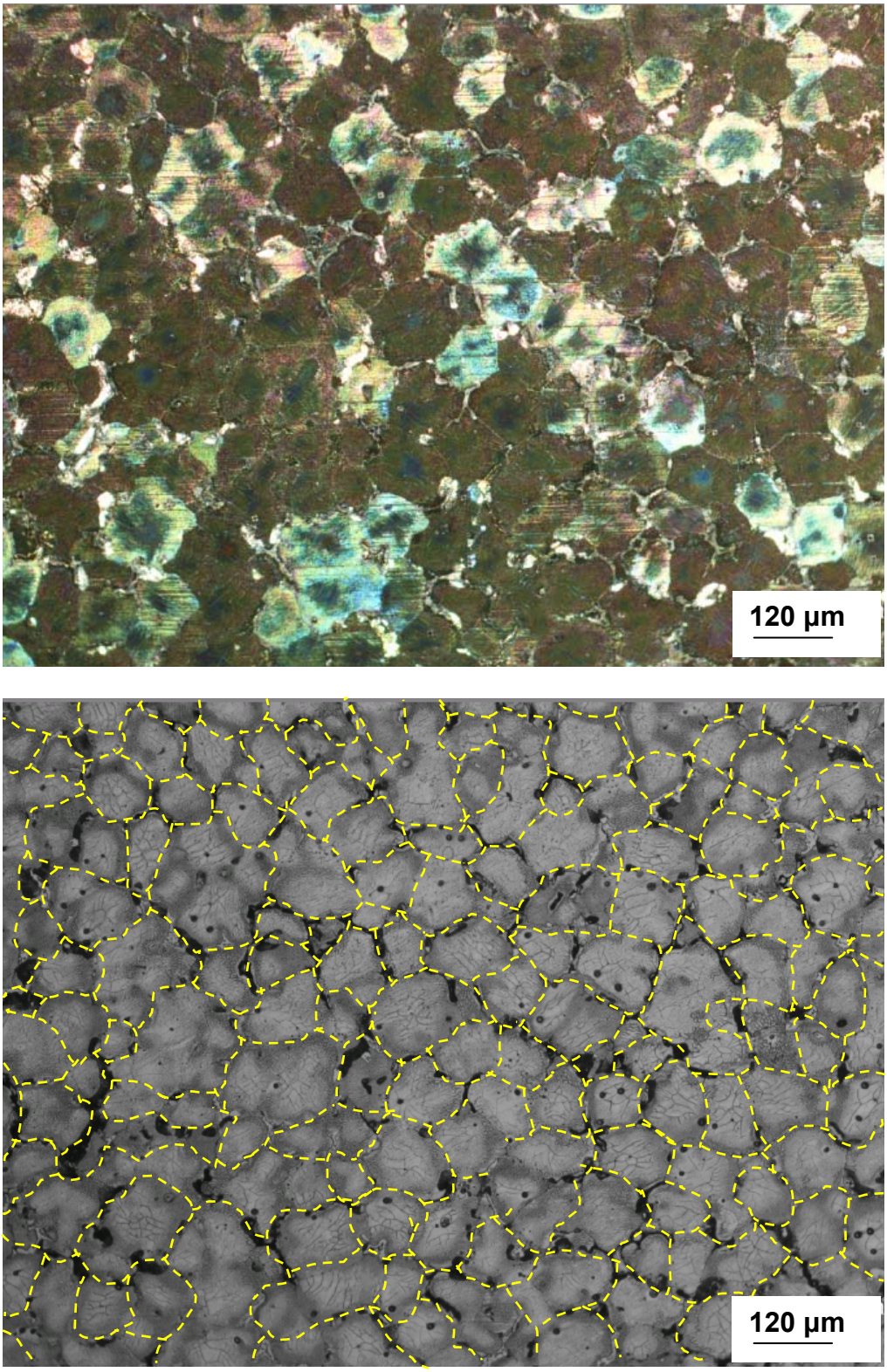

Figure 4-25: Micrographs showing the relationship between the grain structure and the distribution of pores in the rim section of the AZ91E casting treated with 0.02 wt% C. The mean grain size of this sample is 113µm.

Two samples were then chosen for further inspection using Scanning Electron Microscopy (SEM). The first was the rim section of the untreated AZ91E castings and the second, a fully grain refined rim section from the casting treated with the carbon containing tablet. Micrographs were taken of both samples to highlight any changes in microstructure, composition, or pore morphology with a severe reduction in grain size. In the case of these two samples there was an 82% reduction in grain size from 633µm to 113µm.

The first image shown in Figure 4-26 is of the general microstructure of the rim section of the untreated AZ91E casting. There were only small areas of pores throughout the entire rim section, one of which was captured in this image. The pores appear to be surrounding the cored magnesium grains, though there are some small singular pores in the sample that may be located within the grains. The lack of any visible grain boundaries under SEM makes this distinction difficult. Also surrounding the grains are small pockets of fully divorced eutectic. These are shown more clearly in Figure 4-27 with Energy Dispersive X-Ray (EDX) analysis of the light particles (Figure 4-28) confirming they are the $Mg_{17}Al_{12}$ intermetallic particles formed through an eutectic reaction.

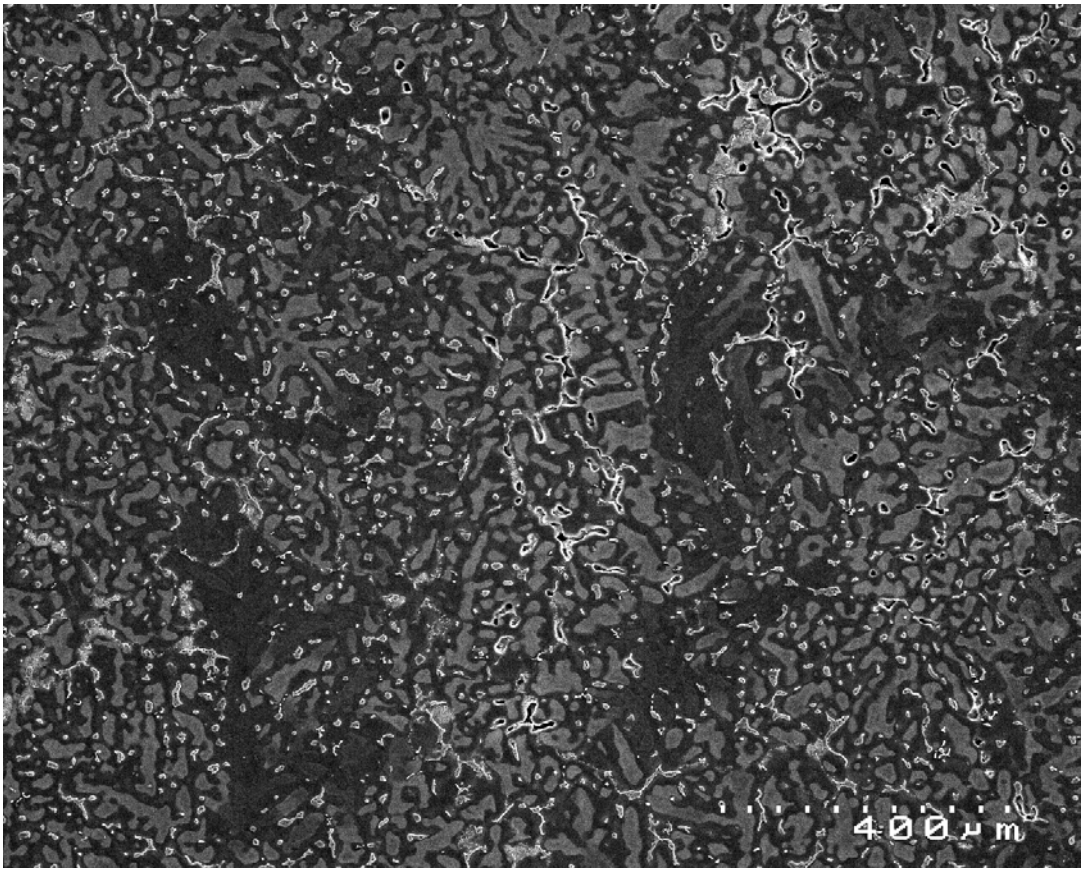

Figure 4-26: SEM micrograph of the rim section of the untreated AZ91E casting. A few small areas of localised pores were found in the centre of the rim section.

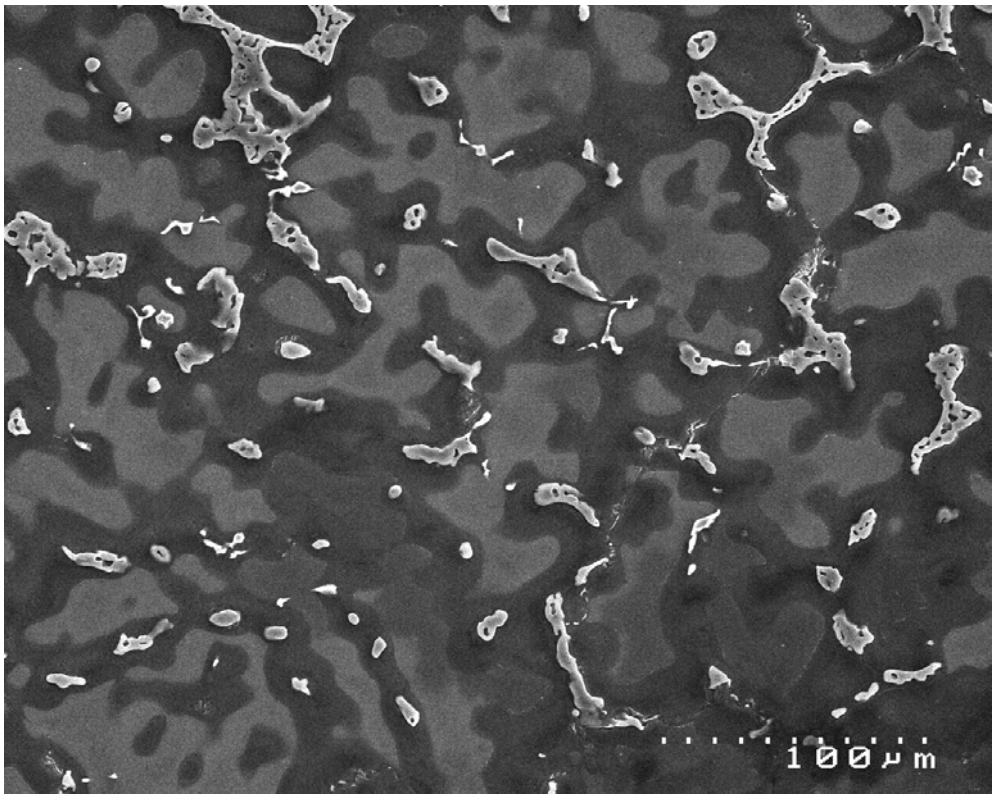

Figure 4-27: Higher magnification SEM micrograph of the rim section of the untreated AZ91E casting. Dark and light grey areas are the cored magnesium grains, with the lighter particles being the $Mg_{17}Al_{12}$ particles.

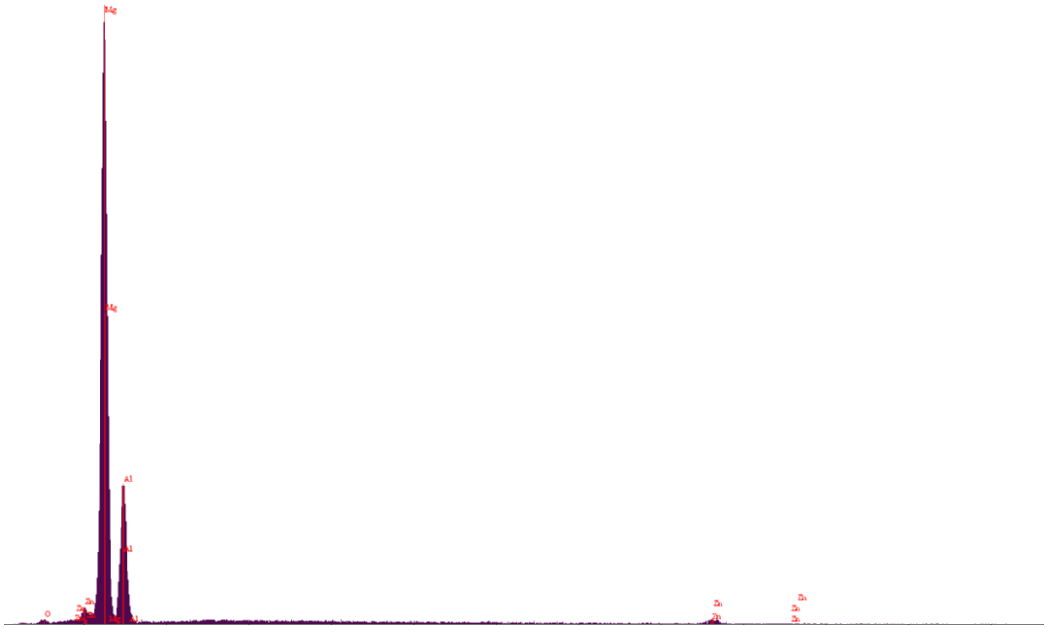

Figure 4-28: Energy Dispersive X-Ray (EDX) analysis of the lighter coloured particles confirming they are in fact the $Mg_{17}Al_{12}$ particles.

The next sample to be examined using SEM was a sample of the rim section from a fully grain refined AZ91E casting. This is the casting that was treated with the carbon containing tablet. In this sample small, cored globular grains were almost completely surrounded by fine interconnected pores. An example of the porous microstructure can be seen in Figure 4-29. Note that this image is at a higher magnification than Figure 4-26.

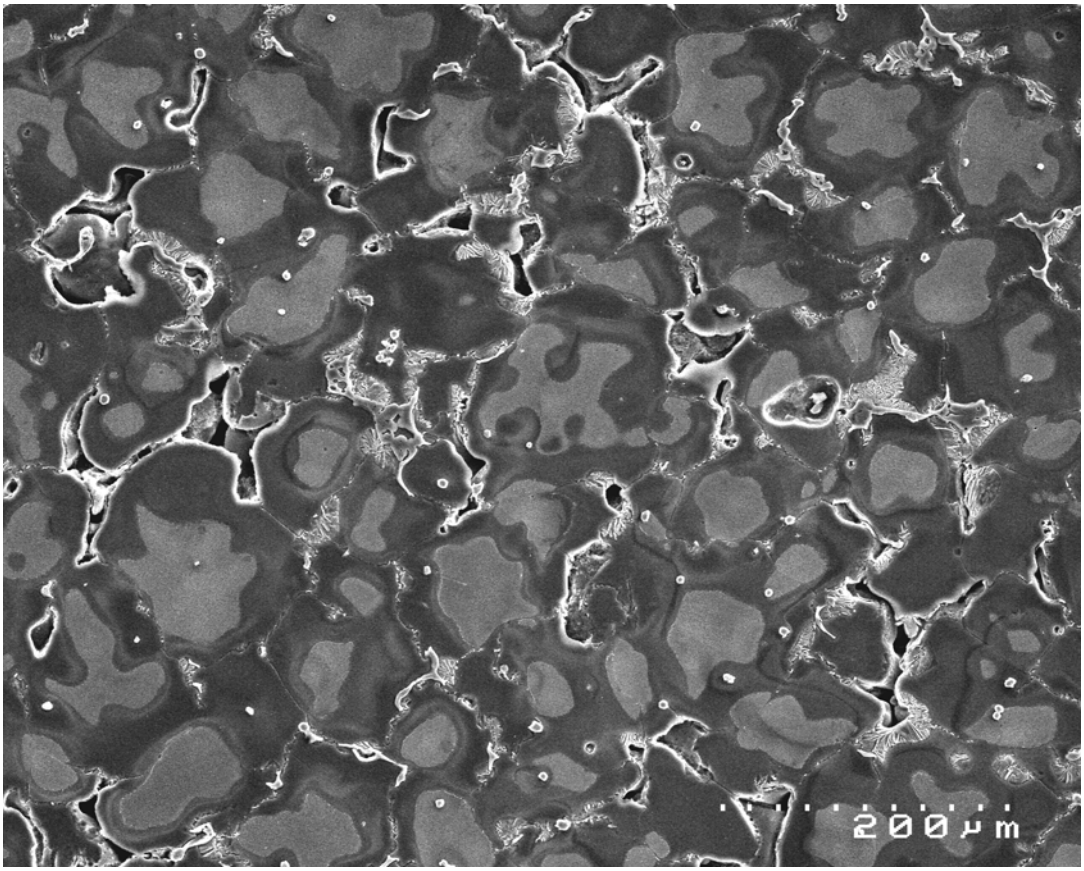

Figure 4-29: SEM micrograph of the microstructure of the rim section of the fully grain refined AZ91E casting.

An elemental map was produced of the above image to determine the distribution of the major elements thought to be present in the casting sample. The resulting X-ray elemental maps of magnesium, aluminium, manganese, zinc and carbon are shown in Figure 4-30.

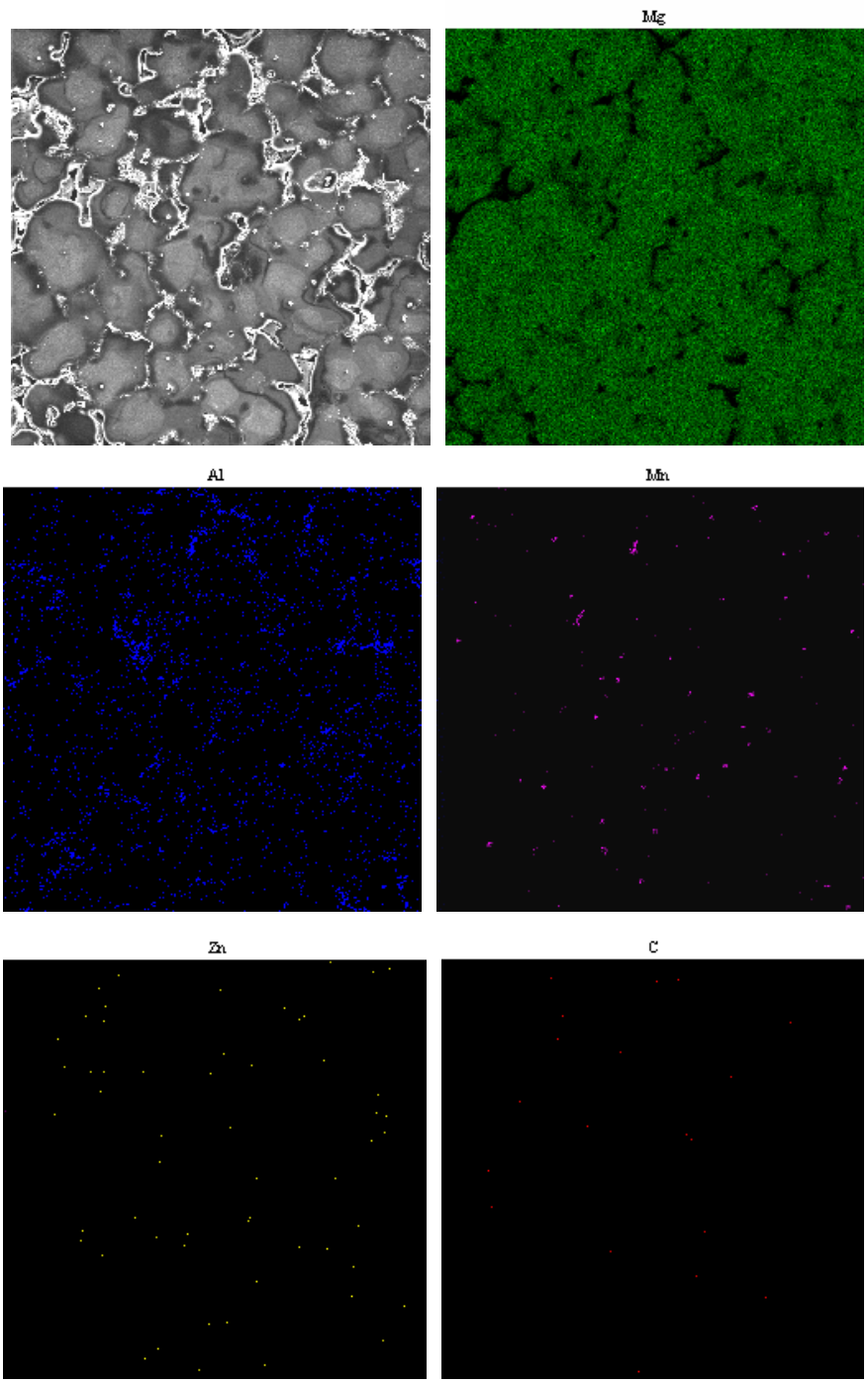

Figure 4-30: Elemental map of the casting sample taken from the same location as Figure 4-29.

The X-ray elementals map shown in Figure 4-30 show that along with the already known alloying elements of Mg, Al, Mn, and Zn present in the alloy there is also small traces of carbon. While these may be indicate the presence of carbon containing nucleant particles

such as Al_4C_3, there appears to be little correlation between the distribution of the carbon and the distribution of aluminium in the elemental map. There is a possibility that the particles may have been affected during sample preparation through reaction with the water used for lubrication and cooling. It is also important to note that the use of diamond particles during the polishing process may have also introduced carbon particles into the soft magnesium microstructure. The confirmation of the nucleant particles with carbon grain refinement using SEM is an area requiring future detailed work, though it is outside the scope of this thesis.

4.4 Discussion

4.4.1 Grain Size Measurement

Before discussing the effects of the grain refinement on the castability of AZ91E alloy it is important to review the techniques chosen for grain size analysis in this study and explain how they differ from conventional research, and why these results have more relevance to the casting industry. Much of the grain size data presented in the literature reviewed in Chapter 2 arises from samples that have been solution treated subsequent to casting and prior to grain size measurement. This is done to dissolve the $Mg_{17}Al_{12}$ eutectic compound that forms at the grain boundaries of Mg-Al alloy castings and hinders detection of grain boundaries, hence making grain size measurement difficult. The solution treatment often utilised for this eutectic dissolution involves heating the sample to around 400 °C and holding at this temperature for up to 24 hours [12, 15, 16]. As heating of metals to above 0.5Tm (where Tm is the melting point or liquidus temperature of a metal or alloy in Kelvin) often leads to grain growth, it is expected that such heat treatment to magnesium-aluminium alloys would cause the grains to grow, resulting in a larger measured mean grain size of the castings.

The dissolution of the $Mg_{17}Al_{12}$ eutectic compound combined with a possible alteration of grain size and morphology produces a major change to the microstructure of a casting

sample. As this investigation is focussed on the effects of grain refinement on the castability of Mg-Al alloys, it would be remiss not to report the grain size in its as-cast state. Therefore, the relationship between the grain size of the casting and its corresponding defect and porosity levels can be confidently identified.

A few researchers have managed to find ways of measuring the as-cast grain size of Mg-Al alloys without the need for solution treatment [17-20]. Methods usually involve the use of etchants that produce colour contrast between grains under polarised light or the employment of advanced image analysis software and grain boundary reconstruction. For the grain size measurements made in this investigation a combination of these methods was employed. Etchants such as acetic-picral and a newly developed AZ91 reagent [20] were used to distinctively colour individual grains in the casting specimens. A high-resolution digital image was then produced of the samples using a digital scanner. ImagePRO analysis software was employed to adjust the image brightness and contrast. This produced an image that could be clearly magnified showing distinct boundaries between the grains. This method is illustrated in Figure 4-31. Grain size measurements were made following the ASTM standard E-118 and at least 50 grains were counted in each of the five fields chosen for each sample. Employing this method of sample preparation and image analysis, along with the large number of grains counted for each sample, means that statistically accurate measurements were made for the as-cast grain size of the castings.

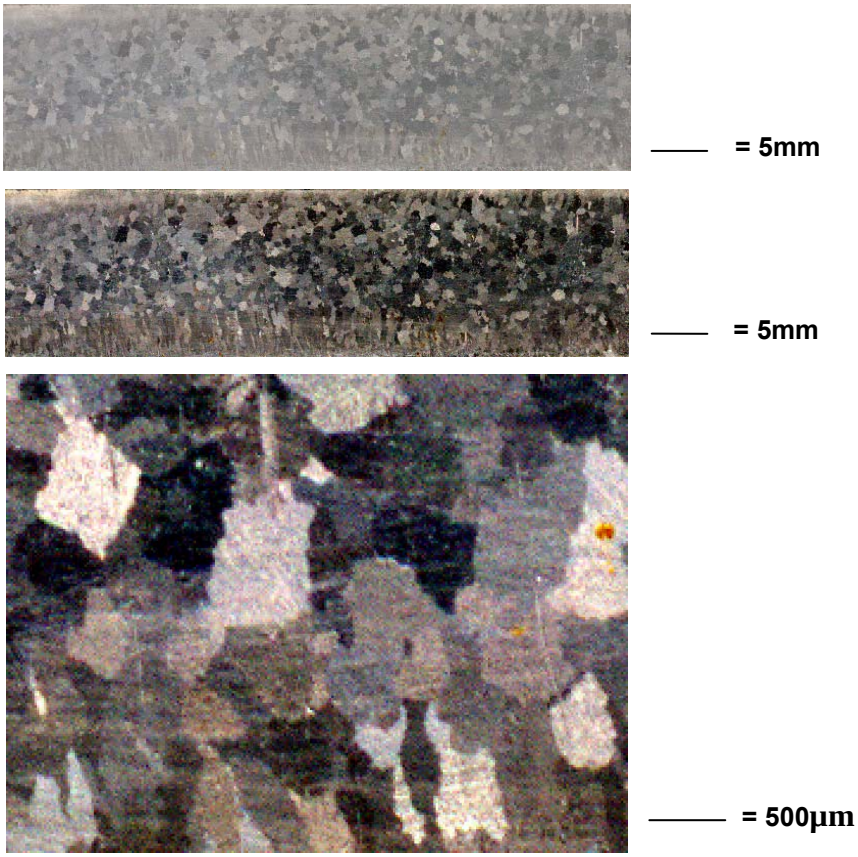

Figure 4-31: Illustration of the grain size measurement preparation used in the investigation. The image at the top is a digitally scanned image of the spoke section of a casting. The middle image is the same sample after image processing using ImagePRO software.

4.4.2 The Grain Refinement of AZ91E Castings

The literature review presented in Chapter 2 of this thesis suggested a range of potential grain refiners for AZ91E castings [4, 10, 12, 13, 15, 16, 19, 21, 22]. Due to the two established theories of solidification based on the effect of solute elements or the presence of suitable nucleation sites, one grain refiner of each type was chosen. Strontium was added to the AZ91E melts as a solute element, and carbon was added to promote suitable sites for heterogeneous nucleation.

The addition of strontium in the form of an Al-10wt% Sr master alloy enabled the concentration of strontium in the AZ91E to be raised to the desired levels of 0.05 wt% and 0.10 wt% Sr respectively. The strontium addition produced grain refinement in all

sections of the castings. In the thinner casting sections of the spoke and the rim, where solidification is faster, the level of grain size reduction increases linearly with an increase in strontium. In the thicker casting sections of the hub and the spoke/rim junction, the results were not as consistent. The hub exhibited significant refinement with 0.05 wt% Sr, but no further refinement when 0.10 wt% Sr was added. The spoke/rim junction showed no refinement with the initial addition rate but significant refinement with 0.10 wt% Sr.

Overall, a grain size reduction of approximately 200μm was realised with the use of Sr as a grain refiner. The results experienced in this investigation correlate well with other studies on the effect of Sr as a grain refiner for AZ91 castings. Wallace et al [22] found 0.05 wt% Sr had significant grain refinement effects on AZ91E especially in the slower cooling casting sections. This is in agreement with the results of this study, as the smallest grain size achieved using AZ91E was in the spoke/rim junction where the grain size was reduced to 300μm with 0.10wt% Sr added. Lee et al [23] reported that the addition of between 0.1 and 1.0 wt% Sr to a Mg-9 wt% Al alloy yielded fluctuating results, although reductions to grain size were noted. In their study on the effect of strontium on microporosity levels of magnesium sand castings, Aliravci et al [19] noted that even after grain refinement with carbon containing C_2Cl_6 tablets, the addition of Sr lead to a further reduction in casting grain size.

The reason for the grain refining effect of strontium is not fully understood. However, the effect that strontium has on the growth of α-Mg grain during solidification can be explained by the growth restriction effect as discussed in Chapter 2. The rejection of the solute ahead of the growing solid/liquid interface slows the growth of the grains. It has been suggested [24] that strontium poisons the grain surface during solidification, or poisons the fast growing direction of the grains due to preferential adsorption of strontium in these areas. The addition of strontium is said to cause films of strontium to be formed at the boundaries of growing crystals which slow their growth. The slowing of the growth rate at the individual faces of primary Mg crystals also provides sufficient time for the melt to create more nucleation events [19] and therefore a smaller mean grain

size. It is not in the scope of this thesis to investigate the reasons for grain refinement but rather to investigate the effect of grain refinement on the castability of Mg-Al alloys. Therefore, no further work has been done in this area.

The major issue surrounding the grain refinement of Mg-Al alloys with carbon relates to the introduction of sufficient carbon to the melt in order to achieve successful grain refinement. In this study it was found that when carbon was added to the melt in the form of carbon black powder wrapped in an aluminium foil neither of the nominal carbon addition levels were achieved in the castings. Table 4-5 shows that when the 0.05 wt% C was added to the melt in the form of carbon black powder wrapped in an aluminium foil, only 0.005 wt% C was present in the final casting, and when 0.10 wt% C was added to the melt only 0.007 wt% C was present in the final casting. The solubility of carbon in magnesium is very low at approximately 20 ppm [8] therefore there is more carbon in the final casting than just dissolved carbon, but not nearly as much as had been added to the melt in the first instance. It is suspected that the majority of carbon added in this way is trapped in the oxide layer on the top of the melt in the crucible and is removed prior to pouring of the casting.

Despite the low levels of carbon content achieved in the final castings, significant grain refinement was still experienced. A reduction in grain size from approximately 600μm to around 200μm was achieved with an addition of 0.005 wt% C. Further refinement was not achieved by increasing addition to 0.007 wt% C, in fact the resulting grain size was slightly larger than that achieved with the lesser addition. This result proves that the addition of ultra-fine carbon black particles is an effective form of producing suitable nucleation sites for solidification. It also proves that adding the powder in this manner is not an efficient method of introducing carbon into the castings.

The development of the carbon-containing pressed tablets during this study produced interesting results. The carbon level detected by the leco-combustion analysis in the castings produced using the tablet was 0.02 wt% C. This is much closer to the desired nominal addition level of 0.05 wt% C. It would appear that the design of the tablet for

slower release of carbon into the melt has been effective in giving more contact time between the carbon and the melt. The use of these tablets during melt preparation has resulted in the smallest grain sizes achieved in the study. An example of this is seen in the spoke section of the AZ91E casting where the grain size is reduced by 80% from 650μm to 130μm. This shows that adding carbon in the form of pressed tablets of magnesium alloy, aluminium, and carbon composite powder is an effective means of introducing carbon to the Mg-Al melt.

As discussed in Chapter 2, carbon is only effective as a grain refiner to magnesium alloys that contain aluminium and adding carbon to pure magnesium melts has no effect on casting grain size. This suggests that the grain refinement effect produced is due to a reaction between the aluminium in the alloy and carbon. The exact nature of the particles responsible for the heterogeneous nucleation has not been identified, though it is strongly believed to be Al_4C_3 or a compound of Al-C-O [8].

Overall, the use of strontium and carbon as grain refiners for AZ91E has been very successful, with a wide range of grain sizes achieved in the castings. The wide range of grain sizes achieved in the casting samples allows further investigation to fully understand the effect of grain refinement on the castability of the alloy.

4.4.3 The Effect of Grain Refinement on External Casting Defects

The first stage in assessing casting quality in any casting operation is the initial visual inspection for external defects. Castings need to be inspected for shape abnormalities arising through misruns (when the casting mould is not filled completely) or from slumping of the casting surface. The surface must also be inspected for the presence of defects resulting from hot tearing or porosity. This initial examination allows for castings to be rejected prior to any further machining or painting processes that add to the cost of production. Obviously an alloy with good castability is the one that allows production of complex castings which would, for the most part, pass this initial inspection.

While the visual inspection of castings is always a qualitative assessment, efforts have been made in this work to quantify the assessment, as explained in Section 4.3.4. Subsequently plotting this severity against corresponding grain size, allows the effect of grain refinement on the castability of AZ91E to be better identified.

In the experimental castings, the surface slumping defect is located on either side of the hub and spoke/rim junction sections of the castings. For consistency the mean grain size of only one of these sections was used for the analysis. In this case it was the grain size of the spoke/rim junction, although there is little discrepancy between the two. Figure 4-32 shows the effect of grain refinement on the surface slumping of AZ91E castings. A strong linear trend is apparent between the level of grain refinement achieved and the severity of surface slumping; as grain size is decreased in the castings the surface slumping severity increases greatly.

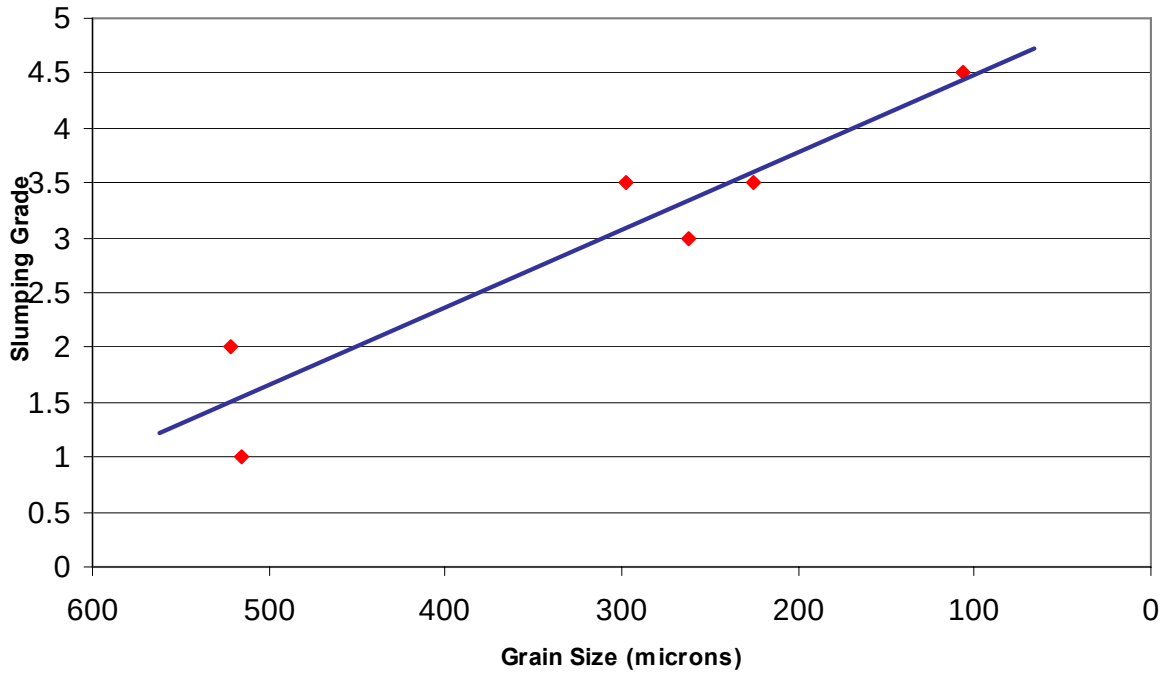

Figure 4-32: Severity of surface slumping in AZ91E castings as a function of average grain size.

The mechanism responsible for the occurrence of surface slumping is solid feeding of the casting. This occurs in the latest stages of solidification when the internal pressure

created from volumetric shrinkage is accommodated by the drawing in of the casting surface. In a casting that has a large grain size, the channels that are utilised during interdendritic feeding of a hot spot remain open for a longer amount of time. Therefore, a grain refined casting will have more volumetric shrinkage to overcome in the final stages of solidification. Hence grain refined castings are more likely to have a large amount of solid feeding/surface slumping.

The grain refinement of the AZ91E casting had little effect on the occurrence of external shrinkage porosity. One trend that was apparent however, was that when shrinkage was noted at the surface of the castings, the corresponding surface slumping levels were lower. This is due to some of the pressure created by the volumetric shrinkage in the hot spot being alleviated when the macroscopic shrinkage pore formed, creating less pressure on the surface of the casting causing it to slump.

As stated previously, hot tearing is one of the most serious defects from which a casting can suffer [25]. It is a defect that has the appearance of a tear in the casting and results from uniaxial tensile failure in a weak material. Hot tearing was apparent in a few of the experimental castings produced with AZ91E, and once again when plotting the severity of the defect against its corresponding grain size a significant trend is apparent as shown by Figure 4-33.

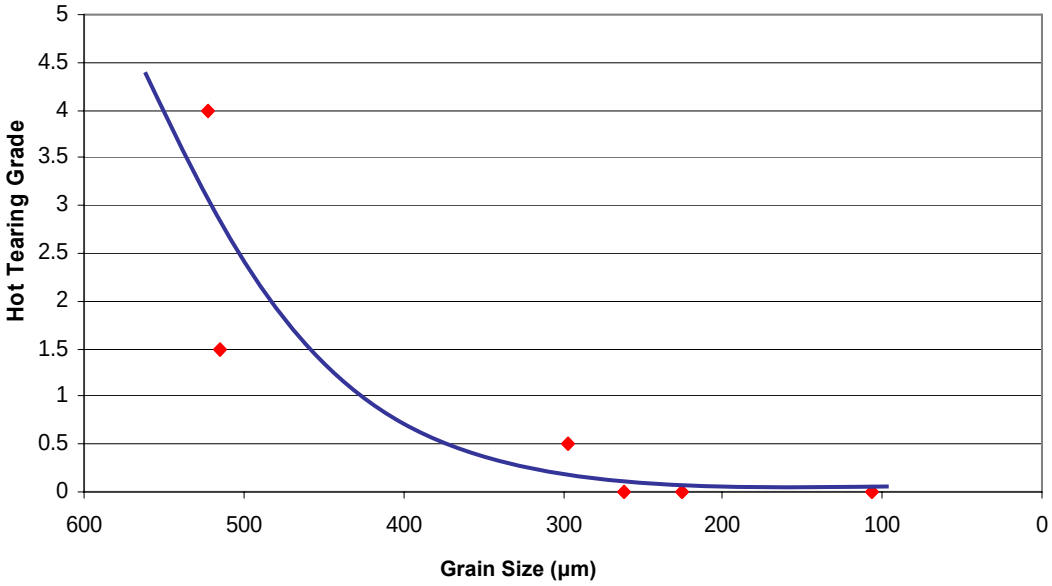

Figure 4-33: Hot tearing severity in the AZ91E castings as a function of average grain size.

This study proves that the occurrence and severity of hot tearing is strongly dependent on grain size. An increase in the degree of grain refinement of AZ91E casting leads to a reduction in the tendency for hot tearing. This is a trend which is also seen in aluminium alloys, with Easton et al [26] showing that grain refinement of A356 reduced hot cracking tendency.

Little research has been published on the effect of grain refinement on the hot tearing susceptibility of magnesium alloys. One study of different grain refiners for AM50A [22] showed that there was no hot tearing in the castings when C_2Cl_6 was used as a degassing/grain refinement addition, although there was little tearing in the unrefined castings to begin with. The advantage of the current research is that it not only reports on the presence or absence of hot tearing, but also the severity of the defect. This gives an idea as to how the defect behaves with different levels of grain refinement and indicates the sensitivity of the defect to grain size.

A hot tearing defect results from the uniaxial tensile failure of the casting due to the stresses imparted on it by solidification shrinkage. Magnesium alloys have a long

freezing range, which means that like other alloys of this nature, they are particularly susceptible to this defect [27]. A long freezing range means that there is often a large amount of semi-solid material present when the shrinkage forces are acting, and this causes castings to fail more easily. The reason this study showed that increased grain refinement caused a decrease in hot tearing is because having a smaller grain size makes it more difficult for cracks to propagate through the casting structure. Any semi-solid material is also spread more thinly so its impact on hot tearing susceptibility is greatly reduced. The decrease in average grain size also leads to an increase in strength of the granular network, meaning it is more difficult for the material to be torn apart.

4.4.4 The Effect of Grain Refinement on the Level of Porosity

As AZ91E has a relatively large freezing range of 130°C, the formation of pores during solidification through the mushy zone is more difficult to avoid than in many other casting alloys. There is much conjecture with aluminium alloys as to the effects of grain refinement on the occurrence of porosity [26, 28] and little work has been published on the effect of grain refinement on the porosity levels of magnesium castings. The results presented in Sections 4.3.5 and 4.3.6 show that the reduction in grain size through the addition of both strontium and carbon had a negative impact on porosity levels. The porosity level data from the separate casting section are more indicative of the absolute level of internal porosity in the castings, therefore it is these results that will be discussed here.

To more clearly illustrate the effect of grain refinement on porosity levels, the data was plotted in such a way that each separate grain size measurement was matched with its corresponding porosity level. This is regardless of which grain refiner was used or its level of effectiveness. The data was also separated by casting section size to clarify the trends, as thinner casting sections have inherently lower porosity levels than thicker sections. Gathering the data in this way allows the effect of grain refinement on porosity level in AZ91E to be clearly illustrated.

Figure 4-34 shows the relationship between grain size and porosity level for the thin spoke and rim sections of the AZ91E castings. It shows that an increase in grain refinement leads to an increase in the level of internal porosity in the spoke and rim of the AZ91E castings. It appears that there is a critical grain size of around 300µm where casting porosity levels rise sharply in the thinner casting sections. The porosity levels of both sections increase rapidly around this point, although the porosity level in the spoke section appears to increase more rapidly. This is due to position of the spoke being located between the two large casting sections of the hub and spoke/rim junction, and so it relies more heavily on the efficient feeding of liquid metal to the required areas during solidification. In the case of the rim section the feeding efficiency is also greatly reduced, however it had little reliance on feeding from the reservoirs of the hub or spoke rim junction due to its location.

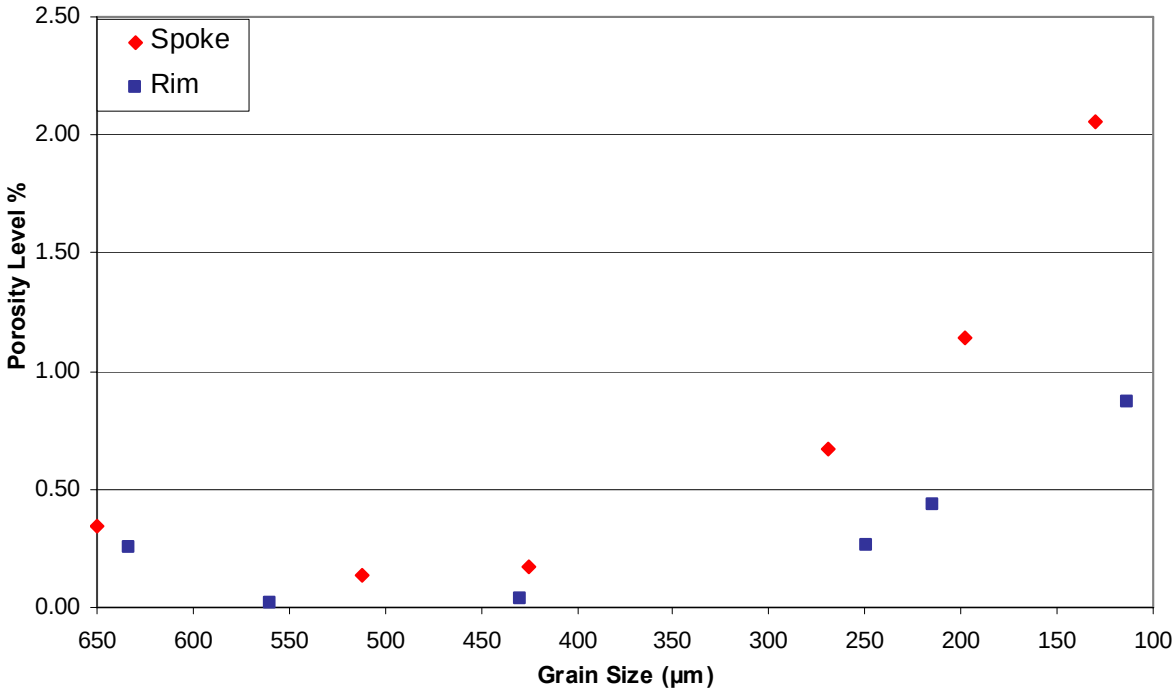

Figure 4-34: The relationship between average grain size and porosity level in the spoke and rim sections of the AZ91E castings.

Figure 4-35 shows the effect of grain refinement on the thicker casting sections of the hub and spoke/rim junction. As with the thinner sections, an increase in grain refinement of the spoke/rim junction leads to a dramatic increase in internal porosity level. In the

hub section however, as the degree of grain refinement is increased the casting porosity levels remain largely unchanged. The reason for the increase in porosity level with increased grain refinement has been discussed previously. The reliance on feeding late in solidification through the interdendritic network means that as grain size is reduced, the interdendritic network becomes a finer. This means that the pressure which is required to be overcome for interdendritic feeding is increased greatly, and feeding efficiency is greatly reduced. The large increases in porosity level experienced in the spoke/rim junction clearly illustrates this phenomenon, as this section obtains feeding liquid through the hub and spoke sections so the constriction of feeding paths through grain refinement in these areas would have a significant effect on the occurrence of porosity.

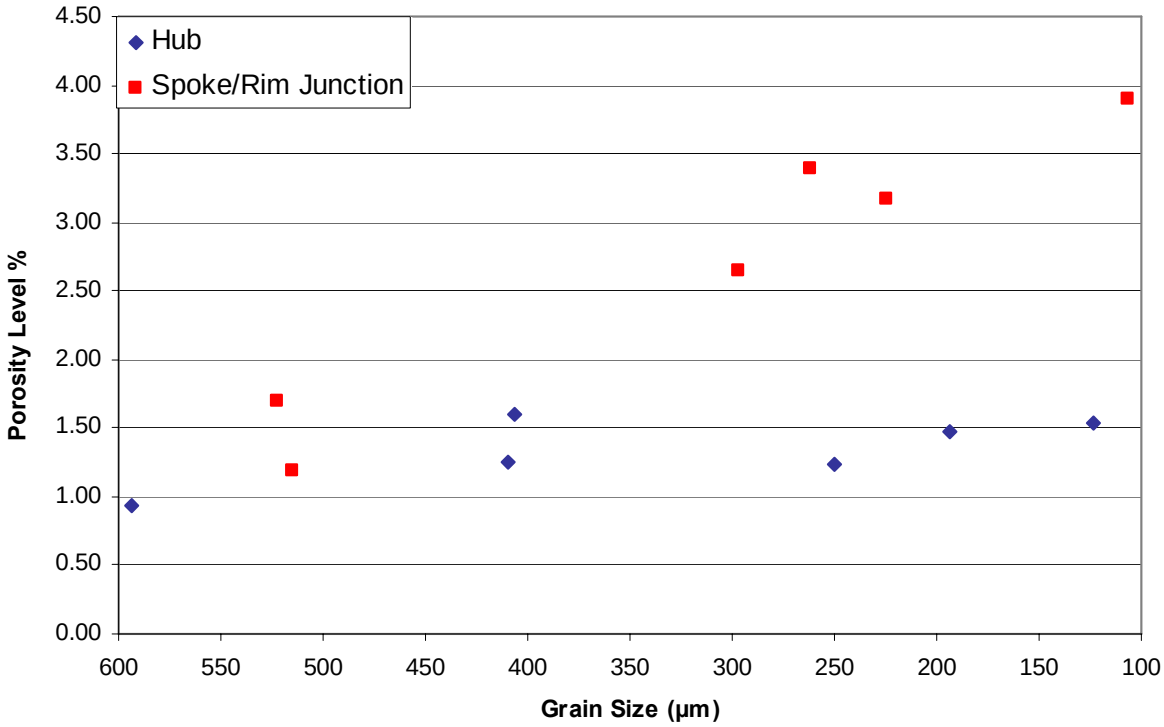

Figure 4-35: The relationship between grain size and porosity level in the hub and spoke/rim sections of the AZ91E castings.

In aluminium castings that solidify directionally, it has been found that grain refinement actually decreases the level of shrinkage porosity. Assuming that this is consistent for magnesium castings, the explanation as to why this work has shown an increase of

porosity level with grain refinement can be found by inspecting the way that the separate feeding mechanisms operate. In castings that are grain refined the dendrites are shorter and so the coherency point is reached later. Therefore, mass feeding continues for longer in the solidification process resulting in the grain refined casting being fed more efficiently in the earlier stages of solidification. It will only be for shorter feeding distances that interdendritic feeding plays an important role, and this is why grain refinement may benefit directionally solidified castings.

As shown in the MAGMAsoft simulations in Figure 4-15 and Figure 4-16, the experimental casting mould used in this investigation does not solidify directionally and so the feeding of castings through the interdendritic network in grain refined castings is more difficult. Therefore, although grain refinement increases feedability at a lower fraction of solid in a casting with finer grains, the pressure required for feeding will increase more rapidly with fraction of solid than in a casting with coarser grains [26]. This is shown schematically in Figure 4-36.

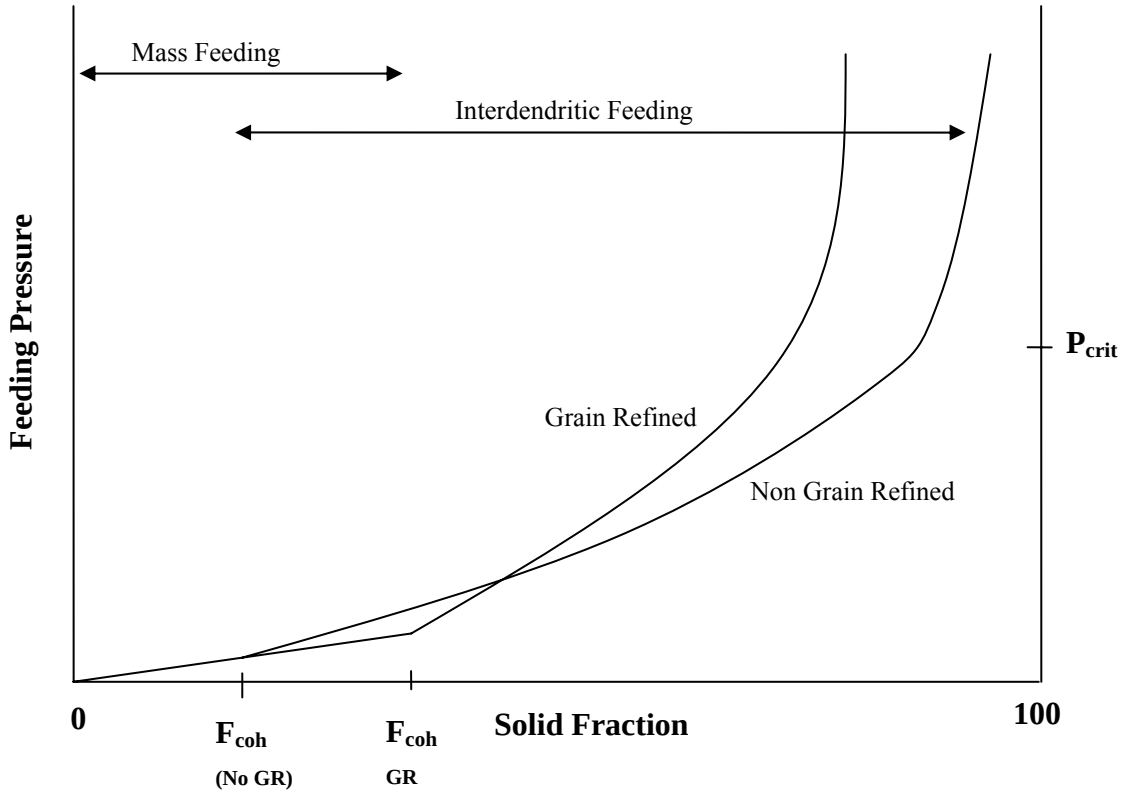

Figure 4-36: A hypothetical schematic of the pressure required for feeding as a function of fraction of solid for grain refined and non grain refined castings. It is assumed that P_{crit} is the same for both castings, although there is no evidence to suggest this is the case. Modified from Easton and StJohn [26].

Figure 4-36 shows that although dendrite coherency occurs later in grain refined castings, interdendritic feeding becomes more difficult as solidification proceeds. Therefore there will be a point where the feeding channels will cease to be effective, denoted as P_{crit} in the diagram. This point is reached sooner in grain refined castings. P_{crit} is the point where the spoke/rim junction of the experimental casting will cease to be fed and so grain refinement has an effect on the level of porosity in this area as was found to be the case. Therefore, the advantage of increased mass feeding is of little consequence to a casting of this nature when the casting geometry allows for such a hot spot to occur.

4.5 Conclusions

This study produced significant results and has lead to a greater understanding of the effects of grain refinement on the castability of AZ91E alloy. The specially designed experimental casting mould was successful in emulating many common casting defects, and the correlation between the severity of these defects and the average grain size of the castings has been established. The use of strontium and carbon as grain refiners for AZ91E produced a range of grain sizes allowing the sensitivity of casting defect occurrence and severity to grain size to be further understood. The main conclusions from this study are as follows:

- Strontium had a significant effect of the grain size of all sections of the castings produced. The highest level of grain refinement was obtained with an addition of 0.10 wt% Sr to the melt prior to casting.

- The addition of carbon black powder wrapped in aluminium foil was effective in refining the microstructure of the castings although results were inconsistent. This lead to the development of an effective means of introducing carbon into a Mg-Al melt, which resulted in higher carbon contents and significant grain refinement in all castings produced. The grain size of the castings treated using this method was reduced by approximately 80%. This method of introducing carbon involved producing a magnesium alloy/carbon powder by high energy mechanical milling and subsequent pressing of this powder to form small tablets that facilitate the slow release of carbon when added to the casting melt.

- Grain refinement was found to have a strong negative effect on the severity of surface slumping in the castings produced. As grain size was reduced, the severity of surface slumping increased dramatically.

- A relationship between grain refinement and hot tearing severity in AZ91E has also been established. Increased grain refinement leads to the reduction of the severity of hot tearing, and eventually a complete elimination of this defect.

- Grain refinement has also been found to have a profound effect on the internal porosity levels of AZ91E castings. The study found that in the thinner casting sections, the porosity level increases sharply once the grain size was reduced below 300μm. The thicker spoke/rim junction section of the casting displayed a strong trend of increased porosity with decreasing grain size. This was due to the refinement of the interdendritic network in the castings reducing the efficiency of feeding network, which in turn lead to an increase in pore formation

- Microscopic examination of the internal structure of the castings showed that as grain size is reduced, the location of pores tends to shift from both within the grains and along grain boundaries, to being situated solely along the grain boundaries.

4.6 References

[1] Sequeira, W. P., Murray, M. T., Dunlop, G. L. and StJohn, D. H., *Effect of Section Thickness and Gate Velocity on the Microstructure and Mechanical Properties of High Pressure Die Cast Magnesium Alloy AZ91D.*

[2] Han, Q., Kenik, E. A., Agnew, S. R. and Viswanathan, S., *Solidification Behaviour of Commercial Magnesium Alloys.* Magnesium Technology 2001 J. R. Hyrn TMS (2001).

[3] Li, P., Tang, B. and Kanalova, E. G., *Microstructure and Properties of AZ91D Alloy with Ca Additions.* Materials Letters **59** 671-675 (2005).

[4] Renger, K. and Simon, R., *Grain Refinement of AZ91 by Nucleant 5000.* 1st Int. Light Metals Technology Conf. 2003 A. K. Dahle Brisbane (2003).

[5] Avishai, A., Bamberger, M., Kaplan, W. D. and EAghion, E., *The Effect of Cooling Rate on the Solidification of AZ91 Magnesium Alloy.* 3rd International Magnesium Conference.

[6] *www.matweb.com Online Materials Database.*

[7] Nelson, C. E., *Grain Size Behaviour in Magnesium Casting Alloys.* AFS 52nd Annual Meeting Chicago, IL. American Foundryman's Society 1-23 (1948).

[8] Qian, M. and Cao, P., *Discussions on Grain Refinement of Magnesium Alloys by Carbon Inoculation.* Scripta Materialia **52** 415 - 419 (2005).

[9] Jin, Q., Eom, J. P., Lim, S. G., Park, S. W. and You, B. S., *Reply to Comments on Grain Refining Mechanism of a Carbon Addition Method in a Mg-Al Alloy.* Scripta Materialia **52** 421-423 (2005).

[10] Glasson, F. L. and Emley, E. F., *Heterogeneous Nucleation in the Solidification of Aluminium and Magnesium Alloys.* The Solidification of Metals London 1-9 (1967).

[11] Jin, Q., Eom, J. P., Lim, S. G., Park, W. W. and You, B. S., *Grain Refining Mechanism of a Carbon Addition Method in a Mg-Al Magnesium Alloy.* Scripta Materialia **49** 1129-1132 (2003).

[12] Thomson, J. P., Liu, P., Sadayappan, M. and Sahoo, M., *Effect of C_2Cl_6 on Mechanical Properties and Microstructure of Gravity Permanent Mold Cast AZ91E.* 108th American Foundryman's Society Metalcasting Congress Des Plaines, IL, USA AFS (2004).

[13] Thomson, J. P., Xu, S., Sadayappan, M., Newcombe, P. D., Millette, L. and Sahoo, M., *Low Pressure Casting of Magnesium Alloys AZ91 and AM50.* 108th American Foundryman's Society Casting Congress Des Plaines IL, USA AFS (2004).

[14] Davis, J. A., Eastwood, L. W. and DeHaven, J. C., *Grain Refinement in Magnesium Casting Alloys.* AFS Transactions **53** 352-362 (1945).

[15] Thomson, J., Fasoyinu, F. A., Sadayappan, M. and Sahoo, M., *Casting Characteristics of Permanent Mold Cast Mg-Alloy AZ91E.* AFS Transactions (2002).

[16] Nishino, N., Kawahara, H., Shimizu, Y. and Iwahori, H., *Grain Refinement of Magnesium Casting Alloys by Boron Addition.* Magnesium Alloys and their Applications K. U. Kainer Wiley-VCH 59-64 (2000).

[17] Avishei, A. and Bamberger, M., *Relation Between Cooling Rates and Microstructures in Gravity Cast AZ91D Disks.* Metallurgical and Materials Transactions B **30B** 723-729 (1999).

[18] Riddle, Y. W., Barber, L. P. and Makhlouf, M. M., *Characterisation of Mg Alloy Solidification and As-Cast Microstructures.* Magnesium Technology 2004 A. Luo 203-208 (2004).

[19] Aliravci, C. A., Gruzleski, J. E. and Dimayuga, F. C., *Effect of Strontium on the Shrinkage Microporosity in Magnesium Sand Castings.* AFS Transactions 1992 AFS **100** 353-362 (1992).

[20] Maltais, A., Dube, D., Fiset, M., Laroche, G. and Turgeon, S., *Improvements in the Metallography of as-cast AZ91 Alloy.* Materials Characterization **52** 103-119 (2004).

[21] Dahle, A. K., Lee, Y. C., Nave, M. D., Schaffer, P. L. and StJohn, D. H., *Development of the As-Cast Microstructure in Magnesium-Aluminium Alloys.* Journal of Light Metals **1** 61-72 (2001).

[22] Wallace, J. F., Schwam, D. and Zhu, Y., *The Influence of Potential Grain Refiners on Magnesium Foundry Alloys.* AFS 2003 1-15 (2003).

[23] Lee, Y. C., Dahle, A. K. and StJohn, D. H., *Grain Refinement of Magnesium.* Magnesium Technology 2000 H. I. Kaplan, et al. TMS 211-218 (2000).

[24] Gruzleski, J. E. and Aliravci, C. A., *Low Porosity Fine Grained Strontium Treated Magnesium Alloy Castings.* United States Patent Office (1992).

[25] Campbell, J., *Linear Contraction of the Casting.* Castings Butterworth-Heinemann Ltd 209-240 (1991).

[26] Easton, M. and StJohn, D. H., *The Effect of Grain Refinement on the Formation of Casting Defects in Alloy 356 Castings.* Int. J. Cast Metals Res. **12** 393-408 (2000).

[27] Viano, D., StJohn, D. H., Caceres, C. H. and Grandfield, J., *Hot tearing of Aluminium-Copper Alloys.* 1st Int. Light Metals Technology Conf. 2003 A. K. Dahle Brisbane 247-250 (2003).

[28] Kashyap, K. T. and Chandrashekar, T., *Effects and Mechanisms of Grain Refinement in Aluminium Alloys.* Bull. Mater. Sci. **24** 345-353 (2001).

5.0 The Effect of Grain Refinement on the Castability of Magnesium Alloy AM60B

This chapter presents the results of the investigation assessing the effect of grain refinement, achieved by additions of strontium and carbon, on the castability of commercial purity Mg-Al alloy AM60B. The chapter begins with an introduction to AM60B, followed by a brief summary of the experimental techniques used. This is followed by the presentation of the results gathered and a discussion of the results analysed in relation to the literature. The chapter ends with a section summarising the conclusions drawn from the investigation.

5.1 Introduction

The AM60 alloy was chosen as the subject of this investigation as, along with AZ91, it is one of the most common magnesium alloys used in producing cast components. The two major alloying elements in this alloy are aluminium and manganese. Unlike AZ91 there are only two alloys in the AM60 family, those being AM60A and AM60B.

AM60 alloys have greater toughness and ductility than AZ91 alloys, although they possess slightly lower strength. AM60B is often chosen for automotive structural applications such as wheels and suspension components due to its higher ductility and resistance to cracking. The ASTM standard composition specifications for the composition limits of alloy AM60B are listed in Table 5-1.

Table 5-1: ASTM composition specifications of alloy AM60B .

Element	Composition (wt%)
Mg	Balance
Al	5.5-6.5
Mn	0.25-0.6
Zn	0.22 max
Si	0.1 max
Fe	0.005 max
Cu	0.01 max
Ni	0.002 max
Other (each)	0.01 max
Other (total)	0.2 max

The aim of this investigation is to determine the effects of grain refinement on the castability of AM60B. Two separate grain refiners at different addition levels are used to attain different levels of grain refinement. The castings are representative of those produced in industrial automotive setting, but are cast under controlled laboratory conditions. In this way, the effect of grain refinement on the castability of AM60B can be accurately defined. The results of this study are directly applicable to the large scale production of permanent mould castings of AM60B.

5.2 Casting Procedure

Commercial purity Mg-Al alloy AM60B was melted in 1kg batches using an Inductotherm induction furnace under a protective atmosphere of 50% CO_2, 49% dry air, and 1% SF_6. The alloy ingots were first ground, using silicon carbide paper, to remove the thick oxide layer formed on the surface. This prevents the oxide layer from becoming entrained in the melt during melting and casting. The alloy was preheated to

200°C to ensure it was free from moisture, and then placed in a boron nitride coated mild steel crucible

The alloy was heated to 700°C where the melt was drossed to remove the layer of oxide from the surface. The melt temperature was then raised to the required temperature for grain refiner addition (725°C for strontium, 760°C for carbon). Three nominal addition levels of each grain refiner were investigated; 0 wt%, 0.05 wt%, and 0.1 wt%. A 0.05 wt% C (nominal) carbon containing tablet which was developed during the study on the castability of AZ91E was also utilised in this study. Once the grain refiner had been added, the melt was stirred continuously for 60 seconds to ensure dissolution prior to lowering the melt to the required temperature for casting, i.e. 100°C above the liquidus temperature of the alloy.

The experimental casting mould was coated with boron nitride and preheated to the required casting temperature as discussed in Chapter 3. The mould cavity was purged with the protective gas to prevent oxidation and burning during casting. A small 10ppi ceramic foam filter was placed at the entrance to the mould cavity to remove any non-metallic inclusions from the melt. Once the casting was poured, the remaining 10% of the melt was poured into a small cylindrical mild steel chill mould to form a sample for ICP-AES analysis to confirm the melt chemistry for each batch. Once the casting had solidified it was removed from the mould and allowed to cool to room temperature. The castings were analysed in accordance with the techniques outlined in Section 3.5 of Chapter 3, with raw data and summary statistics presented in Appendices I-IV.

5.3 Results

5.3.1 The Effectiveness of the Grain Refiner Addition Method

To confirm that the desired grain refiner levels were being achieved in the experimental castings, a sample from each of the melts was analysed using ICP-AES and leco-combustion analysis. This determined the chemical composition of the melt and showed whether the targeted strontium and carbon levels had been achieved in each case. The results of the chemical analysis are presented in Table 5-2.

Table 5-2: Compositions of the different melts used for the casting experiments.

Nominal Composition	Addition Method	Al	Zn	Mn	Be	Fe	Sr	C
AM60B	Nil	5.82	<0.005	0.29	<0.001	<0.002	**<0.001**	<0.005
AM60B + 0.05 wt% Sr	Al-10 wt% Sr master alloy	6.23	<0.005	0.30	<0.001	<0.002	**0.05**	<0.005
AM60B + 0.10 wt% Sr	Al-10 wt% Sr master alloy	5.92	<0.005	0.34	<0.001	<0.002	**0.10**	<0.005
AM60B + 0.05 wt% C	Carbon black wrapped in Al foil	5.87	0.005	0.29	<0.001	<0.005	<0.001	**0.005**
AM60B + 0.10 wt% C	Carbon black wrapped in Al foil	5.89	0.005	0.30	<0.001	<0.005	<0.001	**<0.005**
AM60B + 0.05 wt% C	Mg/Al/C composite Tablet	5.83	0.003	0.32	<0.001	<0.005	<0.001	**0.010**

The results analysis confirmed that the actual content of strontium in the melt is the same as the nominal content targeted by the strontium addition. However, as is common with carbon addition to magnesium, the nominal carbon levels were not

achieved when carbon was added to the melt in the form of carbon black powder wrapped in an aluminium foil. This method resulted in a final carbon content of 0.005 wt% C when 0.05 wt% was added, and a carbon level even below the detection limit of 0.005 wt% when 0.10 wt% carbon black was added. Once again, the addition of the carbon containing tablet that was developed during the course of this research lead to a much higher carbon level in the resulting castings. This confirms that the slow release of carbon from the tablet is a more effective method of introducing carbon to a magnesium alloy melt than traditional methods.

5.3.2 The Effect of Strontium on the Grain Size of AM60B

After polishing and etching the samples from each section of the castings treated with strontium, the grain size was measured in accordance with ASTM standard E 112-96 using the linear intercept method. A total of at least 50 grains were counted for each field of investigation, with five fields selected in each case. This high sample number allowed reliable statistics to be gathered for the mean, variance and standard deviation of the grain size. The effect of strontium on the grain size of the AM60B castings can be seen in Figure 5-1, which shows that the addition of strontium to AM60B had little effect on the average grain size of the casting sections. The grain size of three of the casting sections (hub, spoke/rim junction, and rim) actually showed a slight increase in grain size with the initial strontium addition of 0.05 wt%, followed by a reduction in grain size when the addition rate was increased to 0.10 wt%. The spoke section of the experimental casting exhibited a decrease in grain size with increasing strontium levels. Examples of the as-cast microstructure of the hub section of the AM60B castings can be seen in Figure 5-2.

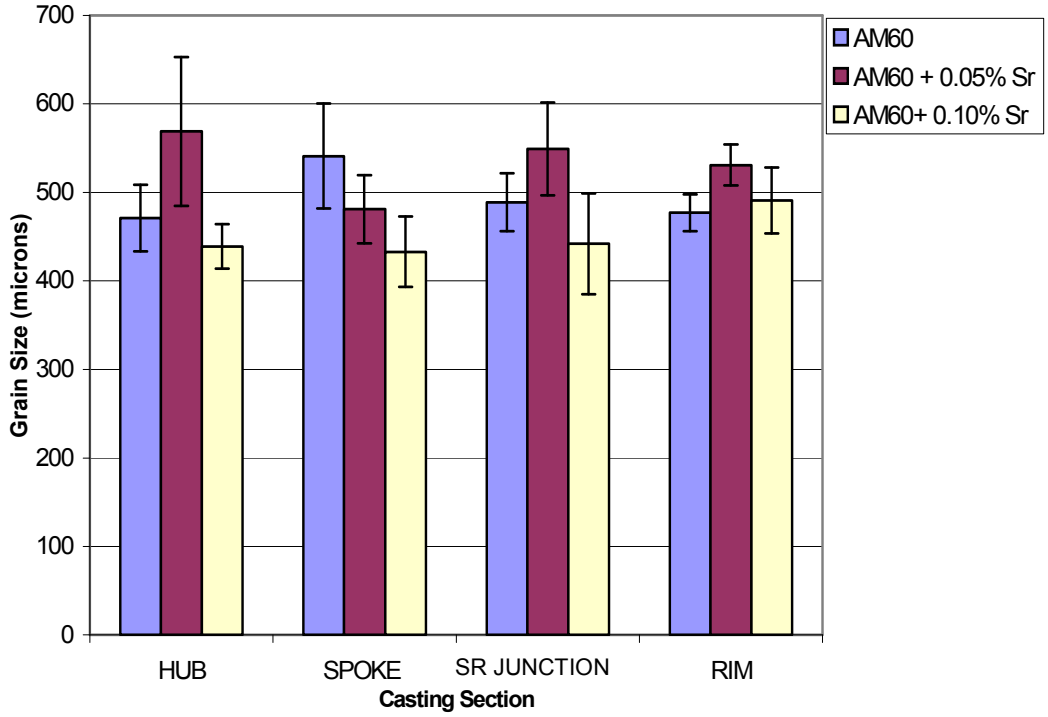

Figure 5-1: The grain sizes of different sections of the AM60B castings achieved with different levels of strontium addition. The error bars represent plus or minus one standard deviation from the mean value.

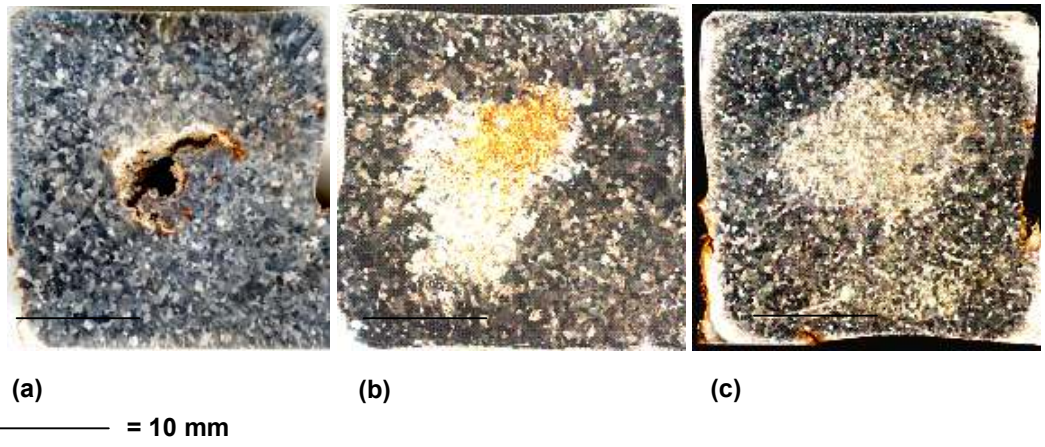

Figure 5-2: Macrographs of the hub section of the AM60B castings with (a) AM60B untreated (b) AM60B + 0.05 wt% Sr, and (c) AM60B + 0.10 wt% Sr. The clouded areas in the centre of the macrographs are due to microporosity in the sample.

Figure 5-3 shows that, although the addition of Sr had little effect on the average grain size of the AM60B castings, a change in the morphology of the grains was apparent. In

the untreated castings, large columnar grains can be seen growing inwards from the walls of the casting sections. These large columnar grains have a detrimental effect to the strength and ductility of a cast component. Grain refinement is used to eliminate the formation of such a structure and produce a more equiaxed microstructure. When 0.05 wt% Sr was added to the melt, the morphology of the grains transformed to a more equiaxed structure. Increasing the strontium content to 0.10 wt% resulted in the complete elimination of the long columnar grains and produced a uniform equiaxed microstructure throughout the casting.

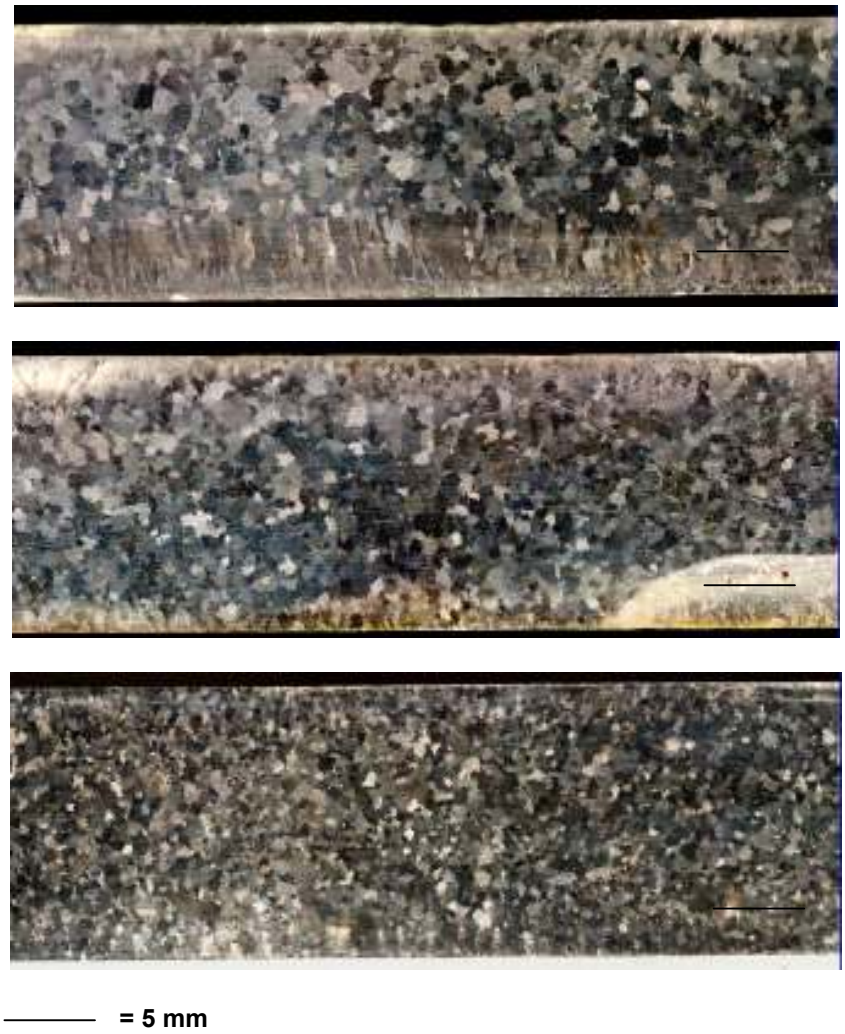

Figure 5-3: Macrographs of the spoke section of the AM60B alloy castings: Untreated AM60B (top), AM60B + 0.05 wt% Sr (middle), and AM60B + 0.10 wt% Sr (bottom). Columnar grains that can be seen to grow from the base of the casting in the untreated sample are eliminated with the addition of Sr to the melt.

5.3.3 The Effect of Carbon on the Grain Size of AM60B

The addition of carbon to the AM60B melt lead to more effective grain refinement than was experienced with strontium addition. Figure 5-4 shows that the AM60B castings without carbon added, and with a carbon level below the detection limit of leco combustion analysis (<0.005 wt% C) have a grain size of around 500µm. When the carbon level is raised to 0.005 wt% the mean grain size of the casting was reduced significantly in all sections. Increasing the carbon content further to 0.01 wt% C resulted in further refinement still. A prime example can be seen in the rim section of the casting treated with 0.01 wt% C where the grain size is reduced by over 50%.

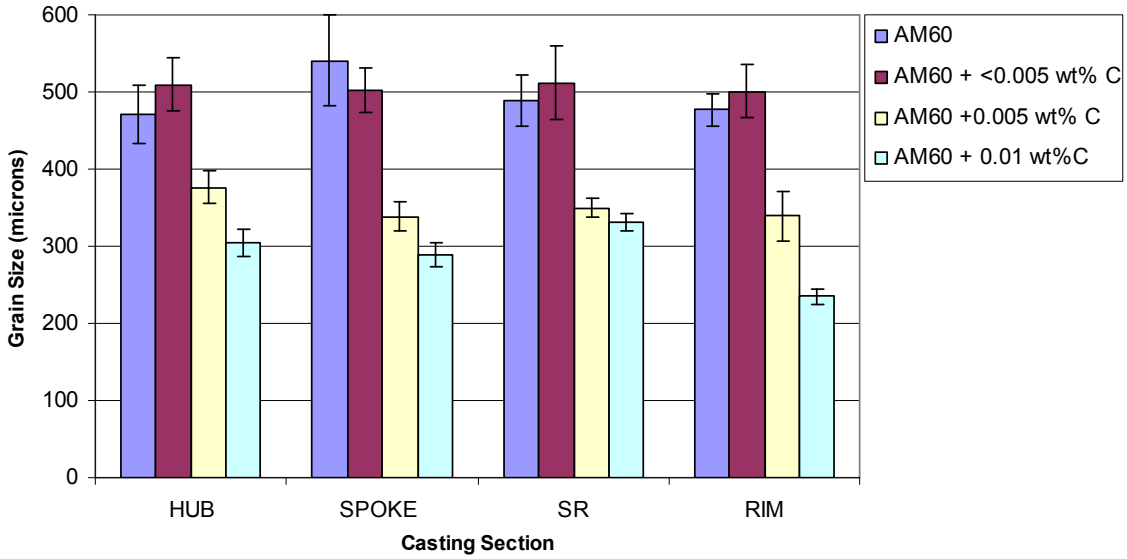

Figure 5-4: The effect of carbon addition on the grain size of alloy AM60B. The error bars represent plus or minus one standard deviation from the mean. The stated composition is that measured by leco combustion analysis in wt%.

Another trend apparent in Figure 5-4 is that the variability of grain size is reduced significantly, as shown by the size of the error bars, as carbon content is increased. This is an important effect of grain refinement as is means that the grain size is reduced consistently through the casting, and also that the grains have become equiaxed which is desirable for consistent mechanical properties. Macrographs showing the as-cast

grain structure of the rim sections of the castings produced in the investigation are shown in Figure 5-5.

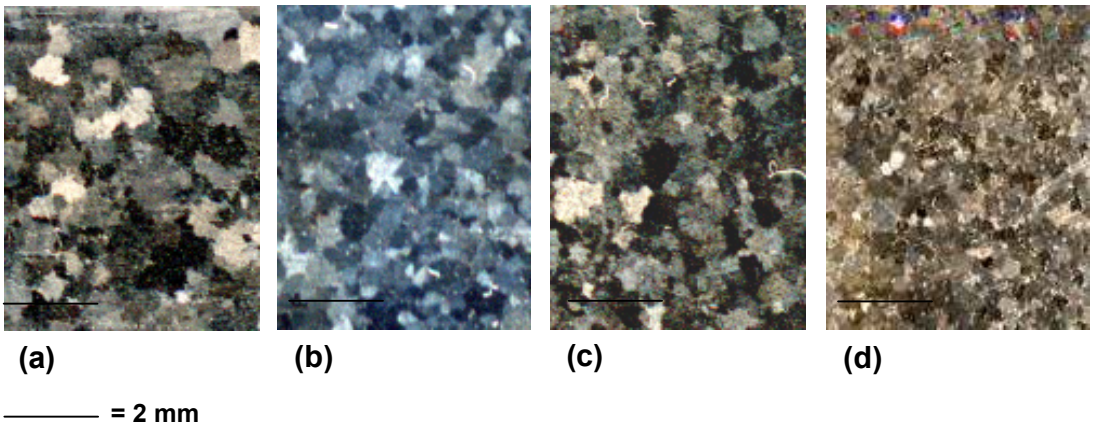

Figure 5-5: Macrographs of the rim section of the AM60B castings with (a) AM60B untreated, (b) AM60B + <0.005wt% C, (c) AM60B + 0.005 wt% C, and (d) AM60B + 0.01 wt% C.

5.3.4 Summary on the Study of Grain Refiner Effectiveness

The results of the AM60B grain size measurements are presented in Appendix II and unlike the results for the AZ91E castings detailed in Chapter 4, the grain refiners employed during this investigation yielded somewhat inconsistent results. The addition of strontium at nominal levels of 0.05 and 0.10 wt% respectively resulted in the desired strontium level being achieved. The addition of carbon black wrapped in an aluminium foil was not effective in introducing carbon to the alloy melts. In the case of the nominal addition of 0.05 wt% C, the carbon level in the casting was raised to a level of 0.005 wt%, which was sufficient to cause clear grain refinement in the castings, but with a nominal addition of 0.10 wt% C the carbon level was below even the detection limit of the analysis. This is most likely due to the rapid rising of the carbon black powder to the melt surface, causing it to become entrained in the oxide layer at the surface of the melt and subsequently removed prior to pouring of the casting. The most successful method of adding carbon to the AM60B melt was by using the carbon containing tablet produced by compacting a magnesium alloy/aluminium/carbon composite powder produced by high-energy mechanical milling of a mixture of

magnesium, aluminium, and carbon powder. Here the carbon level achieved in the castings was much higher at 0.01 wt% C when the nominal addition level was 0.05 wt% C.

In terms of the effectiveness of the grain refiners, the addition of 0.05 or 0.10 wt% Sr had no tangible effect on the grain size of AM60B. Adding carbon on the other hand, did result in significant refinement of the casting microstructure. Adding 0.005 wt% C to the alloy reduced the average grain size markedly, and raising the carbon level to 0.01 wt% resulted in significantly higher levels of grain refinement.

5.3.5 External Defect Inspection

Each of the AM60B castings produced was qualitatively assessed for the level of external defects present as described in Section 3.5.2 of Chapter 3. Two castings were produced for each experimental parameter to ensure that the results (presented in Appendix III) were consistent and reproducible. As with the AZ91E castings, the three defects assessed were slumping of the casting surface, external shrinkage porosity, and hot tearing. The severity of each defect was graded from 0-3 with grade 0 corresponding to no apparent defect, and grade 3 indicating that the defect was severe.

The results of the external defect assessment for alloy AM60B are presented in Table 5-3. The figures in the table were produced by averaging the defect grades of each set of castings, with the total for each defect shown at the right of the table. The results show a fair degree of scatter which is to be expected, as the grain size measurements detailed in Section 5.3.4 also displayed a substantial degree of scatter. One notable trend is apparent when looking at the total severity of the defect levels which shows that the occurrence of external shrinkage porosity has been eliminated when strontium was added to the melt[1]. This is shown graphically in Figure 5-6, which shows an example of an AM60B casting before and after strontium addition. Strontium addition had no

[1] The external shrinkage porosity is defined as porosity that is visible from the surface of the casting, it is not the total amount of shrinkage porosity in the casting.

effect on the occurrence or severity of either surface slumping or hot tearing defects. In Chapter 4, it was found that these defects were extremely sensitive to grain size, so the results of the above table link well with the results of the grain size measurements of Section 5.3.2 which showed that strontium addition had little effect on grain size of AM60B.

Table 5-3: External defect levels of the AM60B castings treated with strontium.

AM60B + 0 wt% Sr					
	A	**B**	**C**	**D**	**TOTAL**
Slumping	0.5	1	1.5	0.5	**3.5**
Shrinkage	1.5	0	1	1.5	**4**
Hot Tearing	0	2	0	0.5	**2.5**
AM60B + 0.05 wt% Sr					
	A	**B**	**C**	**D**	**TOTAL**
Slumping	0	0.5	1	0.5	**2**
Shrinkage	0	0	0	0	**0**
Hot Tearing	0	1	2	0.5	**3.5**
AM60B + 0.10 wt% Sr					
	A	**B**	**C**	**D**	**TOTAL**
Slumping	0	2	1	0	**3**
Shrinkage	0	0	0	0	**0**
Hot Tearing	0	1	1	0.5	**2.5**

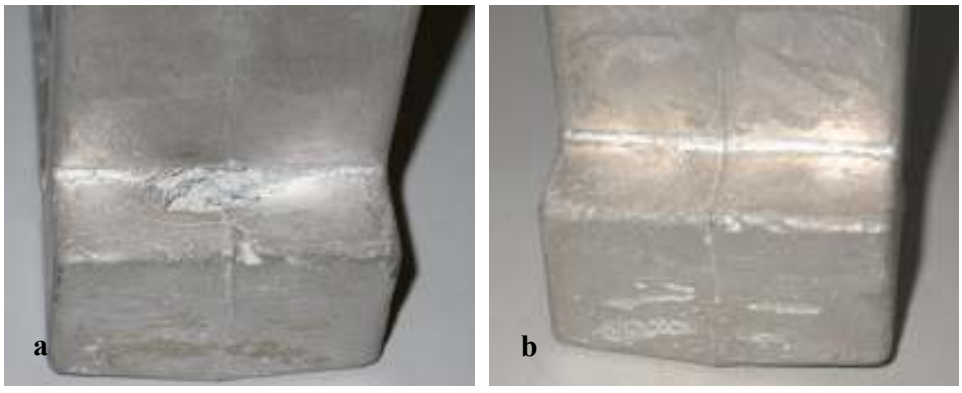

Figure 5-6: Images of region D of a casting without Sr addition (a) and after the addition of 0.05wt% Sr (b) respectively. Note the elimination of externally visible shrinkage porosity.

The results of the external casting defect assessment for the castings treated with carbon are shown in Table 5-5. The numbers presented in the table measure the average severity rating for each experimental parameter. The table shows that the addition of 0.01 wt% C to the melt leads to an increase in surface slumping severity and a significant reduction in hot tearing. The addition of carbon also appears to reduce the occurrence of externally visible shrinkage porosity, but when reviewed against the results of the grain size measurements presented earlier, the presence of this defect appears to be independent of grain size.

Table 5-5: External defect levels of the AM60B castings treated with carbon.

AM60B					
	A	**B**	**C**	**D**	**TOTAL**
Slumping	0.5	1	1.5	0.5	**3.5**
Shrinkage	1.5	0	1	1.5	**4**
Hot Tearing	0	2	0	0.5	**2.5**
AM60B + <0.005 wt% C					
	A	**B**	**C**	**D**	**TOTAL**
Slumping	2.5	0	1	1	**4.5**
Shrinkage	0	0	1	0	**1**
Hot Tearing	1	2.5	0.5	0	**4**
AM60B + 0.005 wt% C					
	A	**B**	**C**	**D**	**TOTAL**
Slumping	1.5	1	1	0	**3.5**
Shrinkage	0	0	0.5	0	**0.5**
Hot Tearing	0	0.5	1.5	0.5	**2.5**
AM60B + 0.01 wt% C					
	A	**B**	**C**	**D**	**TOTAL**
Slumping	1	1.5	1	1	**4.5**
Shrinkage	0	0.5	1.5	0.5	**2.5**
Hot Tearing	0	0	0.5	0	**0.5**

As with the study on the castability of AZ91E, all of the castings produced were subsequently x-rayed to inspect their internal soundness and determine whether internal porosity was visibly affected by the addition of grain refiners to the castings. Examples

of the x-ray radiographs of the castings produced for alloy AM60B can be seen in Figure 5-8 and Figure 5-9. Figure 5-8 shows that without any strontium added there are large internal pores in the thicker casting sections of the hub and the spoke/rim junction. This is illustrated by the darkened areas inside the lighter coloured magnesium casting. These large cavities are not as severe with 0.05 wt% strontium and disappear completely when the melt is treated with 0.10 wt% strontium. Figure 5-9 shows the x-ray radiographs of the castings produced from the melts treated with carbon as a grain refiner. Once again in the case where the addition of carbon grain refiner was successful the presence of large internal cavities is eliminated. With a carbon content of <0.005 wt% the casting was not successfully grain refined, and a large area with a high level of porosity can be seen in the hub section. However, with a carbon content of 0.005 wt% or greater there are no large pores present in the castings Another point of interest is the large amount of surface slumping seen in the spoke/rim junction of the casting with 0.01 wt% C. This indicates that, just as was seen with the AZ91E castings, the reduction in grain size leads to a marked increase in slumping of the casting surface.

	AM60B	**AM60B + 0.05 wt% Sr**	**AM60B + 0.10 wt% Sr**
Hub			
Spoke			
Spoke/Rim Junction			
Rim			

Figure 5-8: X-ray radiographs of the castings produced from the melt treated with strontium.

	AM60B	**AM60B + <0.005 wt% C**	**AM60B + 0.005 wt% C**	**AM60B + 0.01 wt% C**
Hub				
Spoke				
Spoke/Rim Junction				
Rim				

Figure 5-9: X-ray radiographs of the castings produced from the melt treated with carbon.

The x-ray radiographs presented above illustrate varying levels of porosity present in the AM60B castings. Although this is a common method for assessing the quality of castings, a more accurate measure of porosity is gained by calculating the apparent density of the castings, and the results of this analysis are the focus of Sections 5.3.6 and 5.3.7.

5.3.6 Overall Casting Porosity Levels

The effects of strontium and carbon additions on casting porosity level were investigated by measuring the apparent density of the entire casting samples using the Archimedes principle, and comparing this to a fully densified sample to determine the porosity levels of the castings. Both castings produced for each alloy condition were measured for porosity with the results averaged to yield the porosity level for that condition. The results of the porosity measurements for the strontium and carbon treated castings can be seen in Figure 5-10 and Figure 5-11 respectively. In Figure 5-11, the casting sample with a measured carbon content of <0.005 wt% C was not included in the graph as it could not be confidently positioned in relation to the other data points.

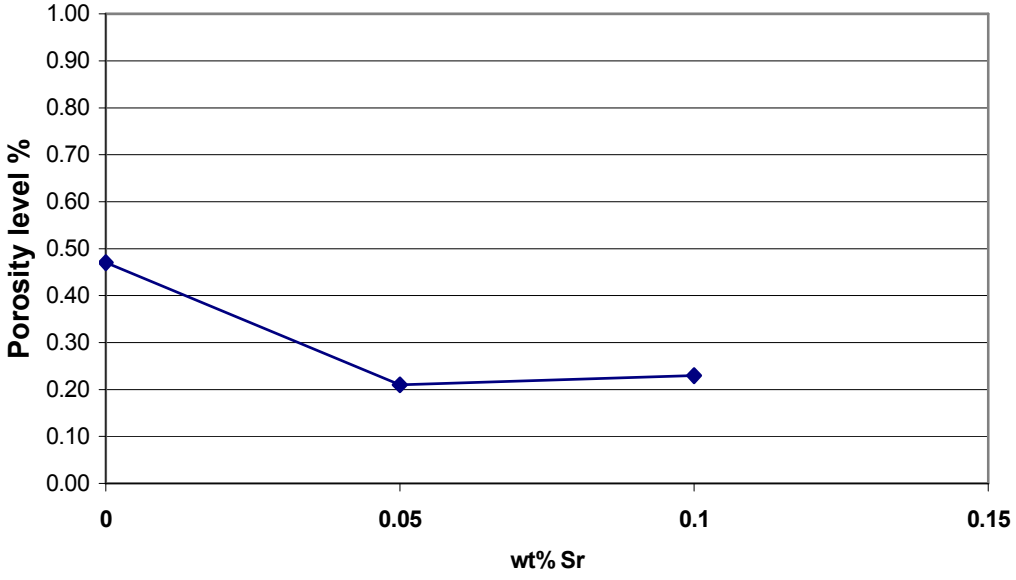

Figure 5-10: The porosity level of AM60B castings as a function of strontium content.

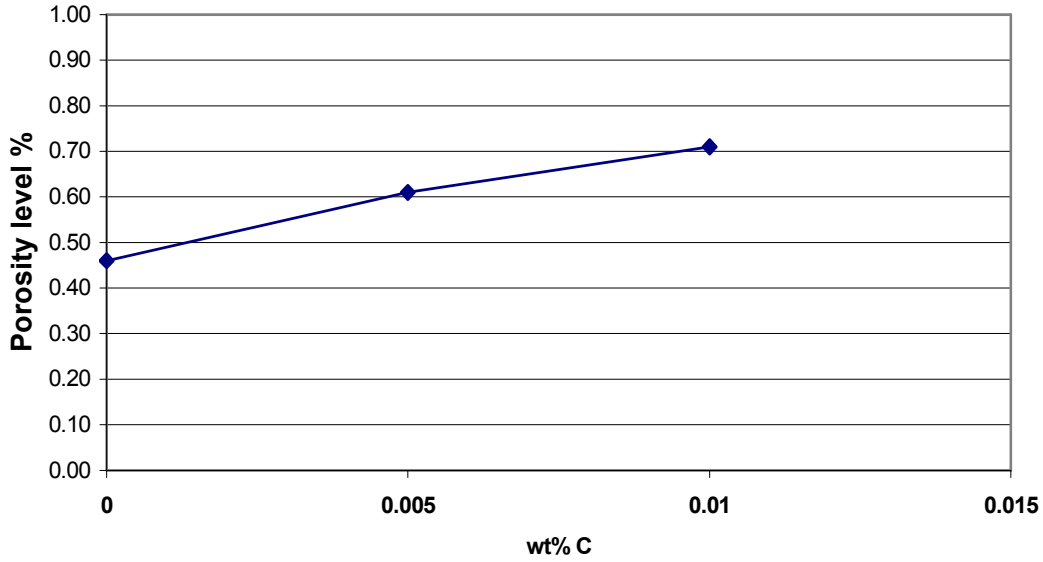

Figure 5-11: The porosity level of AM60B castings as a function of carbon content.

The first point that is obvious from the above graphs is that the castings produced from AM60B had much lower overall porosity level compared to the AZ91E castings presented in Chapter 4. With the AZ91E castings, the porosity levels ranged from 0.74% to 1.68% whereas in the case of the AM60B castings, the porosity levels range from 0.24% to 0.71%. This is due to the fact that AM60B has a much shorter freezing range of only 70°C compared with 125°C for AZ91E . A longer freezing range alloy relies more on the feeding of liquid through interdendritic networks to accommodate shrinkage during solidification. This type of feeding is not as efficient as liquid or mass feeding, therefore an alloy with a shorter freezing range is less likely to suffer from shrinkage porosity.

It is clear that the addition of strontium had a significant effect on the overall porosity level of the castings produced. Without any strontium added the AM60B castings had an average porosity level of 0.46%. When 0.05 wt% strontium was added the overall porosity level dropped by more than half to 0.20%. Increasing the amount of strontium addition to 0.10 wt% did not cause any further decrease in porosity level. These results are interesting since, as is shown in Figure 5-1, the addition of strontium had no significant effect on the grain size of the AM60B castings. The reduction therefore must

be due to other factors. In their study on porosity formation in AZ91 sand castings, Aliravci et al [1] found that the addition of strontium concentrated the shrinkage micropores to the thickest parts of the casting. They mention that the grain refining effect of strontium improved the mass feeding during solidification and hence, aided in the production of denser castings. This may explain the results seen here as if most of the pores were concentrated in the running system of the casting, which was subsequently removed, than the addition of strontium would have lead to a reduction in porosity level of the casting samples, even if grain refinement was negligible.

In the case of the AM60B castings treated with carbon the overall porosity levels correlated well with the grain size measurements shown in Figure 5-4. The highest porosity level of 0.70% was found in the 0.01 wt% C castings (treated with the carbon tablet) which had the smallest grain size. The largest grain size achieved was the casting with <0.005 wt% C and this possessed the lowest porosity level of 0.24%. The remaining two castings had porosity levels which corresponded well with their as-cast grain size.

5.3.7 Porosity Levels of the Individual Casting Sections

Each casting section was separated from the AM60B casting samples and the internal porosity levels were measured using the Archimedes principle. The results of this analysis are plotted in Figure 5-12 and Figure 5-13. The results of this analysis showed that strontium did not have an obvious effect on the porosity level of the casting sections, which fluctuated with increasing strontium level. One region of the casting which showed a significant change was the hub, where adding 0.10 wt% Sr lead to a large increase in porosity level compared with the untreated casting.

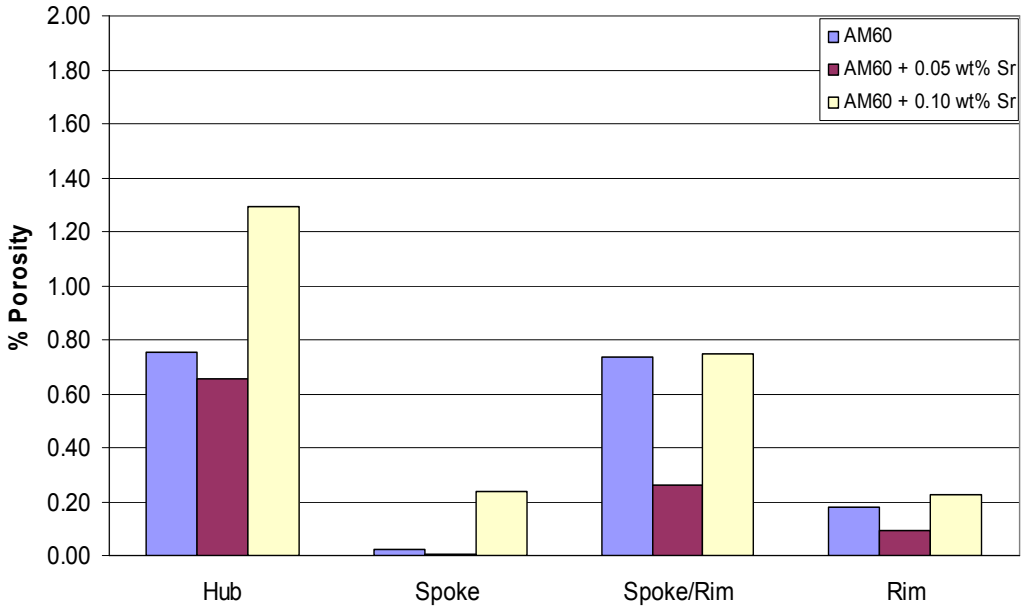

Figure 5-12: Porosity levels of the separate casting sections of the AM60B castings with differing strontium levels.

The results presented in Figure 5-12 do appear to be inconsistent, though the porosity levels that are being measured are extremely low, so a natural variation is to be expected between castings. A prime example is seen in the rim of the casting where adding 0.5 wt% Sr lead to a decrease in porosity level and 0.10wt% lead to an increase, however the total variation was only 0.13%.

Figure 5-13 shows the effect of carbon content on the internal porosity levels of the AM60B castings. It shows that increasing the carbon content to 0.01wt% resulted in a large increase in internal porosity level in the hub and spoke/rim junction sections. It was this carbon level which also provided the finest grain size which again highlights the sensitivity of porosity level to grain refinement in magnesium alloy castings.

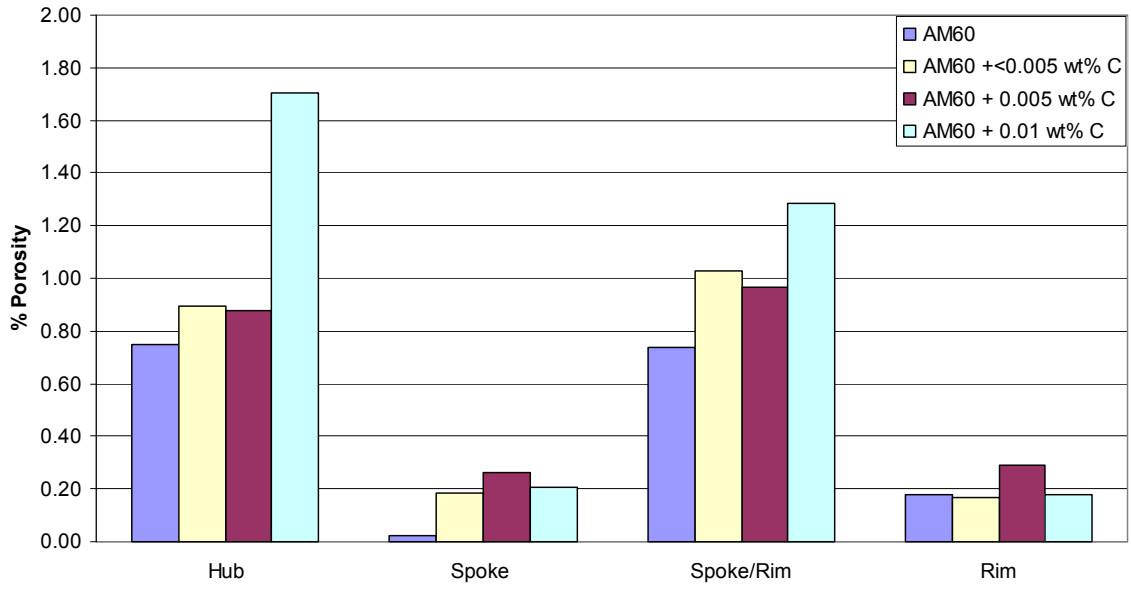

Figure 5-13: Porosity levels of the separate casting sections of the AM60B castings with differing carbon levels.

5.3.8 MAGMAsoft™ Casting Simulation

To further understand the solidification process and porosity formation in the AM60B castings a casting simulation was performed using the MAGMAsoft software package. This illustrated the temperature profile of the casting throughout its solidification process and identified the location and temperature distribution of the hot spots. The screen capture highlights some important features of the solidification patterns in an AM60B casting, and important differences compared to the AZ91E castings. Figure 5-14 shows the simulated AM60B casting at the point of 83% through the solidification process where much of the casting is below the solidus temperature of 545 °C. The lighter coloured regions cover a large area around the hub and spoke rim junction and are only a few degrees above the solidus temperature of 545 °C. There is a much smoother temperature transition than that seen with the AZ91E casting simulation shown in Figure 4-16, so the hot spots are not as detrimental to efficient feeding. This leads to a lower incidence of internal porosity in the AM60B castings.

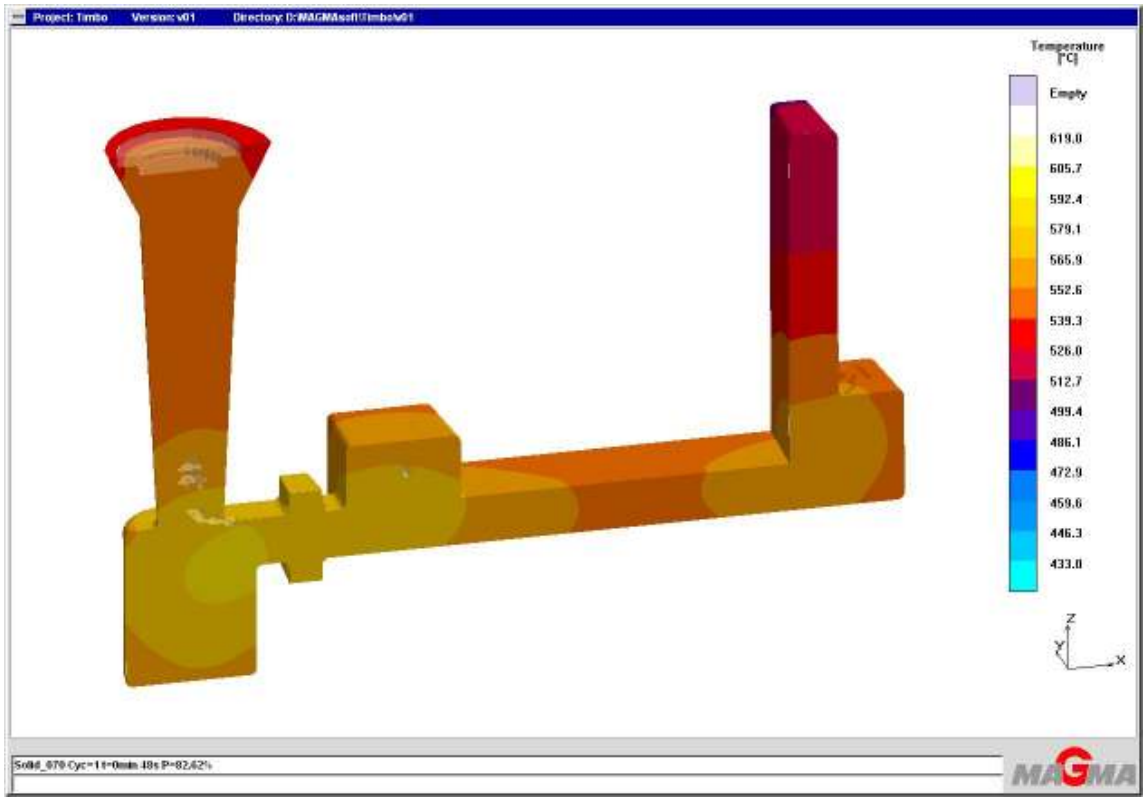

Figure 5-14: Temperature distribution of an AM60B casting 83% through the solidification process.

5.3.9 Microscopic Examination of Pores

As with the AZ91E castings, optical microscopy was employed to determine whether the location, size, and morphology of the pores in the casting changed with respect to grain size. The spoke-rim junction and the rim sections were analysed to give contrasting section thickness, and the samples selected had a range of grain sizes from completely unrefined to fully refined. The samples chosen are listed below, with the contrast in as-cast grain sizes shown in Figure 5-15.

- AM60B untreated
- AM60B + 0.10 wt% Sr
- AM60B + 0.005 wt% C
- AM60B + 0.01 wt% C (carbon tablet)

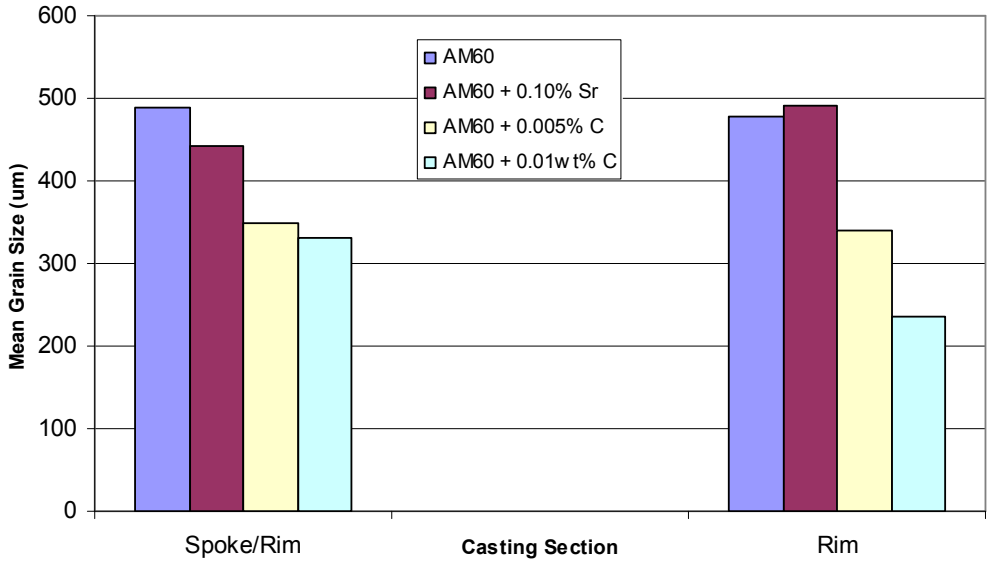

Figure 5-15: The mean grain sizes of the casting samples chosen for the microscopic porosity investigation.

As can be seen in Figure 5-15, the first two rim section samples are basically identical, with the AM60B castings not experiencing any grain refinement in the rim section with the addition of 0.10 wt% Sr. This image is included for consistency with the other alloys and casting sections presented in the thesis.

In the optical microscopy analysis, two images have been captured from identical locations in each casting sample. The first image was taken under polarised light to highlight the grain structure of the sample, while the second image was captured under non-polarised light to show the size, morphology, and distribution of pores in the sample. Using sufficient magnification to clearly distinguish individual grains, the path of the grain boundaries in the first image was traced using the tools available in the image processing software ImagePRO. Once all of the grains had been outlined, the grain boundary profile was extracted and overlaid onto the second image (showing the pore characteristics of the sample) to identify the relationship between grain boundary location and the distribution of pores.

Figure 5-16 through Figure 5-19 show the results of the optical microscopy analysis of the thicker section of the spoke/rim junction from the AM60B casting samples. The first feature that is obvious in the images shown above is the lower incidence of porosity in the AM60B samples compared with the same sections of the AZ91E castings. Figure 5-16 shows the unrefined spoke-rim junction which has a mean grain size of 489μm. In this sample most of the pores are located along the grain boundaries, however there are also pores located inside the grains in some areas. Reducing the grain size slightly to 422μm (Figure 5-16) made little difference to pore characteristics with some pores still visible within the casting grains. Figure 5-17 shows an example of the spoke/rim junction when the mean grain size is reduced further to 350μm. In this example the microporosity tends to follow the grain boundaries in most cases, however there are still some pores located within the grains. The pores are smaller however, than those seen with the larger grain sizes. These pores are the result of small discrete pools of eutectic liquid becoming trapped within the grains during solidification. As these liquid pools feed the solidifying material that surrounds them, they leave behind small isolated pores within the grains.

The smallest grain size achieved of 331μm in the spoke rim junction is shown in Figure 5-19. Here there is no evidence of any pores trapped within the grains, with all pores being located along the grain boundaries.

The results of the optical microscopy investigation of the thicker casting section follow the same trend as was seen with the AZ91E castings. A reduction in the average grain size results in the transformation of pore distribution from a mixture of intergranular and interdendritic, to solely intergranular porosity. In addition, the pores that are located inside the grains tend to change from larger branched pores to small isolated pockets as grain size is reduced until the presence of these pores is no longer detectable inside the grains.

To determine the effect of section thickness on pore characteristics with respect to grain refinement, the optical microscopy analysis was also undertaken on thinner casting sections from the rim of the AM60B castings. It is important to note that due to the faster solidification rate of the thinner section, the rim samples posses a lower porosity

level than the thicker spoke/rim junction. In the rim sections of the casting samples the porosity level ranges from only 0.18% to 0.29% compared with the thicker spoke/rim junction sections where the porosity level ranges from 0.74% to 1.28%. Therefore, the number of pores visible in the images will be lower in the rim sections.

Figure 5-19 and Figure 5-20 show the rim section of the fully unrefined AM60B. Here, once again, the pores are located mostly along the grain boundaries with a only few instances of pores being distributed within the grains. The average grain size of these samples is 477µm and 491µm respectively. Though there are not many pores visible in Figure 5-21 where the grain size is reduced to 339µm, those that are visible are mostly located at the grain boundaries. This trend continues with Figure 5-22, which has the lowest mean grain size of 235µm, as all porosity is located at the grain boundaries.

Overall it appears that grain refinement in both thick and thin casting sections leads to the elimination of porosity inside individual casting grains with only intergranular porosity remaining. These results prove that choosing the correct level of grain refinement is essential for the production of sound castings. The desired improvement in strength and ductility caused by a finer grain size can be negated by a reduction in strength and pressure tightness caused by an increase in intergranular porosity.

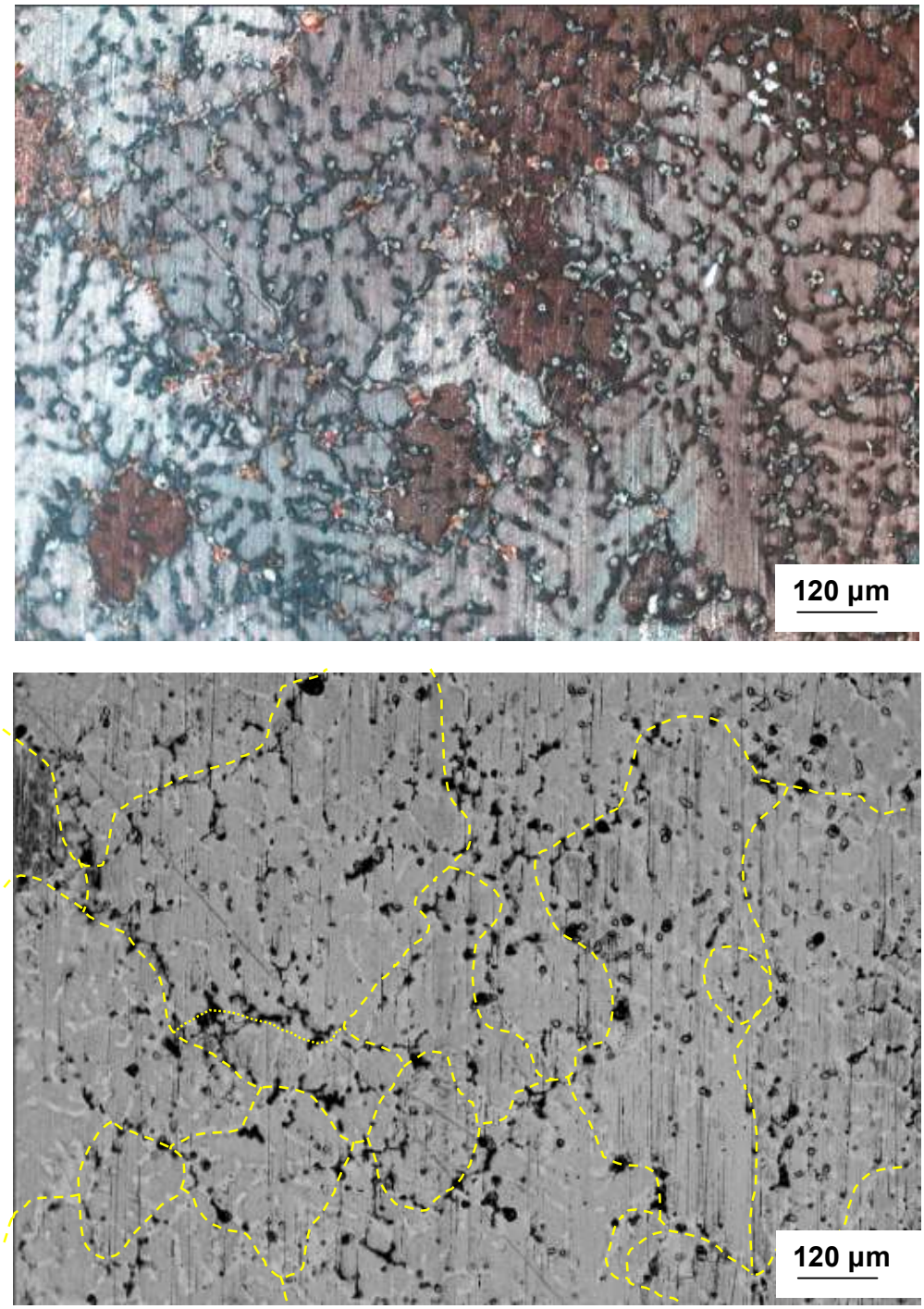

Figure 5-16: Micrographs showing the relationship between the grain structure and the distribution of pores in the spoke-rim junction of the untreated AM60B casting. The mean grain size of this sample is 489µm.

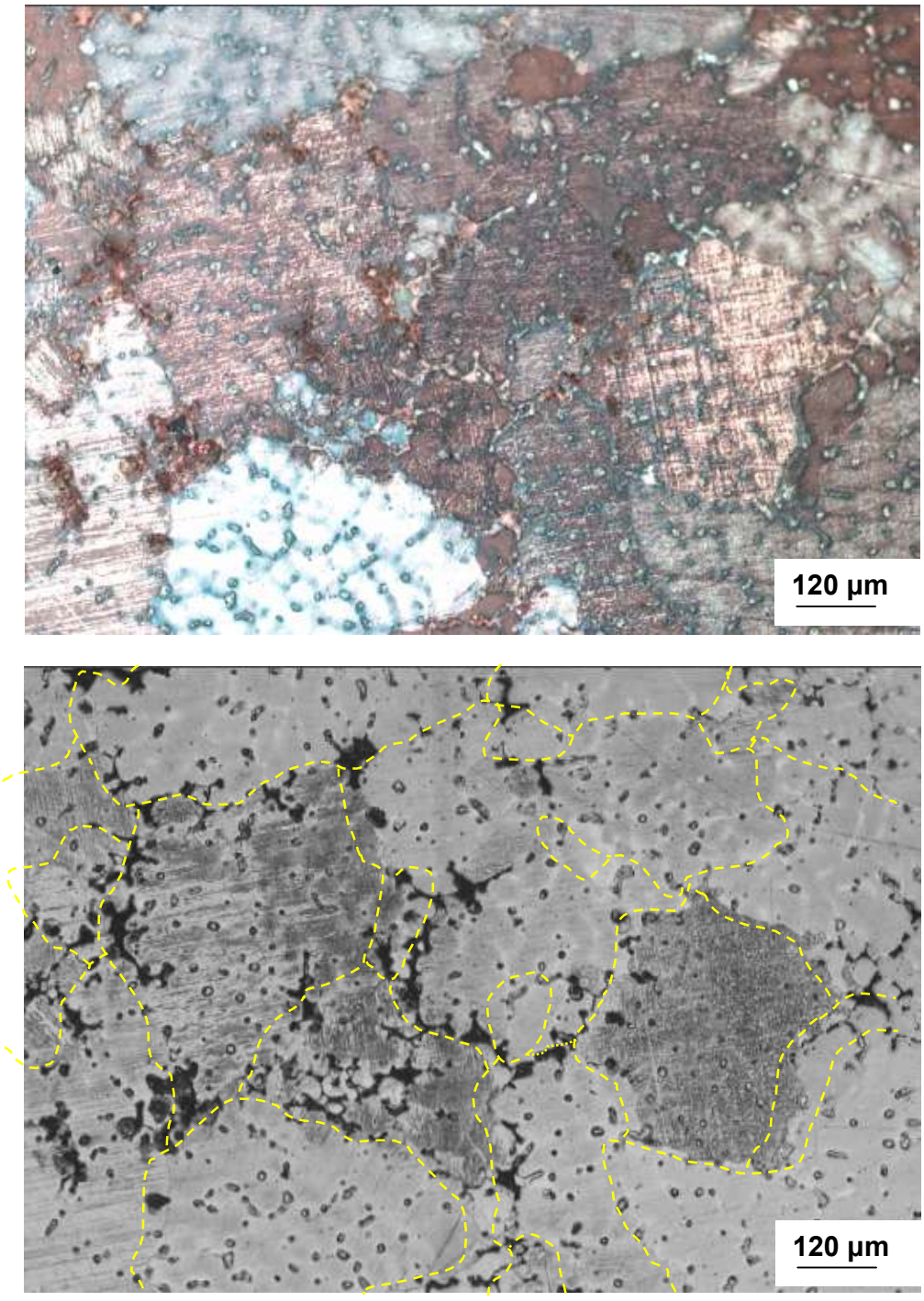

Figure 5-16: Micrographs showing the relationship between the grain structure and the distribution of pores in the spoke-rim junction of the AM60B casting treated with 0.10 wt% Sr. The mean grain size of this sample is 442µm.

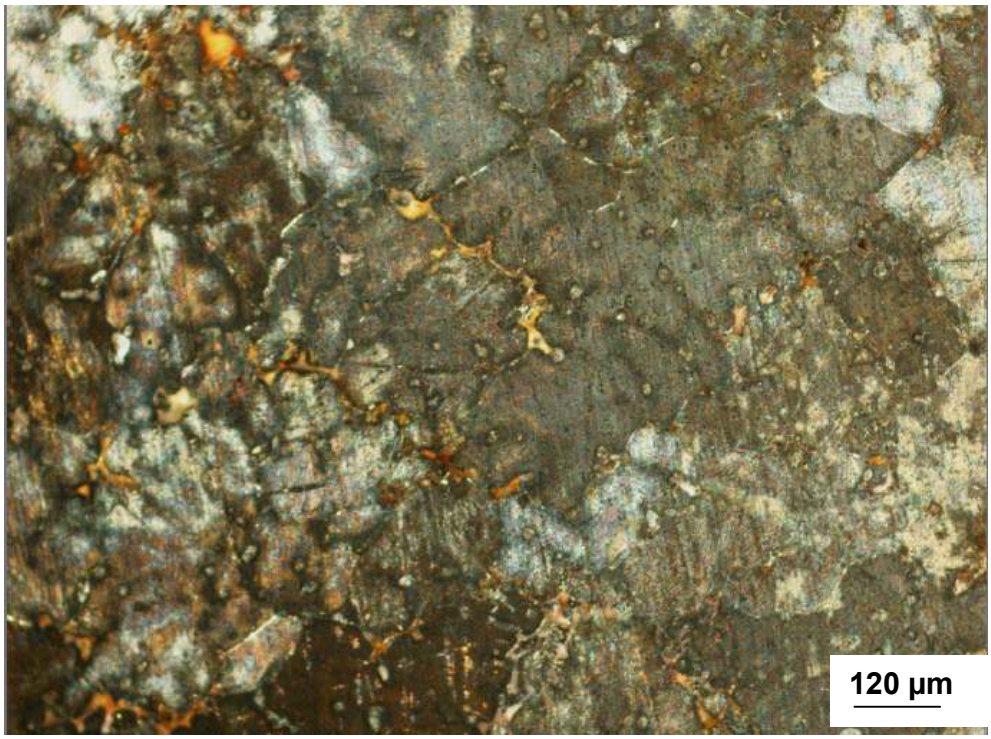

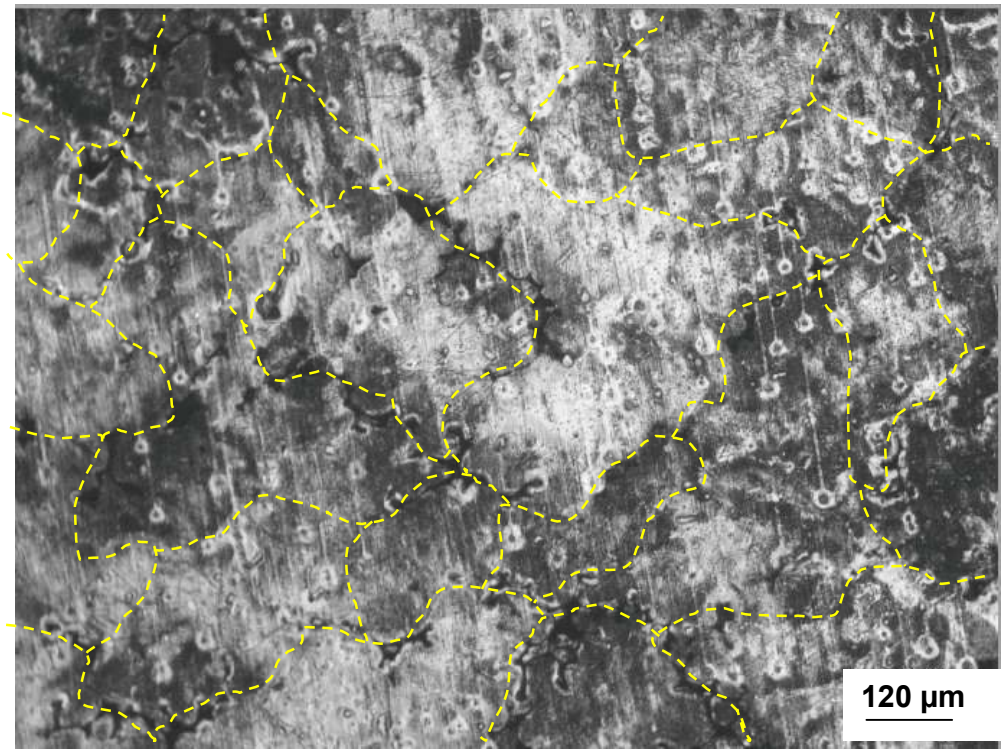

Figure 5-17: Micrographs showing the relationship between the grain structure and the distribution of pores in the spoke-rim junction of the casting treated with 0.005 w% C. The mean grain size of this sample is 350µm.

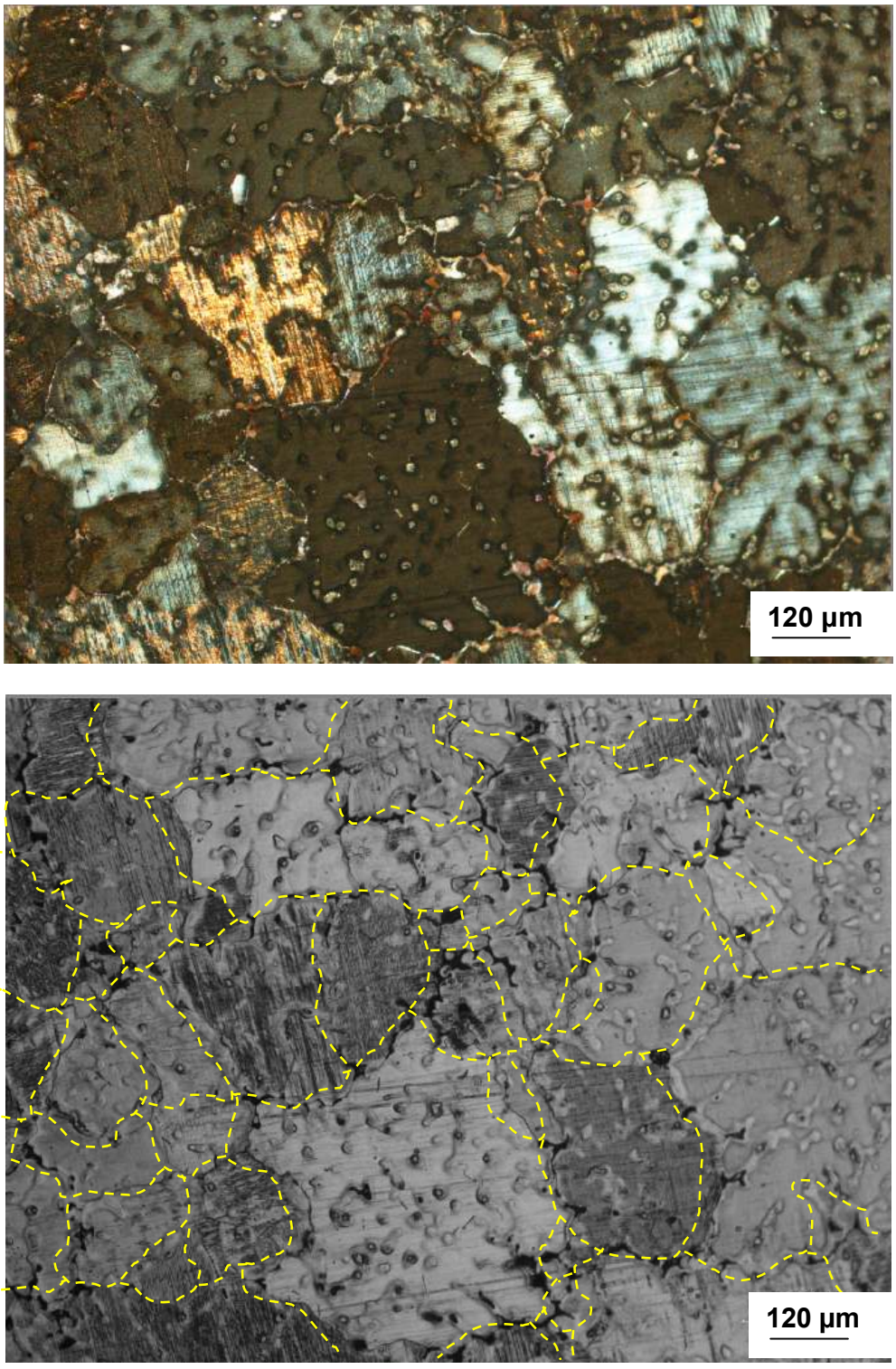

Figure 5-19: Micrographs showing the relationship between the grain structure and the distribution of pores in the spoke-rim junction of the AM60B casting treated with the 0.01 wt% C. The mean grain size of this sample is 331µm.

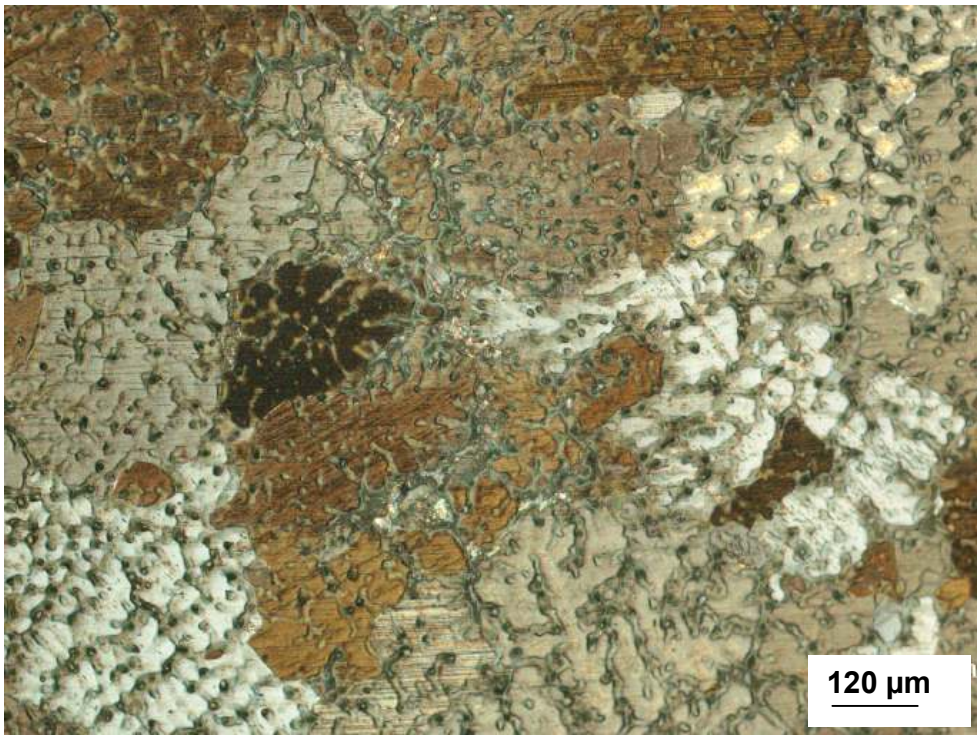

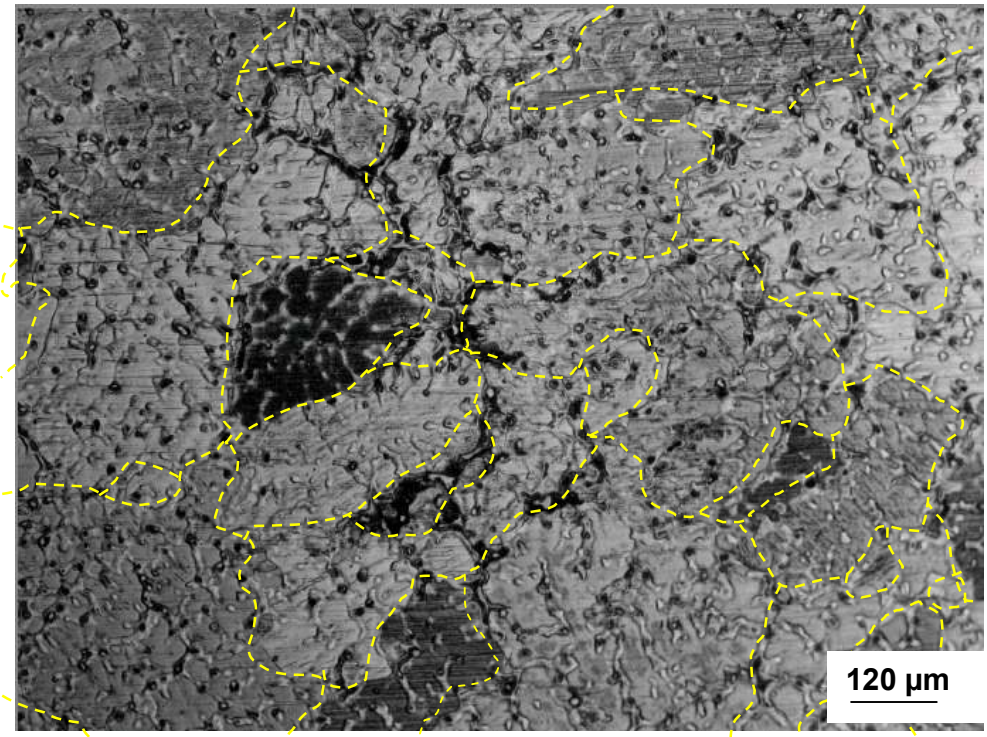

Figure 5-19: Micrographs showing the relationship between the grain structure and the distribution of pores in the-rim section of the unrefined AM60B casting.. The mean grain size of this sample is 477µm.

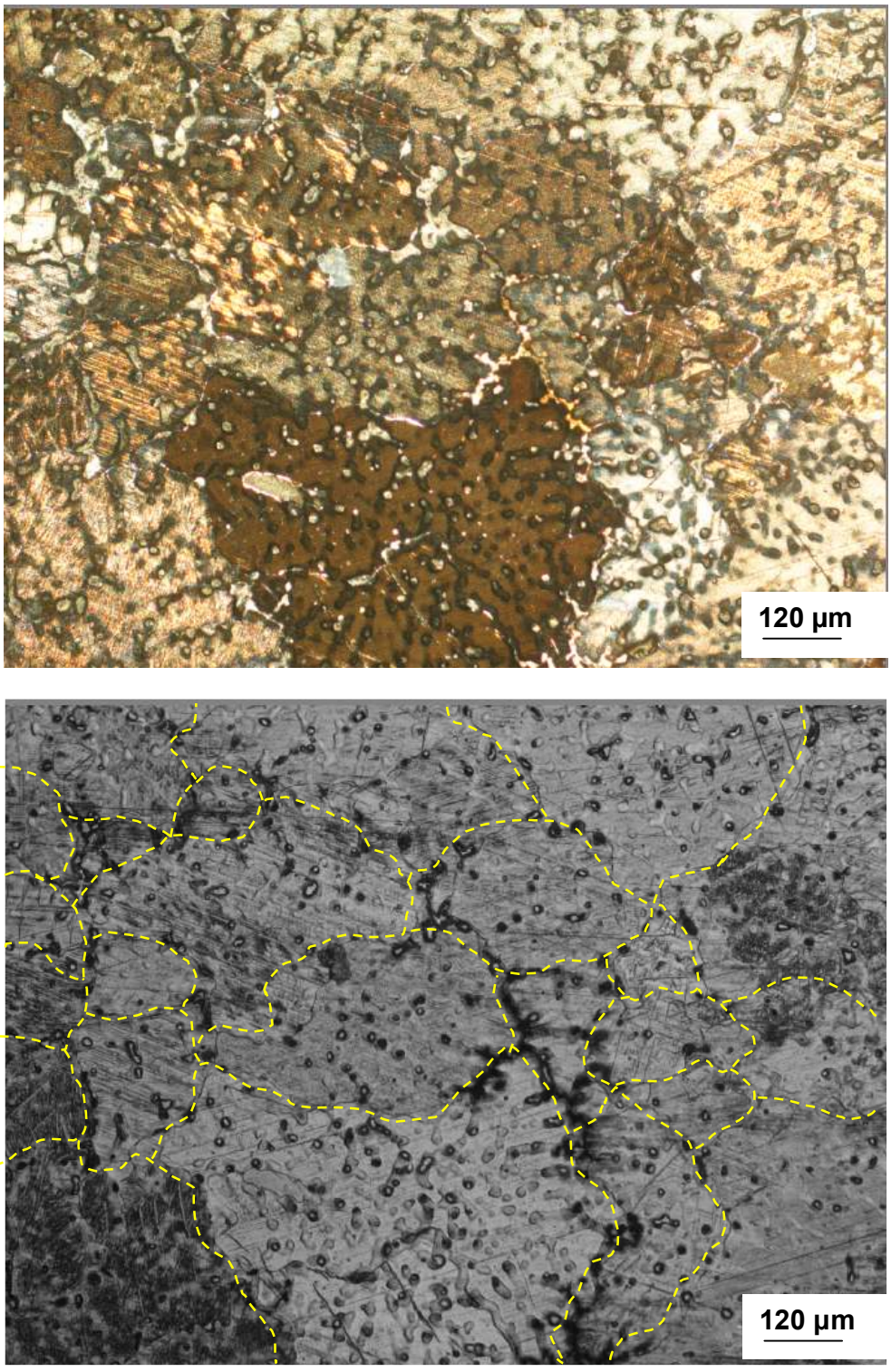

Figure 5-20: Micrographs showing the relationship between the grain structure and the distribution of pores in the rim section of the AM60B casting treated with 0.10 wt% Sr. The grain refinement in this case was unsuccessful with the mean grain size being 491µm.

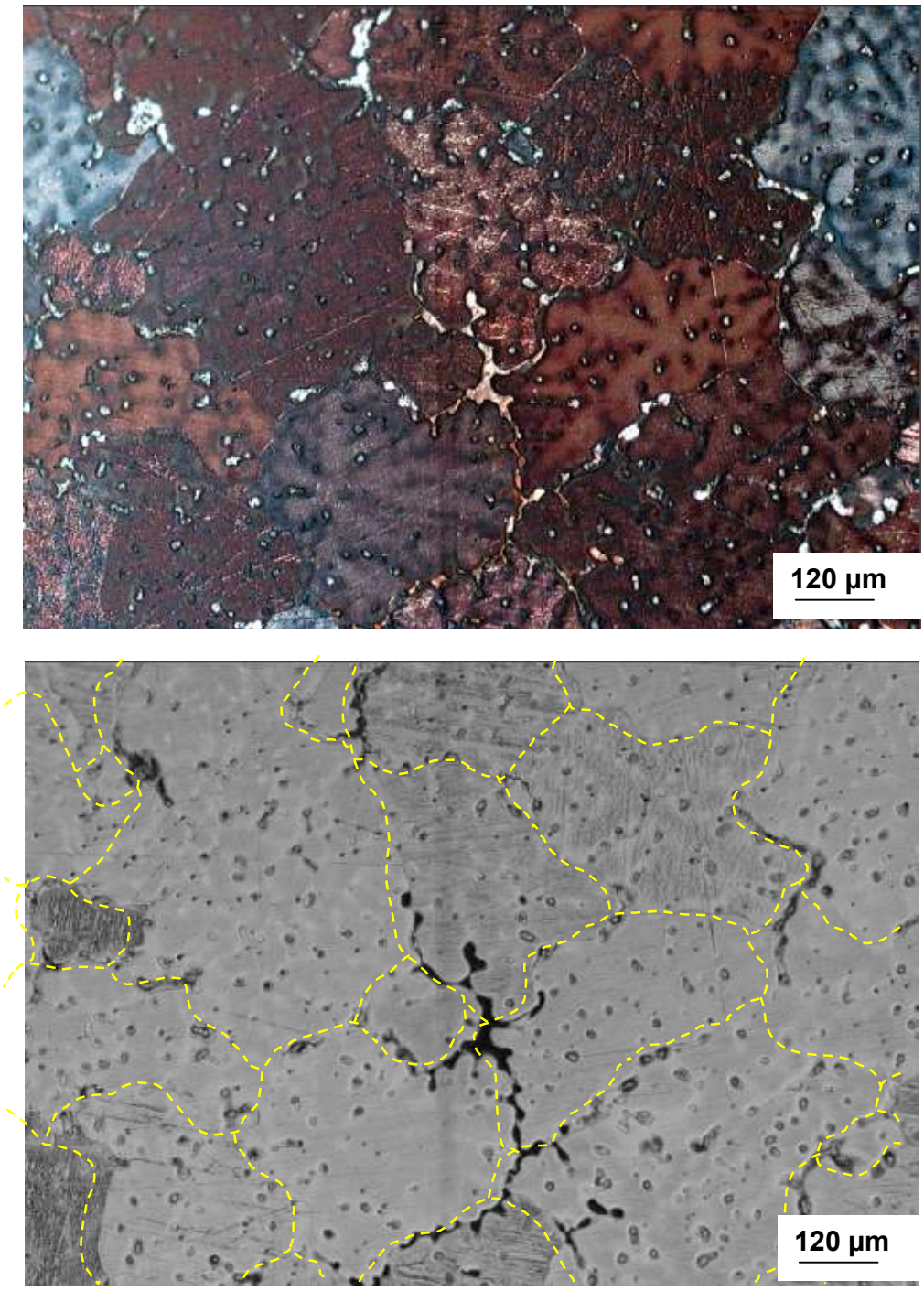

Figure 5-21: Micrographs showing the relationship between the grain structure and the distribution of pores in the rim section of the AM60B casting treated with 0.005 w% C. The mean grain size of this sample is 339µm.

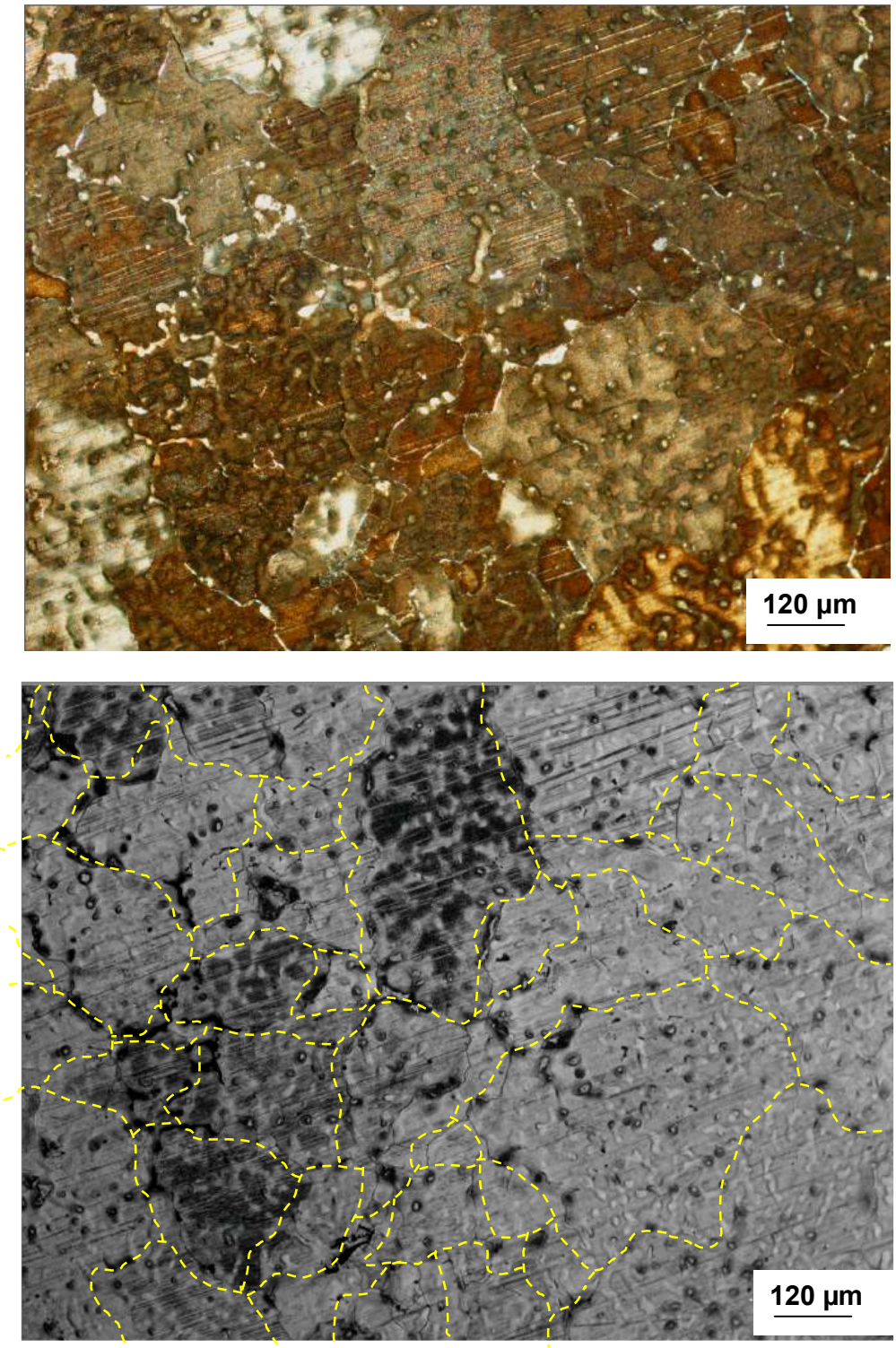

Figure 5-22: Micrographs showing the relationship between the grain structure and the distribution of pores in the rim section of the AM60B casting treated with 0.01 wt% C. The mean grain size of this sample is 235µm.

Two of the above samples were chosen for further inspection using Scanning Electron Microscopy (SEM). The first was the rim section of the unrefined AM60B castings and the second, a fully grain refined rim sample from the casting treated with 0.01 wt% C. Micrographs were taken of both samples to highlight any changes in microstructure composition or porosity morphology with a severe reduction in grain size. In the case of these two samples there was a 51% reduction in grain size from 477μm to 235μm.

Figure 5-23 shows the general microstructure of the rim section of the untreated AM60B casting. There is a noticeable lessening in the amount of $Mg_{17}Al_{12}$ eutectic present in the AM60B sample compared with the AZ91E samples displayed in the previous chapter. A small number of pores can be seen in both this figure and the corresponding higher magnification SEM image shown in Figure 5-24. It is difficult to confirm the location of the pores in relation to the grain boundaries using SEM, due to the lack of visibility of the grain boundaries under SEM. In Figure 5-24, the pores are shown to be extended along in fine branches and almost appear to be linked together. There are also a few incidences of small pores in discrete locations, which may indicate their location in relation to the grain boundaries. The branched pores are likely stretching along the boundary between neighbouring grains and the small round pores are probably located within the grain structure itself.

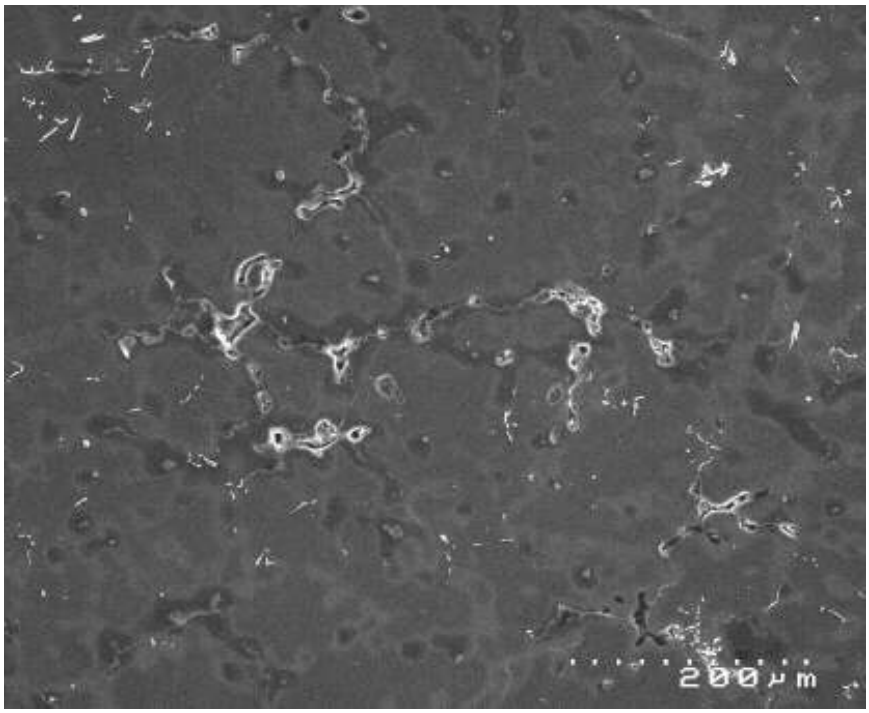

Figure 5-23: SEM micrograph of the rim section of the untreated AM60B casting. Areas of microporosity can be seen along with a small number of $Mg_{17}Al_{12}$ particles.

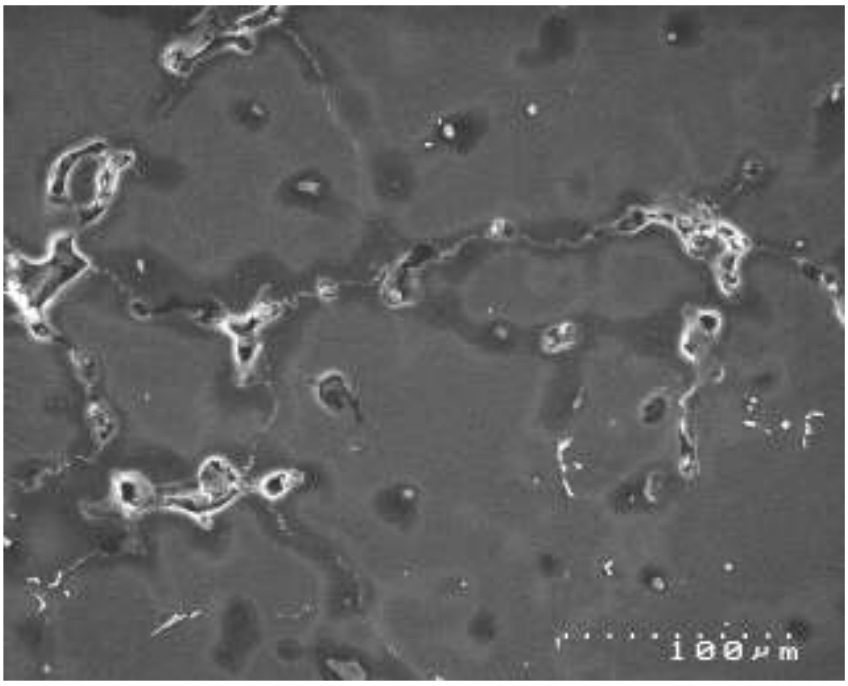

Figure 5-24: A higher magnification of the area shown in Figure 5-23 highlighting the areas of microporosity in the rim section.

There was little difference in the total amount of pores visible under SEM in the rim section of the casting treated with 0.01 wt% C. This was to be expected from the results of the Archimedes porosity measurements for this sample presented in Section 5.3.7. As shown in Figure 5-25, in this sample the pores tended to always branch out slightly from a central point, obviously being pinned at the meeting point of several grains.

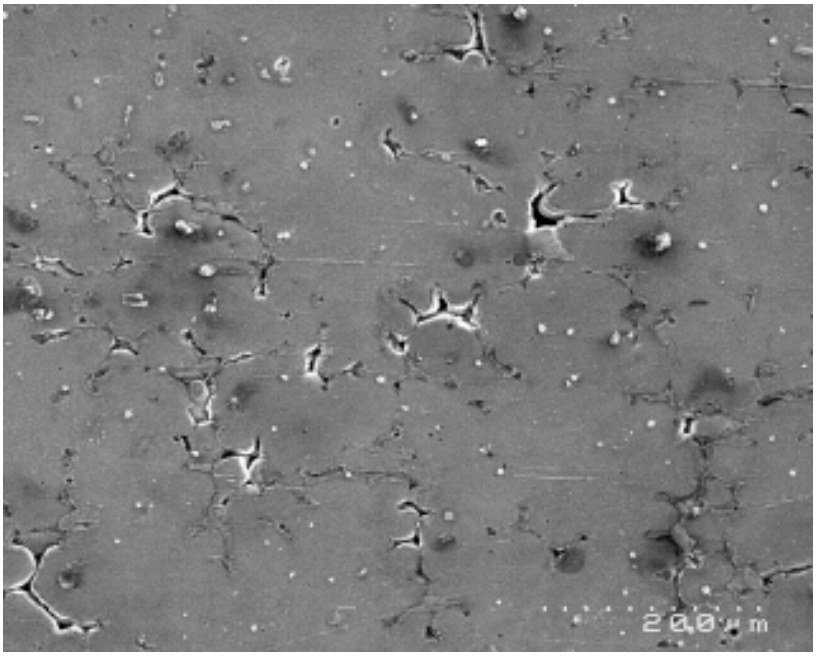

Figure 5-25: SEM micrograph of the rim section of the AM60B casting that was grain refined with the carbon tablet.

A much higher magnification image was taken of this sample and is shown in Figure 5-26. Here the relationship between a magnesium dendrite and an $Mg_{17}Al_{12}$ eutectic particle is shown more clearly. The dendrite arm has grown to the point where a small isolated pool of eutectic liquid has solidified, but in an amount insufficient to fill the remaining void. This has resulted in a small isolated pore between the dendrite arm and brittle $Mg_{17}Al_{12}$ particle.

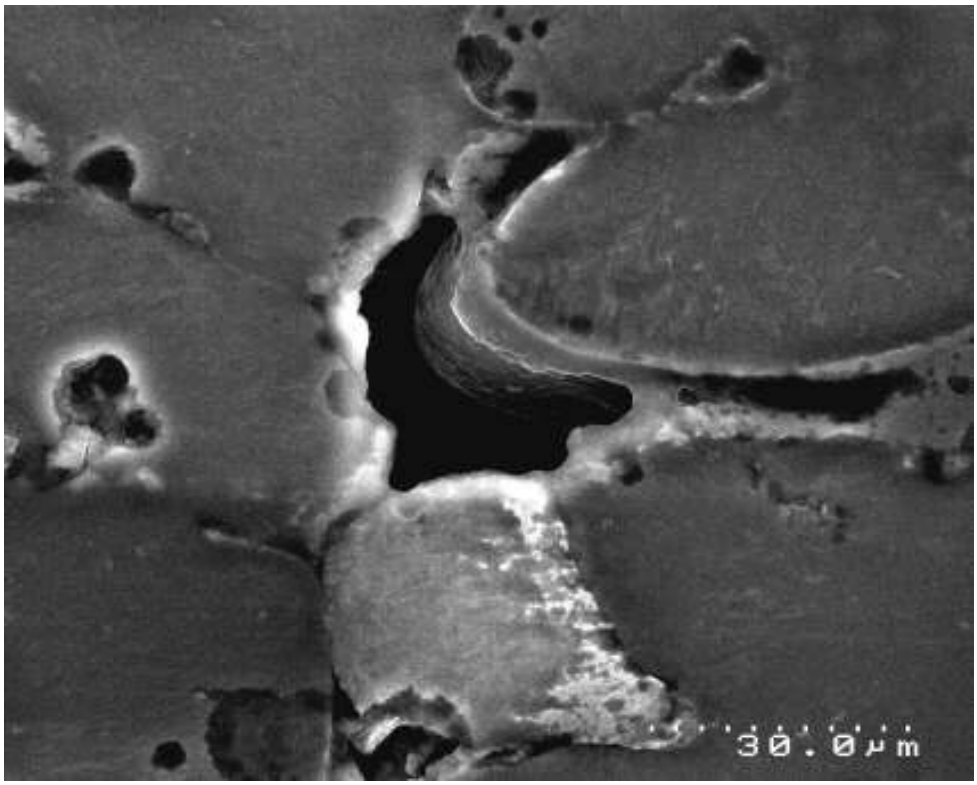

Figure 5-26: A high magnification SEM image of a pore in the rim section of the AM60B casting treated with 0.01 wt% C.

X-ray elemental mapping was performed on the sample to identify the location of the major alloying elements (Mg, Al, Mn, Zn) in the sample, as well as carbon. This was to detect any correlation between the positioning of carbon and aluminium containing particles, which would to some degree, confirm the composition of nucleating particles as Al4C3 or a combination of Al-C-O. The results of the elemental mapping are displayed in Figure 5-27.

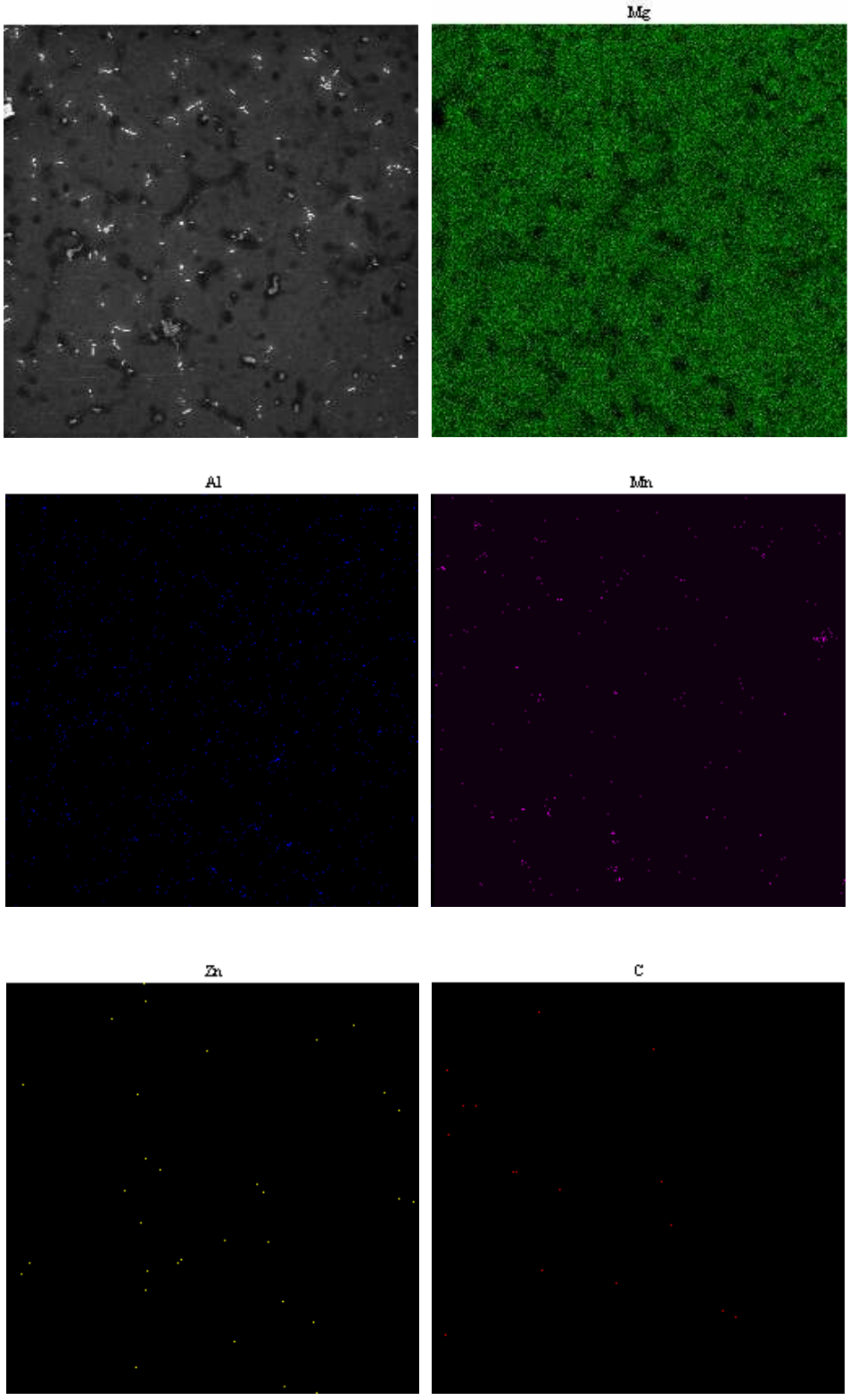

Figure 5-27: X-ray elemental map of the AM60B casting sample treated with 0.01 wt% C.

As with the X-ray elemental mapping of the AZ91E casting sample described in the last chapter, the elemental map shown in Figure 5-27 shows that along with the already known alloying elements of Mg, Al, Mn, and Zn present in the alloy there are also small traces of carbon. While this may indicate the presence of carbon containing nucleant particles such as Al_4C_3, there again appears to be little correlation between the location of the carbon and the location of aluminium in the elemental map. There is a possibility that the particles may have been affected during sample preparation through reaction with the water stream used for lubrication and cooling. The use of diamond particles during the polishing process may have also introduced carbon particles into the soft magnesium microstructure. The correct identification of the nucleating particles when carbon is used as a grain refiner for Mg-Al alloys is an area which deserves further detailed research.

5.4 Discussion

5.4.1 The Grain Refinement of AM60B

As with the castability investigation for AZ91E detailed in Chapter 4, the two grain refiners chosen for this study were based on the nucleant and solute theories of solidification nucleation. Strontium was added to the casting melt to promote constitutional undercooling and solute rejection at the solidification interface, and carbon was added as it is known to form powerful nucleant particles in conjunction with aluminium when added to Mg-Al melts[2-4]. Unfortunately in the case of the AM60B castings the grain refinement effect was not as significant as was seen in the study involving AZ91E.

The first issue to address relates to the introduction of sufficient amounts of grain refiner to the casting melt prior to pouring. Again, as with the AZ91E castings, there were no problems reaching the desired strontium addition rates when using the Al-10 wt% Sr master alloy. This confirms that plunging the master alloy beneath the surface

of the melt and holding for a short period allows enough contact between the master alloy and the melt for the strontium to be taken into solution. Stirring the melt for 60 seconds would have also aided this dissolution. Although strontium is known to oxidise extremely easily at high temperatures [5], the plunging of the master alloy below the melt surface combined with the use of the SF_6 cover gas has prevented any loss of elemental strontium in the castings.

The difficulty in introducing carbon to Mg-Al melts is highlighted in the literature [6]. This study has again shown that plunging fine carbon black powder wrapped in aluminium foil is not a consistently successful method of introducing carbon into the alloy melt. The addition of 0.05 and 0.10 wt % C using this method resulted in carbon levels of 0.005 and <0.005 wt% C respectively. Using the newly developed carbon tablet at a nominal addition rate of 0.05 wt% C, resulted in the highest carbon content in the castings of 0.01 wt% C. Although still lower than the desired addition level, this has again proved to be the most successful method for introducing carbon as a grain refiner to the casting melt. It is likely that when adding the foil wrapped powder, the majority of the carbon black is released from the foil upon contact with the melt and floats to the melt surface where it is removed with the layer of oxide during melt drossing. Using the carbon tablet results in a slow break down of the solid Al/Mg matrix when plunged into the melt, which in turn results in a slower release of carbon or carbon containing particles in the melt. This gives a greater contact period between carbon and the magnesium melt increasing the likelihood of formation of powerful nucleating substrates. The high energy ball milling of the aluminium, magnesium, and carbon powders used to produce the tablets may also have lead to the formation of these particles.

The second issue to be addressed is the success level of the separate grain refinement additions. During the course of this work, it was found that strontium had little effect on the as-cast grain size of the AM60B castings. Whilst a range of grain sizes was achieved throughout the different samples, each of the mean grain size measurements

fell within one standard deviation of each other, indicating strontium has a negligible effect on the grain size of AM60B.

These results follow a similar trend to that observed during experimentation by other researchers. During their in-depth study of the grain refinement of magnesium, Lee et al [3] added strontium to a Mg-Al casting melt and obtained similar results. They found that when the melt contained 3% Al, strontium had a variable effect on grain size when the addition rate was between 0.001-0.1 wt% Sr. The initial addition of 0.001 wt% Sr gave a slight reduction in grain size with a slight increase in grain size achieved with 0.1 wt% Sr. It was not until the strontium level was increased further to 1 wt% that any significant grain size reduction was seen.

Figure 5-4 has shown that a more effective grain refinement is achieved with the addition of carbon to an AM60B melt prior to casting. As discussed previously, adding 0.05 wt% carbon black wrapped in foil resulted in a carbon level below the detection limit of the leco-combustion analysis. The resulting grain sizes displayed in Figure 5-4 indicate that there was no carbon in the castings at all. However, when 0.005 wt % C was introduced to the melt, the grain size was reduced by 30% which highlights the effectiveness of this element in the grain refinement of magnesium. Increasing the carbon content to 0.01 wt% C lead to a further 21% reduction in grain size. This was highlighted best in the rim section, where the mean grain size was reduced from 477μm in the untreated castings to 235μm in the castings treated with 0.01 wt% C. These results compare well with the literature which suggests that once a small amount of carbon can be successfully introduced into an Mg-Al alloy melt, it will provide the highest level of grain refinement compared with other elements [6, 8]. Wallace found that in the grain refinement of AM50A, an alloy with a chemical composition very similar to the alloys used in this study, the three most successful grain refiners (C_2Cl_6, SiC, and CaC_2) all contained carbon [8].

5.4.2 The Effect of Grain Refinement on External Casting Defects

An important aspect of casting quality, and one that often leads to castings being rejected at first inspection, is the slumping of the casting surface. By taking the defect severity data from Section 5.3, and plotting it against grain size, the effect of grain refinement on surface slumping in AM60B can be identified. In the experimental castings, the surface slumping defect is located on either side of the hub and spoke/rim junction sections of the castings. For consistency, the mean grain size of only one of these sections was used for the analysis. In this case it was the grain size of the spoke/rim junction, although there is little discrepancy between the two. The results of this analysis are presented in Figure 5-28.

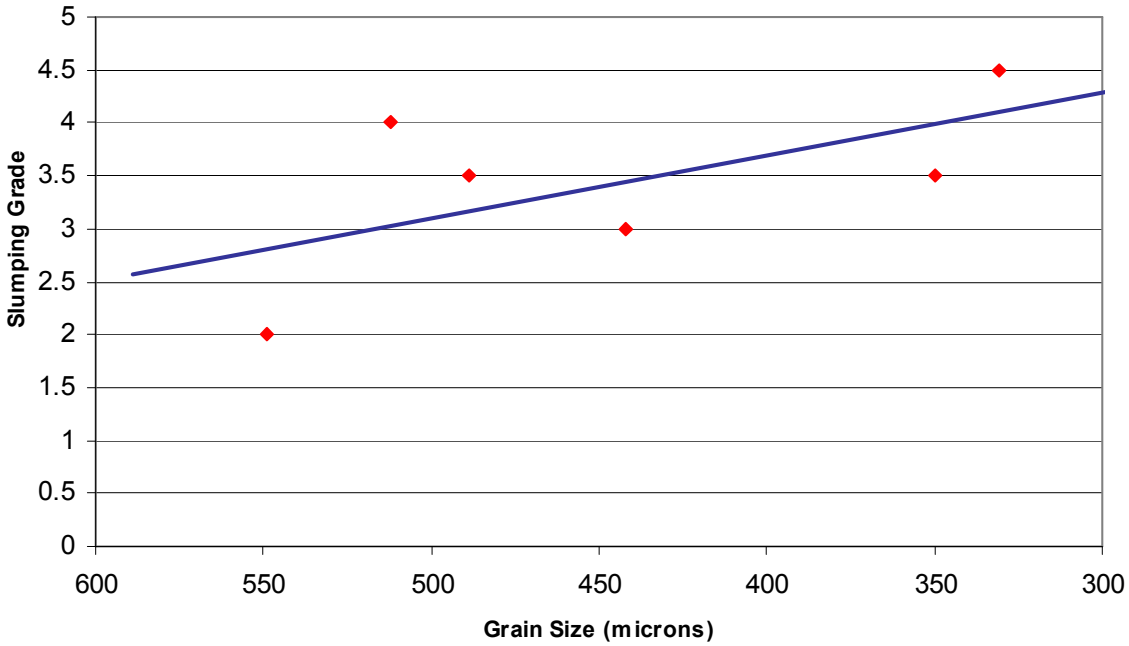

Figure 5-28: Surface slumping defect severity versus grain size in the AM60B castings.

From Figure 5-28 it is obvious that an increase in grain refinement leads to an increase in the severity of the surface slumping defect. The increased dependence on solid feeding to accommodate the solidification shrinkage in the grain refined castings is due

to the closing off of the feeding channels earlier in solidification. The solidification pressure exceeds the yield stress of the outer shell of the AM60B casting, causing the surface of the casting to slump inwards. This explains why an increase in the degree of grain refinement leads to an increase in occurrence of the surface slumping defect.

One of the often stated benefits of grain refinement is an increased resistance to hot tearing due to the improved strength of the internal structure [3, 8-10]. To identify whether this is the case with AM60B, the severity of hot tearing in the castings was plotted against mean grain size to produce Figure 5-29.

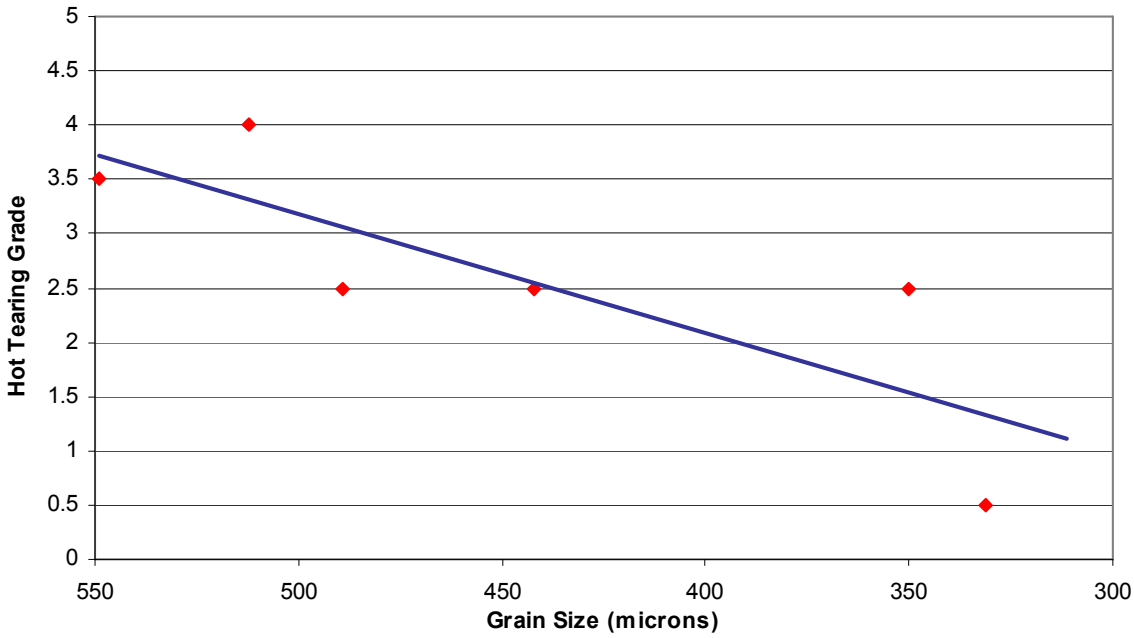

Figure 5-29: Grain size versus hot tearing severity for the AM60B castings.

Figure 5-29 confirms that for the AM60B castings, an increase in the degree of grain refinement leads to a linear decrease in the severity of hot tearing. The fact that the defect was completely eliminated in AZ91E but not in this case, might be due to the much finer grain sizes achieved with the AZ91E castings. Inspection of Figure 4-33 of Chapter 4 shows that once grain size was reduced to around 275µm hot tearing was eliminated. As AZ91E and AM60B have similar strengths (UTS = 230 and 220 MPa at

room temperature respectively [5]) a similar grain size would give a similar resistance to hot tearing. It would be logical to assume that if smaller grain sizes were obtained for the AM60B castings, an elimination of hot tearing would also have occurred. Another important point to note is the location of the hot spot near the spoke/rim junction of the castings. In the AZ91E casting simulation shown in Figure 4-16, the hot spot is centred more towards the junction itself, whereas with the AM60B castings simulation shown in Figure 5-14 it is extended further towards the spoke. This location directly adjacent to the sharp angled transition from the rim to the spoke means that the stresses evolved from solidification shrinkage would have more impact on the occurrence of hot tearing in the AM60B castings. Comparing the results presented in Figure 5-29 of this chapter to Figure 4-33 of the previous chapter confirms this thinking. With the AZ91E castings, only when the grain size is very large (i.e. ~ 500μm) is hot tearing a problem, and the severity of the defect drops sharply with respect to decreasing grain size until it is eliminated at around 300μm. With the AM60B castings, hot tearing severity is also reduced with grain refinement, but not to the same extent and the defect was never eliminated.

Literature detailing the effect of grain refinement on the hot tearing of Mg-Al alloys is scarce. One study of different grain refiners for AM50A [8] showed that there was no hot tearing in the castings when C_2Cl_6 was used as a degassing/grain refinement addition, although there was little tearing in the unrefined castings to begin with. Once again the advantage of the current research is highlighted by the fact that not only is the presence or absence of hot tearing reported, but also the severity of the defect. This allows the correct level of grain refiner addition to be determined by balancing the positive effect on properties with the negative effects on castability.

The results presented here and in the previous chapter highlight the effectiveness of using the specially designed experimental casting mould to determine the castability of magnesium alloys. The mould was not designed to make perfect castings, but rather to promote the occurrence of casting defects so that the behaviour of these defects with differing grain structure could be assessed. By plotting not just the occurrence, but also

the *severity* of the defects, a valuable insight into the effect of grain refinement on castability has been obtained. Work of this nature has not been carried out previously for magnesium-aluminium alloys.

5.4.3 The Effect of Grain Refinement on Porosity

The most inconsistent and variable data collated during this investigation related to the effect of strontium additions on the internal porosity levels of the separate casting sections. This is due to the fact that although the targeted strontium addition levels were achieved in the castings, there was a variable effect on grain size. To clarify the situation further, the internal porosity level for each casting section was plotted against its respective grain size to highlight any trends that may be apparent. This would clarify the effect of grain size on internal porosity in the AM60B castings. The first set of data is presented in Figure 5-30 which shows the effect of grain size on the internal porosity levels of the spoke and rim sections of the experimental castings.

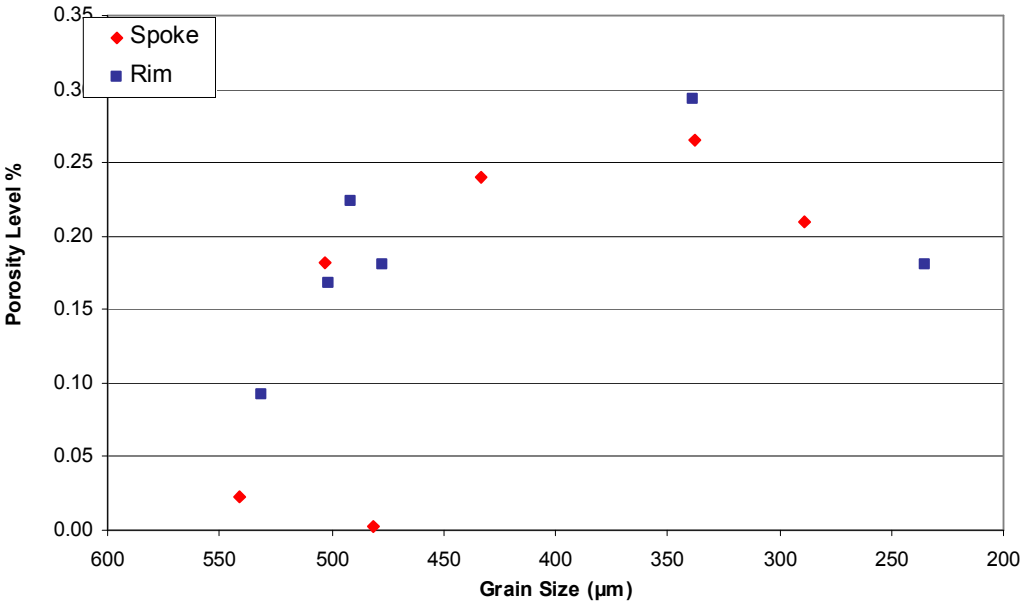

Figure 5-30: The effect of grain size on the internal porosity levels in the spoke and rim of the AM60B castings.

Figure 5-30 shows a general increase in internal porosity in the thinner casting sections as grain size is reduced. There are discrepancies visible in the trend though, in the red spoke section around 500µm and the blue rim section around 235µm. With the spoke section there are two rather different porosity levels obtained for a similar grain size, and in the rim section the porosity level at 235µm is a little lower than expected. These discrepancies can be attributed to the fast freezing nature of the thinner sections leaving limited time for pore formation, leading to natural fluctuations. It also is important to note the scale divisions on the y axis are based on only 0.05% increments due to the low range of porosity levels involved.

A more confident relationship between grain size and internal porosity level can be obtained by analysing the thicker hub and spoke/rim junction casting sections. Here solidification time is longer, and the range in porosity level is large enough, for the effect of grain refinement on porosity level to be confidently established. Figure 5-31 shows that in both of the casting sections an increase in grain refinement leads to a linear increase in porosity levels. When a large grain size in the order of 500-600µm is produced in the casting sections, the porosity level is less than 0.8%. However, when the addition of a grain refiner produces a finer microstructure the porosity level increases steadily. When the grain size was measured to be around 300µm in the thicker casting sections, the internal porosity levels is raised to over 1.5%. These porosity levels are much lower than in the corresponding sections of the AZ91E castings due to the much smaller freezing range of the AM60B alloy.

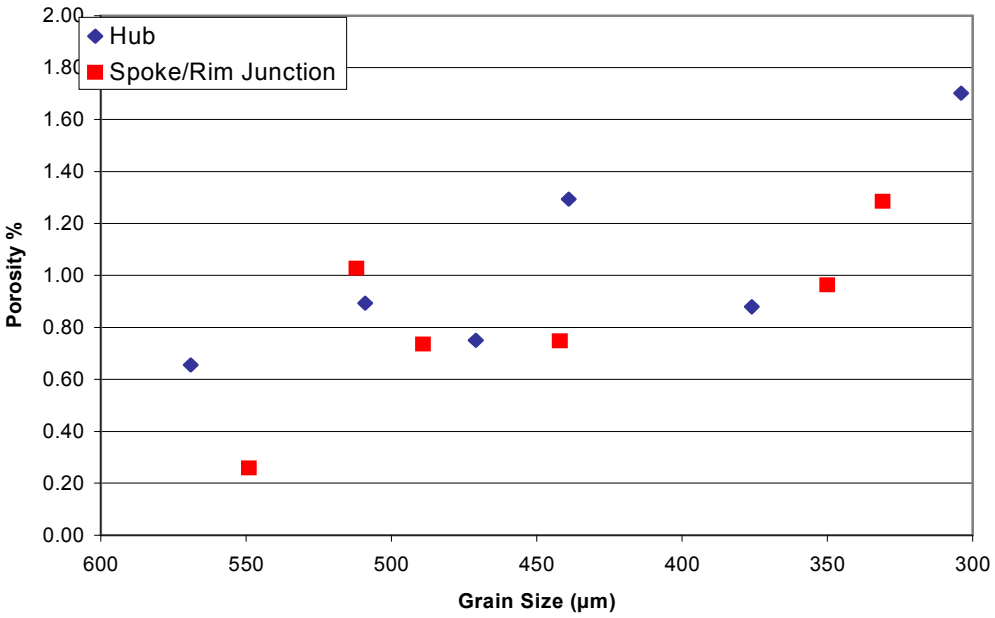

Figure 5-31: The effect of grain size on the internal porosity levels in the hub and spoke/rim junction of the AM60B castings.

As presented in Figure 4-36 of Chapter 4, Easton and StJohn [9] showed that dendrite coherency occurs later in grain refined castings. This is of great benefit to castings that solidify directionally as they rely less on the feeding of liquid through the interdendritic network. In many cases however, solidification does not progress directionally. The temperature profile simulated for this casting (Figure 5-14) shows that there are distinct hot spots around the hub and spoke/rim junction that would solidify much later than the spoke and rim sections. In these areas there is a greater reliance on interdendritic feeding to compensate for solidification shrinkage. This explains the trend seen above in Figure 5-31 and was also seen with the AZ91E castings. A finer grain size results in a much finer interdendritic network, which severely restricts the flow of feed metal, increases the required feeding pressure, and thus leads to an increase in the level of internal microporosity.

The optical microscopy examination has shown that, along with an increase in porosity with decreasing grain size, there is also a change in the distribution of pores. A finer grain size reduces the fraction of pores located within the grains and transforms the

distribution of pores to being completely intergranular. This poses an added risk to casting producers, as intergranular microporosity is likely to be interconnected through the grain boundary network resulting in a decrease in strength, ductility, and pressure tightness of cast components.

5.5 Conclusions

Just as was found for the AZ91E castings in the previous chapter the experimental mould proved to be very successful in highlighting the effects of grain refinement on the castability of magnesium alloy AM60B. The relationship between grain size and the occurrence of casting defects has been established along with how defect severity is affected by grain refinement. The main conclusions from this investigation are as follows:

- The addition of strontium had a negligible effect on the mean grain size of each of the casting sections and it appears strontium is not an effective grain refiner for AM60B. However, the addition of strontium did transform the grain morphology of the castings from partly columnar and partly equiaxed to completely equiaxed throughout.

- The targeted levels of strontium were again reached buy adding the Al-10 wt% Sr master alloy to the alloy melt. The newly developed carbon containing tablet has also been proved to be effective in consistently introducing carbon into an AM60B melt.

- The addition of carbon had a significant effect on the grain size of the castings. As little as 0.005 wt% C was sufficient to reduce grain size by 30% in the experimental castings, with 0.01 wt% C yielding further refinement.

- Grain refinement has been found to decrease hot tearing severity of AM60B castings. However, both surface slumping severity and internal porosity level is greatly increased as grain size is reduced.

- Grain refinement was found to affect the distribution of pores within a casting. As the level of refinement was increased, internal pores became located solely along the grain boundaries.

5.6 References

[1] Aliravci, C. A., Gruzleski, J. E. and Dimayuga, F. C., *Effect of Strontium on the Shrinkage Microporosity in Magnesium Sand Castings.* AFS Transactions 1992 AFS **100** 353-362 (1992).

[2] Liu, Y., Liu, X. and Xiufang, B., *Grain Refinement of Mg-Al Alloys with Al4C3-SiC/Al Master Alloy.* Materials Letters **58** 1282-1287 (2004).

[3] Lee, Y. C., Dahle, A. K. and StJohn, D. H., *Grain Refinement of Magnesium.* Magnesium Technology 2000 H. I. Kaplan, et al. TMS 211-218 (2000).

[4] Qian, M. and Cao, P., *Discussions on Grain Refinement of Magnesium Alloys by Carbon Inoculation.* Scripta Materialia **52** 415 - 419 (2005).

[5] Askeland, D. R., *The Science and Engineering of Materials.* London Chapman and Hall 830-831 (1996).

[6] Nelson, C. E., *Grain Size Behaviour in Magnesium Casting Alloys.* AFS 52nd Annual Meeting Chicago, IL. American Foundryman's Society 1-23 (1948).

[7] Dahle, A. K., Lee, Y. C., Nave, M. D., Schaffer, P. L. and StJohn, D. H., *Development of the As-Cast Microstructure in Magnesium-Aluminium Alloys.* Journal of Light Metals **1** 61-72 (2001).

[8] Wallace, J. F., Schwam, D. and Zhu, Y., *The Influence of Potential Grain Refiners on Magnesium Foundry Alloys.* AFS 2003 1-15 (2003).

[9] Easton, M. and StJohn, D. H., *The Effect of Grain Refinement on the Formation of Casting Defects in Alloy 356 Castings.* Int. J. Cast Metals Res. **12** 393-408 (2000).

[10] Davis, J. A., Eastwood, L. W. and DeHaven, J. C., *Grain Refinement in Magnesium Casting Alloys.* AFS Transactions **53** 352-362 (1945).

6.0 Further Discussion of the Effects of Grain Refinement on the Castability of Mg-Al Alloys

6.1 Introduction

The investigation presented in this work into the effects of grain refinement on the castability of Mg-Al alloys has produced many valuable findings. The alloys investigated, AZ91E and AM60B, are two of the most widely used alloys in the magnesium casting industry. This chapter aims to tie together the results obtained for both alloys, and in conjunction with the literature, further discuss the effects of grain refinement on the castability of Mg-Al alloys.

6.2 Grain Refiner Effectiveness

The grain refiner additions chosen for this study were based on the proposed modes of grain refinement by constitutional undercooling (strontium) and heterogeneous nucleation (carbon). Strontium addition proved successful in grain refining the AZ91E alloy castings, but the results obtained when added to AM60B were not as significant. Although strontium has a low solid solubility in pure magnesium, the potential interaction with aluminium when used with Mg-Al alloys reduces its potency. It is therefore interesting that strontium was more effective in grain refining the higher aluminium content AZ91E than for the AM60B. Aside from chemical composition, another major difference in the two castings was the as-cast grain size of the untreated samples. AZ91E possessed a much larger grain size in the untreated state. This suggests strontium may be effective in the grain refinement of Mg-Al castings when there is a tendency for larger grain growth, though its effect is minimised when growth is already restricted by other factors such as cooling rate. Aliravci et al [1] noted a further reduction in grain size when strontium was added to an AZ91C melt which had already been grain refined using hexachloroethane tablets.

This investigation was carried out on sand cast samples which possess a comparatively large grain size due to the slower cooling rate of this type of casting. The fundamental aspects of grain refinement theory are beyond the scope of this thesis, however this does present an area deserving of further investigation.

Carbon addition proved to be extremely effective in grain refining both alloys used in the investigation. The initial experimentation of adding carbon black powder directly to the melt resulted in grain refinement to varying degrees of success. These results mirror those presented in the literature [2-5] where it is suggested that carbon is an excellent grain refiner of Mg-Al castings, though difficult to introduce to the melt successfully. This lead to the development of a novel method of carbon inoculation, using a pressed tablet of Mg/Al/C based composite powders to facilitate the slow release of carbon as the tablet dissolved. This tablet enabled the carbon level of both alloys to be raised significantly higher than when simply adding carbon black powder, and resulted in unparalleled levels of refinement. The fact that a greater refinement was experienced in the AZ91E castings than with the AM60B is due to the higher aluminium content of AZ91E. When even small amounts of carbon are introduced to Mg-Al alloys, the carbon reacts with aluminium to form powerful nucleating substrates that promote numerous solidification events within the casting melt. Therefore, the effect is expected to be greater as aluminium content is increased for the same level of carbon addition. The successful identification of the particles responsible for nucleation was unable to be accomplished using conventional microscopic techniques, though once again, this was outside the scope of this work. The development of the carbon-containing tablet as a method of adding carbon to the Mg-Al alloy melts is seen as a major contribution arising from this research and one that opens up avenues for further investigation. Overall, the use of both strontium and carbon as grain refiners for AZ91E and AM60B resulted in a wide range of grain sizes being achieved throughout the different casting samples. This allowed thorough investigation into the sensitivity of the castability of Mg-Al alloys to grain refinement.

6.3 The Effect of Grain Refinement on External Casting Defects

External casting defects cause many castings to be rejected soon after they are removed from the casting mould. Elimination of these types of defects is of prime importance to casting manufacturers, as they are costly both in terms of the time spent producing them and the value of the material and energy expended in producing them. This is especially significant with magnesium castings as they are not as easily recycled as aluminium and other castings. This study was able to add quantitative data to a usually qualitative assessment of external casting defects to determine their sensitivity to the level of grain refinement. It was found that the occurrence of hot tearing was closely related to the grain size in Mg-Al castings, with both AZ91E and AM60B showing a considerable decline in hot tearing severity with decreasing grain size. Conversely, the severity of the surface slumping defect was increased considerably with decreasing grain size.

Figure 6-1 shows the sensitivity of the defects with respect to grain size for both alloys combined. Although the graph is based on a combination of two differing alloys, each with their own chemical composition and solidification behaviour, the obvious trends in the graph cannot be ignored.

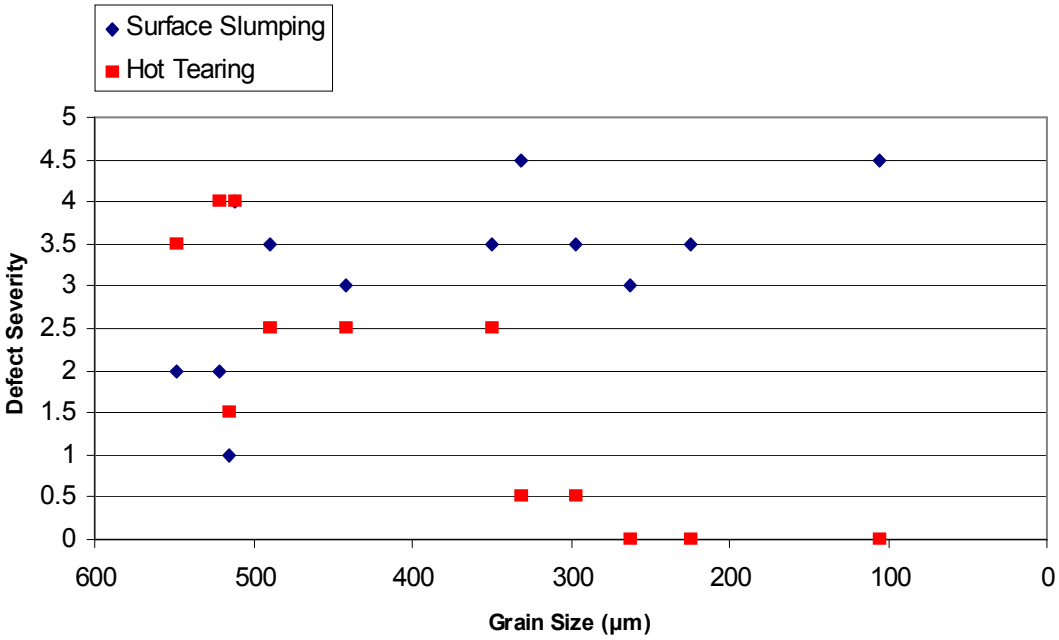

Figure 6-1: Sensitivity of hot tearing and surface slumping defects to grain size in Mg-Al castings.

Surface slumping of a casting results from the solid feeding of a solidifying area through movement of the material surrounding it. The requirement for this feeding arises from a build up of negative pressure inside the casting as the material solidifies and shrinks. This pressure can be alleviated by increasing the head of metal in feeding reservoirs (such as risers), which in turn increases the internal pressure in the system. This has been verified in the literature as an appropriate means of reducing surface slumping by Campbell [6], and means the benefits of grain refinement can still be realised as long as a casting is adequately designed to minimise a resulting increase in slumping susceptibility.

The reason grain refinement results in an increase in the severity of the surface slumping defect is due to the reliance on interdendritic feeding in the latter stages of solidification. In a casting with a larger grain size, once the coherency point is reached the large interdendritic channels allow feed metal to flow more freely than in a grain refined casting. With a smaller grain size, although coherency is reached later, the fine interdendritic channels result in a large increase in feeding pressure

within the casting. This pressure is alleviated in the system through the nucleation of internal porosity, or by solid feeding. Solid feeding causes the inward slumping of the casting surface and this is why a fully refined casting will be more prone to surface slumping.

As mentioned in Chapter 2, hot tearing is one of the worst defects from which a casting can suffer. This defect is a result of shrinkage pressures building in the casting to a point where it is literally torn apart. A grain refined casting is more immune to the hot tearing defect because having a finer grain structure makes it more difficult for cracks to nucleate and propagate through the casting structure. Also, any intergranular liquid which may weaken the structure is spread more thinly making a stronger network. This makes it much more difficult for a casting to be torn apart. The reduction in hot tearing severity with grain size in Mg-Al castings is a valuable finding that reflects similar results discovered with the grain refinement of aluminium alloys [7]. It is widely known that long freezing range magnesium alloys such as AZ91E are highly susceptible to hot tearing, but until now no work has been published that clearly illustrates the sensitivity of this defect to grain size in magnesium castings.

The other phenomenon that can be observed from examining Figure 6-1 is that the decrease of the severity of hot tearing with decreasing the grain size appears to be strongly linked to the increase of the severity of surface slumping with decreasing grain size. The understanding of this phenomenon is related to the discussion made in Section 2.4.5 of Chapter 2. As the solidification of the two hot spots causes the spoke section to be pulled apart in a uniaxial tensile manner, the formation of surface slumping (or internal porosity) at one or both of the hot spots would allow the tensile stress to be reduced as the casting is opened up. Therefore the likelihood of a hot tear appearing at the sharp corner between the spoke and neighbouring hot spots would be reduced. This may help explain the extreme end of Figure 6-1 where a high level of surface slumping led to a complete elimination of hot tearing. The increase in the strength of the material thanks in to a fine grain size, and the alleviation of some of

the tensile stress acting in that area through the formation of the slumping defect, combine to resist the growth of a hot tear. Likewise, if the stresses acting during the solidification of the experimental casting reached the critical stress for hot tearing to arise, the triaxial hydrostatic stress due to shrinkage in the hot spots would be partially reduced, lessening the likelihood of surface slumping occurring.

6.4 The Relationship between Grain Refinement and Porosity

6.4.1 The Effect of Grain Refinement on Porosity Formation

The two most effective means of feeding a casting to compensate for the shrinkage induced as it solidifies are liquid and mass feeding. Liquid feeding, as the name suggests, is the flow of liquid metal to the areas where it is required and mass feeding is the flow of a semi-solid slurry. This slurry contains a mix of liquid metal and solidified casting grains which are carried by the liquid until they begin to interlock and halt movement of the slurry. The point at which the grains fully interlock and mass feeding ceases is termed the coherency point. The addition of grain refiners to a casting melt results in an increased number of casting grains that are smaller than in unrefined castings, and so are able to be carried further by the surrounding liquid until the coherency point is reached. It is for this reason that grain refinement is widely thought to increase the feedability of a casting melt, and thus reduce the formation of casting pores.

This work has shown that for Mg-Al alloy castings an increase in grain refinement leads to an increase in the level of internal shrinkage porosity. By looking at the worst fed area of the experimental casting mould, the spoke/rim junction, it is obvious that an increase in grain refinement has lead to a subsequent increase in the level of internal shrinkage porosity. Figure 6-2 plots the porosity level of both the AZ91E and AM60B castings versus their respective as-cast grain size for that area. It

shows a strong trend of increasing porosity level as the level of grain refinement is increased.

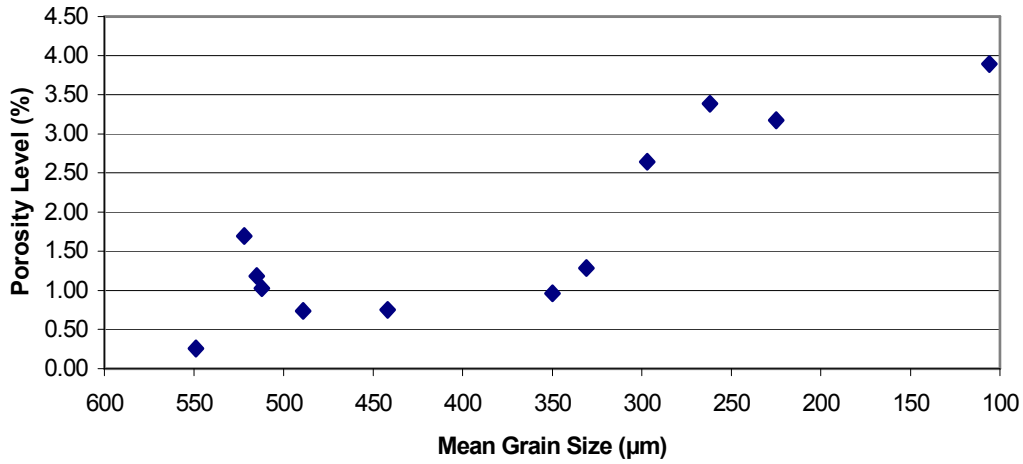

Figure 6-2: Internal porosity level vs. mean grain size for the spoke/rim junction of the experimental AM60B and AZ91E castings.

The reason for the increase in porosity level with increased grain refinement is because once the coherency point is reached, the feeding of this semi solid area in the casting changes to interdendritic feeding. A smaller grain size in the spoke/rim junction means that the interdendritic channels that the liquid metal must flow through to feed the solidifying structure are considerably finer than for a larger grain size. Therefore, the pressure differential required to enable liquid to be drawn through the network is increased significantly. Figure 6-3 shows schematically the differences in solidification tendencies of the spoke/rim junction with large and small mean grain sizes respectively. The coherency point is seen to be reached later for the grain refined casting, however the fine interdendritic network restricts interdendritic feeding, leading to a more porous casting. The internal negative pressure that builds up due to unfed shrinkage in the hot spot created by the casting geometry reaches a point where the surrounding material caves inwards to compensate.

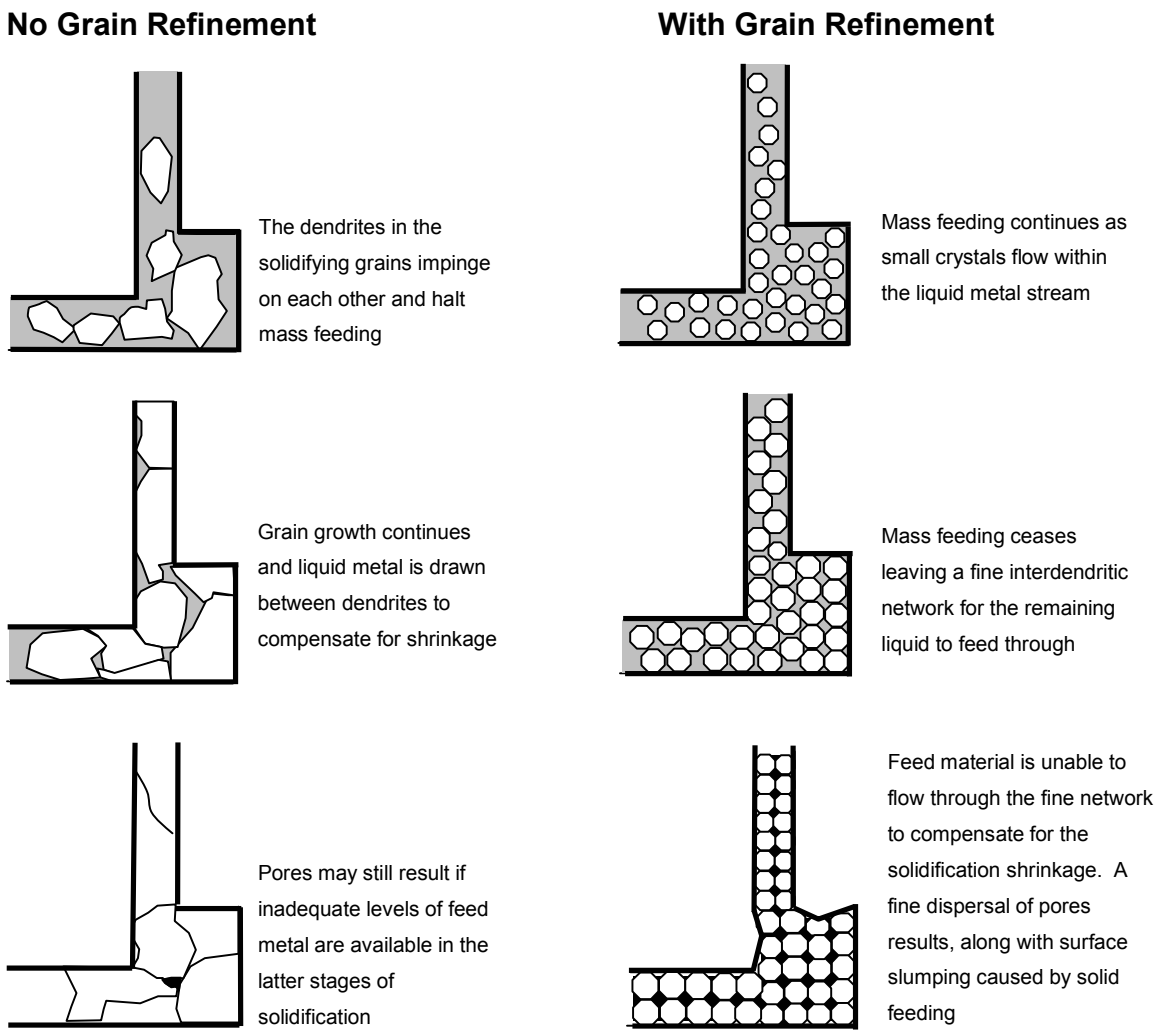

Figure 6-3: Schematic illustration of the different solidification tendencies for non-grain refined (left) and grain refined castings (right).

It is tempting to compare the castability of Mg-Al with the castability of other common casting alloys such as Al-Si alloys, however there are distinct differences that help explain why grain refinement was seen to have such a detrimental effect on porosity formation. Figure 6-4 schematically illustrates the difference in the dendritic structures of aluminium and magnesium alloy castings. Unlike aluminium alloys where the solid dendrites grow with a cubic structure and four-fold symmetry, the hexagonal close packed (HCP) structure of magnesium means the growing dendrites possess a six-fold symmetry. This makes liquid flow through the interdendritic

network more difficult in magnesium castings as grain size, and hence interdendritic spacing, is reduced.

Figure 6-4: Schematic illustration of the different dendritic structure of an aluminium (left) and magnesium (right) alloy casting. The finer dendritic network of the magnesium alloy casting makes interdendritic feeding more difficult.

The equilibrium phase diagram for Al-Si shows that solidification of an aluminium-silicon alloy such as A356 progresses with a mixture of primary α-aluminium crystals and liquid alloy until the eutectic composition is reached. The presence of around 50% eutectic [7] means there is ample liquid available to compensate for solidification shrinkage. The Mg-Al equilibrium phase diagram on the other hand suggests that for alloys with less than 13% Al there should be no eutectic present upon solidification under equilibrium conditions. The non-equilibrium freezing characteristics of permanent mould casting mean that a metastable eutectic of α-magnesium and $Mg_{17}Al_{12}$ is present in the solidifying microstructure, though it is obviously not as prominent as with Al-Si casting alloys.

Literature suggests that in the critical last stages of solidification, both the morphology and formation mechanisms of the eutectic are important [2]. If there is a smooth growth of the solid/liquid interface during eutectic solidification, feeding is less likely to be affected than if the growth of one phase leads the other. If the strong segregation of an element during eutectic solidification leads to one phase growing ahead of the other, the interdendritic channels will become restricted further and feeding will be even more difficult. Zinc is one element that has been found to segregate strongly to the $Mg_{17}Al_{12}$ phase [8], so the presence of this element in

AZ91E may further add to the propensity for pore formation with decreasing grain size in this alloy.

6.4.2 The Distribution and Morphology of Pores

The microscopic examination of casting pores with respect to grain size carried out for successively higher levels of grain refinement of AZ91E and AM60B showed that there is a transition in pore morphology and distribution as grain size is reduced. In the unrefined samples, long branches of interconnected pores are seen to be extending both along the grain boundaries as well as through the interdendritic boundaries within the grains. As grain size was progressively reduced, pores were seen to be located only at grain boundaries in distinct locations. This suggests that once the grain size is reduced to a level where interdendritic feeding of liquid metal becomes too difficult, individual grains tend to solidify independently. With a larger grain size, the interdendritic and intergranular paths through which the feed metal flows are able to pass liquid metal to surrounding grains and compensate shrinkage. As these paths constrict and halt efficient feeding, the liquid left inside is quickly used up leaving an interconnected branch of porosity. In the case where the grain size is reduced to a level where interdendritic feeding of liquid is impossible, even with adequate levels of feed material available in the system, the trapped liquid feeds only its surrounding grains. Once the liquid metal has been completely spent, this results in many small pores pinned at the grain boundaries. The spoke/rim junction and the rim sections of the castings displayed similar results, which suggests this phenomenon may act independently of casting geometry.

6.5 Application to Industry

The findings presented in this study propose a rethink of the level of grain refinement to be selected when attempting to cast sound components from Mg-Al alloys. While the benefits of increased strength, ductility, and corrosion resistance that come from a

small grain size in a casting cannot be ignored, the results of this investigation show that the castability of Mg-Al alloys is extremely sensitive to grain size. It would appear there is no simple answer to the question "how much grain refinement should be used when casting Mg-Al components?" The use of grain refinement may be totally justified in castings of simple geometry where solidification is directional and hot tearing is not a major concern. The increased efficiency of mass feeding that is obtained with small grain sizes would add to the grain refinement benefits already mentioned. However, as is often the case when producing castings of complex geometry where structural integrity and pressure tightness are of prime importance, the answer is not that simple. This study has shown that when castings possess hot spots, frequent changes in section thickness, and non-directional solidification, the addition of grain refiners will have a profound effect on castability. If using an alloy that is prone to hot tearing, grain refinement has been proven to successfully eliminate this defect, which means less focus need be put into designing around this defect. However if hot tearing is not seen to be a significant issue when producing a Mg-Al casting then the benefits of grain refinement must be balanced against an increase in surface slumping and internal porosity.

The experimental mould used in this investigation was designed to emulate the geometry of an alloy wheel casting. When producing such a casting, structural integrity and pressure tightness are two very important properties required for a successful casting. This makes selection of the correct level of grain refinement difficult. Refining the grain size fully would eliminate the risk of hot tearing and produce a strong, ductile casting. However, the increased level of porosity that resulted would reduce pressure tightness, leading to the potential for "leaking" wheels. This is a very expensive defect as it is only identified in the final stages of production after significant time and energy has been expended in producing the component. In this case, attention needs to be paid to the correct positioning of efficient feeding reservoirs around the casting mould, or the use of added pressure during solidification as is used in the low pressure casting process. This would help

combat the reduction in interdendritic feeding efficiency and reduce the potential for porosity formation.

6.6 References

[1] Aliravci, C. A., Gruzleski, J. E. and Dimayuga, F. C., *Effect of Strontium on the Shrinkage Microporosity in Magnesium Sand Castings.* AFS Transactions 1992 AFS **100** 353-362 (1992).

[2] Dahle, A. K., Lee, Y. C., Nave, M. D., Schaffer, P. L. and StJohn, D. H., *Development of the As-Cast Microstructure in Magnesium-Aluminium Alloys.* Journal of Light Metals **1** 61-72 (2001).

[3] Davis, J. A., Eastwood, L. W. and DeHaven, J. C., *Grain Refinement in Magnesium Casting Alloys.* AFS Transactions **53** 352-362 (1945).

[4] Hogg, J. C., Westegen, H. and Albright, D., *Low Pressure Sand Casting of Magnesium Alloys.* Extraction, Refining, and Fabrication of LIght Metals M. Sahoo and P. Pinfold Ottawa Pergamon Press 57-65 (1991).

[5] Kurfman, V. B., *Hydrogen Escape from Magnesium Alloys.* Modern Castings **45** 9-12 (1964).

[6] Campbell, J., *Solidification Shrinkage.* Castings Oxford Butterworth-Heinemann Ltd 175-208 (1991).

[7] Easton, M. and StJohn, D. H., *The Effect of Grain Refinement on the Formation of Casting Defects in Alloy 356 Castings.* Int. J. Cast Metals Res. **12** 393-408 (2000).

[8] Nave, M. D., Dahle, A. K. and StJohn, D. H., *Eutectic Growth Morphologies in Magnesium-Aluminium Alloys.* Magnesium Technology 2000 H. I. Kaplan, et al. TMS 233-242 (2000).

7.0 Conclusions and Recommendations

The substantial investigation that has been undertaken to assess the effects of grain refinement on the castability of Mg-Al alloys AZ91E and AM60B has resulted in many valuable findings which contribute greatly to this field of research. The main conclusions from the study are summarised as follows:

1. The experimental mould that was developed to emulate the filling and solidification of an alloy wheel casting was highly effective in reproducing the parameters and associated defects involved in studying magnesium alloy castability. The methodology developed and the results achieved when using the mould were consistent and repeatable making this a valuable tool for future castability investigations.

2. The method of adding strontium as a grain refining agent via the use of an Al-10 wt% Sr master alloy was successful in introducing the desired strontium levels to both AZ91E and AM60B alloys. When endeavouring to introduce carbon as a grain refining agent to the alloy melts in the form of carbon black powder wrapped in aluminium foil, the results were not as consistent. The subsequent development of a solid carbon-containing tablet, produced by the compaction of mechanically milled magnesium alloy, aluminium, and carbon powders resulted in the successful introduction of carbon into both the AZ91E and AM60B alloy melts. The development of this method of carbon addition to Mg-Al alloy melts is seen as a major contribution arising from this work.

3. The use of both strontium and, to a greater extent, carbon as grain refiners for AZ91E alloy resulted in significant reduction of mean grain size throughout the casting samples. It can be concluded from this investigation that grain refinement has a strong negative effect on the formation of the surface slumping defect in AZ91E castings. As the level of grain refinement is increased, the severity of this defect is increased correspondingly.

Conversely, an increase in the level of grain refinement in AZ91E leads to a substantial reduction of the severity of the hot tearing defect. The occurrence of the hot tearing defect was completely eliminated in this case once the mean grain size is reduced below 250μm. Reducing the average grain size of the AZ91E castings also resulted in a corresponding increase in the level of internal shrinkage porosity. This effect is especially prevalent in poorly fed, non-directionally solidifying casting sections such as the spoke/rim junction of an alloy wheel casting.

4. The addition of strontium had no significant effect on grain size of the permanent mould gravity cast AM60B alloy castings. The addition of carbon however results in significant grain size reduction in all sections of the AM60B castings. Again, as with the AZ91E castings, grain refinement has been shown to increase the severity of the surface slumping defect and decrease the severity of hot tearing. The internal porosity level of the AM60B castings was found to increase markedly with an increase in the level of grain refinement achieved.

5. The internal porosity level of Mg-Al castings increases markedly with increased levels of grain refinement due to a reduction of interdendritic feeding efficiency in the castings. This is an important conclusion to consider when choosing an adequate level of grain refinement in non-directionally solidified castings where interdendritic feeding is heavily relied on in the latter stages of solidification to reduce the occurrence of shrinkage microporosity.

6. It was found that for both of the Mg-Al alloys investigated, the distribution of micropores within the castings transformed from a mixture of interdendritic and intergranular, to solely intergranular as the level of grain refinement was increased. This highlights an area of concern for metal casters as

intergranular porosity can easily become interconnected, leading to a severe reduction in the ductility and pressure tightness of Mg-Al castings.

7.1 Recommendations for Future Work

As with all work of this magnitude, avenues for further investigation open up throughout the course of the study. The recommendations for future investigation arising from this research are summarised as follows:

1. As the use of the experimental mould was successful in determining the effect of grain refinement on the castability of Mg-Al alloys AZ91E and AM60B, the results can be further validated for their application to industry through a carefully designed and monitored industrial trial. A permanent mould gravity or low-pressure die casting of a Mg-Al alloy wheel would be a suitable model for validating the conclusions drawn from this investigation.

2. The investigation of the effects of other potential grain refiners for Mg-Al melts (such as CaC_2, SiC, AlN, or Sc) could be investigated in a similar manner to this study to further broaden the understanding of the effects of grain refinement on the castability of Mg-Al alloys. Similarly, the effect of grain refinement on the castability of other magnesium alloys requires further understanding.

3. Though it was not in the scope of this work, the successful identification of the nucleating particle(s) responsible for the grain refinement of Mg-Al alloys through carbon addition still needs to be addressed. Some type of separation technique (e.g. centrifugation or filtration) may be successful in identifying the particles responsible for carbon grain refinement.

4. The further development of the carbon-containing tablet that was developed during this work is an area deserving of further investigation. Alternative

materials and milling times need to be investigated to identify the most efficient method of producing a successful tablet in terms of grain refiner effectiveness. This would further address the issues related to successfully introducing carbon to a Mg-Al melt and may result in a commercially viable solution for the industry.

8.0 Appendix I – AZ91E Grain Size Measurements

	AZ 0 Hub	AZ 0 Spoke	AZ 0 SR	AZ 0 Rim
Mean	594.13	650.45	522.48	632.68
Standard Error	51.60	56.92	5.38	26.08
Median	570.58	571.63	526.82	641.35
Standard Deviation	115.38	127.27	12.04	58.32
Sample Variance	13313.13	16197.69	144.90	3400.65
Kurtosis	2.43	-3.11	0.98	-2.97
Skewness	1.53	0.58	-1.27	-0.17
Range	281.46	265.21	28.89	122.00
Minimum	504.44	536.72	503.33	571.18
Maximum	785.90	801.93	532.22	693.18
Count	5	5	5	5
Confidence Level(95.0%)	143.27	158.03	14.95	72.41
	AZ 1 Hub	**AZ 1 Spoke**	**AZ 1 SR**	**AZ 1 Rim**
Mean	406.40	511.91	514.78	559.64
Standard Error	7.96	20.01	19.59	14.45
Median	406.08	511.78	519.88	541.75
Standard Deviation	17.80	44.74	43.81	32.30
Sample Variance	316.88	2001.41	1919.53	1043.41
Kurtosis	-0.50	0.57	-0.19	-2.61
Skewness	-0.03	0.57	-0.60	0.51
Range	46.52	119.19	112.90	73.25
Minimum	382.96	458.77	451.23	526.63
Maximum	429.48	577.96	564.14	599.89
Count	5	5	5	5
Confidence Level(95.0%)	22.10	55.55	54.40	40.11
	AZ 2 Hub	**AZ 2 Spoke**	**AZ 2 SR**	**AZ 2 Rim**
Mean	409.72	425.26	296.52	430.32
Standard Error	23.75	17.41	4.80	13.27
Median	408.84	421.06	298.97	433.48
Standard Deviation	53.11	38.92	10.72	29.67
Sample Variance	2820.99	1514.95	115.01	880.54
Kurtosis	0.19	1.56	-1.50	-1.09
Skewness	-0.15	1.09	-0.47	-0.54
Range	142.25	102.63	26.20	72.07
Minimum	336.49	384.31	282.02	388.66
Maximum	478.75	486.94	308.22	460.73
Count	5	5	5	5
Confidence Level(95.0%)	65.95	48.33	13.32	36.85

	AZ 3 Hub	AZ 3 Spoke	AZ 3 SR	AZ 3 Rim
Mean	194.31	198.36	224.76	215.02
Standard Error	10.92	13.50	9.10	3.66
Median	195.24	202.53	227.25	216.33
Standard Deviation	24.42	30.18	20.34	8.19
Sample Variance	596.36	910.87	413.62	67.03
Kurtosis	-1.87	-2.48	0.66	-2.28
Skewness	0.19	-0.06	-0.14	0.01
Range	58.10	68.88	55.39	18.76
Minimum	167.74	165.05	196.51	206.32
Maximum	225.84	233.93	251.89	225.07
Count	5	5	5	5
Confidence Level(95.0%)	30.32	37.47	25.25	10.17
	AZ 4 Hub	**AZ 4 Spoke**	**AZ 4 SR**	**AZ 4 Rim**
Mean	250.10	269.29	261.63	249.25
Standard Error	6.32	6.31	14.16	8.10
Median	248.28	267.09	268.91	249.59
Standard Deviation	14.14	14.11	31.66	18.11
Sample Variance	199.82	198.98	1002.04	327.91
Kurtosis	1.39	-0.56	2.97	-2.24
Skewness	0.60	-0.10	-1.64	-0.21
Range	38.81	36.67	80.60	40.98
Minimum	232.54	250.35	208.24	226.39
Maximum	271.35	287.02	288.84	267.37
Count	5	5	5	5
Confidence Level(95.0%)	17.55	17.52	39.30	22.48
	AZ 5 Hub	**AZ 5 Spoke**	**AZ 5 SR**	**AZ 5 Rim**
Mean	122.58	130.40	106.06	113.27
Standard Error	6.01	3.35	5.10	3.45
Median	121.56	132.46	102.85	117.07
Standard Deviation	13.45	7.50	11.40	7.72
Sample Variance	180.85	56.23	129.89	59.63
Kurtosis	-0.07	-1.95	-0.90	3.16
Skewness	-0.34	-0.56	0.09	-1.80
Range	35.35	17.03	29.26	18.70
Minimum	103.58	120.31	91.42	100.08
Maximum	138.93	137.34	120.68	118.78
Count	5	5	5	5
Confidence Level(95.0%)	16.70	9.31	14.15	9.59

0. No treatment
1. 0.05 wt% Sr
2. 0.10 wt% Sr
3. 0.005 wt% C
4. 0.007 wt % C
5. 0.02 wt% C

9.0 Appendix II – AM60B Grain Size Measurements

	AM 0 Hub	AM 0 Spoke	AM 0 SR	AM 0 Rim
Mean	471.43	541.36	488.51	477.23
Standard Error	16.78	26.52	14.74	9.28
Median	471.70	509.72	479.00	476.54
Standard Deviation	37.52	59.29	32.96	20.75
Sample Variance	1407.60	3515.65	1086.40	430.66
Kurtosis	1.04	0.09	-0.74	-2.73
Skewness	0.42	1.18	0.62	-0.02
Range	102.59	137.15	83.22	45.20
Minimum	423.73	495.95	452.16	453.38
Maximum	526.32	633.10	535.38	498.58
Count	5	5	5	5
Confidence Level(95.0%)	46.58	73.62	40.93	25.77
	AM 1 Hub	**AM 1 Spoke**	**AM 1 SR**	**AM 1 Rim**
Mean	569.16	481.07	548.80	531.21
Standard Error	37.63	17.16	23.48	10.27
Median	552.41	461.61	576.28	539.84
Standard Deviation	84.14	38.37	52.49	22.97
Sample Variance	7079.07	1472.05	2755.71	527.40
Kurtosis	2.96	-1.09	-3.00	-0.76
Skewness	1.36	0.94	-0.46	-0.71
Range	228.81	86.18	113.05	57.50
Minimum	479.43	450.97	488.66	498.23
Maximum	708.24	537.15	601.71	555.73
Count	5	5	5	5
Confidence Level(95.0%)	104.47	47.64	65.18	28.52
	AM 2 Hub	**AM 2 Spoke**	**AM 2 SR**	**AM 2 Rim**
Mean	438.93	433.19	442.23	490.58
Standard Error	11.30	17.82	25.53	16.57
Median	432.06	429.48	452.46	479.61
Standard Deviation	25.26	39.84	57.09	37.04
Sample Variance	638.21	1587.17	3259.36	1372.01
Kurtosis	3.73	2.02	-0.13	-2.88
Skewness	1.79	1.36	-0.30	0.29
Range	65.78	100.35	150.84	79.91
Minimum	416.59	397.90	363.03	450.96
Maximum	482.37	498.25	513.86	530.86
Count	5	5	5	5
Confidence Level(95.0%)	31.37	49.47	70.89	45.99

	AM 3 Hub	AM 3 Spoke	AM 3 SR	AM 3 Rim
Mean	376.25	338.01	350.43	339.26
Standard Error	9.39	8.44	5.81	14.12
Median	373.38	333.72	351.12	323.25
Standard Deviation	20.99	18.87	12.98	31.57
Sample Variance	440.63	356.19	168.61	996.61
Kurtosis	2.07	1.57	1.16	-1.05
Skewness	1.35	1.29	-0.34	0.85
Range	53.87	47.52	35.75	75.81
Minimum	356.65	320.89	331.58	309.15
Maximum	410.52	368.42	367.33	384.96
Count	5	5	5	5
Confidence Level(95.0%)	26.06	23.43	16.12	39.20
	AM 4 Hub	**AM 4 Spoke**	**AM 4 SR**	**AM 4 Rim**
Mean	509.38	502.54	512.40	501.40
Standard Error	15.40	12.85	21.07	15.77
Median	506.69	519.30	532.24	518.33
Standard Deviation	34.44	28.73	47.12	35.27
Sample Variance	1185.79	825.15	2220.70	1243.76
Kurtosis	-1.69	-2.32	-2.28	4.48
Skewness	0.41	-0.74	-0.12	-2.10
Range	79.14	62.78	107.27	83.01
Minimum	476.64	463.94	462.40	439.10
Maximum	555.78	526.73	569.67	522.11
Count	5	5	5	5
Confidence Level(95.0%)	42.76	35.67	58.51	43.79
	AM 5 Hub	**AM 5 Spoke**	**AM 5 SR**	**AM 5 Rim**
Mean	304.28	289.43	331.23	235.09
Standard Error	8.19	7.04	5.16	4.57
Median	311.88	284.35	335.46	240.66
Standard Deviation	18.32	15.75	11.55	10.22
Sample Variance	335.63	248.13	133.33	104.39
Kurtosis	-1.22	-1.97	1.16	-1.08
Skewness	-0.74	0.57	-1.11	-0.93
Range	44.39	36.67	30.07	23.84
Minimum	278.29	273.87	313.07	220.19
Maximum	322.68	310.54	343.14	244.03
Count	5	5	5	5
Confidence Level(95.0%)	22.75	19.56	14.34	12.69

0. No treatment
1. 0.05 wt% Sr
2. 0.10 wt% Sr
3. <0.005 wt% C
4. 0.005 wt % C
5. 0.01 wt% C

10.0 Appendix III – External Defect Analysis

As detailed in Chapter 3, all of the castings produced were assessed for external defects after they were removed from the casting mould. The defects were located in four specific regions of the casting as shown in Figure 10-1.

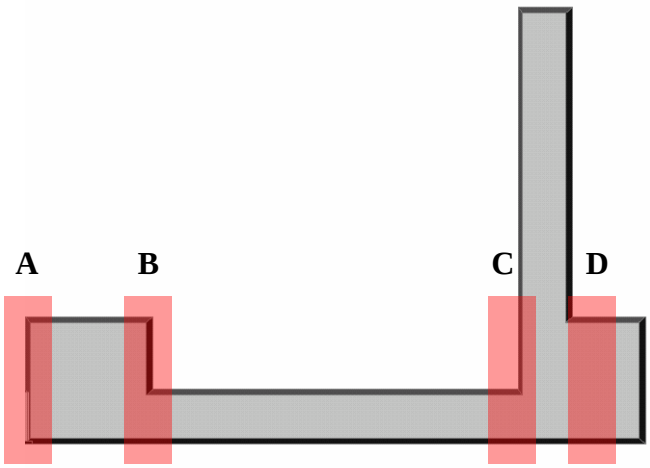

Figure 10-1: Locations of the externally visible defects in the experimental castings.

The severity of each defect was given a grade between 0 and 3 depending on its severity. This provided quantitative data to a usually qualitative assessment. Explanation of the grading system used can be seen in Table 10-1.

Table 10-1: Explanation of the grading system for the externally visible casting defects.

	Surface Slumping	**Shrinkage Porosity**	**Hot Tearing**
Grade 0	No slumping	No visible porosity	No tears present
Grade 1	Small amount of slumping	Slight traces of porosity	Small tears present
Grade 2	Moderate amount of surface slumping	Moderate amounts of porosity visible	Moderate amount of tearing
Grade 3	Large amount of surface slumping	Large amount of porosity present	Large tears apparent

Examples of the types of defects present and their respective grades are below shown in Figure 10-3, Figure 10-5, and Figure 10-7.

Figure 10-2: Example of a grade 2 surface slumping defect.

Figure 10-3: Example of a grade 3 externally visible shrinkage porosity defect.

Figure 10-4: Example of a grade 1 hot tearing defect.

The results of the external defect analysis of the AZ91E castings are presented below in Table 10-3.

Table 10-2: External defect ratings of the AZ91E casting samples.

AZ91E				
	A	**B**	**C**	**D**
Slumping	0,0	1,0	1,0	1,1
Shrinkage	0,0	0,1	0,1	0,0
Hot Tearing	0,0	0,0	3,2	2,1
AZ91E + 0.05 wt% Sr				
	A	**B**	**C**	**D**
Slumping	0,0	0,0	0,1	0,1
Shrinkage	0,0	0,0	0,0	0,0
Hot Tearing	0,0	0,0	2,1	0,0
AZ91E + 0.10 wt% Sr				
	A	**B**	**C**	**D**
Slumping	0,0	2,1	1,1	2,1
Shrinkage	0,0	0,0	0,0	0,0
Hot Tearing	0,0	0,0	0,1	0,0
AZ91E + 0.005 wt% C				
	A	**B**	**C**	**D**
Slumping	1,2	0,0	0,0	1,1
Shrinkage	0,0	0,0	0,0	0,0
Hot Tearing	0,0	0,0	0,0	0,0
AZ91E + 0.007 wt% C				
	A	**B**	**C**	**D**
Slumping	0,0	0,1	2,1	1,1
Shrinkage	0,0	0,0	0,0	1,1
Hot Tearing	0,0	0,0	0,0	0,0
AZ91E + 0.02 wt% C				
	A	**B**	**C**	**D**
Slumping	1,0	0,0	0,1	3,2
Shrinkage	0,0	0,0	0,0	0,0
Hot Tearing	0,0	0,0	0,0	0,0

The results of the external defect analysis of the AZ91E castings are presented below in Table 10-5.

Table 10-3:External defect ratings of the AM60B casting samples.

AM60B				
	A	**B**	**C**	**D**
Slumping	0,1	1,1	1,2	0,1
Shrinkage	2,1	0,0	1,1	1,2
Hot Tearing	0,0	2,2	0,0	0,1
AM60B + 0.05 wt% Sr				
	A	**B**	**C**	**D**
Slumping	0,0	0,1	1,1	0,1
Shrinkage	0,0	0,0	0,0	0,0
Hot Tearing	0,0	1,1	2,2	1,0
AM60B + 0.10 wt% Sr				
	A	**B**	**C**	**D**
Slumping	0,0	2,2	1,1	0,0
Shrinkage	0,0	0,0	0,0	0,0
Hot Tearing	0,0	1,1	1,1	1,0
AM60B + <0.005 wt% C				
	A	**B**	**C**	**D**
Slumping	3,2	0,0	1,1	1,1
Shrinkage	0,0	0,0	1,1	0,0
Hot Tearing	1,1	2,3	0,1	0,0
AM60B + 0.005 wt% C				
	A	**B**	**C**	**D**
Slumping	0,1	1,1	1,1	0,0
Shrinkage	0,0	0,0	0,1	0,0
Hot Tearing	0,0	1,0	2,1	1,0
AM60B + 0.01 wt% C				
	A	**B**	**C**	**D**
Slumping	1,1	1,2	1,1	1,1
Shrinkage	0,0	1,0	2,1	0,1
Hot Tearing	0,0	0,0	0,1	0,0

11.0 Appendix IV – Theoretical Density Measurements

To be able to calculate the porosity level of the casting samples, a theoretical density figure is required to compare with the apparent density of the samples. This figure is then used to determine the porosity level of the sample in question. As detailed in Chapter 3, to calculate this theoretical density a small sample from the rim section of each of the castings was removed and hot isostatic pressed to fully densify the sample. The two samples were then averaged to give a theoretical density value for that casting condition. Table 11-1 shows the calculation of the theoretical density value for each of the casting samples.

Table 11-1: Theoretical density calculations for the AZ91E and AM60B castings.

Sample		Air (g)	Water (g)	Diff (g)	Temp (C)	Water Density (g/cc)	Ap Density	Average
AZ-0	1	29.48	13.24	16.2	16.9	0.998792	1.8131	
	2	31.99	14.38	17.6	16.9	0.998792	1.8144	**1.8137**
AZ-1	1	28.45	12.81	15.6	16.9	0.998792	1.8169	
	2	23.77	10.70	13.1	16.8	0.998809	1.8165	**1.8167**
AZ-2	1	26.28	11.86	14.4	16.8	0.998809	1.8203	
	2	25.00	11.28	13.7	16.8	0.998809	1.8200	**1.8201**
AZ-3	1	14.80	6.64	8.2	14.8	0.999129	1.8121	
	2	15.20	6.82	8.4	14.8	0.999129	1.8123	**1.8122**
AZ-4	1	14.12	6.35	7.8	14.8	0.999129	1.8157	
	2	12.90	5.77	7.1	14.8	0.999129	1.8077	**1.8117**
AZ-5	1	13.98	6.27	7.7	14.8	0.999129	1.8117	
	2	11.75	5.29	6.5	14.8	0.999129	1.8173	**1.8145**
AM-0	1	25.17	11.05	14.1	17.1	0.998757	1.7804	
	2	26.84	11.81	15.0	17.0	0.998774	1.7836	**1.7820**
AM-1	1	27.81	12.26	15.6	17.0	0.998774	1.7862	
	2	24.36	10.74	13.6	17.0	0.998774	1.7864	**1.7863**
AM-2	1	33.11	14.56	18.6	16.9	0.998792	1.7827	
	2	30.10	13.24	16.9	16.9	0.998792	1.7831	**1.7829**
AM-3	1	11.95	5.26	6.7	14.4	0.999188	1.7848	
	2	13.31	5.88	7.4	14.4	0.999188	1.7899	**1.7874**
AM-4	1	10.31	4.52	5.8	14.5	0.999173	1.7792	
	2	10.58	4.66	5.9	14.5	0.999173	1.7857	**1.7824**
AM-5	1	22.50	9.89	12.6	14.5	0.999173	1.7828	
	2	21.98	9.70	12.3	14.5	0.999173	1.7884	**1.7856**